POROUS CRYSTALLINE FRAMEWORKS: SYNTHETIC APPROACHES AND THEIR APPLICABILITY AS MEMBRANE MATERIALS FOR GAS SEPARATION

Thesis Submitted to AcSIR

For the Award of the Degree of

DOCTOR OF PHILOSOPHY

In

CHEMICAL SCIENCES

By

Bishnu Prasad Biswal
(Registration Number: 10CC11A26005)

Under the guidance of
Dr. Rahul Banerjee

Physical & Materials Chemistry Division
CSIR-National Chemical Laboratory
Pune - 411008, MH, India.

August 2016

Dedicated to
My Parents, My Wife
and Daughter for their
Love and Support…

सीएसआईआर - राष्ट्रीय रासायनिक प्रयोगशाला
(वैज्ञानिक तथा औद्योगिक अनुसंधान परिषद)
डॉ. होमी भाभा मार्ग, पुणे - 411 008, भारत
CSIR - NATIONAL CHEMICAL LABORATORY
(Council of Scientific & Industrial Research)
Dr. Homi Bhabha Road, Pune - 411 008, India

CERTIFICATE

*This is to certify that the work incorporated in this Ph.D. thesis entitled "**Porous Crystalline Frameworks: Synthetic Approaches and their Applicability as Membrane Materials for Gas Separation**" submitted by **Mr. Bishnu Prasad Biswal** to **Academy of Scientific and Innovative Research (AcSIR)** in fulfillment of the requirements for the award of the Degree of Doctor of Philosophy, embodies original research work under my supervision. I further certify that this work has not been submitted to any other University or Institution in part or full for the award of any degree or diploma. Research material obtained from other sources has been duly acknowledged in the thesis. Any text, illustration, table etc., used in the thesis from other sources, have been duly cited and acknowledged.*

Mr. Bishnu Prasad Biswal
(Student)

Dr. Rahul Banerjee
(Supervisor)

Communication Channels
NCL Level DID : 2590
NCL Board No. : +91-20-25902000
EPABX : +91-20-25893300
: +91-20-25893400
FAX
Director's Office : +91-20-25902601
COA's Office : +91-20-25902660
SPO's Office : +91-20-25902664
WEBSITE
www.ncl-india.org

DECLARATION

I hereby declare that the matter embodied in this thesis entitled ***"Porous Crystalline Frameworks: Synthetic Approaches and their Applicability as Membrane Materials for Gas Separation"*** *is the result of investigations carried out by me in the Physical & Materials Chemistry Division, CSIR-National Chemical Laboratory, Pune, India under the supervision of Dr. Rahul Banerjee.*

In keeping with the general practice of reporting scientific observations due acknowledgements have been made wherever the work described is based on the findings of other investigators.

Pune, August 2016

Bishnu Prasad Biswal

ACKNOWLEDGEMENT

I would take this opportunity to express my sincere gratitude to my supervisor Dr. Rahul Banerjee. My heartfelt thanks go to him for introducing me to the wonders of scientific research, for his persistent guidance, encouragement, inspiration and support during every stage of my doctoral research work. Again I warmly thank him for his precious advice, analysis, criticism and discussions on my research work. The other important person who has bestowed me with his guidance and encouragement is my co-supervisor Dr. Ulhas K. Kharul. I am very much thankful to him for his pursuance for improving me as a person as well as my scientific skills. His enthusiasm for transforming the science into technology for the improvement of the quality of life was a great inspiration for me to pursuing membrane research as a career. I would also like to sincerely thank my DAC committee members Dr. Nandini Devi, Dr. Sreekumar K. and Dr. Sayam Sen Gupta for their constructive, innovative suggestion and comments throughout my Ph.D. work period at CSIR-NCL, Pune.

I extend my sincere thanks to the Director of CSIR-NCL Prof. Ashwani Kumar Nangia, former Directors Dr. Vijayamohanan K. Pillai and Dr. Sourav Pal, Head of Physical and Materials Chemistry Division Dr. P. A. Joy and Dr. Anil Kumar (Ex-HoD) for their kind help and encouragement during the course of this work. I must earnestly acknowledge the collaborative assistance, valuable scientific discussions and suggestions that I received from Dr. Sreekumar K. and Dr. V. K. Pillai with helpful hands of their students Dr. T. Palaniselvam and Dr. Dhanraj Shinde for electrochemical related works. I also thank Dr. Thomas Heine, School of Engineering and Science, Jacobs University, Germany, for his help in theoretical calculations in few projects.

I am very grateful to UGC, New Delhi for fellowship support to carry out my research work. I thank all the non-teaching staff of CSIR-NCL for their assistance on various occasions. I would like to especially thank my senior Dr. Subash C. Sahoo (Subash Bhai) for his support and help in learning the basic laboratory practice. He has placed a great influence on me at the beginning of my stay at NCL. I wish to thank all my friendly and cooperative labmates Tamas Bhaya, Pradip Bhaya, Arijit Bhaya, Chandan Bhaya, Subhadeep Bhaya, Tanay Bhaya, my dearest friend Sharath, Divya, Harshitha, Suman, Bikash, Mohitosh, Saibal, Arjun, Suvendu, Jayshri Didi, Gobinda Da, Digambar Ji, Manas Da, Shouvik Da, Sujit Da, Kaushik, Himadri, Abdul, Amit Da, Arghya Da, Sushil Bhaya and

Gargi Di for creating a cheerful and enjoyable working atmosphere in the lab. I had a great experience in Dr. Kharul Sir's lab as well. I would like to thank Deepti, Vinaya, Nikita, Smita, Sneha T., Vasanti, Manisha, Rishit, Kiran, Rohit, Bharat, Varsha, Sudhir, Ganesh, Prakash, Praveen, Deekshith, Ramendra, Harsha, Vrushali, Shebeeb, Godavari, Supriya, Chetana, Vijay, Akash, Runali, Swaraj, Taranpreet, Shilpa and Dr. Kanhu who have helped me in all possible ways & have been my extended family during the tenure of my work at NCL. I owe special thanks to my lab mates Harshal, Rupesh Bhaya, Anita, Sayali, and Anand for their constant encouragement & always being with me in all sorts of situations during my stay in NCL. I thank Dr. K. V. Pandare Sir for his support and valuable discussions on scientific and non-scientific topics. I would also like to thank Mr. Swaraj Singh, Sneha D., and Hemchandra for their support in purchasing and indenting of the laboratory materials and other related issues.

My stay on this campus has been pleasant with the association of all the research scholars at CSIR-NCL. I am thankful to Kundan, Sushma, Asish, Chaitanya, Yogesh, Manoj, Anantharamaiah, Joyashish Da, Munmun, Chinmay, Sekhar, Nagesh, Prajitha, Vishal, Sreekuttan, Pandiraj, Beena, Rajashri, Soumen, Saibal B., Dhanya and many more. I would also like to thank the Odiya group at NCL, Pitambar Bhai, Ramakanta Bhai, Chaka Bhai, Jitu Bhai, Mandakini Nani, Rinki Nani, Raju Bhai, Rudra, Manoj, Prajna and Kanhu for their support, guidance, and advice. I am grateful to all my teachers and I expressed my gratitude for their encouragement in different part of my life.

I sincerely acknowledge my wife Mahalaxmi (Sunu) and my daughter Utkalika (Khushi), they deserve the credit for their sacrifice, support and love during my entire Ph.D. period at CSIR-NCL. I also thank my elder brother Dr. K. C. Biswal for his support, guidance and encouragement from my childhood. I thank the entire members of my family for their constant care and wishes. Last but not least, I would like to pay high regards to my parents and in-laws for their constant encouragement and inspiration throughout my research work and lifting me uphill this phase of life. I owe everything to them. Dedicating this thesis to them is a minor recognition for their valuable support and encouragement.

Bishnu Prasad Biswal

PREFACE

Metal-organic frameworks (MOFs) and covalent organic frameworks (COFs) are belongs to a classs of new age porous crystalline frameworks (PCFs) gaining increasing momentum due to their diverse practical applications in gas storage, catalysis, sensing etc. Despite such advancement, the chemical stability and synthetic difficulty are the two major challenges, which hinder their practical applicability. Moreover, separations of industrially relevant gas mixtures are becoming very important now a days. Although, MOFs/COFs have characteristics to being a good candidate for gas separation but the composite membranes based on these materials are barely explored. Therefore, an easy and scalable method to synthesize these porous materials and their applicability as membrane materials for gas separation still remains a key challenge. In this thesis, we emphasize on simple design and easy synthesis of chemically stable MOFs, COFs and their polymer composite membranes for gas separation application. Excluding introduction chapter this thesis is divided into 5 chapters which includes the synthetic development of chemically stable MOFs and COFs, control on the growth of the MOF crystals on polymeric hollow fiber membranes and COF based hybrid membranes to enhance gas separation performance.

Chapter 2 will present the synthesis of a new, highly porous, water stable Co(II) based ZIF [CoNIm (RHO)] and it's in situ solution mediated phase transformation to a less porous SOD ZIF. The phase transformation process has been systematically investigated with the help of PXRD and SEM imaging at different stages of crystallization. The detail synthetic procedures and characterization processes will also be explained. The water stability of both the ZIFs (RHO and SOD) will be discussed thoroughly with reference to the existing literatures. The crystal structures, thermal stability and the adsorption properties, especially H_2, CO_2, N_2 and H_2O adsorption will be demonstrated. (Adapted from ***Chem. Commun.*, 2012, *48*, 11868-11870**).

In Chapter 3, a new, convenient, scalable room temperature interfacial MOF (ZIF-8 and CuBTC) synthesis approach towards the preferred fabrication on inner and outer surfaces of polybenzimidazole hollow fiber membrane will be presented by varying the water immiscible low boiling solvent pairs and synthetic conditions. The mechanism of MOF growth *via* interfacial crystallization method with immiscible solvent combinations, flow

reversal approach, and composite membranes characterizations will be showcased. The growth of MOFs on hollow fiber membranes, their uniformity and the continuity will be discussed thoroughly. Finally the gas separation performance towards He, N_2 and C_3H_8 will be evaluated and discussed. (Adapted from ***Nanoscale,* 2013, *5,* 10556-10561**).

In Chapter 4, the first synthesis of a class of thermally and chemically stable, isoreticular COFs *via* simple room-temperature solvent-free mechanochemical grinding will be presented. The structure and the chemical stability in boiling water, acid (9 N HCl) and base (3 N NaOH) will be discussed. The concept of exfoliation of COF stacked layers to graphene-like sheets during mechanochemical grinding will be presented with reference to HR-TEM images. The analysis of gas and water adsorption properties will be thoroughly explained. In the later part of this chapter, we will also discuss the idea of liquid assisted grinding (LAG) to synthesize diverse Schiff base COF materials with improved crystallinity. (Adapted from ***J. Am. Chem. Soc.,* 2013, *135,* 5328–5331** and ***Chem. Commun.*, 2014**, ***50,* 12615-12618**).

In Chapter 5, we will present a method to fabricate chemically stable, flexible COF@PBI composite membranes by direct blending of COFs (TpPa-1 and TpBD) with Polybenzimidazole (PBI) matrix. All the physical properties and characterizations of these composite membranes will be carefully discussed. The effect of chemical structure of both filler and polymer matrix towards defect-free composite membrane fabrication will be summarized. The gas permeation properties of these composite membranes will be explored. The effect of pore-modulation of filler materials (COFs) to enhance the gas permeability will be evaluated with evidence of experiments. In the later part, we will showcase the fabrication of thin film composite membranes based on COF and Styrene Butadiene Rubber (SBR). At last, the hydrocarbon separation performance of these hybrid TFCs membranes will be presented and discussed. (Adapted from ***Chem. Eur. J.*, 2016, *22,* 4695-4699**).

Finally, Chapter 6 will describe the conclusion of the overall work presented in this thesis. The future direction based on the understanding of this thesis work also presented in the last section of this chapter.

Bishnu Prasad Biswal

CONTENTS **PAGE**

CHAPTER 5

Chemically Stable Covalent Organic Framework-Polymer Hybrid Membranes for Enhanced Gas Separation 123-150

LIST OF FIGURES

LIST OF TABLES

CHAPTER 1

Introduction to Porous Crystalline Frameworks: Synthesis and their Applications

Abstract: *Porous crystalline frameworks (PCFs) such as metal-organic frameworks (MOFs) and covalent organic frameworks (COFs) are gaining increasing attention as new age materials due to their diverse practical applications in gas storage, catalysis, sensing etc. Despite such advancement the chemical stability and synthetic difficulty are the two major challenges, which hinder their applicability. Moreover, separations of gas mixtures are becoming very important for many industrial applications. Although, PCFs have characteristics to being a good candidate for gas separation, PCF based membranes are scarcely explored. Therefore, an easy and scalable method to synthesize these porous materials and their application as membrane materials for gas separation remains a key challenge. In this thesis, we emphasize on simple design and easy synthesis of chemically stable MOFs, COFs and their polymer composite membranes for gas separation. Excluding introduction chapter the thesis is divided into 5 chapters which discuss the facile and scalable method for the synthesis of chemically stable MOFs and COFs, control on the growth of the MOF crystals on polymeric hollow fiber membranes and COF based hybrid membranes to enhance gas separation performance.*

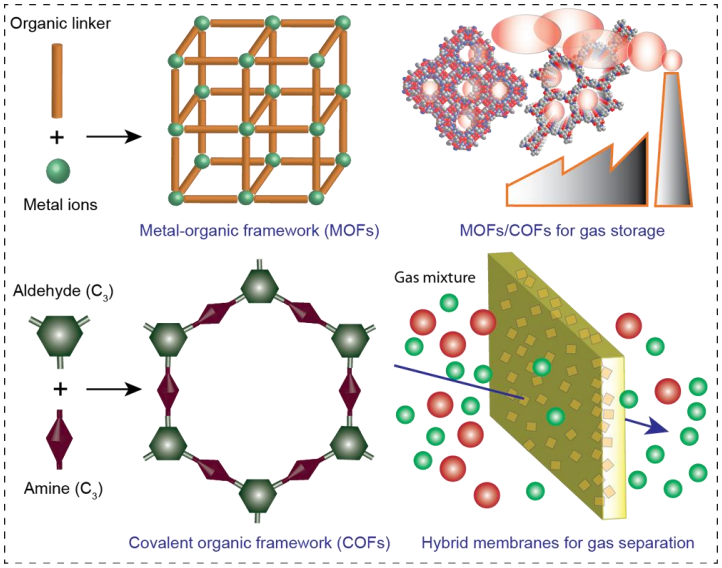

1.1 Background of porous crystalline frameworks

A solid can be defined as a porous material if it contains minute openings on the surface, through which gases, liquids, or microscopic particles can pass. Over the past five decades microporous materials have become a progressively more important and developed area of chemistry. There are many academic and industrial research groups all over the world now exploring these materials for various applications including adsorbent technology, catalysis, gas purification, chemical sensing, optoelectronics etc. [1.1]. This is possible due to their ultrahigh surface area, tuneable pore size, adjustable framework cavity and outstanding surface properties. Surprisingly, the surface area of these porous materials can be in the range of 300 to 10,000 square meters per gram (m^2g^{-1}) depending on the materials [1.2]. Prior to 1970, researchers have extensively used porous carbon for the purpose of gas storage, separation, water purification, solvent removal, etc. [1.3]. However, due to certain limitations such as low surface area, nonuniform pore size and poor crystallinity, application of porous carbon in large scale have been affected. Subsequently, researchers discovered another interesting inorganic porous material called zeolites, which have crystallinity, uniform porosity and very good for various targeted applications [1.4]. In principle, zeolites belong to a family of aluminosilicate made from silicate $[SiO_4]^{4-}$ and aluminate $[AlO_4]^{5-}$ where tetrahedrons are interconnected through oxygen atoms. The resulting three-dimensional framework has nanochannels of molecular dimensions (0.1 – 2.0 nm). Such microporous zeolite structure provides a surface area ranging from 400 – 900 m^2g^{-1} offering numerous potential applications. But zeolites also have some limitations like poor chemical stability and unavailability of opportunity for pore engineering or tuneability. To address the issues faced by zeolites, in the year 1995 researchers have come up with hybrid organic-inorganic porous materials well known as metal-organic frameworks (MOFs) [1.5]. This class of porous materials offer high crystallinity, porosity and opportunity of pore surface engineering for various important applications. However, they also have some drawbacks as the framework density is very high due to metal content and the poor chemical stability arises because of metal-ligand coordination bonds. To tackle the issues associate with MOFs, in 2005 Yaghi and co-workers introduced another class of organic crystalline, porous materials called covalent organic frameworks (COFs) [1.6], which have shown great potentiality for many applications.

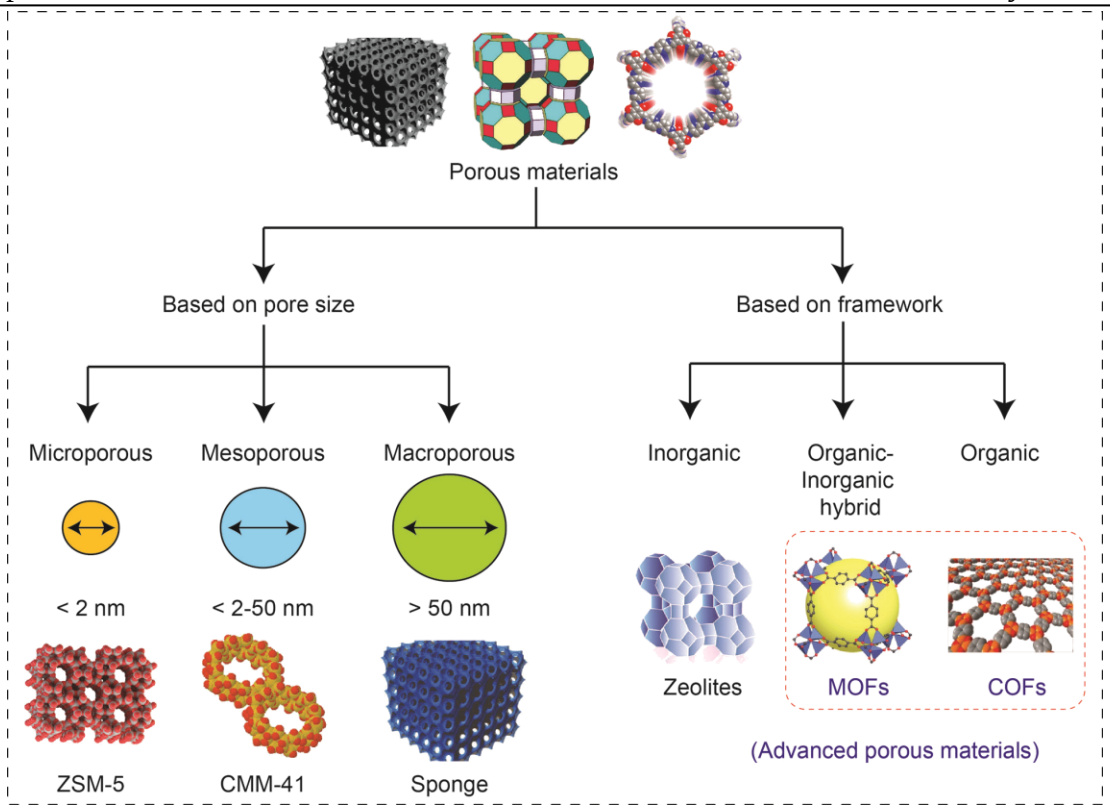

Figure 1.1. *Classification of porous materials based on the pore diameter and framework type.*

On the other hand, according to the International Union of Pure and Applied Chemistry (IUPAC), the porous materials can be classified [1.7] in three major classes based on their pore diameters (nm): i) microporous materials, < 1 nm (*i.e.*, zeolites and MOFs); ii) mesoporous materials, 2.0 nm < < 50 nm (silica and alumina); and iii) macroporous materials > 50 nm (porous glass, carbons, sponge and foams) (***Figure 1.1***). Moreover, based on framework type advanced porous materials can be classified as inorganic (zeolites), organic-inorganic hybrid (MOFs) and pure organic materials (COFs, PAFs, cages). In this thesis, mainly microporous materials (special attention to MOFs and COFs), their easy synthesis and polymer composite membranes for gas separation applications have been discussed.

1.2 Metal-organic frameworks (MOFs)

Metal-organic frameworks (MOFs) [1.5] are belong to a family of advanced crystalline, porous materials comprised of ordered networks resulted from organic electron donor linkers and metal ions/nodes to form 1D chains, 2D layers and 3D frameworks (***Figure***

1.2). This class of materials have emerged as a most promising candidate for sorbent based applications [1.8]. They are synthesized *via* various methods including solvothermal approach wherein organic ligands coordinate with metal ions/nodes (either a single ion or cluster). MOFs offer a very high surface area (up to 10,000 m^2g^{-1}, and pore volume 4.40 cm^3g^{-1}) than other porous materials such as zeolites, carbon and porous polymer materials. In addition, once these frameworks constructed, they do not collapse when guest molecules (most often solvents) are removed from the pores. Their extraordinary compositional and structural variety (>10,000 MOF structures), many of them display permanent porosity and well-defined pores/channels, suitable for a range of applications [1.9]. The single crystal structures elucidation of MOFs can provide accurate pore size/dimension of the channel, which in turn, gives better insight into the structural parameters. On the other hand, by varying the diverse organic linkers the porosity of MOFs can be systematically tuned according to the application requirement. In addition, different active sites of the organic linkers can be installed inside the MOF channels, which facilitate post-synthetic modification and pore functionalization, a unique advantage, which is beyond the scope of other porous materials. The uniform porosity throughout the framework and outstanding thermal stability of MOF have been utilized for important applications like gas adsorption and storage, catalysis, magnetism, proton conduction, chemical sensing, drug delivery etc. [1.8] However, in recent years, the focus has been shifted to other interesting applications such as gas separation, lithium ion battery, charge carrier motion, oxygen reduction catalysis, light harvesting [1.9]. These applications are highly important for the generation renewable energy and to protect the environment.

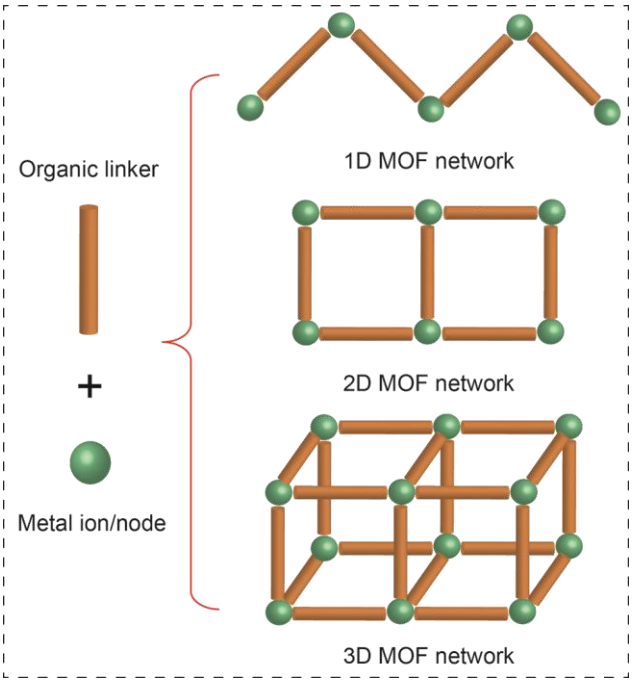

Figure 1.2*. Model representation of 1D, 2D and 3D MOF constructed from organic linker and metal ion/node.*

1.3 Synthesis of metal-organic frameworks (MOFs)

The metal-organic frameworks (MOFs) have been so far synthesized using most metal ions (s-block metals, transition metals and lanthanides) present in the periodic table with a library of organic linkers. The organic linkers suitable for MOF structures formation are mainly polydentate ligands such as aromatic polycarboxylates and other functionality like –OH, $–NH_2$, –SH, $–N_3$, –CN, $–H_2PO_4$, $–SO_3H$. Heterocyclic compounds like imidazole, triazole, tetrazole, pyridine, pyrazine and their derivatives are also been used as potential linkers for MOFs synthesis. MOFs are primarily synthesized using different liquid phase methods (solid phase MOF synthesis are also attempted), in which metal salts and organic linkers are dissolved in suitable solvents and kept for crystallizing at particular pressure and temperature. The advantage of solvent based synthesis is that it maintains the thermodynamic conditions of the system and gives rise to the crystalline product (mostly single crystals) at higher extent. The next section will briefly describe the synthesis methods so far employed for the construction of various MOF structures.

1.3.1 *Solvothermal and hydrothermal synthesis of MOFs*

Solvothermal method is the most common and widely used method for MOF synthesis. About 70% of MOFs have been synthesized by using this approach [1.10]. In this method metal salts and particular organic linkers dissolved in suitable solvents (sometimes mixture of solvents) in a container (*i.e.*, glass vial) having Teflon cap [1.11a]. The caps of these vials are sealed tightly to make a close system. A temperature range of 60 - 100 ºC and the time period of 10–100 h are generally required for MOF synthesis using this solvothermal reaction condition. Another method called hydrothermal synthesis method, which is exactly similar to solvothermal one but only difference it operates at very high-temperature reaction condition (100–200 ºC) has been employed for MOF synthesis. The solvents that are suitable for this particular method includes *N*,*N*-dimethylformamide (DMF), *N*,*N*-diethylformamide (DEF), dimethyl sulfoxide (DMSO), *N*,*N*-dimethylacetamide (DMA), *N*-methyl-2-pyrrolidone (NMP), *N*-methylformamide (NMF), etc. in Teflon-lined autoclave. The reaction time is normally 2-5 days to get single crystalline MOF crystals.

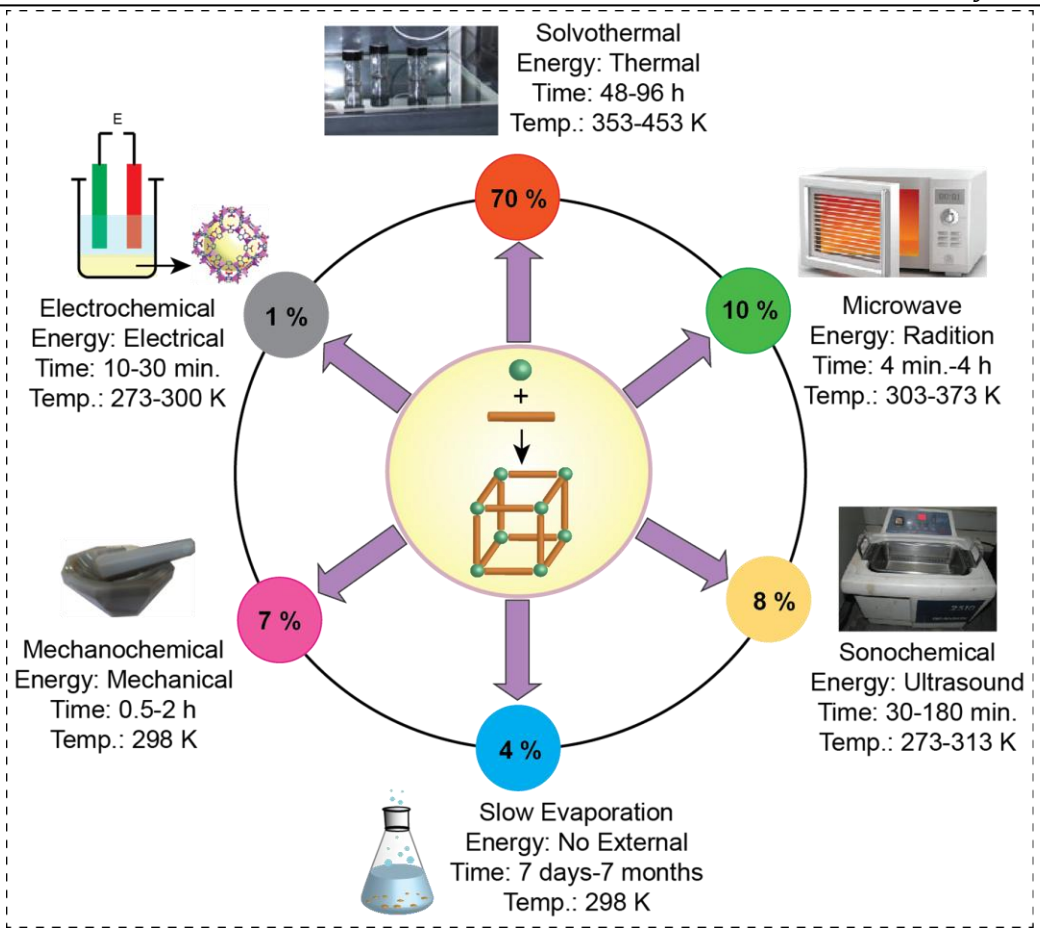

Figure 1.3*. Scheme of various synthetic approaches and conditions used for the preparation of MOFs. [Ref. 1.10b].*

1.3.2 *Room temperature synthesis of MOFs*

There are several reports on room temperature synthesis of MOFs [1.10b]. In general three types of method have been used for this purpose: i) slow evaporation method, ii) layering method and iii) slow diffusion method. About 4% of MOFs synthesized using room temperature synthesis method and does not require any external energy.

I. *Slow evaporation method:* In this method a mixture of metal and ligands are dissolved is low boiling solvents (preferably) in a container and then the solvent is allowed to evaporate slowly. This approach takes a long time for crystallization (7 days to 7 months).

II. *Layering method:* Two different solvents with varying density are used for MOF synthesis *via* layering approach. The dissolved metal salt and ligand are placed in a

container in which the lower density solution forms a layered on top of high-density solution (*e.g.*, methanol solution can be layered on the aqueous solution). The MOF single crystals grow preferably at the junction of the layers.

III. *Slow diffusion method:* This method also employs two different solvents. The metal and ligand are dissolved in a solvent and placed in a saturated vapor of another low boiling solvent. In this approach, the solvent vapor slowly diffuses into the solution and MOF crystallization starts.

1.3.3 *Microwave synthesis of MOFs*

Microwave synthesis method is very important and rapid for the industrial level bulk production of MOFs. Using this process MOFs can be synthesized in gram scale within few minutes. In this approach, metal salt and ligands are dissolved in a solvent and the reaction vessel kept inside a microwave reactor. In most cases a microcrystalline MOF powders are recovered and getting single crystal is extremely difficult using microwave technique [1.11b].

1.3.4 *Mechanochemical synthesis of MOFs*

Mechanical method is a famous method to synthesize a wide range of materials at room temperature. In mechanochemical synthesis, the mechanical force plays a very crucial role in bringing molecules together, breaking of intramolecular bonds and to carry out the chemical transformation. Commonly mortal and pestles used to carry out the reaction in a laboratory level and in industries ball mills are used to do mechanochemical reactions. In this approach sometimes solvents are also used (liquid assisted grinding) to enhance the product rate formation and to improve the crystallinity of the product. The mechanochemical method takes 0.5 h to 2 h to synthesize highly crystalline and single-phase MOFs [1.11c-e]. The entrapped guests molecules can be removed by thermal activation to obtained guest-free porous MOFs.

1.3.5 *Electrochemical synthesis of MOFs*

The electrochemical synthesis of MOFs is employed to prohibit the entry of anions like nitrate, perchlorate or halides during the syntheses, which are of concern to large-scale production processes. It is believed that the large scale synthesis of MOFs using metal

precursors and organic linkers can be achieved following electrochemical synthesis approach in a continuous manner. A highly crystalline and phase pure MOF materials are anticipated in this synthetic procedure. The time required for the MOF synthesis in this method is very short say 10 to 30 minutes [1.11f].

1.3.6 *Sonochemical synthesis of MOFs*

Sonochemistry is a process wherein molecules experience chemical change subject to the ultrasonic radiation (20 kHz–100 MHz). Ultrasound induces physical or chemical changes to the MOF precursors and the crystal growth occurs within very short time period (30 to 180 minutes). Sonochemical methods can produce MOFs with uniform crystal sizes and a considerable reduction in crystallization time compared with other conventional hydrothermal methods [1.11g and h].

1.4 Properties and applications of MOFs

Porous materials have been offering many potential applications that include gas storage, gas/vapour adsorption and separation, shape/size-selective catalysis, drug delivery, chemical sensing, optoelectronic etc. In order to get full advantage of any porous material like MOFs and to explore their physical properties both chemical stability and crystallinity is need to be considered. MOF materials have attracted a great deal of scientific attention in the past two decades because of their fascinating applications (***Figure 1.4***). MOFs have structural attractiveness and ability to tune the framework architectures, thus properties of MOFs provides a significant advantage over other inorganic porous materials (*i.e.*, zeolites). In addition to these MOFs also hold several outstanding features as mentioned below.

I. A wide variety of easy synthesis method so far developed for MOF synthesis like room temperature synthesis, mechanochemical, electrochemical synthesis, etc.
II. Ultrahigh porosity, systematic tunable pore sizes, easy incorporation of functional groups is possible in MOFs.
III. Isoreticulation is possible and the prospect of structure predictable provides tailored materials for specific applications.
IV. The surface properties of nanochannels can be modified with different organic substituent’s on the ligand without altering the basic framework.

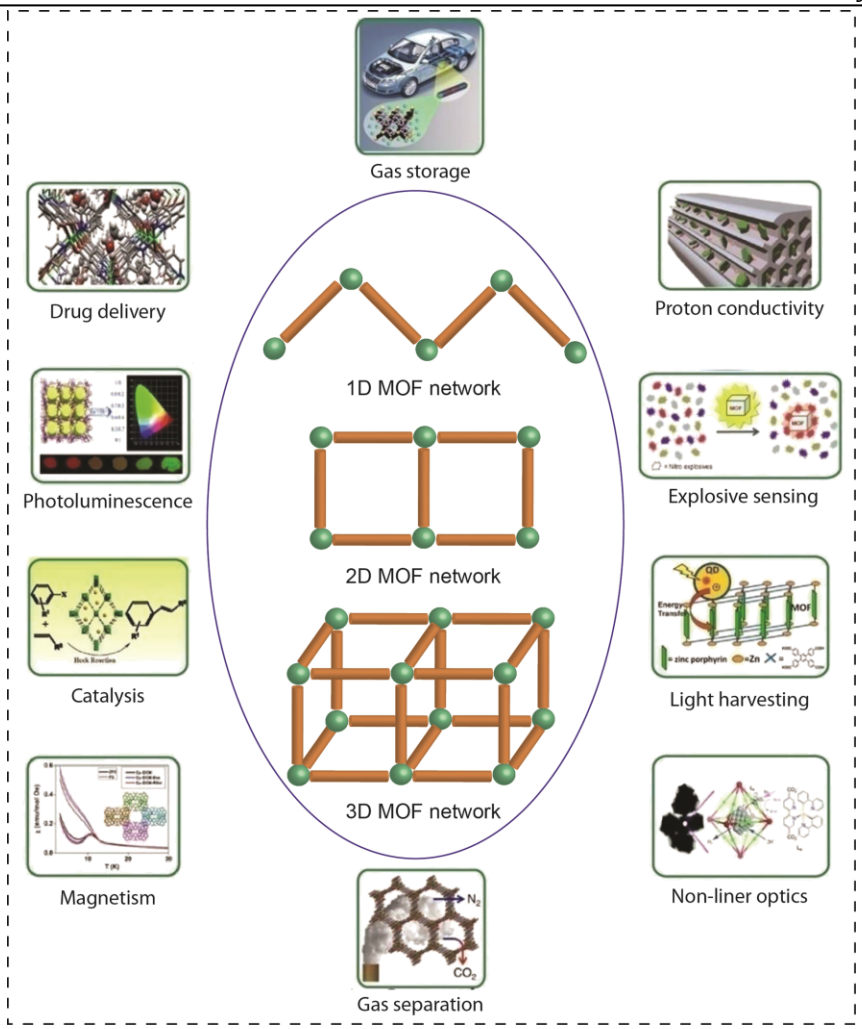

***Figure 1.4**. Various applications of MOFs such as gas storage, separation, catalysis, drug delivery, magnetism, proton conductivity, non-linear optics, light harvesting, photoluminescence, explosive sensing etc. [Ref. 1.10b].*

Considering these highlighting aspects MOFs show superior ability over other porous materials. Although, MOFs have been successfully synthesized using various methods and potentially applied for numerous applications, still there are challenges to developing this class of materials in terms of stability and gas separation ability. In the next section of the introduction is devoted to the chemical stability of MOFs, gas/water vapour storage in MOFs and their polymer composite membranes for gas separation.

1.4.1 *H_2 storage in MOFs*

Storage of H_2 is crucial due to its application in mobile or portable fuel cells. However, the storage of H_2 is considered as a great challenge because of its low volumetric

density (0.0899 kg m^{-3} at STP); hence, storing hydrogen at ambient condition is extremely difficult [1.12]. In the last decade, MOF materials have been used for the effective storage of H_2 owing to their permanent porosity and outstanding structural features [1.13]. H_2 storage in MOFs is shown to be reversible in nature and avoids complicated heat treatments to recover [1.14]. Therefore, MOFs are the dominating class of materials over metal hydrides, clathrates etc. In general MOFs are recovered as single crystals and their high-resolution crystal structures allow the analysis of basic structural features such as pore size and geometry as compared to other porous materials. Moreover, post-synthetic modification is possible in MOFs, which offers the introduction of potential active sites for stronger H_2 binding and thus higher uptake. The hydrogen adsorption in MOFs was firstly reported in 2003 [1.15a]. The MOF-5 with a high BET surface area (3800 m^2g^{-1}) showed a gravimetric H_2 uptake of 7.1 wt% at 40 bar and 77 K. After this report, > 300 MOF structures have been elucidated and tested for H_2 uptake study. So far, the highest H_2 uptake is reported for NOTT-112 as 10 wt% at 77 bar and 77 K [1.15b]. On the other hand, NU-100 [1.15c] and MOF-210 [1.16] exhibited the H_2 uptake of 7.9 to 9.0 wt% at 56 bar respectively and for MOF-210, 15 wt% at 80 bar (***Figure 1.5***). Further, we have also tabulated the potential MOFs with their H_2 storage capacities at low pressure (***Table 1.1***).

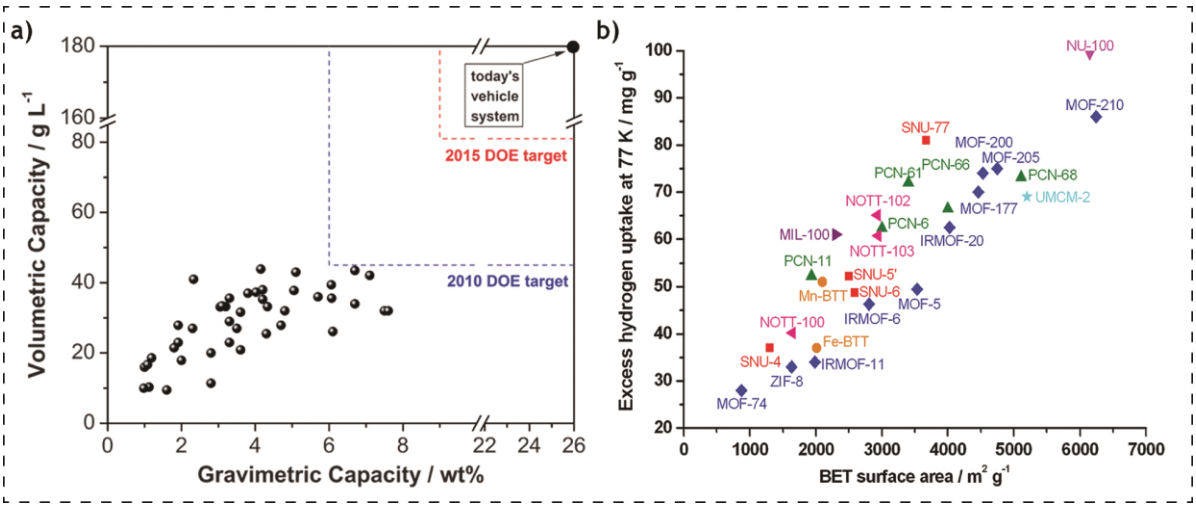

Figure 1.5. *a) Current status of MOFs' towards hydrogen storage capacity at 77 K versus targets; b) high-pressure H_2 uptake capacities at 77 K versus BET surface areas of highly porous MOFs. [Reprinted with permission from Ref. 1.14, Copyright American Chemical Society, 2012].*

Table 1.1. *Low-pressure H_2 adsorption in Metal-Organic Frameworks (MOFs) at 77 K and 1 atm.*

MOFs	**H_2 Uptake (wt.%)**	**MOFs**	**H_2 Uptake (wt.%)**
PCN-12[1.19a]	3.05	MOC-2[1.17h]	2.17
UTSA-20[1.19b]	2.80	UMCM-150[1.17i]	2.10
PCN-14[1.19c]	2.70	Ni\DOBDC[1.17j]	2.10
NOTT-103[1.19d]	2.56	Zn_2(BDC) (TMBDC)(DABCO)[1.17k]	2.10
PCN-11[1.19e]	2.55	$Ni_3(BTC)_2(3\text{-}PIC)_6(PD)_3$[1.18a]	2.10
HKUST-1[1.7]	2.54	$(In_3O)(OH)(ADC)_2(IN)_2$ $4.67H_2O$[1.19k]	2.08
Cu_2(tptc)[1.19f]	2.52	$Zn_2(BDC)_2$ (DABCO)[1.17k]	2.00
NOTT-100[1.19d]	2.52	Mg\DOBDC[1.17j]	1.98
NOTT-140[1.19g]	2.50	PCN-6[1.18b]	1.90
MOF-505[1.19h]	2.48	NOTT-116[1.18c]	1.90
NOTT-101[1.19d]	2.46	CPM-6[1.18d]	1.88
NOTT-105[1.19d]	2.46	PCN-68[1.17c]	1.87
$Cu_4Cl(btt)_{3/8}$[1.19i]	2.42	Cd-ANIC-1[1.8k]	1.84
$Cu_6O(tzi)_3(NO_3)$[1.19j]	2.40	Co\DOBDC[1.17j]	1.81
PCN-12′[1.19a]	2.40	IRMOF-3[1.18e]	1.80
PCN-10[1.19e]	2.34	PCN-66[1.17c]	1.79
$(In_3O)(OH)(ADC)_2(NH_2IN)_2$ $2.67H_2O$[1.19k]	2.31	$Zn_2(C_2O_4)(C_2N_4H_3)_2.(H_2O)_{0.5}$[1.27q]	1.70
NU-100[1.17a]	2.29	Co-ANIC-1[1.8k]	1.64
NOTT-112[1.17b]	2.30	$[Co_4(OH)_2(p\text{-}CDC)_3DMF_2]_n$[1.18f]	1.61
NOTT-109[1.19d]	2.28	ZTF-1[1.18g]	1.60
PCN-61[1.17c]	2.25	CUK-1[1.8l]	1.60
Mn-BTT[1.17d]	2.25	$H_3[(Cu_4Cl)_3\text{-}(BTTri)_8]$[1.27p]	1.58
Cu_2(qptc)[1.17e]	2.24	Zn\DOBDC[1.17j]	1.54
NOTT-106[1.19d]	2.24	Bio-MOF-11[1.18h]	1.50
NOTT-107[1.19d]	2.21	ZIF-11[1.26a]	1.37
$[Zn_2(1)(DMF)_2]_n(DMF)_m$ [MOF(4)][1.17f]	2.20	MOF-5[1.8t]	1.32
NOTT-102[1.19d]	2.19	ZIF-8[1.26a]	1.30
$[Zn_3(OH)(p\text{-}CDC)_{2.5}(DEF)_4]$[1.17g]	2.10	MOF-177[1.8s]	1.25

In general, it has been seen that the functionality of organic building blocks for MOFs has little influence on hydrogen adsorption, whereas the pore volume and the surface area has remarkable effects on enhancing the gravimetric H_2 uptake at 77 K under high-pressure condition [1.12]. However, for volumetric H_2 capture, adsorption enthalpy of hydrogen (Q_{st}) plays a vital role compared to the surface area of MOF materials. In such condition, unsaturated open metal sites are the most effective tool in order to enhance the H_2 uptake capacity of MOF structures. Here, we have noted few important strategies, which can help to design the MOF materials to improve H_2 storage. The key points includes i) high pore size, pore volume and surface area; ii) open metal sites; iii) incorporation of functional groups which will have good affinity to H_2 gas; iv) interpenetration or catenation in the MOF framework; v) doping of metal nanoparticles or alkali metals in the MOF matrix.

1.4.2 *CO_2 storage in MOFs*

The steady growth of global population and the industrialization consequences in a huge increase in energy demand. About 85% of total energy produced results from burning of natural fossil fuels, which eventually releases a vast amount of CO_2 to the atmosphere. Over the last five decades, the concentration of CO_2 in the atmosphere rises to ~80 ppm. This increase is considered to be remarkable and is one of the greatest environmental concerns now-a-days [1.20]. CO_2 is a major component of greenhouse gasses, which is primarily responsible for global warming. On the other hand, to minimize the concentration of CO_2 from the atmosphere, the excess amount of CO_2 is being dissolved inside sea water, which harms the life of aquatic animals. To address this concern, carbon

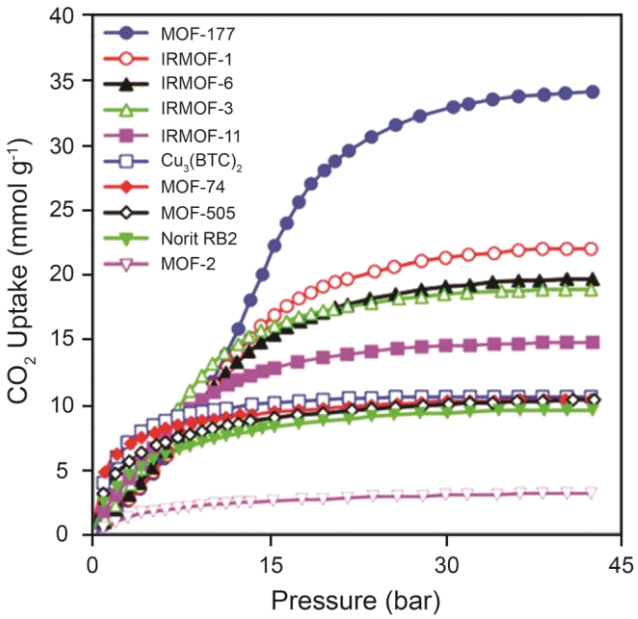

Figure 1.6. *Comparison of gravimetric CO_2 capacities of MOFs with activated carbon at ambient temperature and pressures up to 42 bar. [Reprinted with permission from Ref. 1.24a, Copyright American Chemical Society, 2005].*

capture systems (CCS) must confine the CO_2 from flue gas in an efficient and reversible fashion. Although there are methods which utilize the chemicals such as alkanolamines and aqueous ammonia for CO_2 capture. However, the difficulty arises due to the regeneration of these chemicals for further use [1.21]. In addition to this, few solid porous adsorbent materials like zeolites, activated charcoals, porous alumina, and porous silica have also been employed for the selective capture of CO_2 from flue gases. But their amorphous nature and poor chemical stability under operational conditions restrict their uses [1.22]. From an applications point of view, MOF materials have attracted significant attention towards CO_2 capture due to their extraordinary surface areas, finely tunable pore surface and scalability opportunity [1.23]. It is believed that, highly ordered structures with suitable topologies, tunable pore sizes, and incorporation of appropriate functional groups *via* post-synthetic modification will make MOFs as a potential candidate for highly efficient CO_2 capture system. There are certain features that can affect the CO_2 adsorption capacities in MOFs. For example, it has been seen that high CO_2 uptake is offered by the interpenetrated MOFs than that of their non-interpenetrated analogs [1.24a]. Also, it is known that MOFs with open metal sites significantly enhances the performance for polar/non-polar gas pairs separation (CO_2/CH_4) [1.24b and c]. For example, HKUST-1 [1.24d] and Mg-MOF-74 [1.24e] have high CO_2 uptake due to the presence of open metal sites. In more specific, to establish a clear relation between the surface area and porosity with CO_2 uptake nine well-known MOFs were studied [1.16] (***Figure 1.6***). Among these MOFs, the IRMOF-1 and MOF-177 have high surface area. Hence, MOF-177 has highest CO_2 uptake at high pressure (60 wt % at 35 bar). Similarly, the MOFs with free functional groups (*e.g.*, amine, arylamine, alkylamine, hydroxyl groups, etc.), enhances the capacity and selectivity towards CO_2 on MOFs. These functional groups establish a good interaction with CO_2 molecules compared to the parent non-functionalized material. The other MOFs such as Bio-MOF-11 and ZTF-1 has shown a very high CO_2 uptake due to amine functionalized pores. Sometimes it has been noticed that, despite amine and other nitrogen-based functionalities, organic linkers with polar functional groups (–NO_2, –OH, –CN, –Cl and –Br) also influence the CO_2 capture in MOFs. Thus, from the above discussion it is clear that CO_2 uptake capacities at high pressures depend on surface areas and pore volumes of the MOFs similar like other porous materials. However, it should be noted that, materials which adsorb CO_2 gas at high pressure region have less

importance in coal fire power plants. They also emit N_2 and other gases such as H_2O, O_2, CO, NO_x and SO_x. The gas stream contains all these components released at 1 bar total pressure (approximately). Hence, for CO_2 capture, materials, which can adsorb at low pressure (especially at 1 bar) region and room temperature are most important for industrial carbon capture [1.24g]. Therefore, we have also tabulated the low-pressure (up to 1 atm) CO_2 adsorption capacities for few MOFs at 273 and 298 K (***Table 1.2***).

Furthermore, a systematic study was conducted on the functionality and polarization strength in zeolitic imidazolate frameworks (ZIFs), a well-known sub-class of MOF towards CO_2 uptake. Due to the existence of their large and modifiable pores ZIFs have received substantial interest for storage of CO_2 and H_2 gases [1.25]. ZIF frameworks mainly composed of imidazolate linkers with metal centers (Zn^{2+}, Co^{2+} and Cd^{2+}) capable of generating tetrahedral coordination environment (***Figure 1.7***) [1.26]. Hence, there is a huge opportunity for synthesizing a wide number of isostructural compounds with different functional groups. On this line, a series of ZIFs with mixed imidazolate linkers with GME topology were synthesized by Banerjee *et al.* and examined for CO_2 adsorption capacity [1.26c and d]. From these reports it can be concluded that the polar groups have a great impact on the CO_2 adsorption. Therefore, it is understandable that, by manipulating the surface polarization of MOFs introducing functional groups the CO_2 capture can be enhanced.

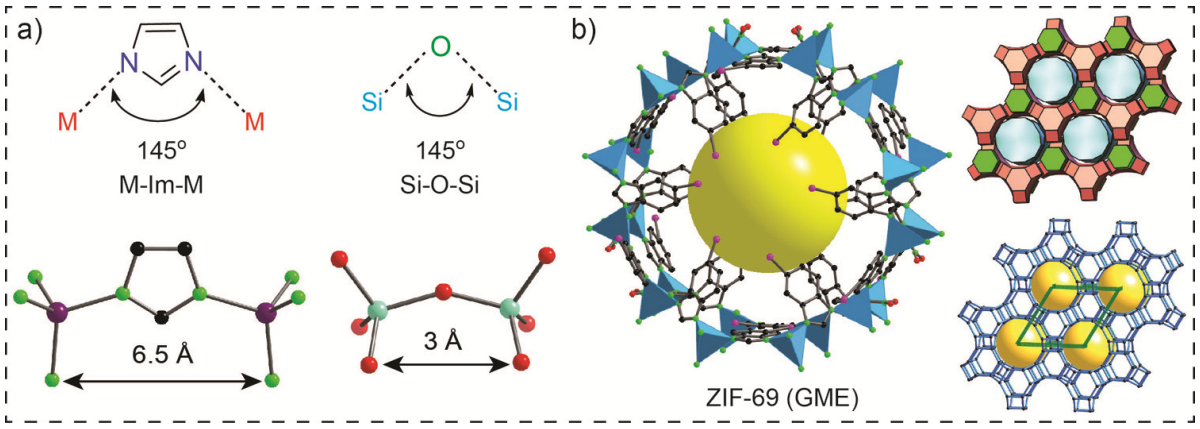

Figure 1.7. *a) Structural similarity between zeolite and ZIF; b) Represents the ball and stick model, net and tile image of ZIF-69 with GME topology (yellow ball indicate the space availability inside the cage). [Redrawn with permission from Ref. 1.26a, Proc. Natl. Acad. Sci. U.S.A., 2006 and from Ref. 1.26d, Copyright American Chemical Society, 2009].*

Table 1.2. *Low-pressure CO_2 adsorption capacities for Metal-Organic Frameworks (MOFs) at 273, 298 K and 1 atm. (NA: Data not available).*

MOF	CO_2 Uptake (mmol/g)		MOF	CO_2 Uptake (mmol/g)	
	273K	298K		273K	298K
Mg\DOBDC[1.27e]	NA	8.08	MOF-505[1.26h]	NA	3.27
Co\DOBDC[1.27e]	NA	7.11	$H_3[(Cu_4Cl)_3$-$(BTTri)_8]$[1.27p]	NA	3.25
Ni\DOBDC[1.27e]	NA	5.80	$(In_3O)(OH)(ADC)_2(NH_2IN)_2$ .2.67 H_2O[1.8o]	NA	3.21
Zn\DOBDC[1.27e]	NA	5.51	CPM-6[1.8p]	4.76	2.90
UTSA-20[1.27e]	NA	5.01	TMA@ Bio-MOF-1[1.8q]	4.5	NA
HKUST-1[1.27i]	NA	4.72	TEA@ Bio-MOF-1[1.8q]	4.2	NA
Zn + 4,4’ bipy + (BTA-TBA) [1.27w]	NA	4.10	TBA@ Bio-MOF-1[1.8q]	3.5	NA
Bio-MOF-11[1.27o]	6.0	4.01	UMCM-150[1.8r]	NA	2.80
$[Zn_2(1)(DMF)_2]_n(DMF)_m$[MOF(4)] [1.27x]	5.80	NA	$Zn_2(BDC)_2$ (DABCO) [1.8s]	NA	2.71
$[Zn_3(OH)(p\text{-}CDC)_{2.5}]_n$[1.27y]	NA	4.00	CPM-5[1.8p]	3.62	2.43
Cd-ANIC-1[1.8k]	4.72	3.84	ZIF-78[1.26d]	3.348	2.23
ZTF-1[1.18g]	5.35	3.79	ZIF-96[1.26i]	NA	2.16
$Zn_2(C_2O_4)(C_2N_4H_3)_2.(H_2O)_{0.5}$[1.27q]	4.30	3.78	IRMOF-3[1.26g]	NA	2.14
Co-ANIC-1[1.8k]	4.22	3.48	$(In_3O)(OH)(ADC)_2(IN)_2$. 4.67 H_2O[1.8o]	NA	2.08
CUK-1[1.8l]	NA	3.48	MOF-177[1.8s]	NA	1.72
YO-MOF[1.8m]	NA	3.39	ZIF-69[1.26d]	3.03	1.69
SNU-M10[1.8n]	NA	3.30	MOF-5[1.8t]	NA	0.92

1.4.3 *Water adsorption in MOFs*

Water adsorption in crystalline, porous materials is very important for various real life applications like dehumidification, thermally operated batteries, and portable delivery of drinking water in many remote areas [1.28]. Also, water vapour is present in various industrial gas streams and should not be neglected when choosing adsorbent materials for purification systems. Similarly in air separation units, air compressor outlet and industrial flue gases contain ~10% to 40% of relative humidity (RH) that adsorbs on the adsorbent materials and interfere with the process [1.29]. In another case the dehydration step in the

biofuel stream, can require significant energy that exceeds the amount of energy released by the combustion process [1.30]. On this line, although MOFs has shown tremendous potentials for adsorption applications but their behaviour in the presence of water/moisture is an importance topic of interest (***Figure 1.8***). The water stability of several MOFs has been well documented and the stability in real operating conditions considered being a major challenge. Important MOFs namely MIL-100, MIL-101, MIL-53, HKUST-1, MOF-74, UiO-66, and ZIF-8 have received significant attention over the past decade in terms of applications [1.31]. If we debate on the water stability of MOFs, mainly three points come into picture i) basicity of the organic ligand, ii) the extent of coordination of the metal and ligand, iii) the shielding of functional groups on coordination sites.

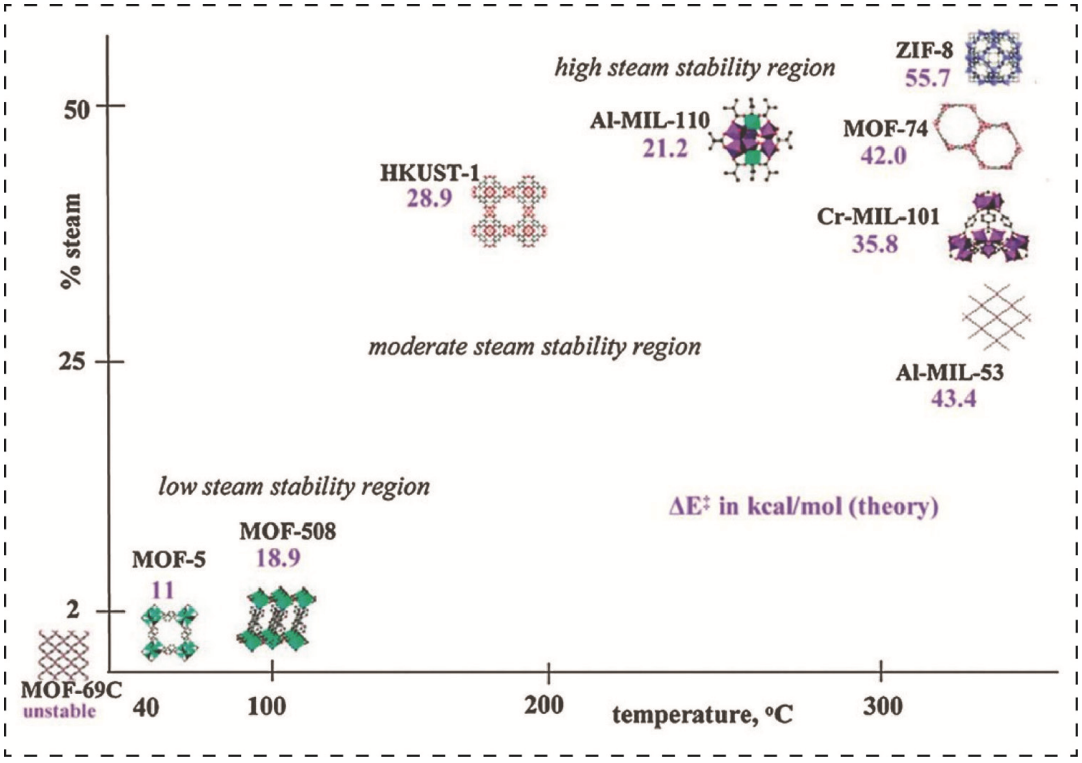

Figure 1.8. *Steam stability map based on reported MOFs. The position of the structure in the map is placed with maximum structural stability as probed by PXRD, while the activation energy for ligand displacement by a water molecule as determined by molecular modelling is represented by the numbers (in kcal/mol). [Reprinted with permission from Ref. 1.32, Copyright American Chemical Society, 2009].*

Table 1.3. *Summary of literature reported porous MOFs and their water adsorption capacities measured at 298 K (unless specified).*

MOFs	Pore dia. (nm)	S_{BET} (m^2g^{-1})	Pore vol. (cm^3g^{-1})	Uptake (cm^3g^{-1})	Ref.
Ni-CPO-27	1.1	1040	0.46	0.5	1.33a
Mg-CPO-27	1.1	1400	0.65	0.68	1.33b
HKUST	0.9/0.6	1270	0.62	0.51	1.33b
Al-fumarate	NA	1300	NA	0.41	1.33c
Fe-MIL-100	2.5/2.9	1549	0.82	0.81	1.33d
Al-MIL-100	2.5/2.9	1814	1.14	0.5	1.31b
Cr-MIL-101	2.9/3.4	3017	1.61	1.28	1.33d
Cr-MIL-101-NH_2	<2.9/3.4	2690	1.6	1.06	1.33e
Cr-MIL-101-NO_2	<2.9/3.4	2146	1.19	1.08	1.33f
UiO-66	0.75/1.2	1032	0.52	0.4[a]	1.33g
UiO-66-fumarate	0.5/0.7	690	0.27	0.28	1.33h
UiO-66-NH_2	<0.75/1.2	1328	0.7	0.38[a]	1.33g
UiO-66-NO_2	<0.75/1.2	792	0.4	0.37	1.33i
UiO-66-1,4-naphtyl	NA	757	0.42	0.26	1.33i
UiO-66-2,5-$(Ome)_2$	NA	868	0.38	0.42	1.33i
UiO-67	1.2/1.6	2064	0.97	0.18[a]	1.33g
MOF-841	0.9	1390	0.53	0.48	1.33a
MIL-125-NH_2	0.6/1.2	1220	0.55	0.37[a]	1.33g
In-MIL-68	0.6/1.2	1100	0.42	0.32	1.33j
In-MIL-68-NH_2	0.6/1.2	850	0.30	0.32	1.33j
DUT-67	0.9/1.7	1560	0.6	0.3	1.33a
CAU-6	0.5/1.0	625	0.25	0.32	1.33k
CAU-10	0.7	635	0.25	0.31	1.33l
CAU-10-NO_2	NA	440	0.18	0.15[b]	1.33l
Al-MIL-53	NA	1040	0.51	0.10	1.33j
Ga-MIL-53	NA	1230	0.47	0.05	1.33j
ZIF-8	1.1	1530	0.48	0.01	1.33d
ZIF-90	1.1	1200	0.48	0.29	1.33m
SIM-1	0.6	470	0.23	0.12	1.33j
Zn(NDI–SEt)	1.6	888	NA	0.25[a]	1.33n
Zn(NDI–SO_2Et)	<1.6	764	NA	0.25[a]	1.33n

[a]Measured at 293 K; [b]Measured at lower relative humidity P/P_0 = 0.5–0.7.

In 2002, the first water adsorption isotherm for HKUST-1 (Cu-BTC) was studied by Bulow and co-workers [1.31f]. As HKUST-1 has a well-known open metal site with a pore diameter of 9 Å, and the smaller pockets of about 6 Å, it shows very good water uptake. In addition to this report, Kaskel and co-workers (2009) reported a more thorough study on water adsorption of HKUST-1, along with few other MOFs [1.31a]. These two reports confirm that HKUST-1 exhibits a type I water adsorption isotherm and the open metal sites are primarily responsible for the water adsorption at low relative pressure (P/P_o), 25 mol/kg (45 wt%). The water uptake behaviour shown by HKUST-1 is analogous to that of microporous zeolites such as Zeolites 5A and 13X which also display a type I water isotherms with similar saturation capacities of 15 mol/kg (29 wt%). However, nitrogen adsorption analysis indicates that after the water adsorption analysis there is loss of 50% of the surface area for HKUST-1 compared to that of unexposed samples. This is due to the degradation of the framework upon exposing to water for longer time. However, Li and Yang *et al*. showed that HKUST-1 is stable at 40% RH for 7 days [1.34]. On this line, another well-known MOF series called MIL [MIL100 (Fe), MIL-100(Cr), and MIL-100(Al)], has also been extensively studied for water adsorption application [1.31a-e]. These MILs possess a BET surface area of approximately 2000 m^2g^{-1} and with a pore volume of 1.0 cm^3. The water adsorption isotherm for MIL-100 (Fe) signifies that well-defined steps at approximately P/P_o = 0.25, 0.40, and 0.45 before fully saturating at 0.8 g/g was observed. The comparison of different MOFs on water uptake has assembled in ***Table 1.3***. Looking at these reports, it can be concluded that, MOFs have great promises to be potential water adsorbing material but the basic criteria such as condensation pressure of water in the pores, water uptake capacity, recyclability and water stability need to be taken into account while designing such materials for water uptake applications.

1.5 MOF-based membranes for gas separation

MOFs are considered to be a most promising porous material for the gas/liquid separation/purification application. However, due to their granular nature fabrication of free standing MOF membranes are still remaining as a challenging task. Moreover, control over the growing position and growing shape of MOF crystals into supports are also difficult and that needs to overcome to realize the full potential of MOFs as membrane materials. There

are a number of challenges and prospects in designing MOFs as membrane materials, which are discussed here in this section. In the conventional dense membranes the gas separations are driven by the solubility difference of gas molecules into the membrane. However, these membranes suffer a critical trade-off between permeability (energy consumption) and selectivity (separation quality) [1.35a]. More simply, thicker membranes are required for good separation of gases, but impose gas permeation resistance simultaneously (***Figure 1.9a***).

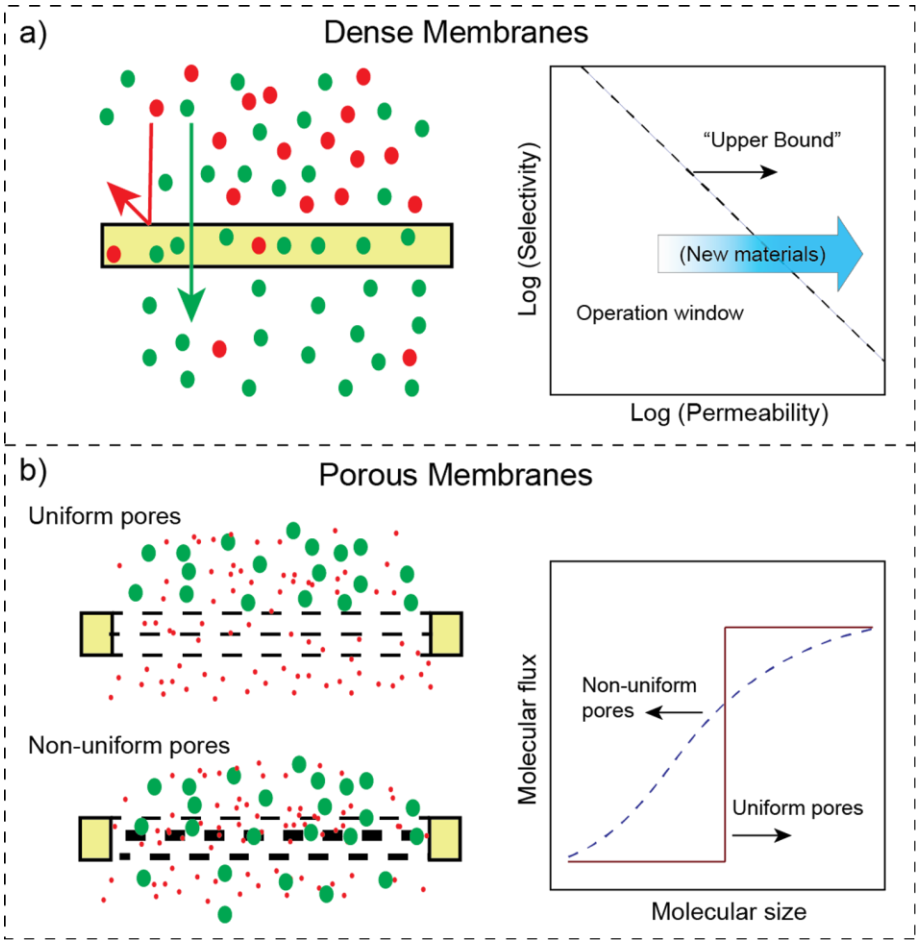

Figure 1.9. *Molecular separation characteristics for a) dense membranes and b) porous membranes with uniform and non-uniform pores. [Redrawn with permission from Ref. 1.35b, Copyright Science, AAAS, 2011].*

Compared to dense membranes, that derived from porous materials shown promises. In such membranes the molecules can pass through the pore aperture exclusively in competition with the other molecules, this process is also referred to as molecular sieving. If

the pores of the porous material are uniform, the selectivity can be very sharp and offers 100% separation for gas mixtures. This is the ideal situation in which the molecule sizes are lower than the pore aperture can pass through the membranes and those are larger completely reject. However, porous membranes with non-uniform pores can still separate gas mixtures; but, non-uniform pores mostly by-pass the larger molecules, which impose a poor separation. In such cases, the difference of diffusion rate among the molecules passing through the membrane act as primary drive for the separation. This mechanism commonly referred to as Knudsen diffusion effect (***Figure 1.9b***) [1.35b]. Before the advancement of MOFs, zeolite has been considered as an excellent material in order to fabricate composite membranes for gas separation [1.36]. However, the pore sizes of zeolites are very limited and cannot be tuned systematically or functionalized either, which completely restricted specific gas molecules. In the case of MOFs, there are no such limit and thanks to MOF for their outstanding features. Moreover, the selection of building units and control of metal-ligand coordination provides almost infinite choices for pore topologies and sizes, which so far considered as the most promising porous materials for gas separation applications [1.8].

1.5.1 *Criteria of MOFs for membrane-based gas separation*

The gas separation through MOF membranes are mainly governed by two factors i) solubility and ii) diffusivity. The solubility of a gas molecule is defined as the thermodynamic affinity between the gas molecule and membrane surface, whereas the diffusivity is mainly governed by the relative size of the gas molecules with respect to the pore size of the membrane matrix. In principle, if a gas strongly adsorbs and faster diffuses through a membrane the higher separation factor (selectivity) could be achieved. The solubility and/or diffusivity can be dramatically varied in the presence of functional groups of the organic linkers in the MOF structure. For gas separation through solubility-based mechanism, the separations of gas molecules happen due to the difference in the solubility. In such case, the framework pores are normally larger than the size of the gas molecules. Consequently, both the thermodynamic and kinetic behaviors of gas molecules can contribute towards membrane separation performance. However, in the case of molecular size-based mechanism, the kinetic diameters of the gas molecules should not be neglected to choose a MOF material suitable for particular gas separation. The flexibility of the MOF structures and the swing effect of the linkers are also important for governing the separation of gas

molecules in the composite membrane. Some of the other important factors that should be considered while choosing MOF as membrane materials for gas separation are given below.

I. Facile and quick synthesis of MOFs.
II. Appropriate pore size and pore diameters.
III. Ease of activation to create guest free MOF framework.
IV. Active metal centers/organic linkers which can interact with the gas molecules.
V. Gate opening or breathing effect in MOFs.

1.6 MOF-based membrane fabrication

So far as the MOF membrane fabrication is concern, still the solvothermal method is the most commonly adopted one. In this typical approach, a solution containing the precursors of MOF *i.e.* metal ions and organic linkers, are heated to allow MOF crystal growth [1.10]. On the other hand methods such as room temperature method, non-solvent precipitation, gel formation-crystallization etc. have also been developed. MOF synthesis is some extend simple but the major problem arises when someone trying to use these materials for gas separation applications in the form of membranes. It is extremely difficult to grow MOF crystals into various shapes of choice other than their natural particulate form. It is also equally difficult to grow directly into certain position or orientation on a support, where it can form as a part of the membrane. These challenges are to some extent addressed by researchers from both membrane and materials background [1.37]. The MOF membrane fabrication technique is mainly directed into two ways i) growth of MOFs on a surface, in-situ or by seeding-secondary growth approach and ii) fabrication of mixed-matrix membranes in which already synthesized MOF particles blended with other structural materials such as polymers. In the next section we will discuss these approaches in detail. However, we are particularly interested in the first approach and contributed to the same in a completely different manner than the existing methods, which is described in chapter 3.

1.6.1 *In-situ and seeding-secondary growth of MOF membranes*

In this general approach, a suitable porous surface generally termed as support is demanded for MOF crystal growth. Many evidences are there in which the support is extensively modified before the MOF growth to make it compatible and don’t allow the

MOF crystals to detach from the support [1.38a]. Mainly negatively charged organic groups in the support material have very good interactions with the metal ions are preferred (***Figure 1.10a***). Then the support is dipped into a mother solution (either metal or ligand) to let the in-situ growth of MOFs occur on the surface, *i.e.* referred as in-situ growth. If the MOF seeds are first formed and then transferred onto the surface followed by a secondary solvothermal growth that is called seeding-secondary growth.

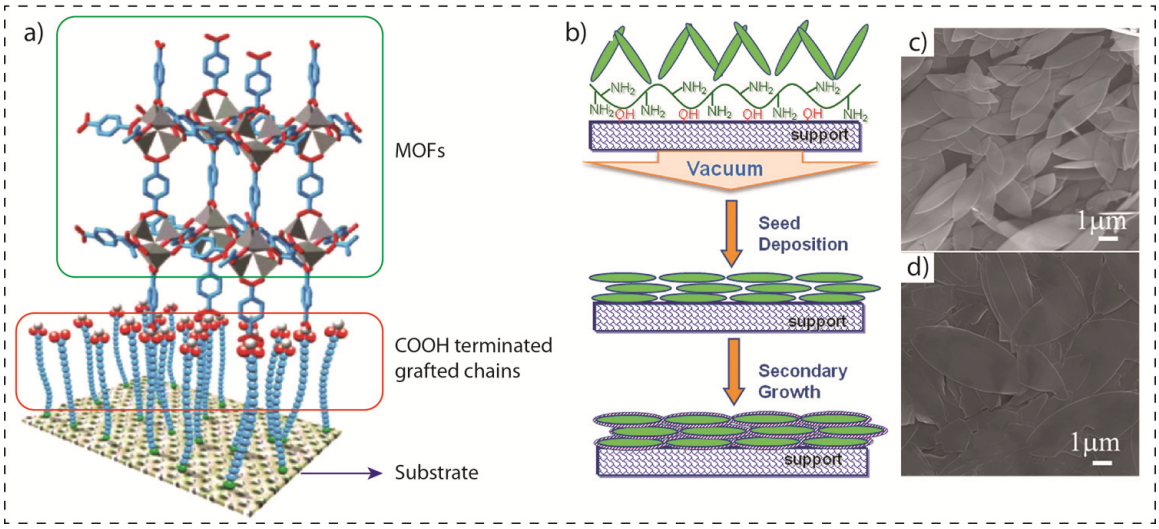

Figure 1.10. *a) The concept of surface modification to increase the compatibility of MOF with the support; b) Schematic representation of filtration-deposition of ZIF-L and followed by secondary growth; c) SEM images of ZIF-L seeding immediately after vacuum filtration and d) ZIF-L membranes after 0.5 h of secondary growth process. [Reprinted with permission from Ref. 1.38a, Copyright American Chemical Society, 2005 and Ref. 1.38h, Copyright Royal Society of Chemistry, 2015].*

In the year 2005, Hermes *et al.* reported the first work on templating growth of MOF-5 on a flat gold surface having –COOH or $–CF_3$ terminated self-assembled monolayer (SAM) [1.38a]. Yoo and Jeong in 2008 reported rapid fabrication of MOF-5 seeded anodic-disk membrane using microwave-induced thermal deposition within 5-30s [1.38b]. The achievement of this work was the membrane formation within short time (seconds), compared to hours normally required during conventional solvothermal methods. They also observed that if the graphite is grafted into the substrate surface, a far better MOF membrane could be obtained. This is believed to be due to the rapid temperature increase of graphite under microwave heating can induce fast crystallization of MOF-5. Similarly, Arnold *et al.*

(2007) presented with an in-situ growth of manganese formate [$Mn(HCO_2)_2$] on a porous alumina and graphite support using a solvothermal approach [1.38c]. It has been stated that a high crystal density on alumina support surface was achieved by anchoring –OH groups (by treating with NaOH). They have also shown for the first time that the MOF crystals can be grown in a controlled manner on the substrate. Gascon *et al.* in 2008 reported a densely coated HKUST-1 film on an alumina support, in which alumina disc surface was pre-seeded prior to secondary MOF growth [1.38d]. Although this approach not results in a fully continuous MOF membrane but the cracks between MOF grains are very less. Soon after this report, Guo *et al.* presented that by in-situ solvothermal growth HKUST-1 can be densely deposited on the pre-oxidized copper net surface [1.38e]. Liu *et al.* (2009) synthesized a uniform and continuous MOF-5 membrane for the first time by dipping a pre-treated alumina disk into a mother solution followed by solvothermal synthesis [1.38f]. This report marked a milestone and treated as the first example of MOF membranes that could demonstrate for real gas separation application. In 2010, Li and Caro *et al.* obtained a continuous ZIF-7 membrane on the top of α-alumina support and ZIF-8 on titanium support by using a microwave-assisted solvothermal synthesis [1.38g]. Further, a new method called van der Drift type growth was followed by researchers to manipulate the MOF membrane morphology by aligned the crystals in a particular direction. Zhong *et al.* synthesized oriented two-dimensional ZIF-L membranes *via* van der Drift method [1.38h] and studied their gas permeation properties (***Figure 1.10b-d***). As mentioned, by varying the ratio between MOF precursors and amine (used as a catalyst), they have managed the MOF growth onto certain crystal faces. In this process, a rod-shaped MOF grains resulted, which aligned vertically to the substrate surface. In 2011, a new step-by-step seeding method was reported by Nan *et al.* to prepare HKUST-1 membrane on porous α-alumina support and evaluated the gas permeation performance (***Figure 1.11a***) [1.38i]. In addition, for the first time, an electrospinning technique was introduced to synthesize ZIF-8/PVP composite membrane by Fan *et al.* in 2012 (***Figure 1.11b***) [1.38j]. They have mentioned that this approach is suitable for various substrates including tubes, with a large-area processing possibility. In 2013, Nagaraju *et al.* reported that ZIF-8 and CuBTC can be effectively grown at room temperature on a polysulphone (PSF) ultrafiltration support and showed the gas separation performance through these membranes [1.38k]. In another report, a rapid thermal

deposition (RTD) method for the growth of MOF film on α-alumina support was demonstrated by Shah *et al.* (***Figure 1.11c***) [1.38l]. The RTD-prepared MOF membranes displayed good improvement in the gas separation performances as compared to those prepared *via* conventional solvothermal methods.

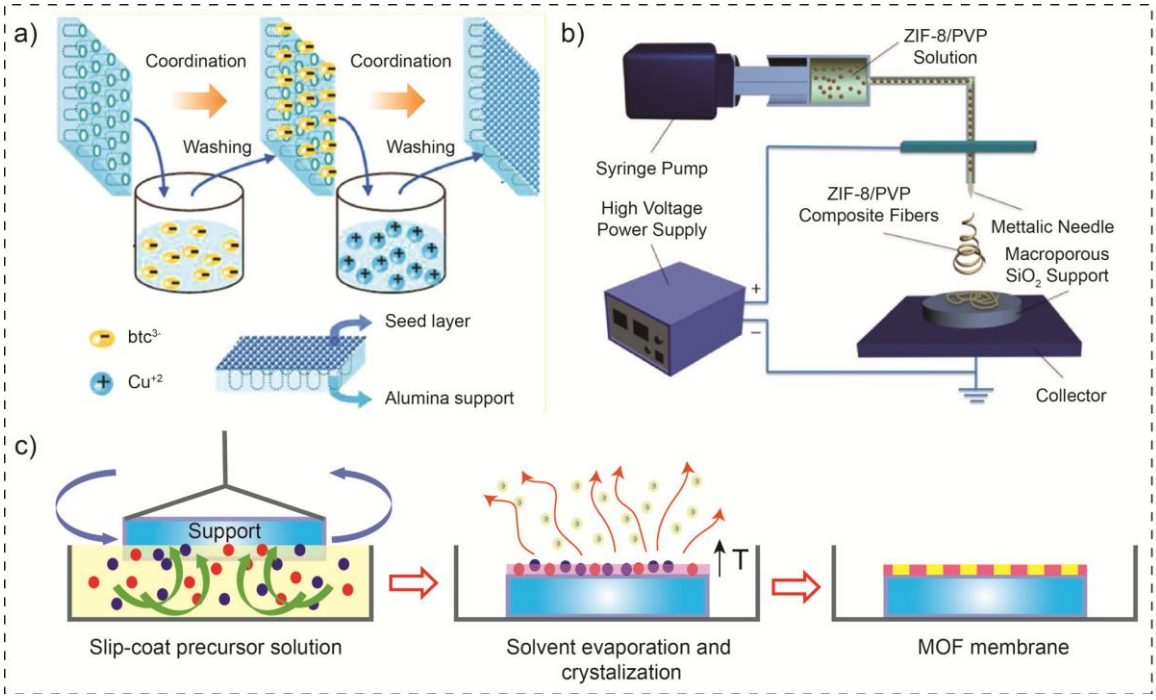

Figure 1.11. *a) Schematic diagram of step-by-step deposition of Cu^{+2} and btc^{-3} on alumina support to form CuBTC membrane; b) Electrospinning process for the support (macroporous SiO_2 wafer) seeding; c) Illustration of rapid thermal deposition (RTD) technique to prepare MOF membranes. [Redrawn with permission from Ref. 1.38i, Copyright American Chemical Society, 2011; Ref. 1.38j, Copyright Royal Society of Chemistry, 2012 and Ref. 1.38l, Copyright American Chemical Society, 2013].*

In addition to these abovementioned methods, a newly introduced advanced liquid-phase epitaxy (LPE) method was reported by Shekhah *et al.* in 2013 [1.38m]. This method was efficiently implemented to construct ultrathin (0.5-1 μm) continuous, defect-free ZIF-8 membranes on gold and α-alumina supports. Further, the permeation properties of different gas pairs were evaluated using the time lag technique.

Moreover, during in-situ approach a major problem encountered is the growth of MOF crystals inside the mother solution as compared to the substrate surface (<5%). This signifies that a large amount of materials wasted during the process. Also the disturbance created by solution nucleation and MOF growth process also results in a low density and

poor attachment of MOF crystals on the support to form a defect-free membrane. Although this in-situ and seeding-secondary growth protocol for MOF membranes has some extend success at the later stage but there are still lots of challenges exist and need urgent attention to realize this class of materials for real application.

1.6.2 *Mixed-matrix membranes based on MOFs*

Mixed-matrix membranes (MMMs) belong to a category of composite membranes in which potential fillers can be dispersed in a matrix material (commonly polymers) [1.39a]. A long ago, zeolites fillers into polymers matrix introduced to fabricate MMMs and has been widely studied for gas separation application [1.36]. These initial works on MMMs provided a foundation for explorations of MOF-based MMMs for gas separation. Till date, there has been several interesting developments on this topic. In 2010, Hu *et al.* reported the synthesis of HKUST-1/polyimide hollow fiber MMMs *via* a dry/wet spinning approach [1.39b]. An interesting opposite change in selectivity of H_2 and CO_2 was observed with the increase of MOF loading. In 2010 and 2011, Basu *et al.* prepared MMMs composed of Matrimid® and HKUST-1, ZIF-8 and MIL-53 [1.39c and d]. It has been noticed that by increasing the MOF loading the mechanical properties of the MMMs decreases to a great extent. The key issue to fabricate high performing MMMs is the compatibility between MOFs and matrix materials. Polymers such as polysulfone (PSF), polyimide, polyphenylene oxide (PPO) and Matrimid® have been widely used as matrix material because of their very good interaction with MOF crystals. To support this fact Bhasker *et al.* reported MMMs based on ZIF-8 and polybenzimidazoles and found to have very promising gas separation performance with only 30% of filler loading [1.39e]. In addition, it has been observed that there is a strong interaction exists between the PBIs and a ZIF-8 crystal as both contains imidazolate moieties. Based on the above literature reports, typically the maximum MOF loading reported was in the range of 15 to 40 wt%, beyond which the membrane becomes fragile. Also, compared to the MOF membranes formed on potential supports described in the above section, it is also unlikely that the MOF layer can be found inside the MMMs. Hence, in the MMMs, there is a chance of by-pass of gases by the free volume inside the matrix material and the gaps between MOF and matrix material, which hampers the selectivity. Therefore, this approach is commonly employed to improve the gas permeability and/or selectivity of existing polymer membranes (***Figure 1.12***). As a result, the separation can only be based on Knudson

diffusion effect, to separate gasses based on their rate differences in passing through channels across the MMM. Notably, the higher selectivity can generally be obtained in the supported MOF membranes due to the size-exclusive effect where the pore sizes of MOFs can be employed to select a certain gas passing through the membrane. Although, the category of MOF based MMMs is well mature and fabrication is simpler, their potential is limited compared to the continuous MOF layer based membranes.

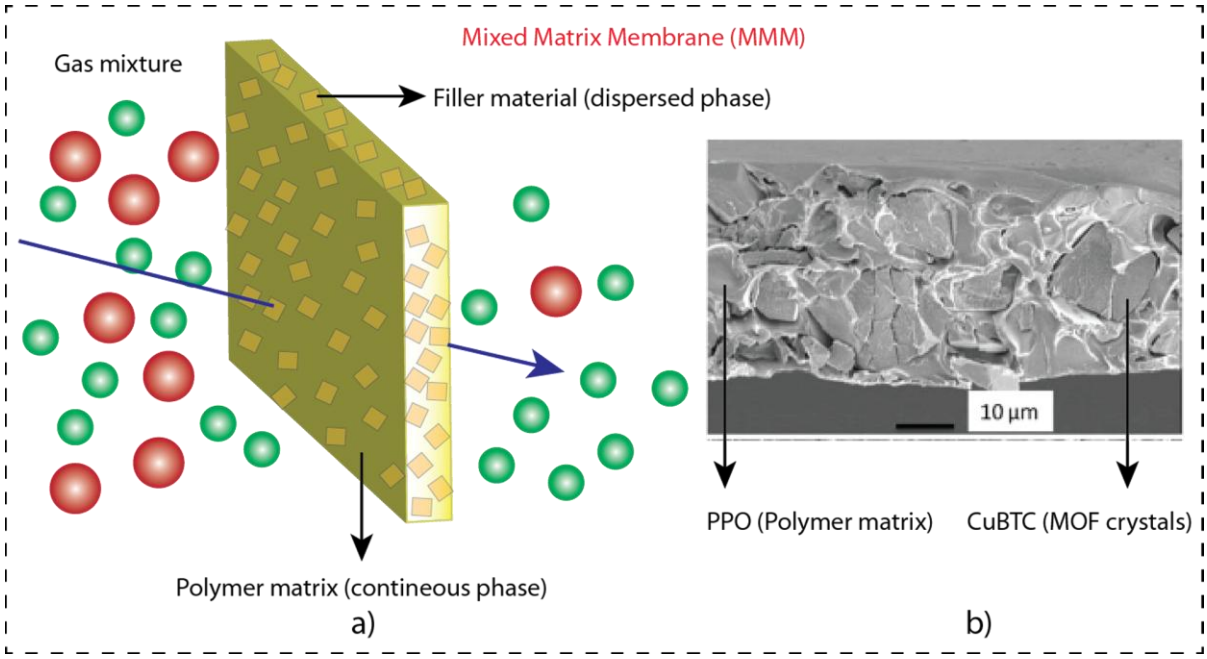

Figure 1.12. *a) Schematic of a mixed matrix membrane and gas separation through them; b) SEM image of Cu-BTC/PPO MMMs. [Reprinted with permission from Ref. 1.39f, Copyright Royal Society of Chemistry, 2013].*

1.6.3 *Other methods developed for the MOF membrane fabrication*

Apart from the methods mentioned above a significant progress has been made on fabricating MOF membranes *via* employing new and interesting approaches. As an example, in 2011, Yao *et al.* reported a contra-diffusion approach for the fabrication of ZIF-8-nylon composite membranes (***Figure 1.13a,b***) [1.40a]. In this method, the MOF precursors are separated by two independent solutions placed on different sides of a nylon membrane. The crystal growth was allowed to occur while the metal and ligands met inside the membrane. Another interesting work reported by Carbonell *et al.* based on the fabrication of single-crystal arrays of HKUST-1 (***Figure 1.13c)*** [1.40b]. The HKUST-1 precursors were injected

precisely on a substrate surface with the help of a pen-type lithography technique. Crystallization started when the solvents evaporated and result a precisely aligned MOF arrays. This simple and effective approach has provided a new prospect on how to control the growth position of MOFs to form a membrane which will have potentials to do the separation.

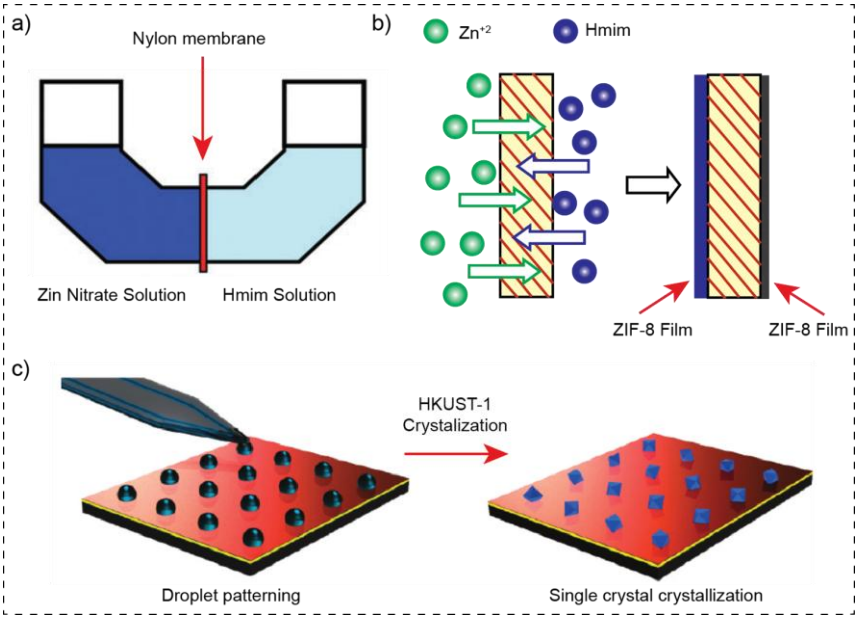

Figure 1.13. *a) Diffusion cell for the preparation of ZIF-8 film and b) Schematic illustration of ZIF-8 film formation on both sides of the nylon support using contra diffusion of Zn^{+2} and Hmim through the pores of the Nylon membrane; c) Schematic Illustration of the fabrication of single crystal MOF (HKUST-1) arrays by employing direct-write FEMTO. [Redrawn with permission from Ref. 1.40a, Copyright Royal Society of Chemistry, 2011 and Ref. 1.40b, Copyright American Chemical Society, 2011].*

1.6.4 *Interfacial synthesis of MOF membranes*

Although MOF films have been synthesized using a variety of methods some of them are described above. However, still there are challenges to grow MOFs in a particular position to form a defect-free membrane. In this regard, interfacial crystallization method looks promising and very limited work has been done on MOFs synthesis *via* this approach. Interfacial MOF synthesis is a method in which difference in solubility of the organic and inorganic precursors can give rise to the preparation of uniform thin MOF layers using a mechanism of self-completing growth (***Figure 1.14a,b***). By employing a biphasic reaction mixture comprising of two immiscible solvents, each contains one of the two MOF

precursors such as metals and ligands. In this process the MOF crystallization only takes place at the liquid–liquid interface. The first attempt on interfacial coordination method for MOF synthesis (HKUST-1 hollow capsules) was made by Ameloot *et al* [1.41a]. In another report Lu *et al.* demonstrated that liquid–liquid interfacial coordination mechanism can be useful for the synthesis of freestanding MOF membranes (***Figure 1.14c-e***) [1.41b]. However, nobody has able use the membranes synthesized *via* such approach for any molecular separation. This is due to the lack of mechanical stability of these membranes formed *via* interfacial approach. In chapter 3, we will discuss how we can grow MOFs preferably on either side of a flexible polymer support using interfacial crystallization approach and to use them for real gas separation applications.

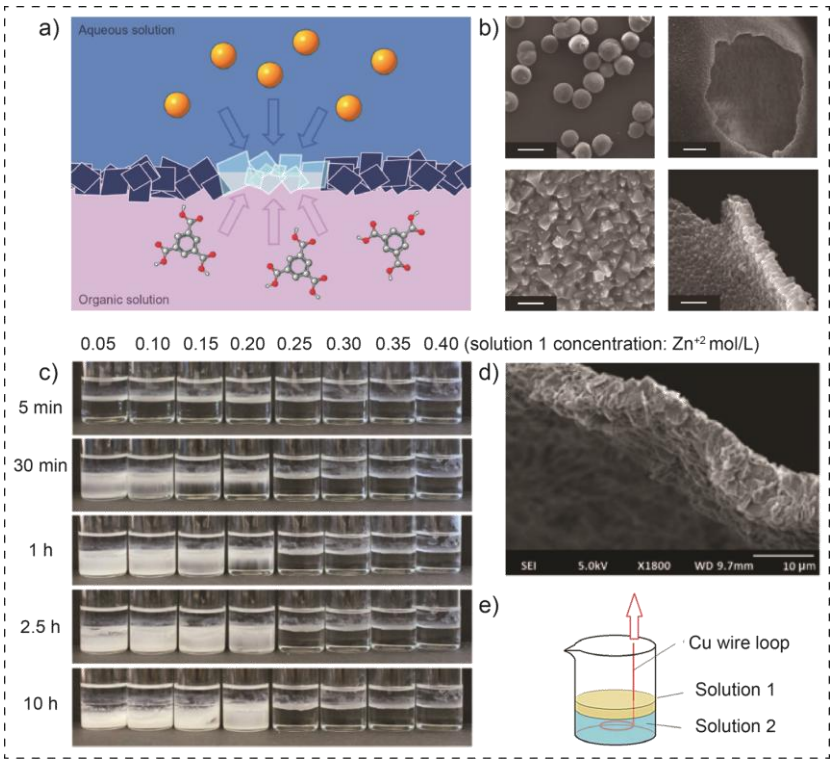

Figure 1.14. *a) Preparation of MOF layer using a biphasic mixture of an aqueous metal-ion-containing solution (blue) and an organic ligand solution (purple) via interfacial crystallization; b) Scanning electron micrographs (SEM) of hollow [Cu(BTC)] capsules; c) Reaction set-up demonstrating how zinc precursor concentration influence the product formation at the interface. Left to right, (solution 1) increases from 0.05 to 0.4 mol/L arithmetically with an increment of 0.05 mol/L, while (solution 2) = 12.5 wt. % TEA; d) SEM cross-section of a free-standing MOF membrane formed via interfacial method and e) Schematic for the collection of membrane samples. [Reprinted with permission from Ref. 1.41a, Copyright Nature Publishing Group, Macmillan Publishers Limited, 2011 and Ref. 1.41b, Copyright Wiley, 2013].*

1.7 Gas separation performance of MOF membranes

Although, fabrication of MOF membrane is very challenging, in terms of gas separation application these materials showed high promises. In this section, we will discuss the gas separation performances of selected MOF based membranes. Firstly, the gas permeation results from the MOF materials have been studied by Ranjan and Tsapatsis [1.42a], this membrane displayed an ideal selectivity of 23 for H_2 over N_2. At the same time low fluxes were also observed due to the randomly oriented seed layers. Membranes composed of ZIF-7, ZIF-8, and ZIF-22 exhibit interesting molecular sieving of small gases such as He, H_2 and N_2 preferentially over larger gas molecules like propane and propylene. ZIF-8 a well known MOF having pore aperture of 3.4 Å and considered as the most studied membrane material in the literature [1.42b-d]. A tubular membrane made up off by ZIF-8 of thickness of 5-9 μm reported by Venna and Carreon [1.42e]. This was realized with a CO_2 permeance of ~2.4×10^{-5} mol/m^2 s Pa with the selectivity ranging from 4 to 7. As stated above, the sharp permeance of gas molecules has not been observed for ZIF based membranes, which is mainly because of the flexible nature of the framework. MOF membranes can be post-synthetically modified by side group functionalization even after the membrane fabrication. This has been proved for many well known MOF membranes such as IRMOF-3,[142f] ZIF-90, [1.43g] and SIM-1 [1.43q]. As an example, functionalization of amine group in SIM-1 results SIM-2, which display enhanced CO_2/N_2 separation and also catalytic activity [1.43q]. Post-synthetic modification of ZIF-90 has also been done to reduce the pore size, which leads to significant enhancement in molecular sieving properties [1.43g]. Moreover, post-synthetic modifications on IRMOF-3 have been demonstrated, which enables the tuning of membrane performance for CO_2/C_3H_8 separation [1.42f]. The results reviewed above signify that MOF has great promises for effective gas separation application. A summary of reported MOF membranes for H_2 separation is given in ***Table 1.4***. Despite the incline progress made over the past few years, MOF membranes for gas separation are still relatively new area and numerous opportunities are there for further improvement.

Table 1.4. *Summary of reported MOF membranes for H_2 separation.*

MOFs	Pore size (Å)	Substrate	Temp. (°C)	Separation factor (α)	H_2 permeance (mol m^{-2} s^{-1} Pa^{-1})	Ref.
$Cu_2(bza)_4(pyz)$	2	α-Al_2O_3 sheet	RT	H_2/N_2 (10[a]) H_2/CH_4 (19[a])	6.88×10^{-9}	1.43a
ZIF-7	3	α-Al_2O_3 disks	220	H_2/CO_2 (13.6) H_2/N_2 (18) H_2/CH_4 (14)	4.55×10^{-8}	1.43b
ZIF-7	3	α-Al_2O_3 disks	200	H_2/CO_2 (8.4)	9.00×10^{-9}	1.38g
ZIF-22	3	TiO_2 disks	50	H_2/CO_2 (7.2) H_2/N_2 (6.4) H_2/O_2 (6.4) H_2/CH_4 (5.2)	1.60×10^{-7}	1.42d
ZIF-8	3.4	TiO_2 disks	RT	H_2/CH_4 (11.2)	6.70×10^{-8}	1.42a
ZIF-8	3.4	Nylon support	RT	H_2/N_2 (4.3)	1.97×10^{-6}	1.40a
ZIF-8	3.4	α-Al_2O_3 tube	RT	H_2/N_2 (10.3) H_2/CH_4 (10.4) H_2/CH_4 (13)	2.00×10^{-7}	1.43c
ZIF-8	3.4	α-Al_2O_3 disks	RT	H_2/N_2 (11.6) H_2/CH_4 (13)	1.70×10^{-7}	1.43d
$Zn_2(cam)_2dabco$	3 × 3.5	Porous ZnO	RT	H_2/N_2 (19.1) H_2/CH_4 (14.7)	2.70×10^{-8}	1.43e
ZIF-90	3.5	α-Al_2O_3 disks	25–225	H_2/CO_2 (11.7) H_2/N_2 (7.3) H_2/CH_4 (15.3) H_2/C_2H_4 (62.8)	2.50×10^{-7}	1.43f
ZIF-90 (post)	3.5	α-Al_2O_3 disks	25–225	H_2/CO_2 (15.3) H_2/N_2 (15.8) H_2/CH_4 (18.9)	$1.9–2.1 \times 10^{-7}$	1.43g
Cuhfipbb	3.5	α-Al_2O_3 disk	25–200	H_2/N_2 (22[a]) H_2/CO_2 (4[a]) CO_2/N_2 (5[a])	1.50×10^{-8}	1.42a
ZIF-95	3.7	α-Al_2O_3 disks	RT	H_2/CO_2 (25.7)	1.95×10^{-6}	1.43h
ZIF-78	3.8	Porous ZnO	RT	H_2/CO_2 (9.5) H_2/N_2 (5.7)	1.00×10^{-7}	1.43i

				H_2/CH_4 (6.4)		
CAU-1	3.8	α-Al_2O_3 tube	RT	H_2/CO_2 (12.3) H_2/N_2 (10.33) H_2/CH_4 (10.4)	1.00×10^{-7}	1.43j
$Zn_2(bdc)_2dabco$	7.5	α-Al_2O_3 disk	RT	H_2/CO_2 (12.1)	2.70 × 10-^{6}	1.43k
NH_2-MIL-53(Al)	7.5	Porous SiO_2	15–80	H_2/CO_2 (30.9) H_2/N_2 (23.9) H_2/CH_4 (20.7)	2.00×10^{-6}	1.43l
MIL-53(Al)	7.3 × 7.7	α-Al_2O_3 disks	RT	H_2/CO_2 (4[a]) H_2/N_2 (2.5[a]) H_2/CH_4 (2.2[a])	5.00×10^{-7}	1.43m
MOF-5	7.8	α-Al_2O_3 discs	RT	H_2, CH_4, N_2, CO_2, SF_6 (Knudsen diffusion)	3.00×10^{-6}	1.38f
MOF-5	7.8	α-Al_2O_3 discs	RT	H_2/CO_2 (2.5) H_2/N_2 (2.7) H_2/CH_4 (2) H_2/CO_2 (4.1[a])	8.00×10^{-7}	1.43n
HKUST-1	9	Copper net	RT	H_2/N_2 (7) H_2/CO_2 (6.8) H_2/CH_4 (5.9)	1.50×10^{-6}	1.38e
HKUST-1	9	PSF	RT/60	H_2/CO_2 (7.2) H_2/C_3H_6 (5.7)	7.90×10^{-8}	1.38k
HKUST-1	9	Porous SiO_2 metal nets	25–60	H_2/CO_2 (9.24) H_2/N_2 (8.91) H_2/CH_4 (11.2)	1.00×10^{-6}	1.38i
HKUST-1	9	α-Al_2O_3 disks	RT	H_2/CO_2 (4.6) H_2/N_2 (3.7) H_2/CH_4 (3)	$4.00–6.00 \times 10^{-7}$	1.43o
HKUST-1	9	α-Al_2O_3 tube	RT	H_2/CO_2 (13.6) H_2/N_2 (8.66) H_2/CH_4 (6.19)	4.00×10^{-8}	1.43p

a = Ideal separation factor.

1.8 Covalent organic frameworks (COFs)

Covalent organic frameworks (COFs) are belong to a family of crystalline porous materials made exclusively from organic building blocks containing light elements (C, Si, H, N, B and O) linked together *via* strong covalent bonds to construct 2 and 3-dimensional frameworks [1.44]. Each connector/linker combination with appropriate symmetry forms a framework with specific geometry embedded with reactive functional groups (***Figure 1.15***). As compared to inorganic framework materials such as MOFs they are light weight (low density) and more robust.

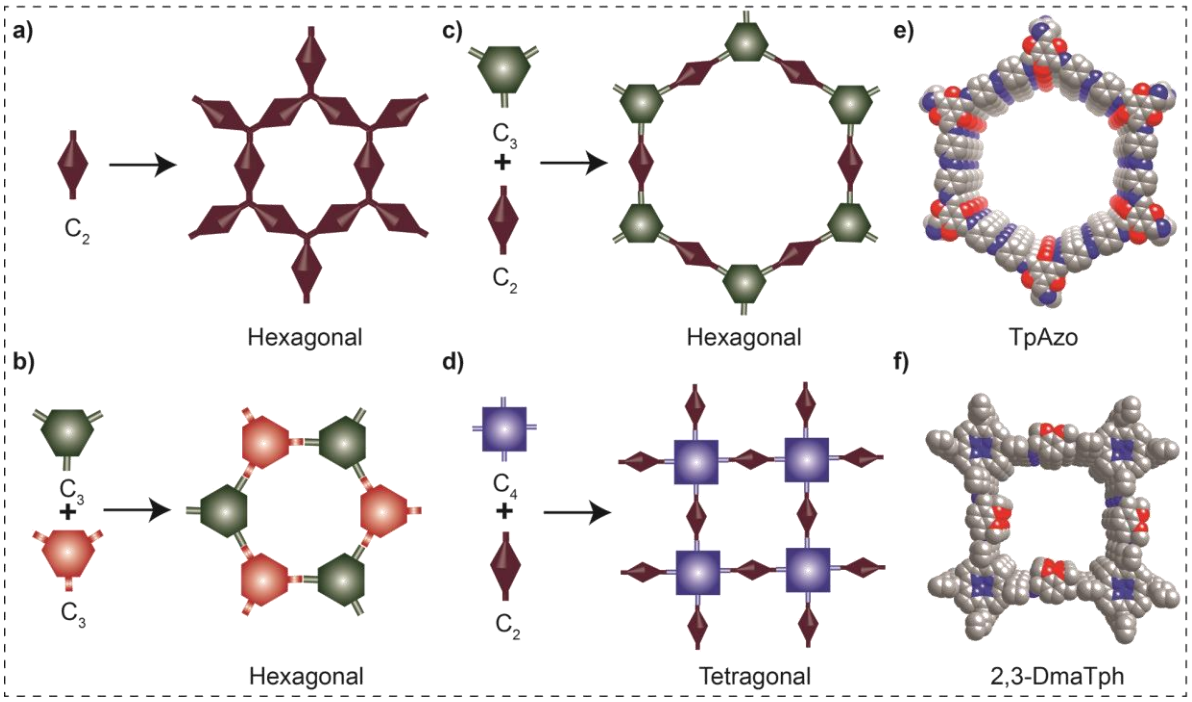

Figure 1.15. *Schematic representation of different symmetry combination to give two-dimensional hexagonal and tetragonal COFs; a) C_2 linker; b) C_3 and C_3; c) C_3 and C_2 combinations gives rise to hexagonal COFs; d) C_4 and C_2 combination gives rise to tetragonal COFs; e) and f) represents the space fill model of 2D chemically stable COF TpAzo (hexagonal) and 2,3-DmaTph (tetragonal) respectively.*

Most of the COFs recovers as microcrystalline powders with rigid internal structures. They also possess long-range order in the atomic domain and high thermal stability (up to 600 °C) coupled with permanent porosity (surface areas, up to 6450 m^2g^{-1}). COFs have been synthesized most commonly using reversible condensation reactions such as trimerization of boronic acid, boronic ester formation, Schiff base formation, trimerization of nitriles etc.

(***Figure 1.16a***) [1.44a]. The void exists within the COF framework provides microporous or macroporous adsorption sites depending on the linker lengths for gas uptake and other applications. This class of materials also follows the same rule of reticular synthesis like MOFs. More importantly, their organic nature offers amazing synthetic flexibility using a library of building units (***Figure 1.16b***) [1.45].

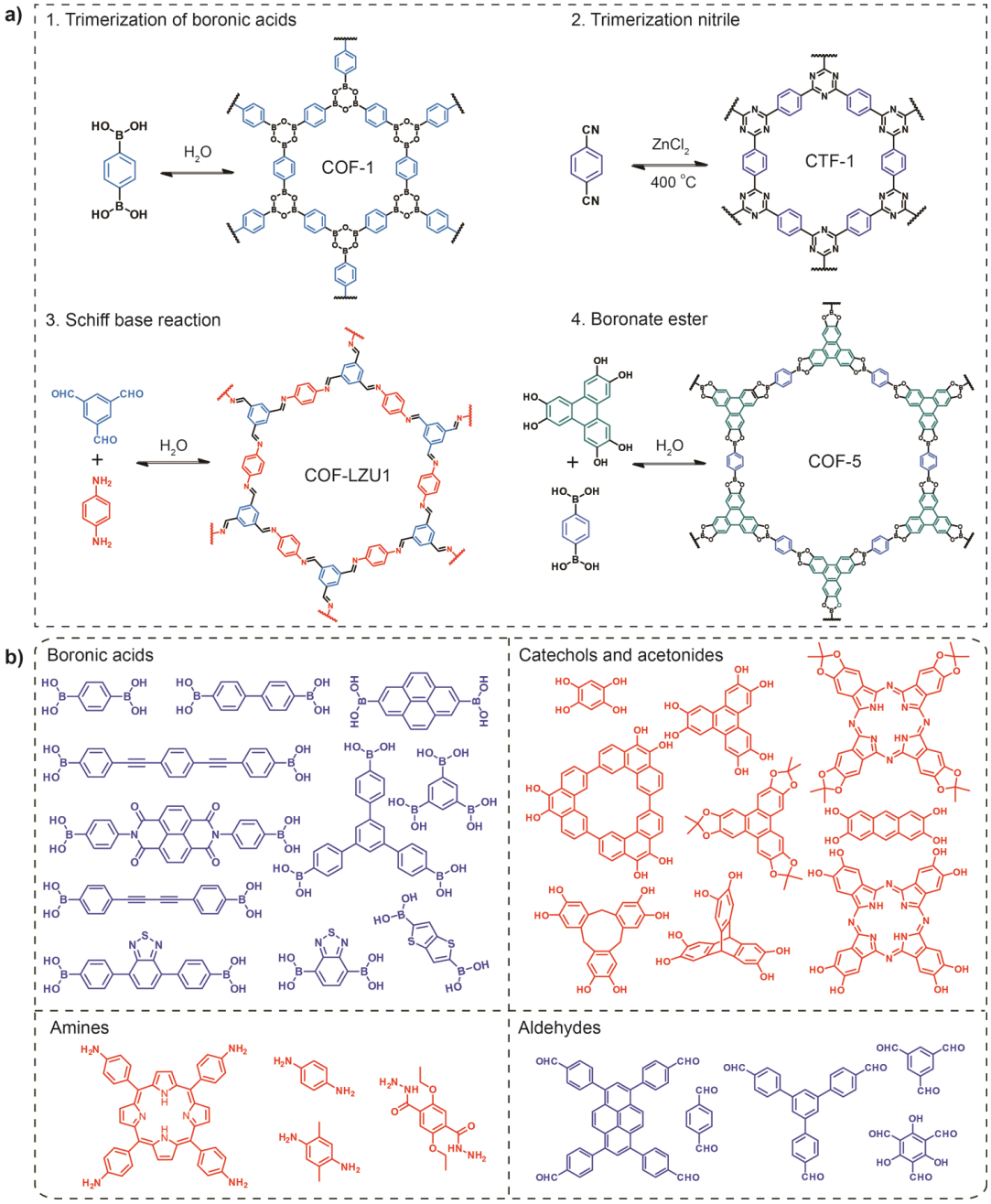

Figure 1.16. *Summary of a) different reversible reactions; b) a library of reported organic linkers used so far for the synthesis of 2D-COFs. [Ref. 1.45].*

The selection of appropriate solvents for the construction of well-ordered and uniform COF structure is highly important as the condensation reaction that forms the COF framework is reversible in nature. Furthermore, the reaction that occurs inside sealed Pyrex tubes, which slows down the reverse reaction and minimizes defects by the self-healing process [1.6]. Due to their fully organic nature, controlled composition and high porosity this class of materials has gained numerous attentions in recent years. These materials have been employed for various applications including gas storage, catalysis, sensing etc. [1.46]. However, they are not so far used for any molecular separation application. This could be due to their poor chemical stability under standard operating conditions. This class of materials also suffers chemical stability issues like MOFs, which limits their potential as useful materials. Hence, construction of chemically stable COF materials and their uses in molecular separation is now an open challenge.

1.9 Synthesis of covalent organic frameworks (COFs)

In order to form a highly ordered covalent network, the regulation of thermodynamic equilibrium between the reactants and the product is the key. For the successful construction of thermodynamically stable, highly crystalline, porous COF, the reaction media, solvents choice and experimental conditions like temperature and pressure should be taken into account. In this section we will briefly discuss the methods that are developed for the COF synthesis in past few years (***Figure 1.17***).

1.9.1 *Solvothermal (seal tube method) for COF synthesis*

Solvothermal method is the widely used method so far for the COF synthesis. In this method, the monomers and the solvents (often used mixture of solvents) are poured in a Pyrex tube and subsequently degassed through three freeze–pump–thaw cycles. The reaction tube is finally sealed and kept inside a programmed temperature oven (set at 90 to 180 ºC) for 3-5 days depending on the chemical reactivity of the building blocks. The precipitate settled at the bottom of the tube is collected, washed with solvents few times, and then dried under dynamic vacuum to recover COFs as microcrystalline solid powder. The solubility, solvent combinations, COF nucleation, crystal growth rate, and self-healing structure are the primary criteria to consider while designing a COF reaction. Essentially, an air-tight closed reaction

environment is highly required to allow the water molecules that could trigger the reversibility of system [1.6 and 1.47].

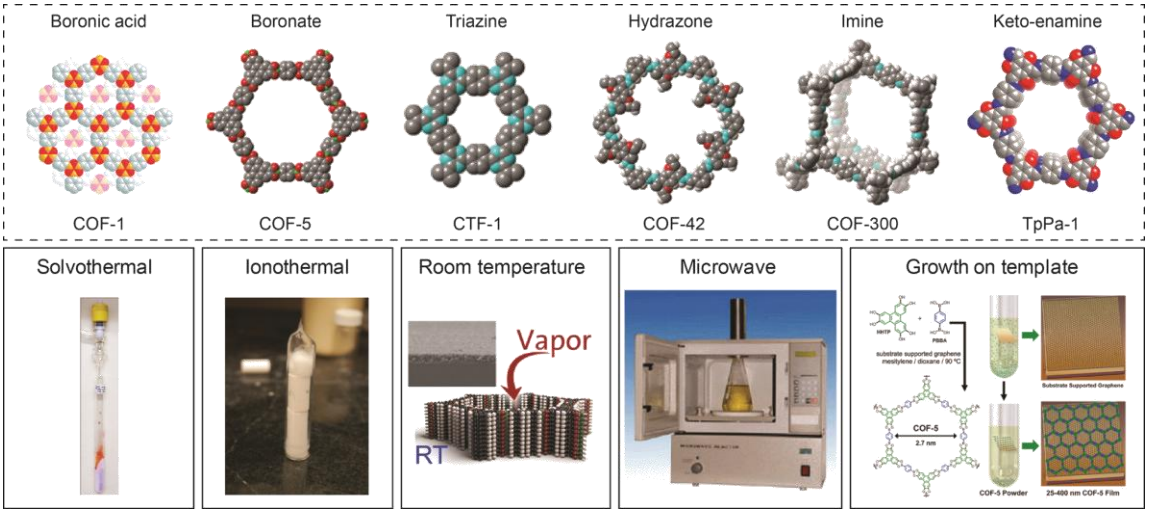

Figure 1.17. *Space-filling models of literature reported COFs (top) and synthetic approaches used so far for the preparation of COFs (bottom). [Ref. 1.48].*

1.9.2 *Ionothermal method for COF synthesis*

Similar to solvothermal approach first time Thomas and co-workers introduced a new method for COF synthesis called ionothermal synthesis method [1.44b]. In this approach firstly, they have done a cyclotrimerization of aromatic nitrile building units in molten $ZnCl_2$ at 400 ºC. This process results in a crystalline conjugated covalent triazine framework (CTF) with outstanding chemical and thermal stabilities. During this process $ZnCl_2$ acts as a solvent and as well as the catalyst for the trimerization reaction. However, this method has not been well explored further as it demands very harsh reaction conditions, which further limit the building block availability. Notably, the CTFs are less crystalline in nature due to lack of long-range molecular order.

1.9.3 *Microwave synthesis of COFs*

As like MOFs, Cooper and co-workers have developed a high-throughput protocol to synthesize COF materials employing a microwave reactor [1.49a]. Microwave synthesis method provides many advantages over solvothermal or any other methods. Using a microwave the product can be formed rapidly, hence large scale production is not an issue.

Also in this technique sealed tube is not required and *via* microwave solvent extraction process the residual impurities can be removed effectively to end off with highly porous materials [1.49b]. Therefore, it is believed that the microwave technique is a powerful one which can replace the existing conventional synthesis methods for COF synthesis.

1.9.4 *Room temperature method for COF synthesis*

Very recently, researchers have attempted to synthesize COFs (COF-5) by vapor-assisted conversion at room temperature. One imine-based COF has been facilely synthesized at ambient condition [1.49c]. This method has advantages over the sealed tube and other methods as it doesn't demand extra energy source. Hence, by using this approach bulk production of the COF materials is possible. However, the generalization of this approach has not been done so far, which means all type of COF frameworks should be synthesized using this room temperature approach.

1.9.5 COF *growth on a surface*

In contrast to the bulk synthesis of COF powders, researchers have attempted the condensation of the building blocks onto a potential metal surface to construct COF thin films of atomic thickness. Dichtel and co-workers have synthesized SCOF-1 and SCOF-2 with hexagonal pores onto a clean Ag(111) by sublimating the building units from heated molybdenum crucible evaporators surface under high vacuum [1.49d]. At the same time they observed the nano-texture *via* scanning tunneling microscopy (STM). It is important to note that, the preparation of defect-free monolayers on any metal surface is challenging and may required proper reaction conditions, building block purity, and an aligned single-crystal metal substrate interface. In another case, COF has been grown on a highly ordered pyrolytic graphite (HOPG) surface. In this approach, THF solutions of biphenyldiboronic acid (BPDA), 1,4-benzene diboronic acid (BDBA), and 9,9-dihexylfluorene-2,7-diboronic acid were drop casted directly onto a HOPG surface and heated in a sealed autoclave at 150 ºC for 1 h to synthesize monolayer COF. The important role of $CuSO_4.5H_2O$ as a water reservoir to regulate the reaction equilibrium for successful COF crystallization in this case should not be neglected. Using similar approach, various COF thin films, like COF-5, TP-COF, HHTP-DPB-COF, NiPc-COF, and ZnPc-PPE-COF have successfully formed on graphene and the thicknesses of layers can also be tuned by controlling the reaction conditions. COF

monolayers prepared by using these methods are of broad scientific interest and significant technological importance.

1.10 Important properties and application of COFs

1.10.1 *Gas storage (H_2, CH_4, CO_2 and NH_3) in COFs*

Ideally COFs can be treated as best materials for many potential applications including gas storage owing to their light weight framework and high surface areas (***Figure 1.18***). In this section we will discuss the storage capabilities of various COFs for gases, like H_2, CH_4, CO_2 and NH_3 along with brief overview of other applications.

Hydrogen storage on porous materials has attracted significant interest as it stand for a major source of future energy based on high abundance, energy/power density and environmentally friendly characteristics. The DOE (US) has set the target for hydrogen storage as 9 wt% at temperature 253–323 K with a pressure of 100 atm by the year 2015. It is also predicted that a material with weak physisorption at cryogenic (*e.g.*, 100 K) temperatures and very high surface areas (43,000 m^2g^{-1}), pore sizes of 0.7 to 1.2 nm, will have the potential to congregate the set DOE 2015 target. So far, the highest hydrogen storage capacity is observed for 3D COF-102 (S_{BET}: 3620 m^2g^{-1}, pore size: 1.2 nm), which uptakes 72 mg g^{-1} at 1 bar and 77 K [1.50a]. This capacity is very well comparable to those of MOF-177 (75 mg g^{-1}, S_{BET}: 4500 m^2g^{-1}), MOF-5 (76 mg g^{-1}, S_{BET}: 3800 m^2g^{-1}), and the porous aromatic framework-1 (PAF-1) (75 mg g^{-1}, S_{BET}: 5600 m^2g^{-1}). COF-10 with BET surface area of 1760 m^2g^{-1} and pore size of 3.2 nm represents the highest hydrogen uptake of 39.2 mg g^{-1} at 1 bar and 77 K. These H_2 uptake capacities clearly signify that COF materials have sufficient potential to become a good material for storage applications.

Methane gas is largely considered as a suitable vehicular fuel. However, the unavailability of an effective, safe onboard and economic storage system is a major hurdle that stops methane-driven automobiles to operate. The DOE has set a target value for methane storage as 180 cm^3 (STP) at 35 bar. COF-102 has shown the highest methane uptake of 187 mg g^{-1}. However, COF-103 also proves to be a potential material for methane uptake (175 mg g^{-1}) [1.50a and b]. The methane uptake observed for these two COFs can be very well compared with potential MOFs with highest methane uptake capacity (*i.e.*, MOF-210; mg g^{-1}) [1.16]. It has been realized that methane molecules can strongly interact with the

faces of the aromatic ring but weakly with the edges. Therefore, COFs can be promising candidates for methane storage application.

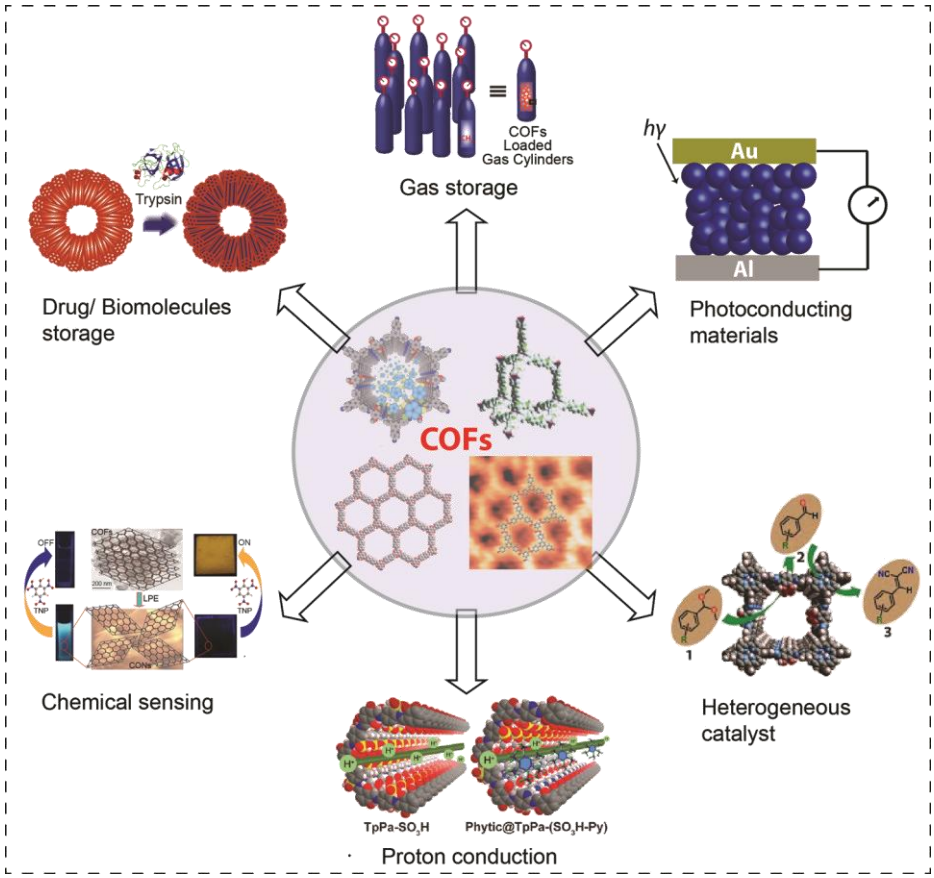

Figure 1.18. *Various applications of COFs such as gas storage, photoconducting materials, heterogeneous catalysis, proton conduction, chemical sensing and drug/bio molecules storage.*

Carbon dioxide is a greenhouse gas and majorly responsible for global warming and rising sea levels. Hence, capturing CO_2 from industrial emission is highly essential and has attracted extensive interest. Among existing CO_2 capture techniques, adsorption by porous materials is technically feasible and energetically efficient. First time, Yaghi and co-workers have studied the CO_2 capture in a family of COFs. The CO_2 uptake for COF-102 was 27 mmol g^{-1} at 298 K and 35 bar [1.50a]. This value is higher than the uptake reported for well known MOF-5 (22 mmol g^{-1}) [1.24a] and zeolite (5–8 mmol g^{-1}) [1.4b]. This could result due to the low density, compact packing, and higher pore volume COF framework as compare to the zeolites and MOFs. It has been also seen that various alkali, alkaline earth, and transition metals, lithium ion doping is very helpful to enhance the CO_2 storage capacity of COFs.

In addition to the adsorption of common gasses such as H_2, CH_4, and CO_2, COFs showed potential for high ammonia uptake. It has been proved that boronate-ester linkages are very useful for adsorbing ammonia due to the availability of Lewis acidic boron sites. Among all COFs reported to date COF-10 has displayed the highest ammonia uptake of 15 mol kg^{-1} (298 K, 1 bar) (***Figure 1.19***) [1.50c]. Also it is stated that, the adsorption of ammonia on COFs are purely based on physisorption and can be cycled several times without any loss in performance. All the results stated above signify that suitably designed COFs with specific functional groups can interact with gas molecules and eventually will give high uptake of gases.

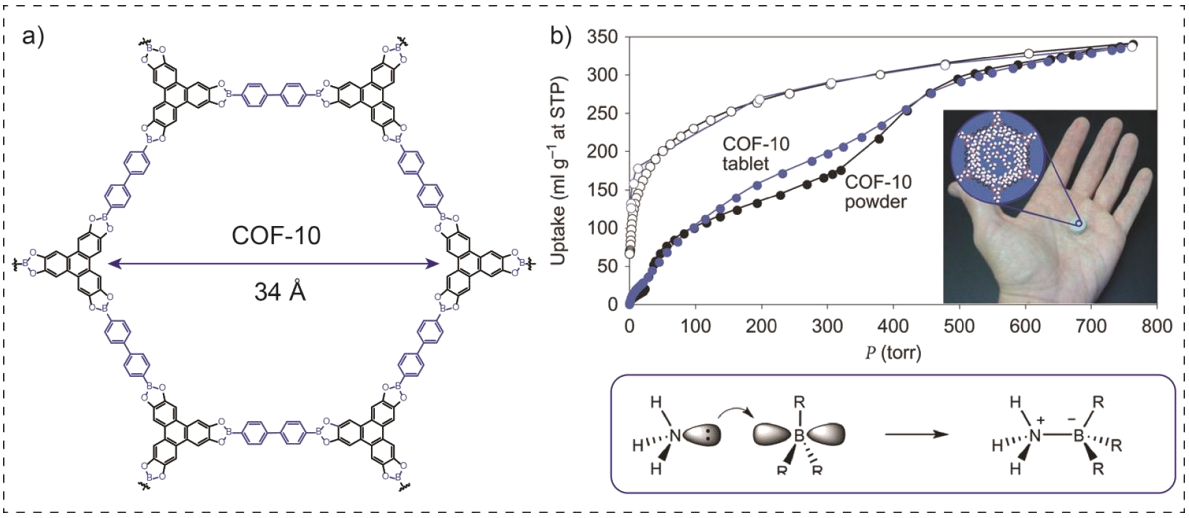

Figure 1.19. *a) Chemdraw model of a COF-10 hexagonal pore showing its atom connectivity; b) Ammonia uptake in COF-10 (black) and COF-10 tablet (blue) at 298 K. Inset, a pressed tablet of COF-10 loaded with ammonia placed in palm. [Redrawn with permission from Ref. 1.50c, Copyright Nature Publishing Group, Macmillan Publishers Limited, 2010].*

1.10.2 *Heterogeneous catalysis*

Apart from gas adsorption COF materials are proved to show catalysis. Due to its robust and high pore volume with the outstanding surface area, COFs can facilitate the loading of various molecules into their nanopores for specific applications. For an example, Pd ions can be loaded onto an imine-based COF-LZU1 to afford Pd/COF-LZU [1.46b]. Interestingly, the Pd ions anchored on the COF walls and in between the layers can act as a heterogeneous catalytic system. Using Pd/COF-LZU1 Suzuki–Miyaura coupling reaction has been demonstrated with outstanding catalytic activity. On the other hand, Shinde *et al.*

recently reported inclusion of bifunctional (acid/base) catalytic sites in the organocatalytic porous, crystalline COF (2,3-DhaTph) for cascade reaction [1.46c]. It has been stated that, due to the presence of acidic (catechol) and basic (porphyrin) sites on 2,3-DhaTph, the catalytic activity and selectivity significantly enhanced. The outcomes stated above suggest that COFs can act as a suitable heterogeneous catalyst for a broad range of reactants scope with outstanding recyclable ability.

1.10.3 *Chemical sensing*

Very recently researchers also have explored the ability of COFs for chemical sensing of nitroaromatics. For example, Jiang and co-workers reported an azine-linked, stable porous framework for quenching based nitroaromatic sensing [1.50d]. It has been stated that due to the columnar ordering of pyrene, the azine-linked framework is highly luminescent and the azine units provide the open docking sites for hydrogen-bonding interactions. These features provide the azine-linked pyrene frameworks with high sensitivity and selectivity towards detection of 2,4,6-trinitrophenol explosive. Later, Das *et al*. demonstrated that imide-based crystalline, porous, and chemically stable covalent organic nanosheets (CONs) can exhibit outstanding sensing ability of nitroaromatics with good selectivity and sensitivity [1.46d]. Interestingly, TfpBDH-CONs exhibit a "turn-on" detection of 2,4,6-trinitrophenol (TNP) in the solid state, and conversely, showed a "turn-off" detection in the dispersion state. Such findings suggest that COF can also be a platform for chemical sensing applications.

1.10.4 *Conducting materials*

The construction of electronic and optoelectronic materials based on COFs was first demonstrated in the year 2008 [1.50e]. In the first design a π-electronic hexagonal 2D TP-COF made from HTTP molecules was synthesized. TP-COF possess a belt-shaped structure and gives a strong blue luminescence. As a result, TP-COF can suitably harvest photons from the ultraviolet to visible regions and successfully convert them to a blue luminescence. Due to the eclipsed stacking, the π-electronic components of TP-COF is semiconducting in nature, which facilitates the hole transport and showed on–off switching of the electric current. On the other hand, the exploration of photo functional materials is highly important for developing artificial photosynthesis, light energy conversion, and optoelectronics. It is to note that the molecular ordering of the π-electronic components in COF materials play a

crucial role for the evaluation of device performance. The first example of a photoconductive COF is PPy-COF. This framework is prepared through the self-condensation of PDBA [1.50f]. These COF showed a cubical morphology with a blue luminescence. From the fluorescence anisotropy measurements it infers that the PPy-COF fluorescence is greatly depolarized, with an anisotropy of only 0.001, which is found to be much smaller than the anisotropy of TP-COF (0.017) reported earlier.

1.10.5 *Biomolecules storage*

Very recently hollow spherical COFs have been used for the storage of biomolecules. The first example was demonstrated by Kandambeth *et al*. In this report a chemically stable, hollow spherical COF-DhaTab with BET surface area ~1500 m^2g^{-1} has been used for the immobilization of tripsin enzyme (uptake of 15.5 µmol g^{-1}) and also systematically studied the release profile. It has been seen that the enzyme take the position within the COF mesoporous walls rather than hollow cavity inside the COF [1.44e].

1.11 Chemical stability of COFs

Even though a diverse number of COFs are been synthesized and used in variety of applications, it suffers from a serious drawback, which is about its chemical stability. Since COFs are synthesized by reversible organic reactions, it is possible that reversible backward reactions can occur in the synthesized COFs and get completely decomposed even in not humid conditions (***Figure 1.20***) [1.51a].

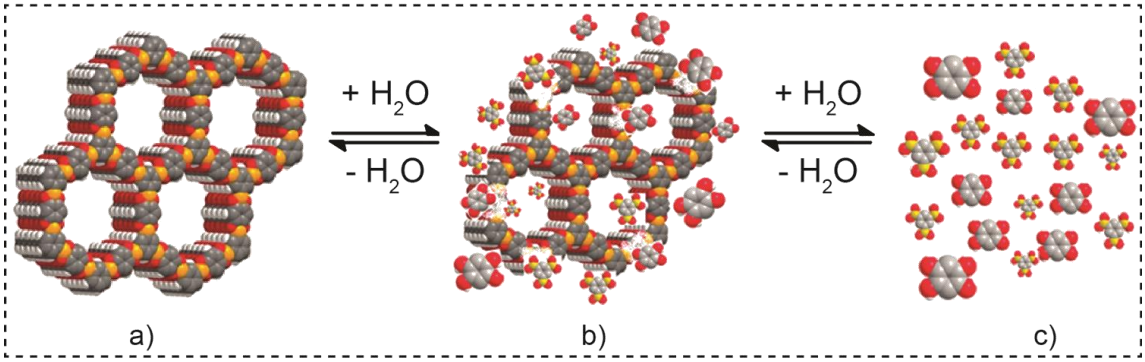

Figure 1.20. *Schematic representation of (a) as-synthesized COF (b) partial hydrolysis and release of monomers into solution upon submersion in water (c) completely hydrolyzed COF. [Reprinted with permission from Ref. 1.51a, Copyright American Chemical Society, 2011].*

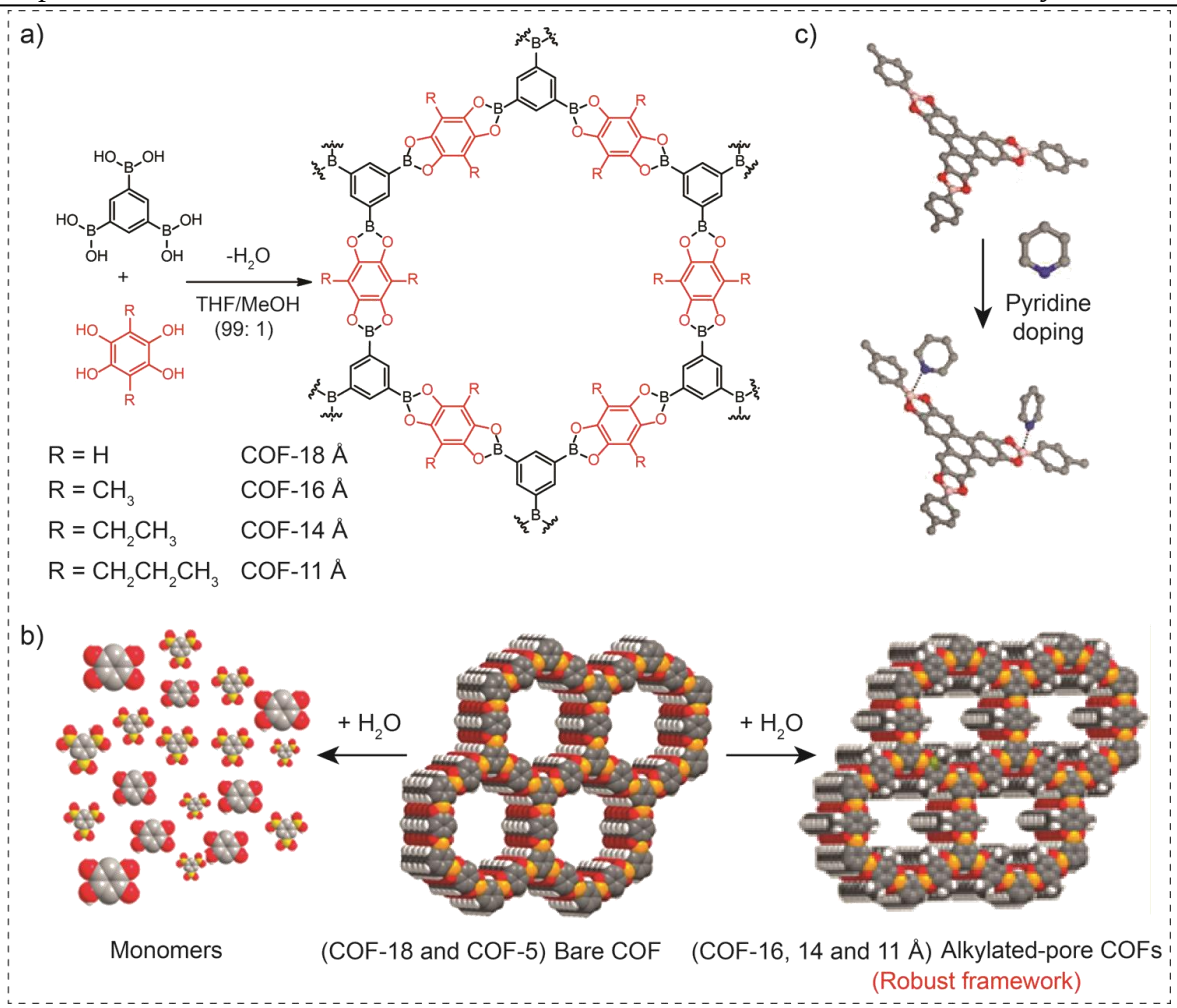

Figure 1.21. *a, b) Introduction of alkyl groups on the COF walls to enhance water stability; c) Pyridine doping onto the active sites to enhance water stability of COFs. [Redrawn with permission from Ref. 1.51a, Copyright American Chemical Society, 2011 and Ref. 1.51c, Copyright Royal Society of Chemistry, 2012].*

A little improvement on water stability of boronic acid-based COF has been achieved by alkylation of COF pore walls and pyridine doping (***Figure 1.21a-c***) [1.51c]. This was with intention that the alkyl and pyridine group introduced into the COF will block the labile Lewis acidic boron sites and prevents the attack of H_2O molecule to bring the stability to COF framework in some extent. (Note: The stability achieved by these methods is only for few days exposed to air, direct contact with water can still degrade the material completely) [1.51]. However, these modifications always result in the decrease of gas adsorption properties. Therefore, stability problem in COFs still was remaining a challenge for a quite long time till 2012, which prevented the usage of COFs for diverse practical applications.

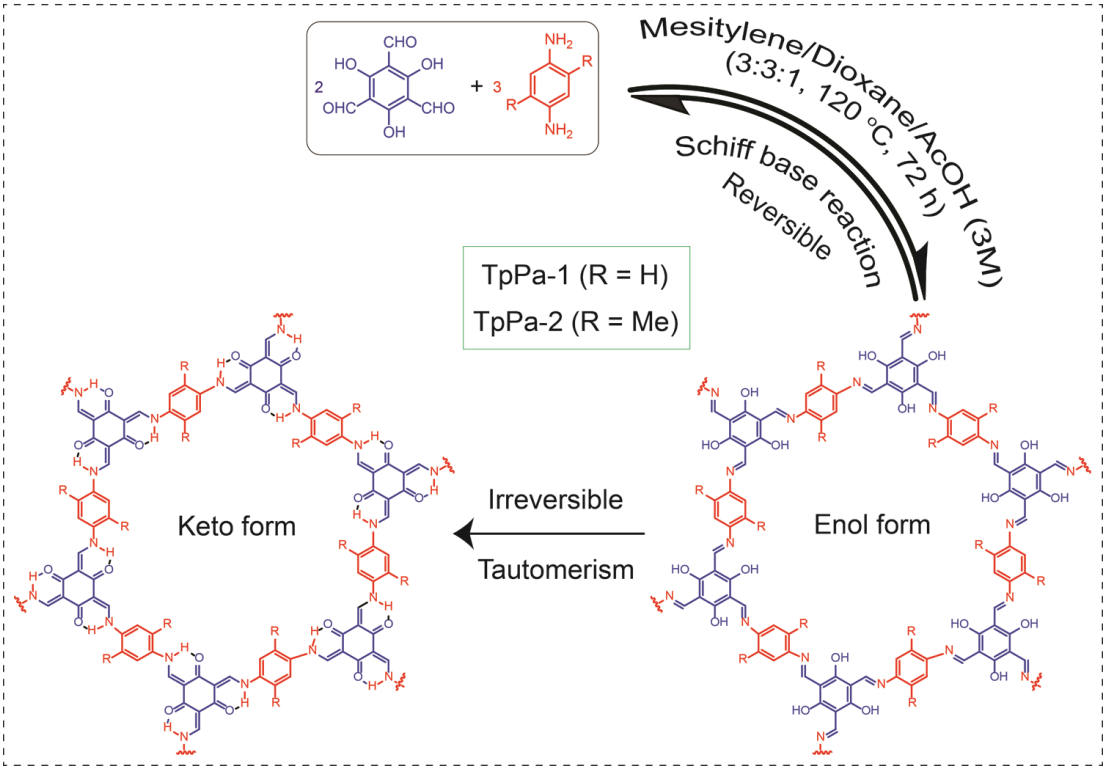

Figure 1.22. *Synthesis scheme for chemically stable COFs (TpPa-1 and 2) via Schiff base condensation reaction. [Redrawn with permission from Ref. 1.47a, Copyright American Chemical Society, 2012].*

In the year 2012, Kandambeth *et al*. for the first time in COF history, developed a methodology of a combined reversible and irreversible Schiff base reaction to construct two new crystalline and porous COFs (*e.g.*, TpPa-1 and TpPa-2) (***Figure 1.22***) [1.47a]. These two COFs displayed outstanding chemical stability towards acid (9 N HCl), base (9 N NaOH) and water for 7 days or beyond. These COFs are resulted by the reaction between 1,3,5-triformylphloroglucinol (Tp) and *P*-phenylenediamine (Pa-1) or 2,5-dimethyl-*p*-phenylenediamine (Pa-2) in a sealed Pyrex tube at 120 ºC for 3 days. It was stated that, the total reaction is divided into two consecutive steps. The first one is reversible Schiff base reaction that is responsible for the formation of the crystalline framework and followed by irreversible enol to keto tautomerization, which brings the chemical stability to the framework. The possible reason behind this type of enol-keto tautomerism is the basicity of imine nitrogen atoms. These imine nitrogen atoms when comes in close proximity with the acidic phenolic –OH, it abstracts the proton, which results in this type of tautomerism. However, such tautomerism is exists even in simple *N*-salicylideneanilines, wherein enol

form is found to be more stable [1.52]. It is believed that, two competing effects decide the stable form of the resulting products *i.e.*, i) Aromaticity, and ii) Basicity of imine nitrogen (–C=N–) over phenolic oxygen (O–H). In case of monosubstituted *N*-salicylideneanilines, the aromaticity is the dominating factor over basicity of imine nitrogen and hence, the compound exists only in enol form (***Figure 1.23***). However, in case of tris(*N*-salicylideneaniline) derivatives, the basicity of three imine nitrogen dominates significantly over the aromaticity factor, as a result equilibrium shifts completely towards the keto-form [1.52]. Once established, the equilibrium does not revert back to the direction of enol form even after heating the sample to a very high temperature and thus this transformation can be considered as an irreversible process.

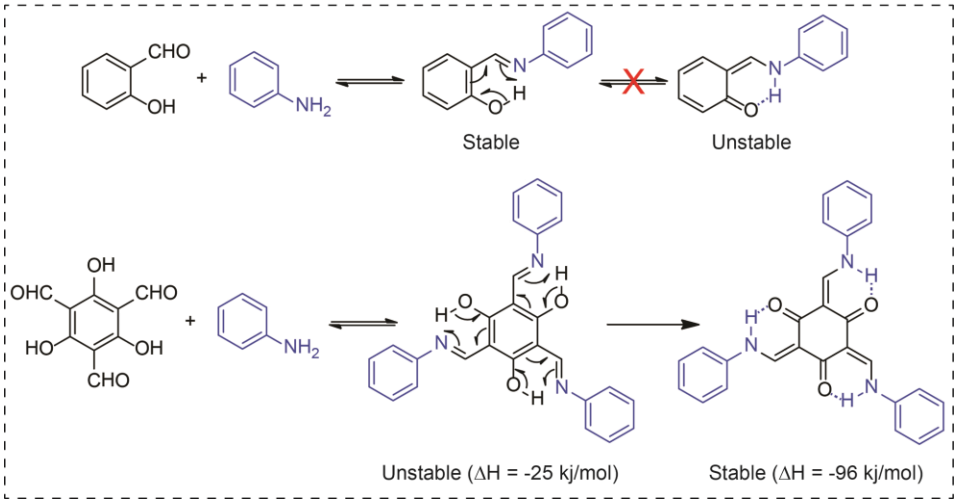

Figure 1.23. *Tautomerism exists in simple N-salicylideneanilines where enol-form is found to be more stable than its keto form. [Redrawn with permission from Ref. 1.52, Copyright American Chemical Society, 2003].*

Despite such advancement in the COF research a suitable method for their synthesis has not been so far explored and remains still a great challenge to achieve. The aim of one part of this thesis is to approach towards the facile synthesis of COFs with outstanding chemical stability and in the later parts devoted to their applicability as a membrane material for gas separation application.

CHAPTER 2

Synthesis of Water-Stable, Porous Cobalt Imidazolate Framework and Solution Mediated Phase Transformation (RHO to SOD)

Abstract: *In this chapter, we presented the entrapment of an unprecedented highly porous, water stable Co based Zeolitic Imidazolate Framework CoNIm (RHO) and studied the time-dependent solution mediated phase transformation to CoNIm (SOD) [known as ZIF-65] via Oswald ripening process. CoNIm (RHO) has a high surface area (BET and Langmuir surface area 1858 m^2g^{-1} and 2087 m^2g^{-1} respectively) among all ZIF materials known. The unusual water stability of CoNIm (RHO) over CoNIm (SOD) was also examined, despite similar framework composition. Large cage in CoNIm (RHO) renders promising H_2 (77 K) and CO_2 (273 K and 298 K, at 1 bar) uptakes, which outperforms many highlighted ZIFs and MOFs. We believe, our finding on phase transformation in ZIFs could contribute towards the structural and morphological evolution in the synthesis of novel frameworks in near future.*

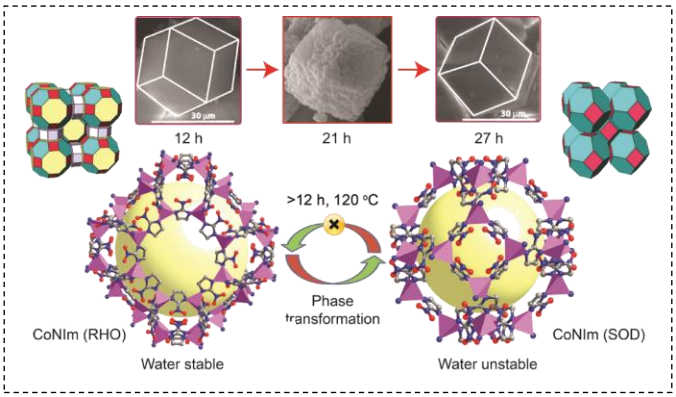

2.1 Introduction

Zeolitic Imidazolate Framework (ZIF) [2.1] belongs to a class of metal-organic frameworks (MOFs) [2.2] where transition metals (Zn/Co/Cd) are linked through imidazolate (Im) type linkers with a variety of functionalities. These tetrahedral metal centres are coordinated through 'N' donors of imidazolate (Im) links to make M–Im–M angle ~145^{o}, which typically found in zeolites (Si–O–Si) [2.3]. Principally, ZIFs have emerged as an ideal candidate for the capture and storage of strategic gases such as H_2 and CO_2 due to its permanent porosity and flexible open frameworks with diverse functionality [2.4]. Apart from gas adsorption, ZIFs have shown numerous potential applications like selective separation [2.5], drug delivery [2.6], organo-catalysis [2.7], sensing [2.8] etc. Interestingly, >40 varieties of diverse net structures with exciting zeolitic topologies (*e.g.,* LTA, ANA, GME, SOD, RHO, DFT, MER, POZ, and MOZ) have been reported [2.9]. However, most of them contain Zn(II) as a metal node, except a few, based on Co(II) and Cd(II) frameworks [2.10]. As a consequence, the water stability of ZIFs based on Co(II) and Cd(II) remains unexplored. On the other hand, crystal growth and phase transformation processes are well known in zeolite chemistry [2.11], but a similar phenomenon in MOFs/ZIFs have not been studied vividly. Taking this as an opportunity, we devote our efforts towards synthesizing water stable ZIF and to understand the crystal growth phenomena, which is very important for the development of this class of materials.

In this chapter, we present an unprecedented highly porous, water stable Co(II) nitroimidazolate based ZIF [CoNIm (RHO)]. Interestingly, CoNIm (RHO), completely transfers to a less porous CoNIm (SOD) phase (previously reported as ZIF-65) [2.1b] *via* Ostwald ripening (***Figure 2.1***) [2.12]. The study on water stability and *in situ* phase transformation from CoNIm (RHO) to CoNIm (SOD) ZIF with time was the principal focus of this study. The structure of CoNIm (RHO) has been determined using single crystal X-ray diffraction (XRD), further identified by FT-IR spectroscopy and powder X-ray diffraction (PXRD). We have also explored the thermal stability of CoNIm (RHO) and compared with CoNIm (SOD) by thermogravimetric analysis (TGA). In addition, *in situ* variable temperature PXRD has been carried out on these ZIFs to analyze their stability and crystallinity at high temperature. The unusual fact, we observed is the remarkably high stability of CoNIm (RHO) in water and other organic solvents compared to CoNIm (SOD),

although both frameworks have similar chemical compositions [$Co(NIm)_2$] as well as same no of Co–N bonds [CoN_4] [2.1b]. Notably, a few ZIF structures have been reported earlier *i.e.*, ZIF-11, ZIF-12, ZIF-71, and ZIF-96 belongs to RHO topology, but most of them are non-porous, low chemical stability or not yet realised in bulk scale [2.1a, 2.14]. CoNIm (RHO) possesses the highest surface area compared to any other ZIFs reported till date. Moreover, polar $–NO_2$ functionality as well as large caged open framework architecture of CoNIm (RHO), renders high H_2 and CO_2 uptake, which outperforms many, highlighted ZIF and MOF materials [2.13, 2.14].

2.2 Result and discussion

2.2.1 *Structural analysis of CoNIm (RHO) and CoNIm (SOD)*

CoNIm (RHO) ZIF crystallizes in highly symmetric *Im*-3*m* (cubic) space group with 48 Co(II) ions with an unit cell, $a = b = c \sim 29.0302(5)$ and volume of 24465.3(7) $Å^3$. The density (*T/V*) of metal atoms per unit volume is 1.96 nm^{-3}, which is comparable with other ZIFs (ranges from 2.0–3.7 nm^{-3}) and much lesser than that of zeolites (lies between 12–20 nm^{-3}) [2.1a]. In CoNIm (RHO), each Co(II) ion is tetrahedrally coordinated to four nitrogen atoms of four 2-NIm moieties to form an extended 3D zeolitic (RHO) framework. The Co–NIm–Co angle is found to be varied from 135.7^o-139.2^o (reported RHO ZIFs withstands a variation from 141.8^o to 151.3^o). The framework composed of three different faces with 8, 6, and 4 member ring windows [$4^{12}.6^8.8^6$; where m^n stands form rings and n faces] are connected with neighbouring cages, including an α cage with 48 vertices and 26 faces, which is comprised of 6 octagons, 8 hexagons, and 12 squares. Each *α* cage is further connected to six other α cage by sharing double 8 member ring units (***Figure 2.2a-c***). In comparison to the CoNIm (RHO), the CoNIm (SOD) is crystallized in a cubic space group (*I*-43*m*) [$a = b = c$ ~17.2 Å] with a unit cell volume of 5152.2(2) $Å^3$ [2.1b]. The density (*T/V*) of metal atoms per unit volume is 2.32 nm^{-3}, which is higher than CoNIm (RHO) (1.96 nm^{-3}). The framework of CoNIm (SOD) ZIF contains *β* cages [24, Co(II)], composed of two different faces with 6, and 4 member ring windows [$4^6.6^8$] connected to neighbouring pores. The $–NO_2$ group of 2-NIm in CoNIm (SOD) point towards the pore windows in both 6 and 4 membered rings

respectively, which results in very small pore aperture (d_a) ~3.4 Å as well as pore diameter (d_P) ~10.4 Å (***Figure 2.2d-f***).

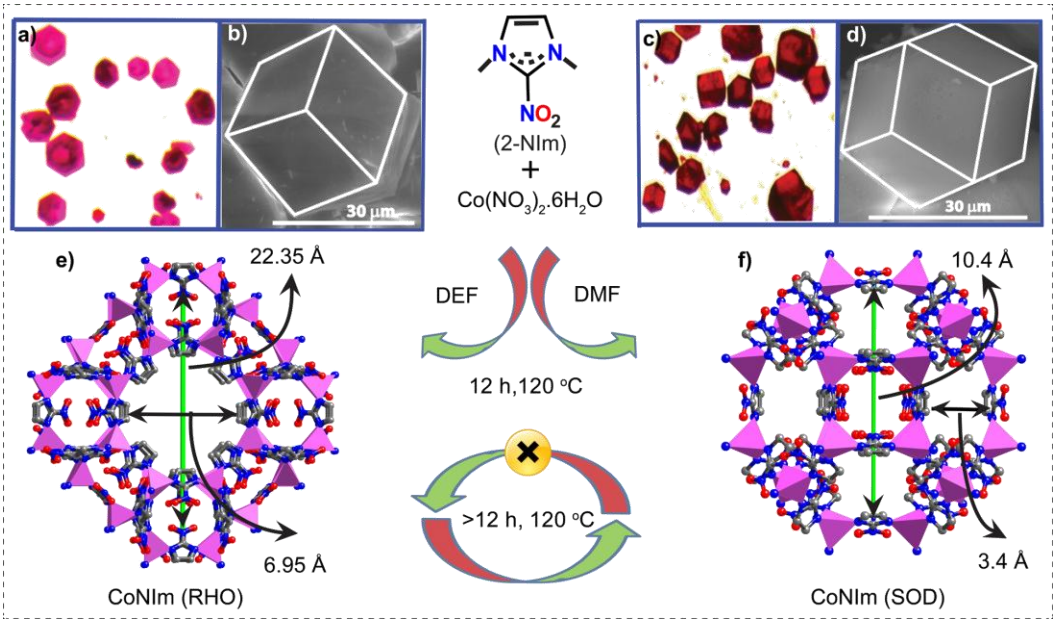

Figure 2.1. *Synthesis scheme for CoNIm (RHO) and CoNIm (SOD) ZIFs; (a, c) Digital photographs of CoNIm (RHO) and CoNIm (SOD) crystals; (b, d) SEM image of individual single crystal of CoNIm (RHO) and CoNIm (SOD) ZIF; (e, f) CoNIm (RHO) and CoNIm (SOD) ZIF cages from single crystal XRD structure, with CoN_4 pink tetrahedra [both sided arrow indicates the pore diameter (d_p) and pore aperture (d_a) in each case]. H atoms have been omitted for clarity. C, gray; N, blue; O, red; Co, pink.*

In ZIFs, we have noticed that imidazole functionalized at 4 and 5 positions (–CH_3, –Cl, –CHO, –NH_2, –CN, –C_4H_4, –C_2N_2 and –CH_2OH) tend to produce RHO topology in which these functional groups are directed towards the pore windows [2.14]. As a consequence, it constricts the pore aperture (d_a~3-4 Å, d_a~14-16 Å). On the other hand, small and rigid functional groups (–CH_3, –Cl, –Br, and –CHO) at 2 positions prefer to adopt the SOD zeolitic topology (***Figure 2.3***) [2.15]. CoNIm (RHO) has small 2-NIm as the linker, where rigid –NO_2 groups occupy the 2 positions and yet it forms both RHO as well as SOD net. From the crystal structure, it is seen that all the –NO_2 groups of 2-NIm in CoNIm (RHO) are away from the pore windows of 8 and 6 member rings, which results in large pore aperture (7.1 Å) and pore diameter (22.3 Å) (***Figure 2.1e***). The pore diameter of CoNIm (RHO) ZIF (22.3 Å), is higher than most of the reported ZIFs, but less than only ZIF-100 (~ 35.6 Å), ZIF-95 (~ 24 Å) [2.16a] and rho-ZMOF (~ 26.9 Å) [2.16b].

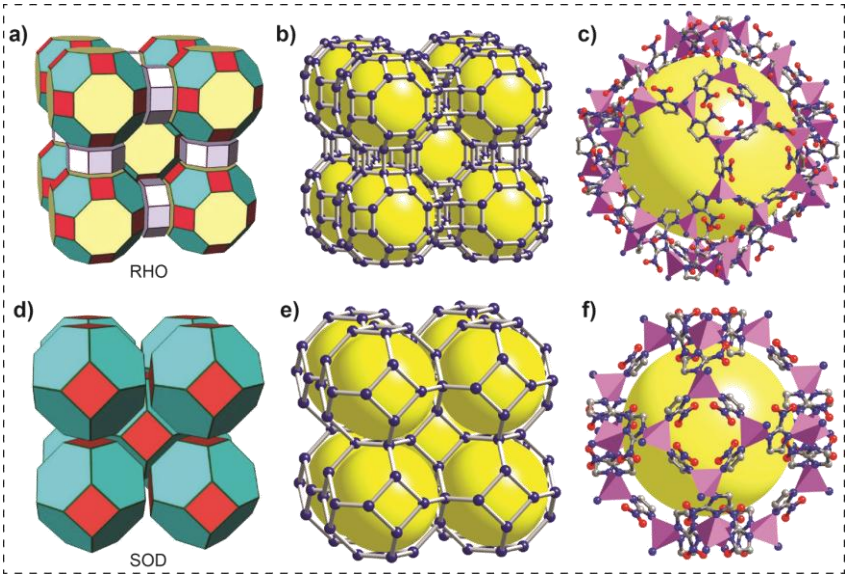

Figure 2.2. *a, d) Tiling shows subdivision of space in RHO/SOD topologies; b, e) nets (gray line and deep blue dots) representing 2-NIm linker and Co centre, yellow ball inside indicates the free space inside the framework; c, f) a cutaway view of one of the [CoNIm (RHO)/CoNIm (SOD) ZIFs] Zeolitic Framework cage from single crystal XRD structure, CoN_4 pink tetrahedral with ball and stick links (yellow ball represents the empty space inside the framework). H atoms have been omitted for clarity. C, gray; N, blue; O, red; Co, pink.*

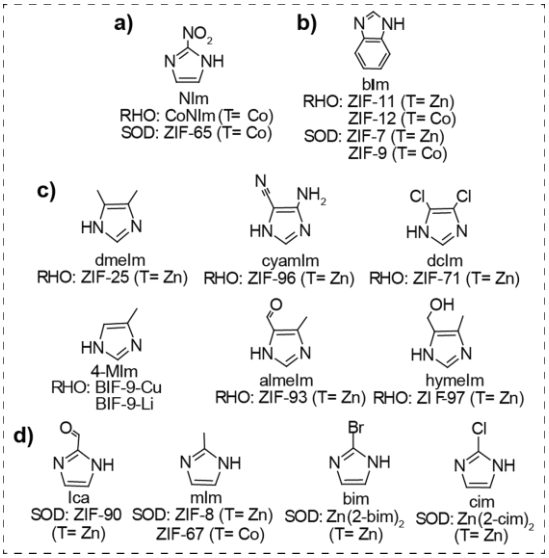

Figure 2.3. *Imidazolate-type links used for the synthesis of ZIFs with RHO and SOD topology. a) 2-NIm is the only 2-substituted linker adopts both RHO and SOD topology; b) bIm is the only 4, 5, substituted linker which adopt both RHO and SOD topology; c) Series of 4, 5, substituted imidazolate links which gives only RHO topology; d) Series of 2 substituted imidazolate links which form only SOD topology. (Each category of linkers is enclosed; 'T' represents the metal atom used for ZIF synthesis) [2.1a and b].*

The pore aperture of CoNIm (RHO) ZIF is 7.13 Å, which also stands at higher position in ZIF series but it is less than the pore aperture (d_a) of few ZIFs such as ZIF-70 (13.1 Å), ZIF-80 (9.8 Å), ZIF-10 (8.2 Å), ZIF-82 (8.1 Å), ZIF-68 (7.8 Å), ZIF-79 (7.5 Å) and ZIF-60 (7.2 Å) with GME and MER topologies [2.1a and b]. [Note: The pore aperture (d_p) and pore diameter (d_a) are calculated by subtracting twice the *van der Waals* radius of H atom from the opposite diagonal atoms in the cage].

2.2.2 *Phase transformation from CoNIm (RHO) to CoNIm (SOD)*

Although a number of ZIF structures have been reported, only a few on crystal growth and no attempt was made to understand the phase transformation during ZIF crystallization [2.14].

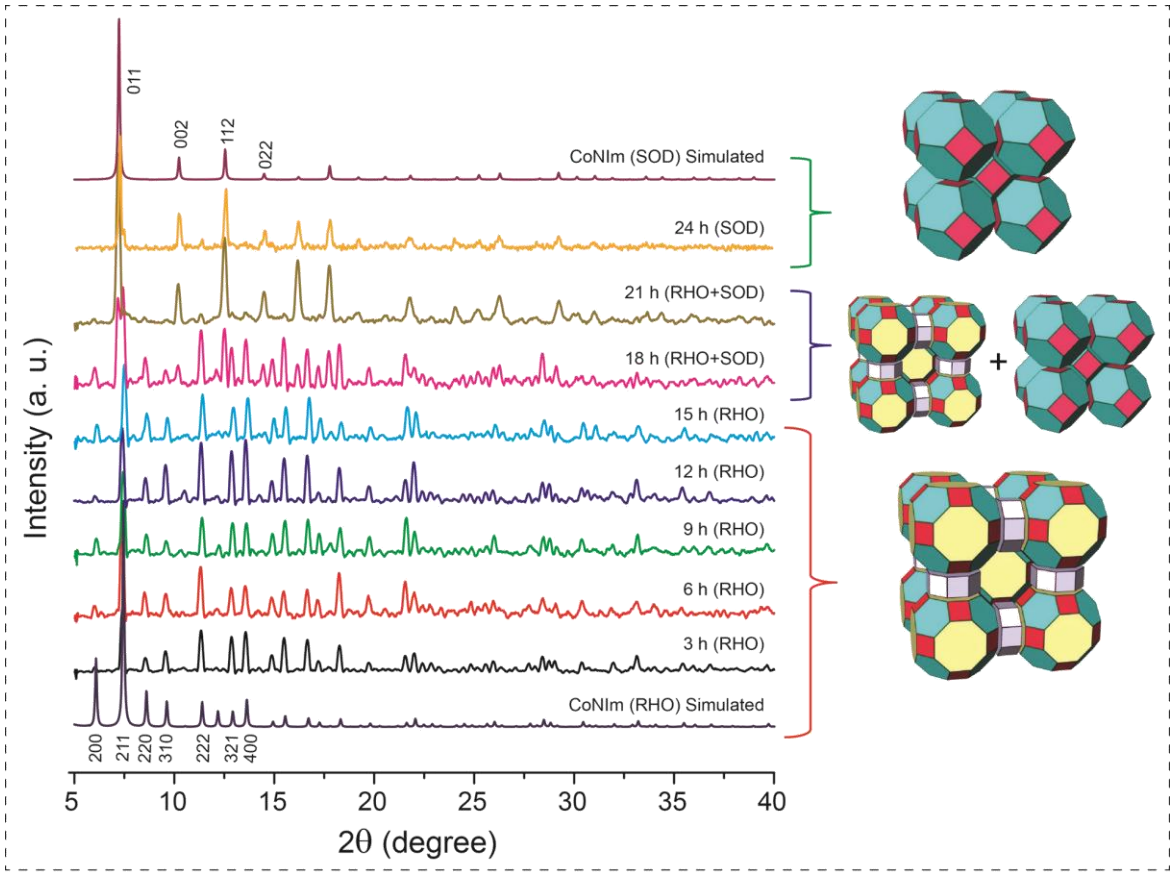

Figure 2.4. *Experimental PXRD pattern demonstrating phase transformation at different stages (each 3 h interval) from CoNIm (RHO) 3 h (black) to CoNIm (SOD) ZIF; 24 h (golden yellow), comparison with simulated CoNIm (RHO) (blue, bottom) and CoNIm (SOD) (brown, top) from its single crystal structure. Red (bottom) and black (top), three digit numbers represent the planes correspond to the characteristic peaks of CoNIm (RHO) and CoNIm (SOD) ZIF.*

In this work, we demonstrate the crystal growth and phase transformation in ZIFs. For this typical study, we have chosen previously reported Co(II) based zeolitic framework CoNIm (SOD) [2.1b]. CoNIm (SOD) have been synthesized by reacting 0.2 M 2-NIm and $Co(NO_3)_2.6H_2O$ solution (2: 1) in *N*,*N*-dimethyl formamide (DMF) at 120 °C for 24 hours (h). However, when the same experiment was attempted in *N*,*N*-diethyl formamide (DEF), we observed that small crystals at early stages of synthesis (10-12 h) with slightly different external morphology (rhombic dodecahedron) than CoNIm (SOD) (sharp cut edged rhombic dodecahedron).

PXRD patterns indicated a completely different phase than CoNIm (SOD) (***Figure 2.4***). To get the exact crystal structure, we have done single crystal X-ray analysis, which revealed an RHO net named as CoNIm (RHO), with large cage. When the same reaction mixture in DEF was kept undisturbed for 24 h or more, we could obtain the phase pure CoNIm (SOD) crystals. The above observations motivated us to study in detail the phase transformation process. We observed that the nucleation followed by crystal growth starts as early as on the 3 h of synthesis and on slow cooling very small crystals, could be found in the reaction vial. We investigated the entire phase transformation process up to 24 h by following similar protocol at each 3 h intervals (***Figure 2.4***). After 12 h of aging good quality crystals suitable for mounting in a single crystal X-ray diffractometer was observed. As the aging process goes on till 15 h, the size of CoNIm (RHO) crystals starts gradually decreasing. At 18 h, we found that a mixture of RHO and SOD phase present in the reaction vial. From this observation, it is clear that during the period (15 to18 h), CoNIm (SOD) phase starts growing at the expense of CoNIm (RHO) phase, which is nothing but Oswald ripening. We continued monitoring the phase transformation process and at 21 h, characteristic peaks of CoNIm (RHO) starts disappearing and relative peak intensity of SOD phase starts intensifying. After 24 h, pure CoNIm (SOD) crystals recovered from the reaction vial. We anticipate that during the synthesis several bulk phenomena like nucleation, crystal growth, and simultaneous phase transformation takes place from one crystal form to another. In order to understand any further phase change beyond 24 h of synthesis, we kept the same reaction ongoing for 36 and 48 h, but no further change from CoNIm (SOD) phase was observed. In order to check the stability of the recovered CoNIm (RHO) crystals; we added fresh 2-NIm (0.2 M, in DEF) solution into the dry CoNIm (RHO) crystals and maintain the reaction

condition (120 ^{o}C, 24 h). However, this experiment does not result in any phase change. From this observation, it is clear that CoNIm (RHO) is highly stable once they are recovered from the reaction mixture.

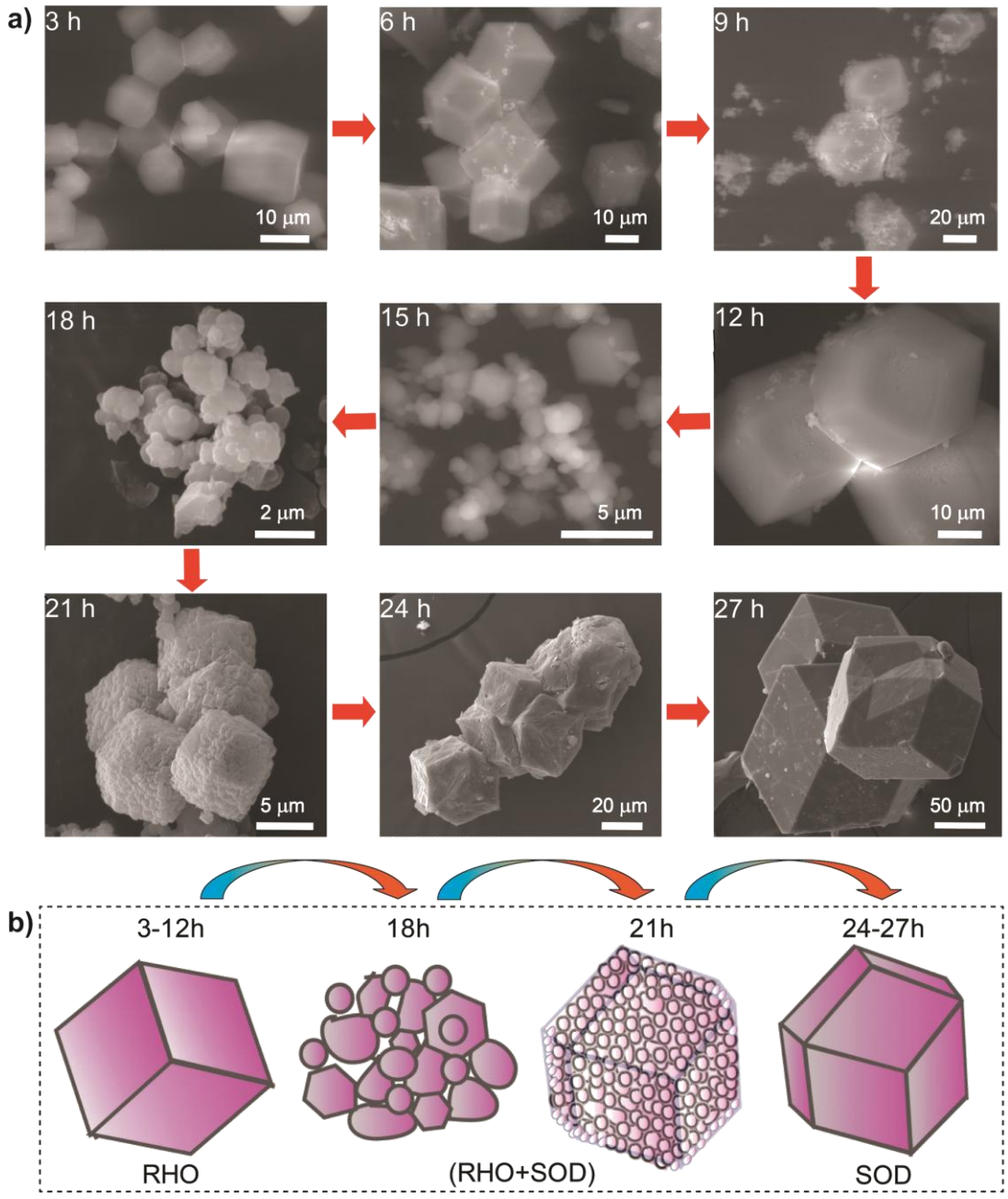

Figure 2.5. *a) SEM images at different time interval of synthesis; 3 h, 6 h and 12 h for CoNIm (RHO) ZIF, 18 h and 21 h for CoNIm (RHO+SOD) and 27 h for CoNIm (SOD) respectively; demonstrating the crystal morphology while phase transformation from CoNIm (RHO) to CoNIm (SOD) ZIF; b) Carton representation of the overall solution mediated phase transformation process form RHO (3-21h) to SOD (24-27h) via RHO and SOD (18-21h) mixed phase with time. (Hours abbreviated as h).*

In order to understand the external morphology of CoNIm (RHO), CoNIm (SOD) and ZIF to ZIF phase transformation process with respect to time, we collected Scanning Electron Microscopy (SEM) images of crystals (***Figure 2.5***). These images indicate that CoNIm (RHO) crystals have well defined homogeneous rhombic dodecahedron shaped morphology (~10±5 μm) at the beginning (3 h). As the time progress, the average crystal size increases and it continue till 12 h (size 30±5 μm). But after that, the crystal size starts decreasing and so as the shape changes from rhombic dodecahedron to semi-spherical (average size 0.5–1 μm). At 18 h, we found small semi-spherical shaped crystals of ~1-3 μm and at 21 h small crystallites gets agglomerated on top of each other to form crystals with rhombic dodecahedron morphology (size 10±2 μm). Since the smaller crystals have a lower thermodynamic stability and a higher surface-to volume ratio, we believe that the Ostwald ripening process leads to the slow disappearance of small CoNIm (RHO) crystals and thereby leading to an increase in the average particle size resulting a different phase [CoNIm (SOD)] to minimize the surface free energy. Further, as mentioned sample collected after 18 and 21 h of reaction contains a mixture of RHO as well as SOD phase. After 24 h of reaction, these sphere-shaped crystals take a sharp cut edge rhombic dodecahedron shape and size increases to 180±10 μm (***Figure 2.5***). PXRD profile indicates this phase as exclusively CoNIm (SOD). This transformation of phase from CoNIm (RHO) to CoNIm (SOD) ZIF accompanies the increase in density (from 0.92 to 1.09), which linearly follows framework energies. Also during solvothermal process, the cavitation of ZIF results the change of pressure and temperature significantly, which is higher than that of the surrounding medium (only solvent, ligand and metal salt). Hence, we also hypothesize that the high cavitational effects lead to the dissolution of the CoNIm (RHO) particle surfaces, followed by diffusion of the dissolved species to undergo rapid recrystallization to form bigger CoNIm (SOD) crystals. Experimentally, we also found that at early stages, a structure with high solvent accessible volume (60.7%) favours but as time progress, meta-stable CoNIm (RHO) ZIF isomerises to a relatively low energy and denser CoNIm (SOD) phase with low solvent accessible volume (51.5%).

2.2.3 *Chemical and thermal stability*

Many ZIFs such as ZIF-8, ZIF-11, ZIF-78 and ZIF-82 [2.1a and b] has shown significant chemical stability. Among which, ZIF- 8 (SOD) is highly stable in water as well as in alkaline medium. This happens as the hydrophobic windows of ZIF-8 pores created by $-CH_3$ group of 2-methylimidazole repels water molecules that attempt to react with Zn centres. ZIF-11 with an RHO topology was also reported to be stable in boiling water for 3 days, due to the similar hydrophobic pore windows formed by benzimidazolate ring.

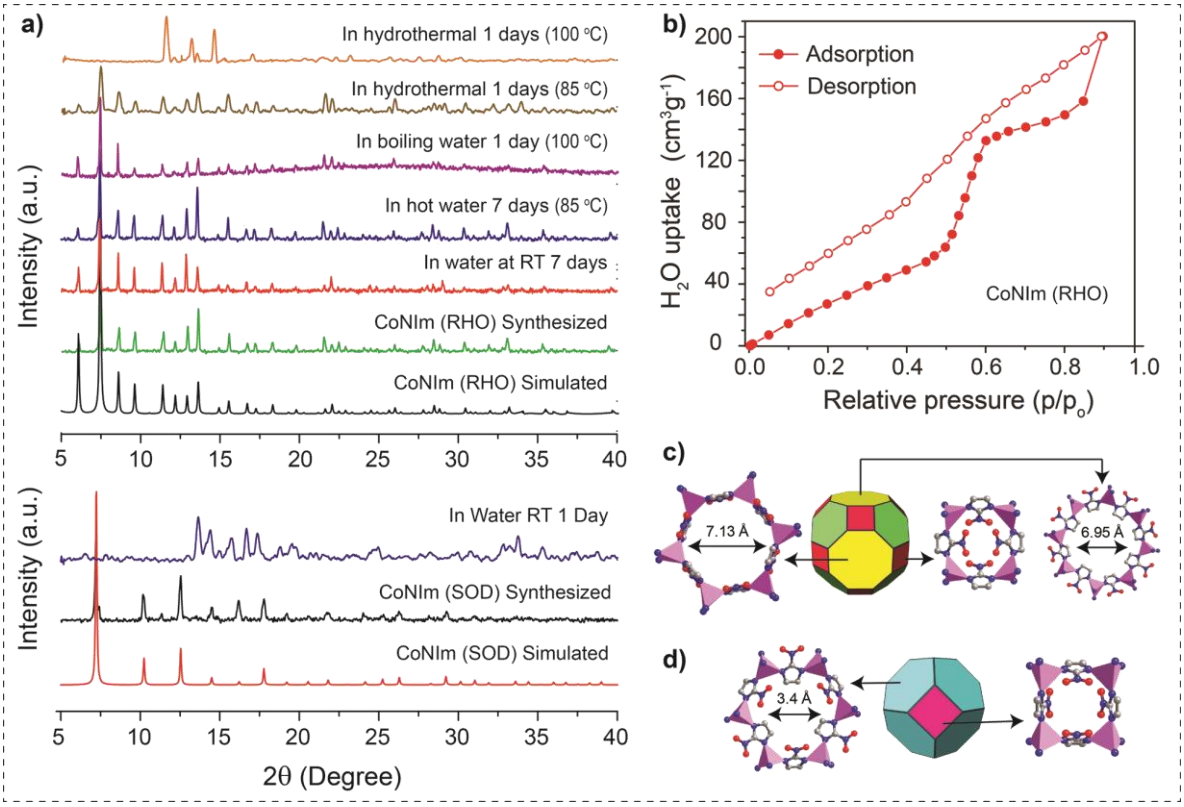

Figure 2.6. *a) Experimental PXRD pattern to show the water stability test and phase purity of CoNIm (RHO) and CoNIm (SOD) ZIF in deionized water; b) Water vapour adsorption isotherm of CoNIm (RHO) at STP (293 K and P/P_o= 0.9); c) Tiling shows subdivision of space in CoNIm (RHO) ZIF and CoNIm (SOD) ZIF cage, a side view of 8 member ring face (yellow) of CoNIm (RHO), from SCXRD data, showing the hydrophobic pore with aperture 6.95 Å, 6 member ring face (green) of CoNIm (RHO) ZIF cage, showing the large pore aperture 7.13 Å, 4 member ring face (red) of CoNIm (RHO) ZIF, showing the hydrophilic pore environment (pore aperture negligible); d) 6 member ring face (cyan) of CoNIm (SOD) ZIF cage from SCXRD data, showing the hydrophilic pore with narrow aperture of 3.4 Å, 4 member ring face (dark red) of CoNIm (SOD) ZIF, showing the hydrophilic pore environment (pore aperture negligible); H atoms have been omitted for clarity. C, gray; N, blue; O, red; Co, pink tetrahedra.*

We investigated the water stability of CoNIm (RHO) by submerging pink crystals in deionized water as well as in hot water (85 ^{o}C) for 7 days. PXRD patterns of these samples have been analysed to conclude that CoNIm (RHO) ZIF crystals retain their physical morphology as well as crystallinity in deionized water and hot (85 ^{o}C) water for 7 days and 3 days respectively (***Figure 2.6a, top***). In boiling water, CoNIm (RHO) remains stable only for 24 h and beyond that the crystals disintegrate into a pink crystalline solid with a different PXRD pattern. CoNIm (RHO) also retains its stability as well as crystallinity under hydrothermal condition but only up to 24 h at 85 ^{o}C. It is noteworthy that, CoNIm (SOD) crystals are unstable to water and transfer into a different crystalline phase within 12 h (***Figure 2.6a, bottom***). This phenomenon was unusual as CoNIm (RHO) has larger solvent accessible voids (60 %) and should, let the water molecule reacts with Co(II) centre, disintegrate much easily than the CoNIm (SOD) contains much less solvent accessible voids (51 %). We believe that, due to the hydrophobic nature of the 8 member rings, as all the –NO_2 groups of 2-NIm remain away from the pore windows. This could oppose the easy approach of water molecule towards the pore (***Figure 2.6c***). However, all the cage windows in CoNIm (SOD) are hydrophilic as the –NO_2 groups are directed towards the pore gate and facilitate the hydrolysis of Co(II) centres (***Figure 2.6d***). There have been several reports of water adsorption in MOFs including only two reports on water sorption in Zn(II) based ZIF [ZIF-71 and ZIF-8] [2.17a and b]. Taking the advantages of water stability of CoNIm (RHO), we further tested the water vapour uptake capacity of CoNIm (RHO) and found a high water vapour uptake of 200 $cm^3(STP)g^{-1}$, at a relative pressure (P/P_o) of 0.9 (***Figure 2.6b***). This water uptake is higher than the water uptake shown by ZIF-71 (~10 cm^3g^{-1}) and ZIF-8 (~150 cm^3g^{-1}) performed under similar experimental conditions [2.17a and b]. Since CoNIm (SOD) [as well as ZnNIm (SOD)] is unstable in water, we could not able to perform the water adsorption experiments on the same.

TGA was performed on both as-synthesized (AS) and activated samples (AE, after the solvent exchange and strong evacuation at 120 ^{o}C) of CoNIm (RHO) and CoNIm (SOD) respectively under N_2 atmosphere (***Figure 2.7***). TGA curve of as-synthesized CoNIm (RHO) shows initial weight loss (32-35%) till 150 ^{o}C due to the escape the amide guest (DEF) from the pores. Then a long plateau was observed in the range of 150-310 ^{o}C, which indicates the thermal stability of the guest free framework. Further, the framework decomposes suddenly

with a significant weight loss of 60% after 310 ^{o}C, upon a narrow temperature difference (5 ^{o}C). In the case of CoNIm (SOD), a continuous weight loss (20-22%) after 100 ^{o}C and up to 150 ^{o}C was observed, which could be due to the loss of entrapped DEF/DMF molecules.

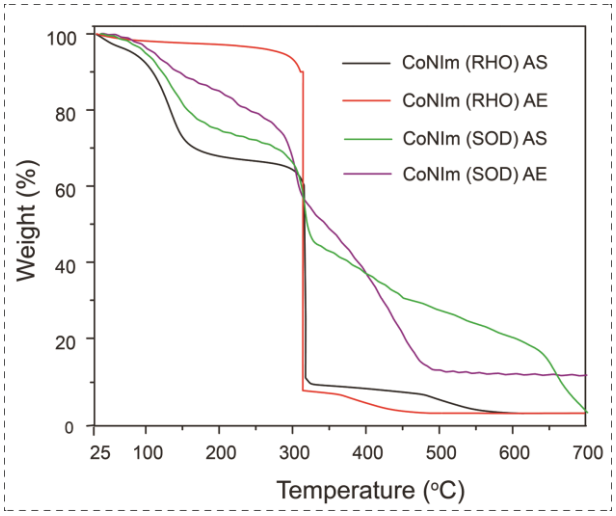

Figure 2.7. *Comparison of TGA thermogram of as-synthesized (AS), activated (AE) CoNIm (RHO) and CoNIm (SOD) ZIFs.*

The guest does not come out easily due to the small opening of the cage in case of CoNIm (SOD). Further, the framework starts decomposing after 310 ^{o}C with a weight loss of 30%. Large pore opening in CoNIm (RHO) ZIF allows the bulky DEF molecule to escape easily from the framework, which implies a straight plateau from 30-310 ^{o}C in the TGA plot, for the activated (AE) sample.

To understand more on the crystallinity and phase change at a different temperature, we performed *in situ* variable temperature powder X-ray diffraction [VT-PXRD, in the range of 25-300 ^{o}C] for both CoNIm (RHO) and CoNIm (SOD) ZIFs (***Figure 2.8***). From VT-PXRD experiment, it is clear that the CoNIm (RHO) framework is stable up to 300 ^{o}C, without phase change and all the characteristic peaks matches well with the respective simulated one. But in the case of CoNIm (SOD), the framework is stable up to 150 ^{o}C only, after that an extra peak appears at 7 degree (2θ), which indicates some structural change. However, the rest of the diffraction pattern remains identical with few broadening and reduction of intensity in peaks. This could be the result of the escape of solvent molecule (DEF/DMF) at high temperature, which induced some structural change into the framework of CoNIm (SOD) ZIF.

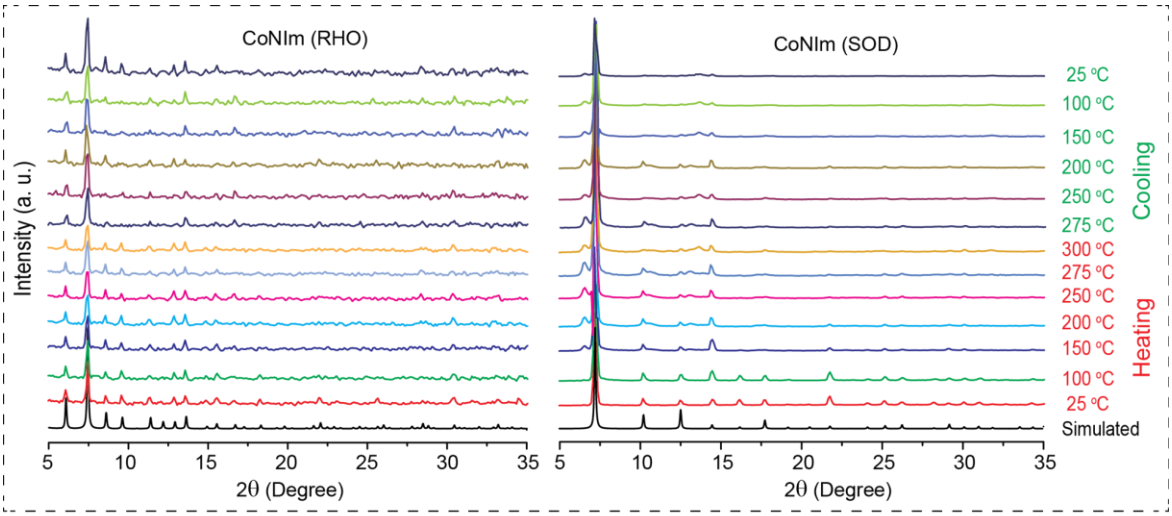

Figure 2.8. *Experimental VT-PXRD patterns of CoNIm (RHO) and CoNIm (SOD) ZIF from 25 ℃ to 300 ℃ and 300 ℃ to 25 ℃.*

2.2.4 *Surface area determination and gas adsorption measurements*

Nitrogen adsorption-desorption experiments were performed to examine the architectural rigidity and permanent porosity of guest-free CoNIm (RHO) and CoNIm (SOD) frameworks (***Figure 2.9a***). In order to make the framework guest-free, these samples were immersed in dry methanol/dichloromethane (DCM) (v/v, 1: 1) mixture for solvent exchange, followed by thermal activation at an optimized temperature of 120 °C, up to 48 h. The N_2 adsorption isotherms collected at 77 K temperature and 1 bar pressure shows typical type-I behaviour with a steep increase in low relative pressure for CoNIm (RHO), suggesting the dominating micropore characteristic. The activated sample of CoNIm (RHO) exhibits the Brunauer-Emmet-Teller (BET) and Langmuir surface area as high as 1858 m^2g^{-1} and 2087 m^2g^{-1} respectively, using the data point on the adsorption branch in the range of P/P_o = 0.01-0.1. To best of our knowledge, the surface area values obtained for CoNIm (RHO) are highest among all ZIFs reported till date (***Table 2.1***). Also, we looked for the micropore volume and is 0.827 cm^3g^{-1} for CoNIm (RHO) based on the single data point at P/P_o = 0.1. Similarly, N_2 adsorption isotherm of CoNIm (SOD) shows type-I at low pressure, with BET and Langmuir surface area of 1097 m^2g^{-1} and 1235 m^2g^{-1} respectively and a micropore volume of 0.477 cm^3g^{-1}, at P/P_o = 0.1. It is noteworthy that, previously reported RHO topology ZIFs, ZIF-11 and -12 (d_a~3 Å) are non-porous towards nitrogen, as the pore

apertures was below the kinetic diameter of N_2 (3.6 Å). ZIF-71 (d_a~4.2Å) due to the presence of two –Cl group at 4 and 5 positions, result into moderate BET surface area of 652 m^2g^{-1} [2.17a]. A recent report of a ZIF [Zn(nim)(pur)] with RHO net also shows a surface area of 900 m^2g^{-1}, which is much lower than CoNIm (RHO) [2.18]. High surface area of CoNIm (RHO) results due to the large cage [22.3 Å] with high pore aperture [(d_a) of 7.1 Å], which allow more N_2 gas molecules migrate towards the cage (***Figure 2.9b***). But in the case of CoNIm (SOD) due to narrow pore aperture (3.4 Å) with pore diameter (10.4 Å), less amount of N_2 gas molecules can be absorbed into the cage, which results in less surface area. From previous literature reports, it is clear that the H_2 and CO_2 uptake can be enhanced by pore architecture as well as functionalization of the pore [2.1a,b and 2.2]. Since CoNIm (RHO) has high surface area, large pores and exposed $–NO_2$ functionality with imidazolate linkers, we decided to collect H_2 and CO_2 adsorption isotherms for both CoNIm (RHO) and CoNIm (SOD) ZIF. CoNIm (RHO) showed high H_2 uptake of 1.5 wt% at 77 K and 1 bar pressure, which is comparable with Bio-MOF-11 (1.5 wt% at 77 K) [2.19] and higher than ZIF-11 (RHO, 1.4 wt%), ZIF-8 (SOD, 1.3 wt%)[2.1a], MOF-177 (1.25 wt%) [2.19b], CPM-5 (1.2 wt%) [2.19c], BIF-9-Li (RHO, 1.2 wt%) [2.19d], ZIF-20 (LTA, 1.1 wt%) [2.19e] and rho-ZMOF (0.91 wt%) [2.16b] but less than that of SNU-6 (1.6 wt%) [2.19f], MOF-74 (1.7 wt%) [2.19g] and MOF-5 (2 wt%) [2.19h]. CoNIm (SOD) showed lower H_2 uptake of 1.1 wt% at identical conditions.

Table 2.1. *List of most highlighted ZIFs and their BET surface area*.*

Sr. no.	ZIFs	Topology	Surface area (BET) in m^2g^{-1}	Reference
1	CoNIm (RHO)	RHO	1858	This work
2	ZIF-70	GME	1730	2.4a
3	ZIF-8	SOD	1630	2.1a
4	BIF-9-Li	RHO	1523	2.19d
5	ZIF-82	GME	1300	2.4a
6	BIF-9-Cu	RHO	1287	2.19d
7	ZIF-90	SOD	1270	2.1e
8	ZIF-25	RHO	1110	2.14
9	CoNIm (SOD)	SOD	1097	This work
10	ZIF-68	GME	1090	2.4a
11	ZIF-91	SOD	1070	2.1e
12	Rho-ZMOF	RHO	1067	2.1f
13	ZIF-95	POZ	1050	2.16a
14	ZIF-96	RHO	960	2.14
15	ZIF-69	GME	950	2.4a
16	Zn(nIm)(pur)	RHO	897	2.18
17	ZIF-93	RHO	864	2.14
18	ZIF-79	GME	810	2.4a
19	ZIF-81	GME	760	2.4a
20	ZIF-71	RHO	652	2.14
21	ZIF-78	GME	620	2.4a
22	ZIF-100	MOZ	595	2.16a

**Except CdIF-4 and -9[2.1g] as BET surface area data was not available.*

The H_2 adsorption behaviour of both CoNIm (RHO) and CoNIm (SOD) shows type-I isotherms (***Figure 2.9c***). However, the initial uptake (P/P_o <0.24) of CoNIm (SOD) ZIF is slightly higher than that of CoNIm (RHO) at low pressure (0.2 bar) but as the pressure approaches 1 bar, because of large cage in CoNIm (RHO) with more exposed imidazolate linker which facilitates more H_2 gas adsorbed (kinetic diameter 2.89 Å) into the cage. High

surface area and a large cage with suitable pore opening support well for high H_2 adsorption in CoNIm (RHO). On the other hand, CoNIm (SOD) framework has comparatively low H_2 uptake that could be because of the narrow pore opening with small cage which favours only limited amount of H_2 gas into the cage.

CO_2 capture in ZIFs became an area of interest owing to their stability compared to many literature reported MOFs [2.19h]. From previous reports, it has been proved that the polar functional group (*i.e.*, $–NH_2$) on the frameworks interact with the CO_2 molecules and enhances the CO_2 capture due to the change of quadruple moment [2.20].

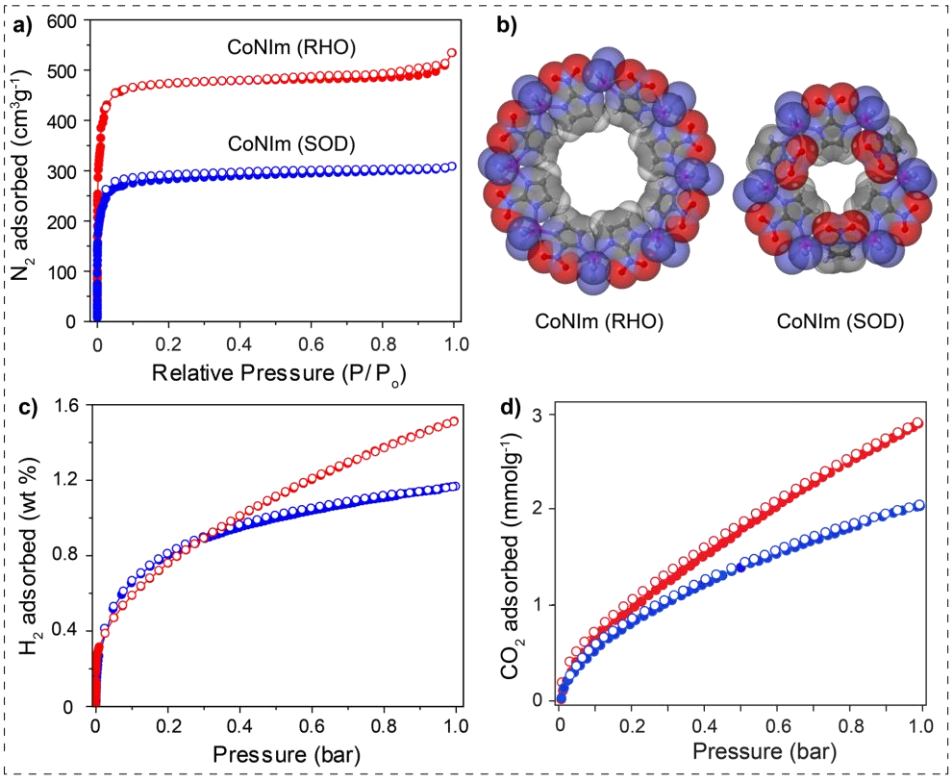

Figure 2.9. *a) N_2 adsorption isotherms of activated samples at 77 K temperature; b) space fill models indicate the pore opening for gas access; c) H_2 adsorption isotherms at 77 K temperature; d) CO_2 adsorption isotherms at 273 K (indicated by spheres) and 298 K (indicated by squares) temperatures. A filled and open circle represents adsorption and desorption respectively.*

As CoNIm (RHO) and CoNIm (SOD) contains free $–NO_2$ functionality to interact with CO_2 and this feature encouraged us to examine the CO_2 adsorption properties of both the CoNIm (RHO) and CoNIm (SOD) ZIFs at 273 and 298 K (***Figure 2.9d***). CoNIm (RHO) ZIF adsorbed 2.99 mmol g^{-1} (273 K) and 1.92 mmol g^{-1} (298 K) of CO_2 at 1 bar pressure, which outperforms all RHO ZIFs reported; such as ZIF-93 (1.6 mmol g^{-1} at 298 K), ZIF-25 (0.9

mmol g^{-1} at 298 K), ZIF-71 (0.65 mmol g^{-1} at 298 K) etc. [except ZIF-96 (2.16 mmol g^{-1} at 298 K)] [2.14], as well other ZIFs belonging to GME topology with large pore aperture and polar functionality, like ZIF-70 (2.45 mmol g^{-1} at 273 K), ZIF-69 (1.69 mmol g^{-1} at 298 K), ZIF-79 (2.36 mmol g^{-1} at 273 K), ZIF-81 (2.81 mmol g^{-1} at 273 K) [2.4a]. But CoNIm (RHO) has less CO_2 uptake than ZIF-78 (3.48 mmol g^{-1} at 273 K) and ZIF-69 (3.03 mmol g^{-1} at 273 K) [2.4a]. The CO_2 uptake for CoNIm (SOD) ZIF was 2.0 mmol g^{-1} (273 K) and 1.6 mmol g^{-1} (298 K) respectively at 1 bar pressure. These data suggests that relatively strong interaction between the CoNIm (RHO) framework with CO_2 and H_2 exists at relatively low pressure.

2.3 Conclusions

We have entrapped highly porous, water stable Co(II) based ZIF [CoNIm (RHO)] and thoroughly observed the crystal growth and time-dependent phase transformation from CoNIm (RHO) to a less porous CoNIm (SOD) ZIF. As the CoNIm (RHO) framework's inner cage diameter is 22.3 Å, with pore aperture 7.13 Å, CoNIm (RHO), which showed the highest BET and Langmuir surface area as 1858 m^2g^{-1} and 2087 m^2g^{-1} respectively. CoNIm (RHO) also display unusually high water stability compared to CoNIm (SOD). In addition, CoNIm (RHO) has promising H_2 uptake capacity of 1.5 wt% at (77 K and 1 bar) along with CO_2 uptake capacity of 2.99 mmol g^{-1} (273 K and 1 bar) and 1.92 mmol g^{-1} (298 K and 1 bar) respectively. These gas sorption uptakes are outperformed most of the highlighted ZIFs and some of the well known MOFs reported in the literature. Our findings, on an understanding of crystal growth and ZIF to ZIF time-dependent solution mediated phase transformation could provide a pathway towards the structural evolution and morphological control in the synthesis of novel ZIFs.

2.4 Experimental procedures

2.4.1 *Materials*

2-nitroimidazole (2-NIm) was purchased from 3B Scientific Corporation (China), $Co(NO_3)_2.6H_2O$, methanol, *N*,*N*-diethylformamide (DEF) and dichloromethane (DCM) were purchased from Sigma-Aldrich Chemicals. *N*,*N*-dimethylformamide (DMF) was purchased from Rankem Chemicals. All starting materials were used without further purification. All experimental operations were performed in 5 mL glass vial inside a programmed oven for CoNIm (RHO) and CoNIm (SOD) ZIF synthesis. Leica M-80 optical microscope with hot stage and camera attachment was used for collecting photographs of ZIF crystals.

2.4.2 *Synthesis of CoNIm (RHO)*

A 0.056 g of 2-NIm in 2.5 mL of DEF (0.20 M, 0.49 mmol) and 0.072 g of $Co(NO_3)_2.6H_2O$ in 1.25 mL DEF solution (0.20 M, 0.24 mmol) were mixed together in a 5 mL glass vial. Then the resulting solution was heated in an oven at 120 °C and allowed to react solvothermally for 12 h. The resulting product was in the form of pink rhombic dodecahedron shaped single crystals. Then washed with DEF and dried in air to get ~10-15 mg of pure crystals of CoNIm (RHO) (Yield: 22%). *FT-IR*: (4000–600 cm^{-1}): 2926(w), 1651(s), 1527(w), 1476(m), 1253(w),1157(m), 1093(w), 946(w), 827(w), 792(s), 657(w). *Elemental analysis (activated)*: Calcd. (%) C, 24.24; H, 1.3; N, 29.67; Found (%): C, 24.16; H, 1.41; N, 27.87.

2.4.3 *Synthesis of CoNIm (SOD)*

A 0.056 gm of 2-NIm in 2.5 mL of DMF (0.20 M, 0.49 mmol) and 0.072 gm of $Co(NO_3)_2.6H_2O$ in 1.25 mL DMF solution (0.20 M, 0.24 mmol) were mixed together in a 5 mL glass vial. Then the resulting solution was heated in an oven at 120 °C and allowed to react solvothermally up to 24-27 h. The resulting product was in the form of pink cube-shaped single crystals, was washed with DMF and dried in air to get ~10-15 mg of pure crystals of CoNIm (SOD). (Yield: 22%). *FT-IR*: (4000– 600 cm^{-1}): 2926(w), 1651(s), 1527(w), 1476(m), 1253(w),1157(m), 1093(w), 946(w), 827(w), 792(s), 657(w). *Elemental analysis (activated)*: Calcd. (%) C, 25.43; H, 1.4; N, 29.67; Found (%): C, 25.09; H, 1.45; N, 28.07.

2.4.4 *General methods for characterization*

a) ***Powder X-Ray diffraction (PXRD)*:** The PXRD patterns were collected on a Phillips PANalytical diffractometer on a Cu Kα radiation (λ = 1.5406 Å), with a scan speed of 2° min^{-1}. The tube voltage and amperage were set at 40 kV and 50 mA respectively. Each sample was scanned between 5 and 50° 2θ with a step size of 0.02°. The instrument was previously calibrated using a silicon standard.

b) ***Thermogravimetric analysis (TGA)*:** TGA was performed on an SDT Q600 TG-DTA analyzer instrument. 5 mg of the sample was added to a platinum crucible and heated from 25 to 800 °C under N_2 atmosphere at a heating rate of 10 °C min^{-1}.

c) ***FT-IR spectroscopy*:** The Fourier transform infrared (FT-IR) spectra were taken on a Bruker Optics ALPHA-E spectrometer with a universal Zn-Se ATR (attenuated total reflection) accessory in the 600-4000 cm^{-1} region or using a Diamond ATR (Golden Gate).

d) ***Scanning Electron Microscopy (SEM)*:** SEM images were obtained with an FEI, QUANTA 200 3D Scanning Electron Microscope with tungsten filament as electron source operated at 10 kV. The samples were sputtered with Au (nano-sized film) prior to imaging by an SCD 040 Balzers Union as well as by sprinkling the powder on carbon tape.

e) ***Gas adsorption measurements***: Low-pressure volumetric gas adsorption measurements were performed at 77 K for N_2, maintained by a liquid nitrogen bath, with pressures ranging from 0 to 760 Torr on a Quantachrome, Quadrasorb automatic volumetric instrument. CO_2 adsorption measurements were carried out at 273 K within the same pressure range. Ultra-high-purity H_2 was obtained by using calcium aluminosilicate adsorbents to remove trace amounts of water and other impurities before introduction into the volumetric system. The pink coloured micro-crystals of CoNIm zeolitic framework were soaked in dried CH_2Cl_2 (DCM): MeOH (v/v 1:1) mixture for 12 h. Freshly dried CH_2Cl_2: MeOH (v/v 1:1) mixture was subsequently added and the crystals were kept for additional 48 h to remove free solvates presented in the framework. The so-obtained material was dried under dynamic vacuum (< 10^{-3} Torr) at room temperature overnight. The sample was heated under dynamic at 60 ºC (12 h) to remove the solvent present on the surface and then further heated to 120 ºC (24 h) to remove the non-coordinated solvent molecule (DEF and DMF).

Apparent surface areas of 2087 m^2g^{-1} (Langmuir model) and 1864 m^2g^{-1} (Brunauer–Emmett–Teller (BET) model [2.21] for CoNIm (RHO) and CoNIm (RHO) ZIF has apparent surface areas of 1235 m^2g^{-1} (Langmuir model) and 1097 m^2g^{-1} (Brunauer– Emmett–Teller (BET) were obtained by using the data points (P/P_o= 0.01-0.1) on the adsorption branch.

f) ***Water adsorption measurements of CoNIm (RHO)*:** Low-pressure volumetric water adsorption measurements were performed at 293K, with pressure ranging from 0 to 0.9 [relative pressure (P/P_o)] on a Quantachrome Autosorb-iQ-MP automatic volumetric instrument. The pink coloured crystals of CoNIm (RHO) were activated using the standard protocol described above.

2.4.5 *X-ray crystallography*

2.4.5.1 *General data collection and refinement procedures*

All Data was collected on a Super Nova Dual source X-ray diffractometer system (Agilent Technologies) equipped with a CCD area detector and operated at 250 W power (50 kV, 0.8 mA) to generate Mo Kα radiation (λ = 0.71073 Å) and Cu Kα radiation (λ = 1.54178 Å). The crystal reported in this paper was mounted on nylon CryoLoops (Hampton Research) with Paraton-N (Hampton Research). Initial scans of each specimen were performed to obtain preliminary unit cell parameters and to assess the mosaicity (breadth of spots between frames) of the crystal to select the required frame width for data collection. CrysAlis^{Pro} program software has used the suite to carry out overlapping φ and ω scans at detector (2θ) settings (2θ = 28). Following data collection, reflections were sampled from all regions of the Ewald sphere to re-determine unit cell parameters for data integration. In no data collection was evidence for crystal decay encountered. Following an exhaustive review of collected frames, the resolution of the dataset was judged. Data were integrated using CrysAlis^{Pro} software with a narrow frame algorithm. Data were subsequently corrected for absorption by the program SCALE3 ABSPACK [2.22a] scaling algorithm. These structures were solved by a direct method and refined using the SHELXTL 97 [2.22b] software suite. Atoms were located from an iterative examination of difference F-maps following least-squares refinements of the earlier models. The final model has refined anisotropically (if the number of data permitted) until full convergence was achieved. Hydrogen atoms were placed in

calculated positions (C-H = 0.93 Å) and included as riding atoms with isotropic displacement parameters 1.2-1.5 times Ueq of the attached C atoms. In some cases, modeling of electron density within the voids of the frameworks did not lead to the identification of recognizable solvent molecules in these structures, probably due to the highly disordered contents of the large pores in the frameworks. Highly porous crystals that contain solvent-filled pores often yield raw data were observed strong (high intensity) scattering becomes limited to ~1.0 Å at best, with higher resolution data present at low intensity. A common strategy for improving X-ray data, increasing the exposure time of the crystal to X-rays, did not improve the quality of the high angle data in this case, as the intensity from low angle data-saturated the detector and minimal improvement in the high angle data were achieved. Additionally, diffused scattering from the highly disordered solvent within the void spaces of the framework and from the capillary to mount the crystal contributes to the background and the 'washing out' of the weaker data. The only optimal crystals suitable for analysis were generally small and weakly diffracting. Unfortunately, larger crystals, which would usually improve the quality of the data, presented a lowered degree of crystallinity and attempts to optimize the crystal growing conditions for large high-quality specimens have not yet been fruitful. Data were collected at 293(±2) K for the CoNIm (RHO) ZIF presented in this paper. Electron density within void spaces has not been assigned to any guest entity but has been modeled as isolated oxygen and/or carbon atoms. The foremost errors in all the models are thought to lie in the assignment of guest electron density. The structure was examined using the Adsym subroutine of PLATON [2.22c] to assure that no additional symmetry could be applied to the models. SQUEEZE on PLATON has been used to remove highly disordered solvent molecules floating inside the cage. The ellipsoids in ORTEP diagrams are displayed at the 50% probability (***Figure 2.10***). For all structures, we note that elevated R-values are commonly encountered in MOF crystallography for the reasons expressed above by us and by other research groups [2.22d-m]. Crystallographic data (excluding structure factors) for the structures are reported in this work have been deposited with the CCDC as deposition No. CCDC 886561(for SQUEEZE) and 906118 (non-SQUEEZE). Copies of the data can be obtained, free of charge, on application to the CCDC, 12 Union Road,Cambridge CB2 lEZ, U.K. [Fax: +44 (1223) 336 033; *E-mail*: deposit@ccdc.cam.ac.uk].

2.4.5.2 ***Experimental and refinement details for CoNIm (RHO)***

A pink rhombic dodecahedron crystal (0.28 × 0.15 × 0.12 mm^3) of CoNIm (RHO) was placed in 0.7 mm diameter nylon CryoLoops (Hampton Research) with Paraton-N (Hampton Research). The loop was mounted on a Super Nova Dual source X-ray Diffractometer system (Agilent Technologies) equipped with a CCD area detector and operated at 250 W power (50 kV, 0.8 mA) to generate Mo Kα radiation (λ = 0.71073 Å) and Cu Kα radiation (λ = 1.54178 Å) at 293(2) K. A total of 8985 reflections were collected of which 2308 were unique. The range of θ was from 3.73 to 71.42°. Analysis of the data showed negligible decay during collection. CoNIm (RHO) ZIF structure was solved in *Im*-3*m* (cubic) space group with 48 (*Z*= 48) Co atoms with a unit cell [*a, b, c* ~ 29.0302(5) and α, β, γ ~ 90°], using direct methods. All non-hydrogen atoms were refined anisotropically with hydrogen atoms generated as spheres riding the coordinates of their parent atoms. The tetrahedrally coordinated Co(II) is surrounded by four 2-nitroimidazole linkers with mirror symmetry. However, Co1 atom lies on a 2-fold symmetry axis and the two (N2—C1 and N4—C3) bonds of either 2-NIm lie on mirror planes (***Figure 2.10***). As a result, the asymmetric unit contains only 0.5 Co(II) atoms and two 0.5 2-NIm unit. The attempts made to model the guests (solvent molecules) did not lead to the identification of guest entities in any of the structures due to the limited periodicity of the solvent molecules in the crystals. Since the solvent is neither bonded to the framework nor tightly packed into the voids, the solvent disorder can be expected for the MOF structures. Thus, electron density within void spaces which could not be assigned to any definite guest entity was modeled as isolated carbon atoms, and the foremost errors in all the models lie with the assignment of guest electron density. "Solvent" is 1 atom refined as nitrogen atoms of undefined solvent, located in a void of the framework. To assess the correctness of the atomic positions in the framework, the application of the SQUEEZE routine of A. Spek has been performed. However, atomic co-ordinates for the "non-SQUEEZE" structures are also presented. Final full matrix least-squares refinement on F^2 converged to R_1 = 0.0875 [I>2σ (I)] and wR2 = 0.2688 (all data) with GOF = 0.871. For the structure where the SQUEEZE program has not been employed, final full matrix least-squares refinement on F^2 converged to *R*1 = 0.1222 [I>2σ (I)] and *wR*2 = 0.3995 (all data) with GOF = 1.032.

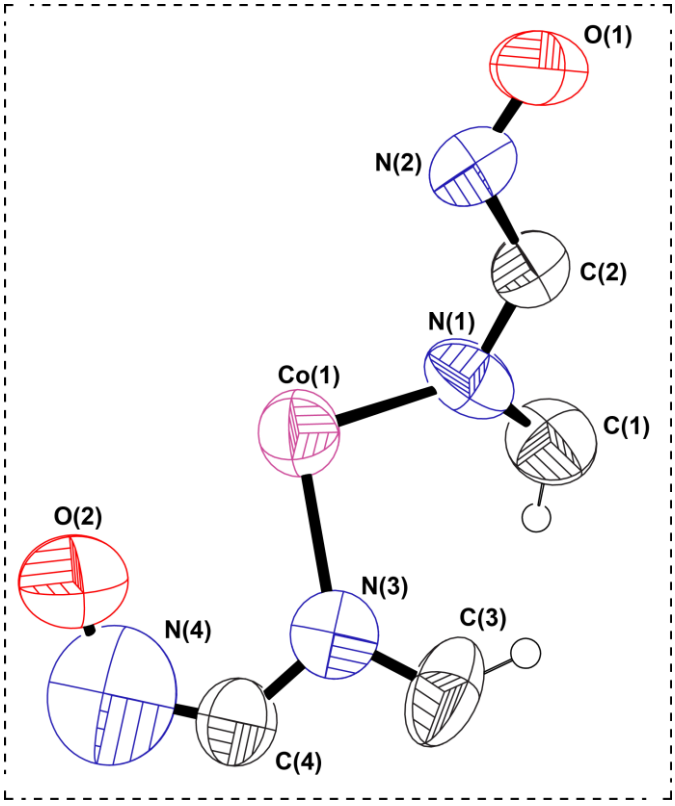

Figure 2.10. *ORTEP drawing of an asymmetric unit of CoNIm (RHO) ZIF generated from SHELXTL 97 software with 50% probability, excluding the guest entities.*

Table 2.2*. Crystal data and structure refinement for CoNIm (RHO).*

Empirical formula	C6 H4 Co N7 O4
Formula weight	297.09
Temperature	293(2)
Wavelength	1.54184 Å
Crystal system	Cubic
Space group	*Im*-3*m*
Unit cell dimensions	a = 29.0302(5) Å, α = 90°
	b = 29.0302(5) Å, β = 90°
	c = 29.0302(5) Å, γ = 90°
Volume	24465.3(7)
Z	48
Density (calculated)	0.968
Absorption coefficient	6.743
F (000)	7104
Crystal size	0.28× 0.15× 0.12 mm^3
Theta range for data collection	3.73 to 71.42°
Index ranges	-19 <= h <= 35, -19 <= k <= 35, -11 <= l <= 35
Reflections collected	9069
Independent reflections	2308
Completeness to theta = 71.42°	98.4%
Absorption correction	Semi-empirical from equivalents
Refinement method	Full-matrix least-squares on F^2
Data / restraints / parameters	2308/0/89
Goodness-of-fit on F2	1.032
Final R indices [I>2σ(I)]	R1 = 0.1222, wR2 = 0.3445
R indices (all data)	R1 = 0.2231, wR2 = 0.3995
Largest diff. peak and hole	0.121 and -0.419 e.$Å^{-3}$

Table 2.3*. Crystal data and structure refinement for CoNIm (RHO) (SQUEEZE).*

Empirical formula	C6 H4 Co N6 O4
Formula weight	283.08
Temperature	293(2)
Wavelength	1.54184 Å
Crystal system	Cubic
Space group	*Im*-3*m*
Unit cell dimensions	a = 29.0302(5) Å, α = 90°
	b = 29.0302(5) Å, β = 90°
	c = 29.0302(5) Å, γ = 90°
Volume	24465.3(7)
Z	48
Density (calculated)	0.922
Absorption coefficient	6.709
F (000)	6768
Crystal size	0.28× 0.15× 0.12 mm^3
Theta range for data collection	3.73 to 71.42°
Index ranges	-19 <= h <= 35, -19 <= k <= 35, -11 <= l <= 35
Reflections collected	8985
Independent reflections	2308
Completeness to theta = 71.42°	97.7%
Absorption correction	Semi-empirical from equivalents
Refinement method	Full-matrix least-squares on F^2
Data / restraints / parameters	2308/0/80
Goodness-of-fit on F2	0.871
Final R indices [I>2σ(I)]	R1 = 0.0875, wR2 = 0.2338
R indices (all data)	R1 = 0.1648, wR2 = 0.2688
Largest diff. peak and hole	0.082 and -0.379 e.$Å^{-3}$

NOTE: The results of this chapter have already been published in *Chem. Commun.*, **2012**, *48*, 11868-11870, with the title: "*Solution Mediated Phase Transformation (RHO to SOD) in Porous Co-Imidazolate based Zeolitic Framework with High Water Stability"*. This publication was the result from the group of Dr. Rahul Banerjee with his student Mr. Bishnu Prasad Biswal from the Physical/Materials Chemistry Division at CSIR-National Chemical Laboratory, Pune, India. Major work was contributed by Mr. Bishnu Prasad Biswal with the help of the instrumental facilities of CSIR-National Chemical Laboratory. Mr. Tamas Panda helped in single crystal data analysis. The manuscript was primarily written by Mr. Bishnu Prasad Biswal under the supervision of Dr. Rahul Banerjee.

CHAPTER 3

Selective Fabrication of Metal-Organic Frameworks on Polybenzimidazole (PBI) based Hollow Fiber Membrane *via* Interfacial Approach for Gas Separation

Abstract: *Metal-organic frameworks (MOFs) are a new class of materials, which have gained immense scientific attention due to their tuneable properties and diverse applicability. Yet, efforts on developing such materials for membrane-based separation, still remains a key challenge. In this chapter, we have demonstrated a new, convenient and room temperature scalable interfacial MOF (ZIF-8 and CuBTC) growth on either outer or inner side of a polybenzimidazole based hollow fiber membrane (PBI-BuI-HF) surface in a controlled manner. The selective growth of MOFs on PBI-BuI-HF was made possible by choosing an appropriate immiscible solvent pair and manipulating synthetic conditions. The growth of MOF crystals on PBI-BuI-HF via interfacial approach was continuous and showed appreciable gas separation performance, conveying promises towards their applicability in the real life.*

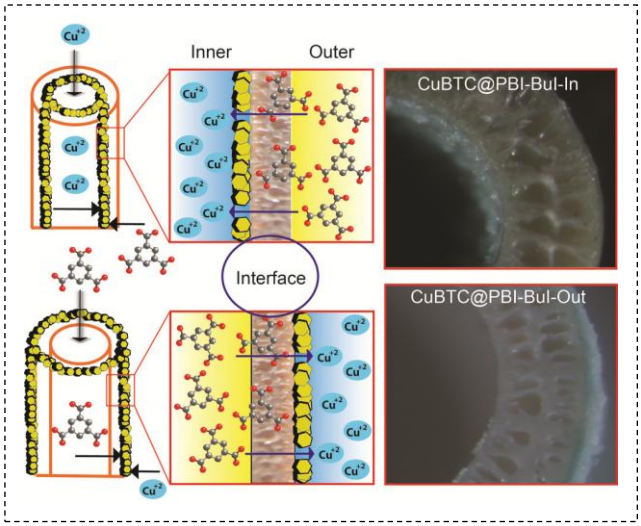

3.1 Introduction

Metal–organic frameworks (MOFs) [3.1] are new age crystalline, porous materials with outstanding properties like gas storage [3.2], catalysis [3.3], sensing [3.4], electronics [3.5], and drug delivery [3.6]. Although MOF research has been studied since last 15 years, the fabrication of MOF-based membranes [3.7] for different gas/liquid separation has geared up only in recent years. A few reports have been demonstrated that porous MOFs can be grown on various inorganic and organic supports such as alumina [3.8], silica [3.9], carbon materials [3.10], etc. for gases/liquids separation. However, these MOF-based membranes suffer some difficulties due to scale-up in hydrothermal synthetic approach, problems in continuous film formation, rigid support, etc. [3.11]. These issues hinder their practical utility in real separation application. To overcome the issues mentioned above researchers thought to grow MOFs on flexible polymeric membrane supports [3.12], in which MOFs can take a position within the pores of the polymeric membrane and will be responsible for interesting molecular separation. Although there have been very few demonstrations on MOF growth on the surface of polymer membranes, but actual benefits of MOF@polymer are so far not realized. Moreover, MOF-based mixed matrix membranes (MMMs), a kind of polymer composite membranes often result in sedimentation, crystal agglomeration and overloading of MOF crystals can result into membrane brittleness [3.13]. Therefore, to design and fabricate a defect-free composite membrane with high performance and flexibility, the development of both support material, as well as MOF-synthetic methodology are highly important to bring anticipated advantages into real practice. To fulfill the criteria, polymeric hollow fiber membranes are suitable over other configurations such as flat sheet and porous inorganic membrane structures. This is owing to their good flexibility, large scale production; high pressure withstands capacity and large membrane surface area available per unit volume [3.14]. Noteworthy that, most of the work reported in the literature based on MOF growth on inorganic tubular/polymeric hollow fiber support uses hydrothermal synthesis approach. Very recently, two reports appeared on microfluidic approach for processing MOF membranes on polymeric hollow fiber supports. The first one by Nair *et al.,* in which interfacial microfluidic membrane processing (IMMP) by two immiscible solvents (octanol/water) was successfully demonstrated for the positional control of ZIF-8 formation on poly(amide-imide) hollow fibers installed within a stainless steel custom-made reactor

[3.15a]. The membranes developed showcase very good permeance with high H_2/C_3H_8 and C_3H_6/C_3H_8 separation factors (370 and 12, respectively). On the other hand a report by Coronas *et al.*, wherein ZIF-7 and ZIF-8 continuous membranes were synthesized on the inner surface of polysulfone hollow fiber using microfluidics [3.15b]. The resultant ZIFs/PSf membranes displayed high CO_2/N_2 and CO_2/CH_4 separation factors (13.6 and 13.5, respectively). Although these initial reports demonstrating new method towards the preparation of MOF@HF membranes, more simple techniques for MOF growth on the hollow fiber membranes in large scale remains a dire challenge and needs urgent attention.

In this chapter, we have demonstrated a facile, scalable and room temperature selective fabrication of MOFs (ZIF-8 and CuBTC, structures are shown in ***Figure 3.1***) on both sides (inner or outer surfaces) of polybenzimidazole based hollow fibers (PBI-BuI-HF) using interfacial synthesis method (***Figure 3.2***). Taking the advantages of high miscibility of organic ligands in volatile solvents such as $CHCl_3$ or isobutyl alcohol (IBA) into immiscible water phase containing metal salt can be a determining factor to obtain preferred MOF growth on either side of the hollow fiber (HF) module.

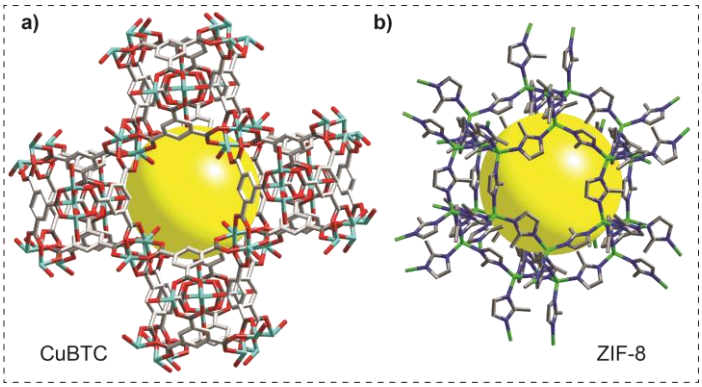

Figure 3.1. *Wire-frame model of a) CuBTC and b) ZIF-8 [cyan: Cu; green: Zn; gray: C; blue: N and red: O]. The yellow ball inside the cage represents the openness of framework.*

We have adopted a solution circulation approach on a HF membrane module to grow MOFs. Such circulation approach offers advantages to forming defect-free continuous MOF membranes on HF support rather than the static growth conditions in which mostly a dense, non-continuous MOF coatings results in the fiber bore [3.15a]. The methodology we have demonstrated herein is very simple than reported earlier and can be easily scalable, as it has been developed directly using membrane module.

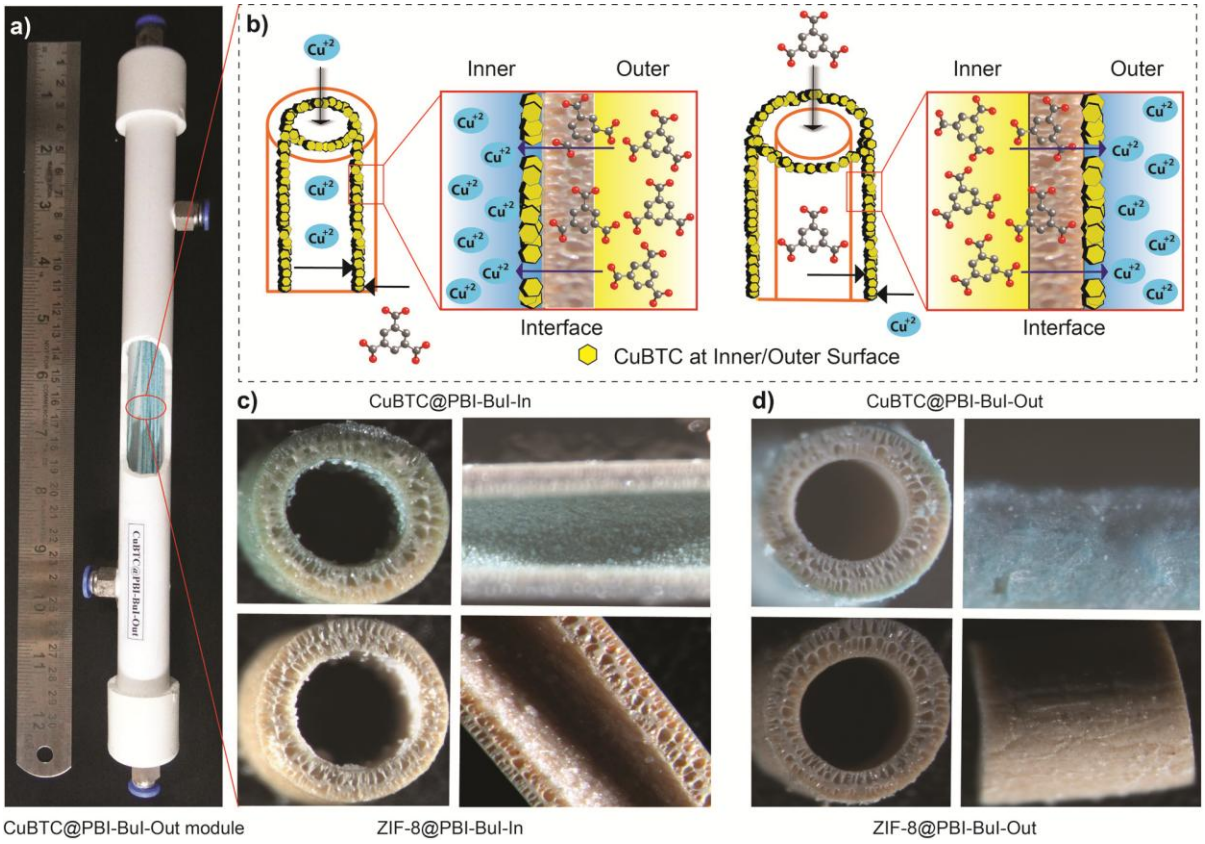

Figure 3.2. *a) Representative digital photograph of a gas separation module [CuBTC growth on the outer surface of PBI-BuI hollow fibers (CuBTC@PBI-BuI-Out) is seen through the cut]; b) Schematic for interfacial synthesis approach of CuBTC@PBI-BuI-In and Out; c) Microscopic images of ZIF-8@PBI-BuI-In, ZIF-8@PBI-BuI-Out, CuBTC@PBI-BuI-In and CuBTC@PBI-BuI-Out composites fabricated.*

In this work, we have chosen polybenzimidazole (PBI-BuI) as membrane material to make hollow fiber membranes and used for MOF growth as it has excellent thermochemical stability [3.16], outstanding mechanical properties even at high temperatures and importantly, a very good compatibility with MOF crystals [3.17]. We have employed an immiscible pair of low boiling solvents [$CHCl_3$, isobutyl alcohol (IBA) and water] for MOF@membrane composite fabrication. These solvents are chosen with an intention that these volatile solvents can be easily removed from the pores of MOF membrane with mild activation process over other high boiling solvents such as octanol (often used for growth of MOFs *via* interfacial synthesis) [3.15a]. Moreover, we have evaluated the gas permeation ability of fabricated MOF@PBI-BuI-HF composite membranes and found that they have potential towards appreciable permeance and selectivity for practical applications.

3.2 Result and discussion

3.2.1 *Wide-angle X-ray diffraction (WAXD) analysis*

We have performed the wide-angle X-ray diffraction (WAXD) analysis to verify the growth of CuBTC and ZIF-8 on PBI-BuI-HF membranes (***Figure 3.3***).

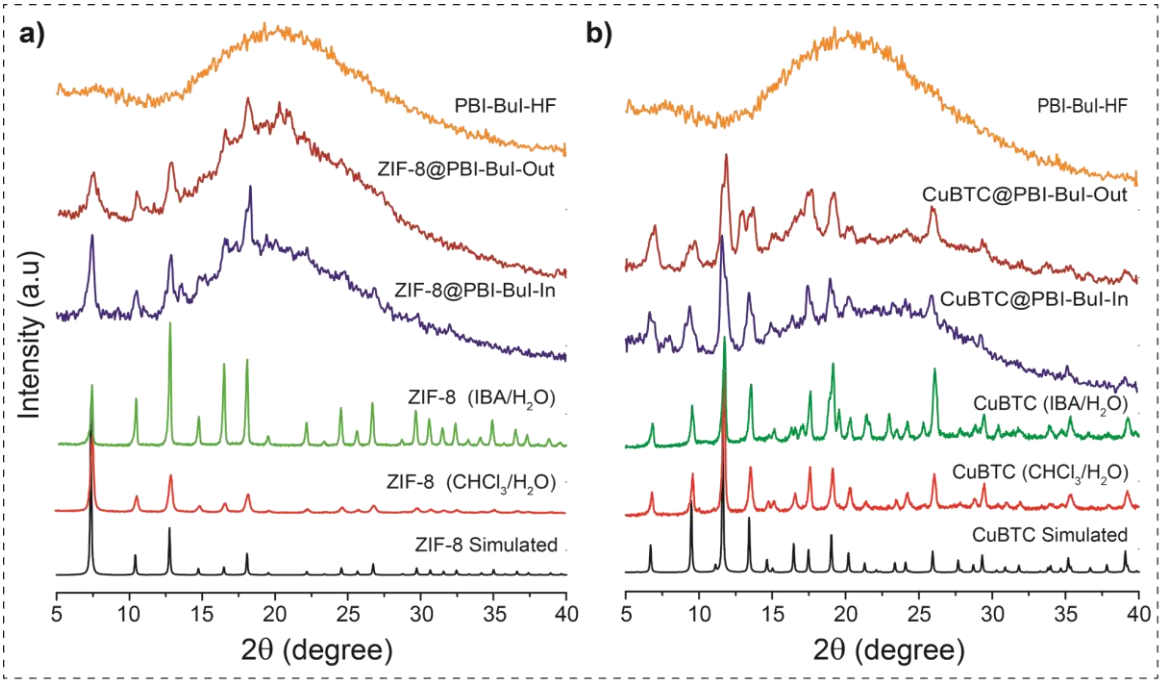

Figure 3.3. *X-ray diffraction of a) ZIF-8 and b) CuBTC; grown on the inner and outer surface of PBI-BuI-HF using interfacial synthesis method in comparison with pristine PBI-BuI-HF, ZIF-8 ($CHCl_3/H_2O$ and IBA/H_2O) and CuBTC ($CHCl_3/H_2O$ and IBA/H_2O).*

Initially, we have collected the WAXD patterns for as-synthesized ZIF-8, CuBTC in $CHCl_3/H_2O$ and IBA/H_2O, matched with their respective simulated patterns obtained from the single crystal X-ray data reported earlier [3.1e and f]. The perfect match between the experimental and simulated patterns confirms that the compound is phase pure and formed successfully in those solvent combinations (***Figure 3.3***). We have also recorded the WAXD profile of pristine PBI-BuI-HF membrane, which showed a broad amorphous hump in the 2θ , 15°-30°, and a smaller hump at 2θ = 6°. Furthermore, the CuBTC@PBI-BuI and ZIF-8@PBI-BuI composites (inner and outer) membranes were analyzed using WAXD to make sure the phase purity of CuBTC and ZIF-8 grown on the membrane surface *via* interfacial synthesis approach. This result confirms that MOF crystals have formed on the PBI-BuI-HF

support is phase pure. This analysis also confirms that MOF growth *via* interfacial synthesis method with different solvent combinations does not affect the crystallinity and structural feature of MOFs.

3.2.2 *Fourier transforms infrared (FT-IR) analysis*

The FT-IR spectrum of pristine PBI-BuI-HF shows an absorption band in the range 1430-1650 cm^{-1} for benzimidazole units. The broadband between ~3145 cm^{-1} and ~ 3410 cm^{-1} was due to the N–H···N hydrogen bonding and the free non-hydrogen bonded N–H stretching. However, the peak at 2862 cm^{-1} in the FT-IR spectrum could be due to the presence of a *tert*-butyl group of PBI-BuI-HF backbone. We have also recorded the FT-IR spectra for the CuBTC@PBI-BuI composite membrane and found that all major bands of CuBTC, *e.g.*, 1647 (C=O symmetric), 1444 (C=C–Ar) and 1369 cm^{-1} (C–O) are appeared, which confirm that the CuBTC crystals are present in the membrane matrix.

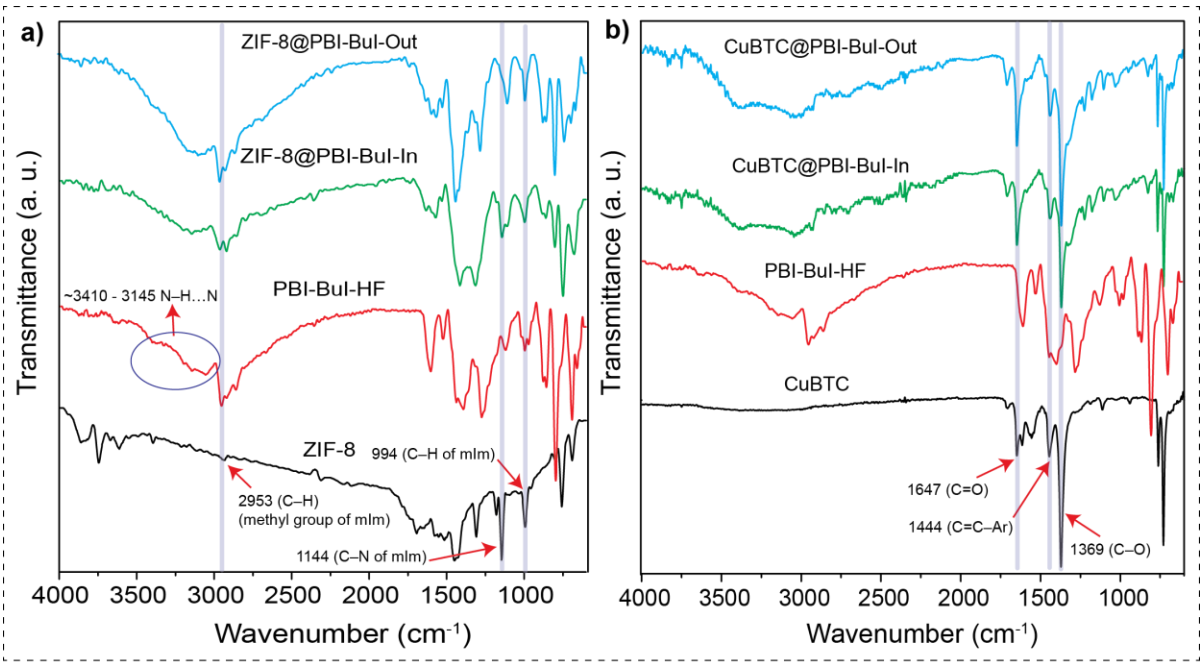

Figure 3.4. *FT-IR of a) ZIF-8@PBI-BuI (In and Out); b) CuBTC@PBI-BuI (In and Out) composite membranes in comparison with pristine PBI-BuI-HF, ZIF-8, and CuBTC.*

Similarly, the weak band at 2953 cm^{-1} (C–H bonds; methyl group of the imidazole ring) appeared for ZIF-8@PBI-BuI composite membranes and was merged with the strong

band of pristine PBI-BuI-HF. Further, it has been seen that few medium bands at 994 cm^{-1} (C–H bonds in the imidazole ring) and 1144 cm^{-1} (C–N bonds in imidazole moiety) of ZIF-8 are also present along with other characteristic bands of PBI-BuI-HF membrane, which confirms the presence of ZIF-8 crystals on the PBI-BuI-HF surface (***Figure 3.4***). However, there is a slight peak shift observed in the FT-IR patterns for In and Out growth of ZIF-8 on PBI-BuI-HF membranes, which could be the result of different extend of interactions between ZIF-8 crystals and HF membrane surface.

3.2.3 *Scanning Electron Microscopy (SEM)*

The SEM imaging was employed to confirm the growth of CuBTC and ZIF-8 crystals on the inner and outer surfaces of PBI-BuI-HF support (***Figure 5a-h***). From the SEM images, it is clear that the crystals are stacked in layers fashion on one another by covering the gaps. This results in a defect-free continuous MOF sheet on PBI-BuI-HF support. ***Figure 3.5*** shows the cross-section SEM images at different magnifications for all the CuBTC@PBI-BuI-HF and ZIF-8@PBI-BuI-HF composites [inner (In) and outer (Out) MOF growth] membranes fabricated. These images infer that the surface of the hollow fiber membrane is covered with MOF crystals as a result of diffusion of metal and ligand ions into the respective immiscible phases. Due to this, MOF crystals were formed extensively at the interface of the two immiscible solvents. As the inner pore voids are not as densely populated as the top surface the chances of diffusion of the metal and ligand ions deeper inside the solution present in fiber pores decrease. Hence, the growth of MOF crystal layers increases on a surface of the HF membrane. This could be a valid reason that drives the crystal growth predominantly on the respective hollow fiber surfaces. The similar observation was also noted for ZIF-8/Torlon membranes reported recently [3.15a]. The crystal shapes of ZIF-8 are dodecahedral and sizes ranging from ~4-8 μm for inner growth (ZIF@PBI-BuI-In) as observed from SEM images. However, relatively small ZIF-8 crystallites (~1-3 μm) with slightly different morphology were observed for the ZIF-8@PBI-BuI-Out membrane. In a similar way, the crystal shapes of CuBTC are a flake like having dimensions ~1 μm thickness/~5 μm length for inner growth and small (~1-2 μm) crystallites agglomerates seen for outer growth on the surfaces of PBI-BuI-HF. Although the exact reason for different morphologies of ZIF-8 and CuBTC crystals of both inner and outer grown hollow fibers are

not fully understood to us, but the sizes and shapes of ZIF-8 and CuBTC are expected to vary. These changes mainly governed by the nature of solvents and the physical parameters like duration of crystallization in the mother liquor, space availability and the environment within the HF membrane. Importantly, it is to note that the WAXD profiles of ZIF-8@PBI-BuI-In/Out and CuBTC@PBI-BuI-In/Out composite membranes matches well with the WAXD profiles of synthesized ZIF-8 and CuBTC, irrespective of their crystal morphologies (***Figure 3.3***).

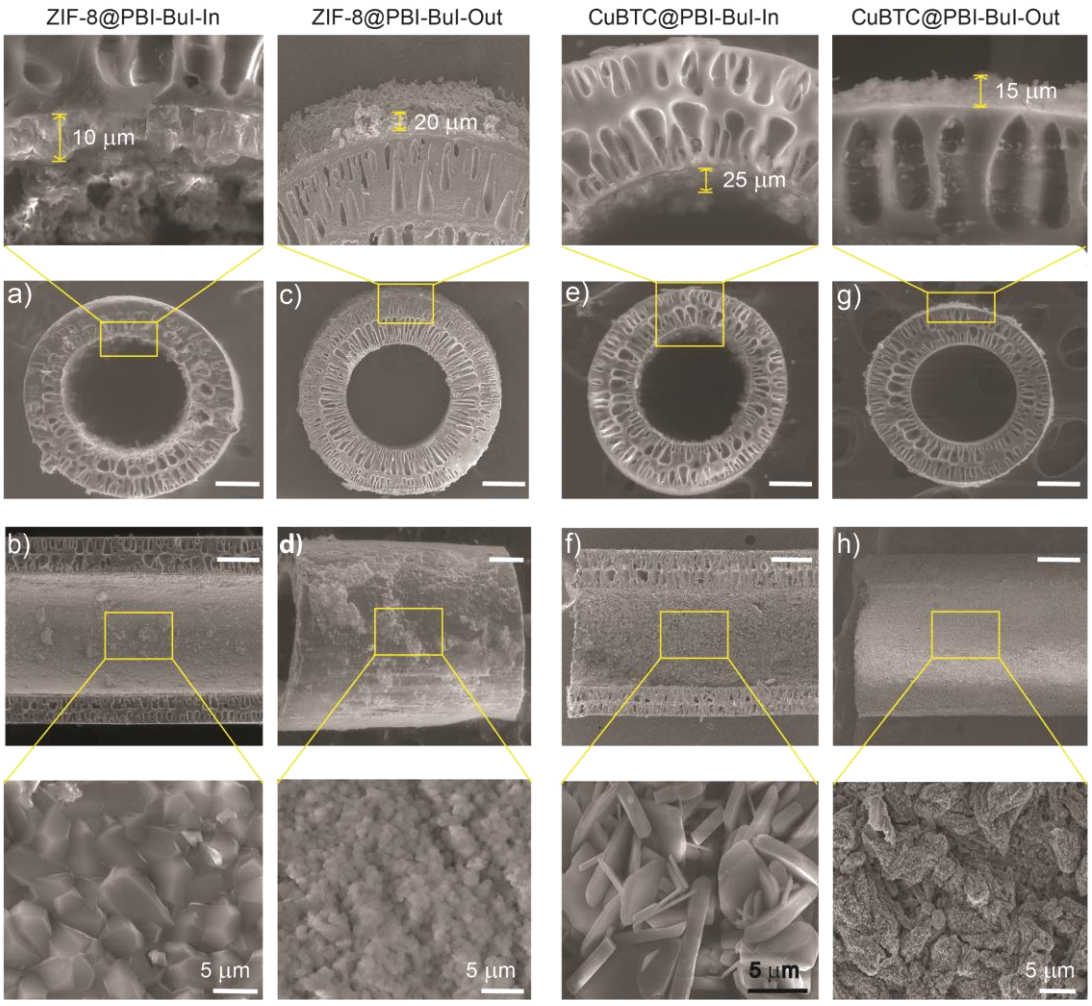

Figure 3.5. *SEM images showing a cross-section of the hollow fiber, its cut along the length and zoomed view; a), b) ZIF-8@PBI-BuI-In; c), d) ZIF-8@PBI-BuI-Out; e), f) CuBTC@PBI-BuI-In; g) and h) CuBTC@PBI-BuI-Out composite membranes respectively. [Top part of a-g represents the zoomed part with a clear cut cross-section showing the thickness of ZIF-8 and CuBTC crystal layer formed on the inner and outer surface of PBI-BuI-HF; whereas bottom part of b-h showing the crystal morphology and continuously packed structures with different magnifications]. (Scale bar for a-h; 200 µm).*

Further, to check the uniformity of MOF layer formation on the PBI-BuI-HF membrane, we obtained cross-sections of the fiber and subsequently measured the membrane thickness at each possible location (***Figure 5a-g, zoomed region***). The average thickness of the CuBTC and ZIF-8 layers on the PBI-BuI-HF membrane was in the range of ~10-25 μm. We have also done the EDAX elemental mapping, which confirms the presence of metals such as Cu and Zn (yellow color) located on the inner circular surface of MOF@PBI-BuI-HF ('N' atoms are designated in red color) composite membranes (***Figure 3.6***).

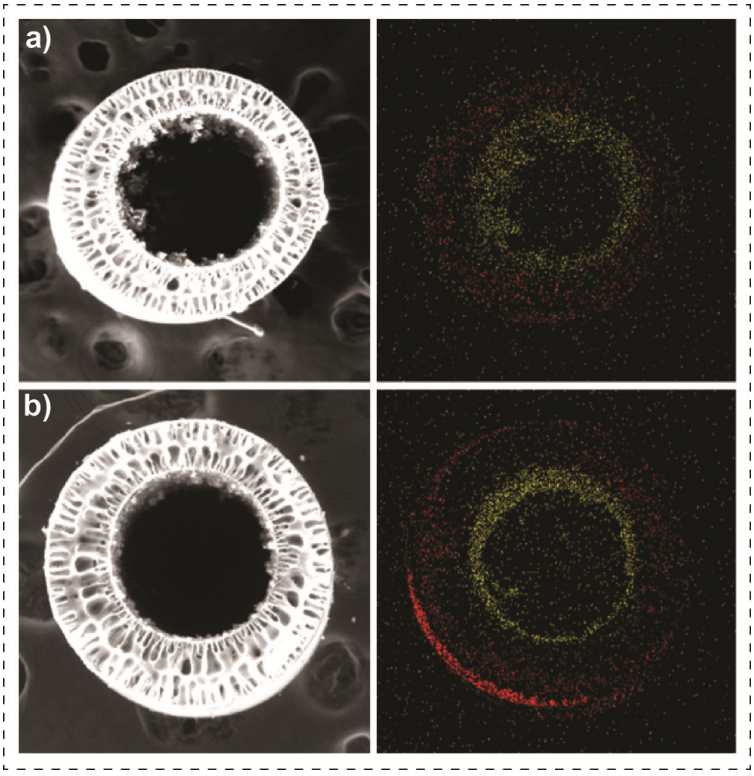

Figure 3.6. *a) and b) Elemental mapping of ZIF-8@PBI-BuI-In and CuBTC@PBI-BuI-In composite membranes [red corresponds to nitrogen signals from PBI-BuI-HF and yellow for Zn and Cu signals from ZIF-8 and CuBTC grew selectively inside the hollow fiber membrane].*

3.2.4 *Selective growth of MOFs on PBI-BuI-HF membranes*

We have successfully employed the interfacial method for the MOF growth on the inner and outer surface of the PBI-BuI hollow fiber membranes by avoiding critical seeding or hydrothermal growth as vastly demonstrated in the literature [3.12 and 3.13]. Our intention was, if we could successfully grow the MOFs selectively on preferred surfaces (inner or outer) with some penetrating within the membrane pores, then the inherent limitation of

MOF films being fragile can be conveniently tackled. Moreover, by using these composite membranes effective molecular level separation can be achieved through MOF pores.

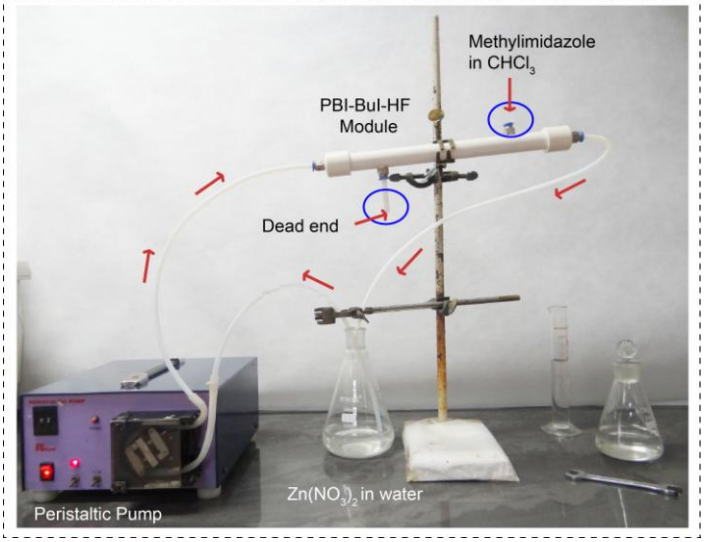

Figure 3.7. *Circulation setup for the growth of ZIF-8 on the inner surface of PBI-BuI hollow fibers (ZIF-8@PBI-BuI-In).*

To achieve selective growth of CuBTC and ZIF-8 crystals on the surface of PBI-BuI hollow fiber membranes, we have used the interfacial MOF synthesis approach, through a well-designed circulation set-up (***Figure 3.7***). The protocol has been optimized *via* a change of solvent pair and flow reversal for the successive growth of MOF films preferentially on inner and outer surfaces as shown in ***Figure 3.1***. Immiscible low boiling solvent pairs such as $CHCl_3$/water and IBA/water were chosen to achieve the interfacial crystallization of ZIF-8 and CuBTC on HF membrane surface, as shown in the digital images (***Figure 3.8***). These solvents were intentionally chosen to take advantages of their easy removal from the MOF pores and membranes after the crystal growth so that they will not interfere with the gas permeation measurements. We have also used an optimized reactants ratio for the formation of both ZIF-8 and CuBTC, the same fixed ratio used to fabricate the MOF on the surfaces of PBI-BuI-HF in an interfacial manner. We also feel that the diffusion of ligands into aqueous phase through the interfacial boundary would control the growth of the crystals than the reactant ratio present in the respective solvent. Our focus was the easy MOF fabrication by using volatile solvents and circulation preferences for the selective MOF growth on either surface (inner and outer) of hollow fiber support. The porous nature of PBI-BuI-HF provides

us high membrane surface area at the immiscible solvent interfaces to achieve effective diffusion of ligand or metal ion.

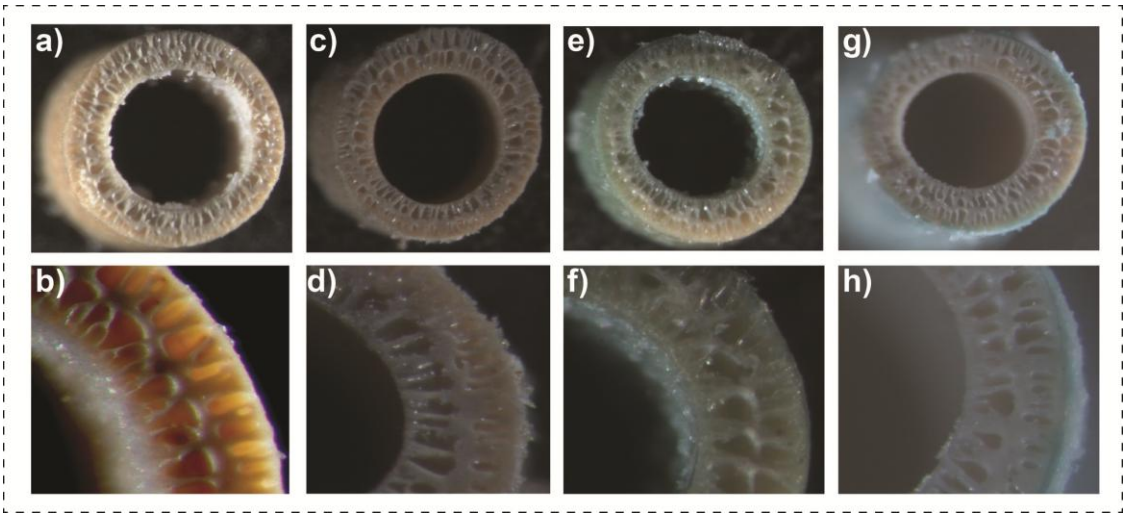

Figure 3.8. *Stereo microscopy images showing MOF growth on PBI-Bu-HF; a), b) ZIF-8@PBI-BuI-In; c), d) ZIF-8@PBI-BuI-Out; e), f) CuBTC@PBI-BuI-In; and g), h) CuBTC@PBI-BuI-Out composites.*

We believe that this would provide not only the MOF nucleation possible at the interfaces but also the effective growth because of the high surface area availability. It is also true that low solubility of metal salts in organic solvents ($CHCl_3$ and IBA) and the high solubility of ligands (2-mIm and BTC) in water are governing the successive growth of MOF on the preferred surface. Further, the affinity of ligand and metal ion to recombine is another key factor for the growth of MOF on preferred surface of PBI-BuI hollow fibers. It has been noticed that the MOF nucleation and growth occurs at the preferred surfaces where an aqueous solution containing metal ions (Zn^{+2} or Cu^{+2}) were present. Such important observations are in very good agreement with the previous report on IMMP of ZIF-8 [3.15a].

3.2.5 *Gas permeation study*

We have evaluated the gas permeance properties of these composite membranes using a variable volume method [3.17] for three gases selected based on their kinetic diameter He (2.89 Å), N_2 (3.64 Å) and C_3H_8 (4.4 Å). ***Figure 3.9*** and ***Table 3.1*** reflects the gas permeance data of the pristine PBI-BuI-HF membrane, ZIF-8@PBI-BuI-In/Out and CuBTC@PBI-BuI In/Out composite membranes, respectively. As pristine PBI-BuI-HF

membranes possess high porosity, it experiences high gas permeance through them. However, when we have conducted the gas permeation experiment on CuBTC@PBI-BuI-In/Out and ZIF-8@PBI-BuI-In/Out composite membranes, the permeance was found to reduce by ~1/3rd compared to the pristine PBI-BuI-HF. All the MOF@PBI-BuI-HF composite membranes prepared retains their flexibility and allows direct contact of the feed gas with MOF so that the pore opening of the MOF can be better utilized as channels for the gases to flow through. Further, between ZIF-8@PBI-BuI and CuBTC@PBI-BuI composites, ZIF-8@PBI-BuI one has higher permeance due to lower coating thickness as evidenced from SEM images (***Figure 3.5***). The difference in MOF membrane thickness could be correlated with the reactivity of Zn^{+2} ions and 2-mIm at the ambient condition leading to a few crystals formation on the support membrane. However, as the reactivity CuBTC is high, the number of crystals formation is also very high and thus the membrane thickness. The permeance in the case of CuBTC@PBI-BuI is low and that led to increasing in the selectivity between gas pairs compared to pristine HF membranes. For example, in the case of CuBTC@PBI-BuI-Out composite membrane, the selectivity of He/N_2 has been increased from 1 to 12 and also He/C_3H_8 from 1.1 to 17. However, the He/N_2 and He/C_3H_8 selectivity was 8 and 8.7, respectively for CuBTC@PBI-BuI-In composite membrane (***Figure 3.9***).

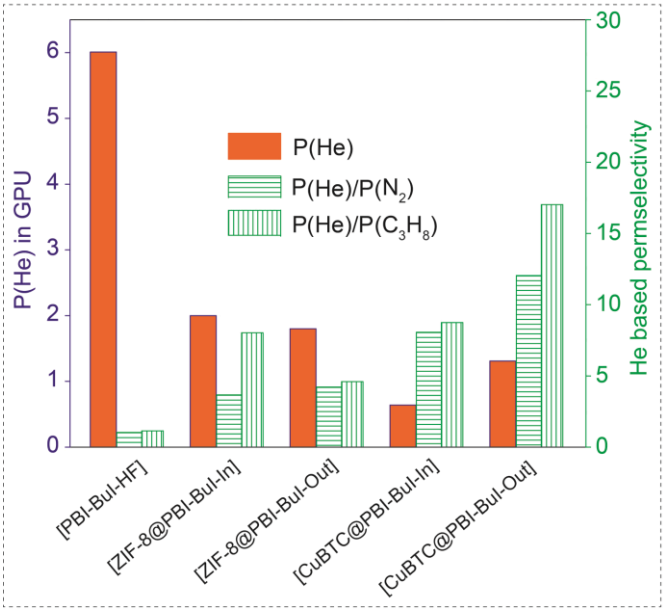

Figure 3.9. *He permeance and its selectivity over N_2 and C_3H_8 for pristine PBI-BuI-HF and MOF@PBI-BuI-HF-In/Out composite membranes.*

Table 3.1. *Permeance and selectivity data of MOF@PBI-BuI-HF composite membranes.*

Hollow Fiber membranes	P(He)	$P(N_2)$	$P(C_3H_8)$	$P(He)/P(N_2)$	$P(He)/P(C_3H_8)$
PBI-BuI-HF	6.01	5.81	5.29	1.04	1.14
ZIF-8@PBI-BuI-In	2	0.54	0.25	3.67	8.03
ZIF-8@PBI-BuI-Out	1.80	0.43	0.39	4.22	4.60
CuBTC@PBI-BuI-In	0.89	0.11	0.10	8.07	8.74
CuBTC@PBI-BuI-Out	1.31	0.11	0.08	12.05	17.02

*Permeance (P) expressed in GPU,
(1 GPU = 1×10^{-6} cm s^{-1} cm Hg^{-1} = 3.348×10^{-10} mol m^{-2} s^{-1} Pa^{-1}).

On the other hand, ZIF-8@PBI-BuI-In composite shows the selectivity of He/N_2 and He/C_3H_8 as 3.7 and 8 respectively, but ZIF-8@PBI-BuI-Out displayed low selectivity (He/N_2, 4.2 and He/C_3H_8, 4.6). Although CuBTC@PBI-BuI-Out showed an appreciable selectivity of 12 (He/N_2), the He permeance value is low (1.3 GPU), compared to other CuBTC@membranes reported in the literature (***Table 3.2***).

Table 3.2*. Permeance and selectivity data of some reported CuBTC@Support membranes.*

MOF	Substrate	$P(H_2)$ in GPU	$P(H_2)/P(N_2)$	Temp.	References
CuBTC	Copper net	4480.3	7	RT	3.18a
CuBTC	PSF	236	-	RT	3.12a
CuBTC	α-Al_2O_3 discs	1194.7	3.7	RT	3.18b
CuBTC	Porous SiO_2 metal net	2986.9	8.91	25-60	3.18c
CuBTC	α-Al_2O_3 tube	119.5	8.66	RT	3.18d
CuBTC	PBI-BuI-HF	1.31 (He)	12.05	RT	*This work*

The low gas permeance of MOF@PBI-BuI-HF composite membranes arises due to the PBI-BuI-HF support used, which itself has a low He permeance of 6 GPU. Importantly, it may be noted that the membrane porosity of any HF support can be increased by lowering the concentration of polymer in the dope solution during the fiber spinning [3.19]. Moreover, the selective permeance of gases through our composite membranes is indicated that the MOF

layer formation is continuous on the top of flexible and scalable PBI-BuI-HF membranes. Indeed, the chemical nature of PBI-BuI (presence of benzimidazole groups) would additionally provide very good hydrogen bonding interactions [3.20] with metal ions (Cu/Zn) and therefore a good adhesion between MOF crystals and PBI-BuI-HF surface is established. As a result, the selective growth of MOFs on PBI-BuI-HF support leads to considerable improvement in the gas selectivity of PBI-BuI-HF. We believe that further optimization and selection of hollow fibers support with high porosity, the methodology, we presented can give rise to better performance for practical utility. More prominently, our methodology offers continuous MOF growth at room temperature and does not need any external seeding, as usually done for such MOF growth on the porous substrates.

3.3 Conclusions

In summary, we reveal a methodology to growth MOF crystals selectively on preferred surfaces (inner or outer) of a porous polymeric (PBI-BuI-HF) substrate employing interfacial synthesis method. The methodology, we have demonstrated has its own merits owing to the ease of MOF growth without any pre-seeding. Moreover, we introduced the use of volatile solvents ($CHCl_3$, IBA and H_2O) to synthesize MOF membranes, wherein solvents can be easily removed from the MOF-membrane system with a mild activation process. The MOF growth and the gas permeance study have been performed using membrane module of practical applicability that can be easily scalable. This work provides an understanding of the benefits of flexible polymeric hollow fiber membrane porosity and its material properties; as well as peculiarities of ligand/metal ion partitioning in immiscible solvent pairs to grow MOFs in a selective manner. The separation performance of gases such as He, N_2 and C_3H_8 through MOF-HF composite membranes demonstrated that MOFs extensively take part in the molecular discrimination. Among all composite membranes synthesized in this work, CuBTC@PBI-BuI-Out displayed an appreciable permeance and selectivity of 12 (He/N_2) and 17 (He/C_3H_8). In closing, we believe that the understanding generated out of this work would help to develop composite membranes for a wider range of gases/liquids separation applications in near future.

3.4 Experimental procedures

3.4.1 *Materials*

2-methylimidazole (2-mIm), zinc nitrate, 1,3,5-benzenetricarboxylic acid (BTC) and cupric nitrate was purchased from Sigma-Aldrich Chemicals. The solvents were purchased from Thomas Baker Chemicals. All other materials were purchased from commercial sources and used without further purification.

3.4.2 *Synthesis of MOFs, spinning of PBI-BuI hollow fibers and fabrication of MOFs@PBI-BuI-HF membranes*

a) ***Optimized protocol for the preparation of ZIF-8 via interfacial synthesis method [ZIF-8 ($CHCl_3/H_2O$)]*:** For the ZIF-8 ($CHCl_3/H_2O$) synthesis, the organic phase was prepared by adding 0.162 g of 2-methylimidazole in 10 mL of $CHCl_3$. The resulting clear solution was used for the preparation of a thin ZIF-8 film by slow addition of a solution of 0.146 g of $Zn(NO_3)_2.6H_2O$ in 10 mL of water in it. The biphasic mixture was left to stand at room temperature for 6 h (***Figure 3.10a***).

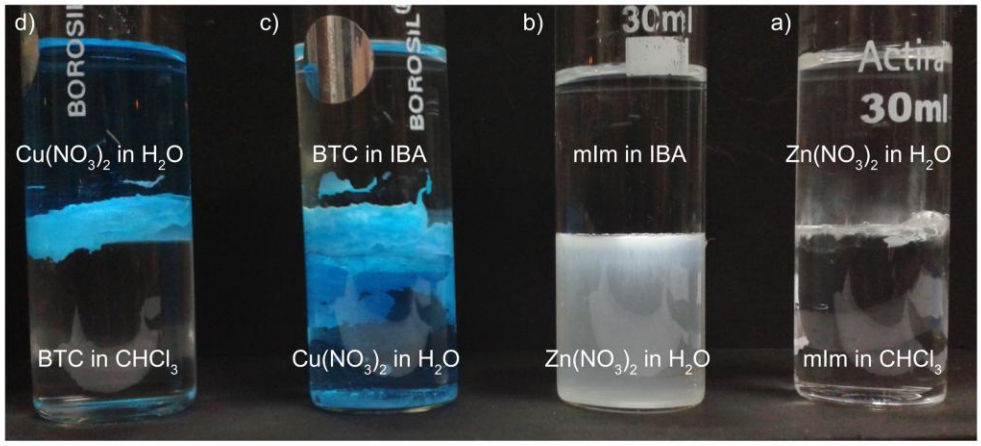

Figure 3.10. *a-d) Demonstrating the synthesis of ZIF-8 and CuBTC using $CHCl_3$/water and IBA/water as solvent systems via interfacial synthesis method.*

b) ***Optimized protocol for the preparation of ZIF-8 via interfacial synthesis method [ZIF-8 (IBA/H_2O)]*:** For the ZIF-8 (IBA/H_2O) synthesis, the aqueous phase was prepared by adding 0.146 g of $Zn(NO_3)_2.6H_2O$ in 10 mL of water. The resulting clear solution was used

for the preparation of a thin ZIF-8 film by slow addition of a solution of 0.162 g of *2*-methylimidazole in 10 mL of isobutyl alcohol (IBA) in it. The biphasic mixture was left to stand at room temperature for 6 h (***Figure 3.10b***).

c) ***Optimized protocol for the preparation of CuBTC via interfacial synthesis method [CuBTC ($CHCl_3/H_2O$)]*:** For CuBTC ($CHCl_3/H_2O$) synthesis, the aqueous phase was prepared by adding 0.68 g of $Cu(NO_3)_2.6H_2O$ in 10 mL of water. The resulting clear solution was used for the preparation of a thin CuBTC film by slow addition of a clear solution of 0.5 g of 1,3,5-benzenetricarboxylic acid (BTC) in 10 mL of $CHCl_3$ and 0.75 mL of triethylamine (TEA) in it. The biphasic mixture was left to stand at room temperature for 6 h (***Figure 3.10c***).

d) ***Optimized protocol for the preparation of CuBTC via interfacial synthesis method [CuBTC (IBA/H_2O)]*:** For CuBTC (IBA/H_2O) synthesis, the organic phase was prepared by adding 0.5 g of 1,3,5-benzenetricarboxylic acid (BTC) in 10 mL of $CHCl_3$ and 0.75 mL of triethylamine (TEA). The resulting clear solution was used for the preparation of a thin CuBTC film by slow addition of a clear solution of 0.68 g of $Cu(NO_3)_2.6H_2O$ in 10 mL of water in it. The biphasic mixture was left to stand at room temperature for 6 hours (***Figure 3.10d***).

e) ***Preparation of dope solution and fabrication of PBI-BuI hollow fiber (PBI-BuI-HF) membrane*:** The PBI-BuI was synthesized using the literature report [3.16c]. It was vacuum dried at 100 ºC for 24 hours prior to the preparation of dope solution (PBI-BuI: DMAc: LiCl = 11: 83: 6 on wt. basis). The spinning of PBI-BuI hollow fiber membranes was carried out using the dry-jet wet spinning process. The dope solution and the bore fluid were passed through a spinneret at the predefined extrusion rate to offer hollow fiber with an internal diameter of 0.46 mm and the outer diameter of 0.78 mm.

f) ***Hollow fiber membrane module preparation*:** The dry hollow fibers of PBI-BuI were used for the preparation of membrane module. A bunch of 10 fibers of 30 cm length was housed in a pipe of ½" diameter using epoxy resin. The photograph of obtained module is given in ***Figure 3.2a***. The active length and active area of the membrane module are 26 cm and 63.6 cm^2, respectively. The prepared module was used as such for the growth of ZIF-8

and CuBTC on either surface (inner or outer) of PBI-BuI hollow fibers present within the module.

g) ***Fabrication of ZIF-8@PBI-BuI-In composite membrane*****:** The $Zn(NO_3)_2$ (2.19 g; 7.34 mmol) dissolved in 150 mL of water was circulated through the tube side of fibers using a peristaltic pump. After 15 minutes, 150 mL $CHCl_3$ solution of *2*-methylimidazole (*2*-mIm, 2.43 g; 29.63 mmol) was held on to the shell side (outer side of the fibers), for 1 hour. During this period, circulation of aqueous $Zn(NO_3)_2$ solution was continued on the tube side. The solutions were then drained and this procedure was repeated twice. Finally, the membrane module was dried at 65 ºC under the vacuum for 12 hours and then used for further characterizations.

h) ***Fabrication of ZIF-8@PBI-BuI-Out composite membrane*****:** The *2*-methylimidazole (*2*-mIm, 2.43 g) dissolved in 150 mL of isobutyl alcohol (IBA) was circulated through the tube side of fibers using a peristaltic pump. After 15 minutes, an aqueous solution of $Zn(NO_3)_2$ (2.19 g in 150 mL) was held on to the shell side (outer side of the fibers), for 2 hours. During this period, circulation of 2-mIm in IBA was continued on the tube side. After that, the solutions from both the sides were drained and the module was dried at 65 ºC under vacuum for 12 hours.

i) ***Fabrication of CuBTC@PBI-BuI-In composite membrane*****:** The $Cu(NO_3)_2$ (3.4 g; 14.07 mmol) dissolved in 150 mL of water was circulated through the tube side of fibers using the peristaltic pump. After 15 minutes, 150 mL of $CHCl_3$ solution of *1,3,5*-benzenetricarboxylic acid (BTC, 2.5 g; 11.9 mmol) and triethylamine (3.5 mL; 25 mmol) was held on to the shell side (outer side of the fibers), for 1 hour. During this period, circulation of aqueous $Cu(NO_3)_2$ solution was continued on the tube side. The solutions were then drained and this procedure was repeated twice. Finally, the membrane module was dried at 65 ºC under the vacuum for 12 hours.

j) ***Fabrication of CuBTC@PBI-BuI-Out composite membrane*****:** The *1,3,5*-benzenetricarboxylic acid (BTC, 2.5 g) was dissolved in 150 mL of isobutyl alcohol (IBA) and triethylamine (3.5 mL), was circulated through the tube side of fibers. After 15 minutes, 150 mL aqueous solution of $Cu(NO_3)_2$ (3.4 g) was held on to the shell side (outer side of the fibers), for 2 hours. During this period, circulation of BTC/IBA/TEA solution was continued

on the tube side. After that, the solutions from both the sides were drained and the module was dried at 65 ºC under vacuum for 12 hours.

3.4.3 *General methods for characterization*

All reagents were commercially available and used as received. Microscopy images of these hollow fibers were taken in Zeiss SteREO Discovery V20.

a) ***Wide-angle X-Ray Diffraction (WAXD)*:** The wide-angle X-Ray Diffraction (WAXD) analysis of MOFs and the composite membranes were carried on a Rigaku SmartLab X-ray diffractometer in reflection mode using CuKα radiation (λ = 1.54 Å). The 2θ range from 5° to 40° was scanned with a scan rate of 3° min^{-1}. The instrument was previously calibrated using a silicon standard.

b) ***FT-IR spectroscopy*:** The Fourier transform infrared spectra (FT-IR) were taken on a Bruker Optics ALPHA-E spectrometer with a universal Zn-Se ATR (attenuated total reflection) accessory in the 600-4000 cm^{-1} region or using a Diamond ATR (Golden Gate). The spectra were measured over the range of 4000-400 cm^{-1}.

c) ***Scanning Electron Microscopy*:** Scanning Electron Microscopy (SEM) was performed on a FEI Quanta 200 3D ESEM (dual beam) instrument with a field emitter as an electron source and in FEI Nova NanoSEM 650 Scanning Electron Microscope. SEM images of membrane cross section were taken after freeze cut off membranes in LN_2. Samples for SEM were gold sputtered before analyses.

3.4.4 *Gas permeance measurements*

Single gas permeation experiments using He, N_2, and C_3H_8 were performed at 35 °C using a variable volume method. The upstream pressure of range 15 psi was used while maintaining permeates side at the ambient.

A schematic diagram of permeation equipment is shown in ***Figure 3.11***. One end of the feed side of the cell was connected through valve V_1 to the feed gas cylinder outlet and an electronic pressure gauge (0-999 psi range). The valve V_2 was a vent and used to control the feed pressure. On the permeate side of the permeation cell, a mercury flowmeter was connected. The displacement of mercury slug was monitored against time.

The permeance (*P*) of was calculated using the Equation 3.1.

$$P = \frac{14.7 \times d \times F.C}{76 \times A \times t \times \Delta P} \qquad (3.1)$$

where, d = Distance travelled by mercury (cm), F.C. = Flow meter constant [volume of the flow meter capillary per unit length (cm^3/cm)], A= Effective membrane area (cm^2), t = Time (sec), P = Pressure (psi), and *P* is the permeance expressed in Gas Permeation Unit (GPU) [1GPU = 1×10^{-6} cm^3 (STP)/ (cm^2 s cmHg)].

The ideal selectivity of various gases was calculated using the Equation 3.2.

$$\alpha = \frac{P_x}{P_y} \qquad (3.2)$$

where, P_x and P_y are the permeance of respective pure gases.

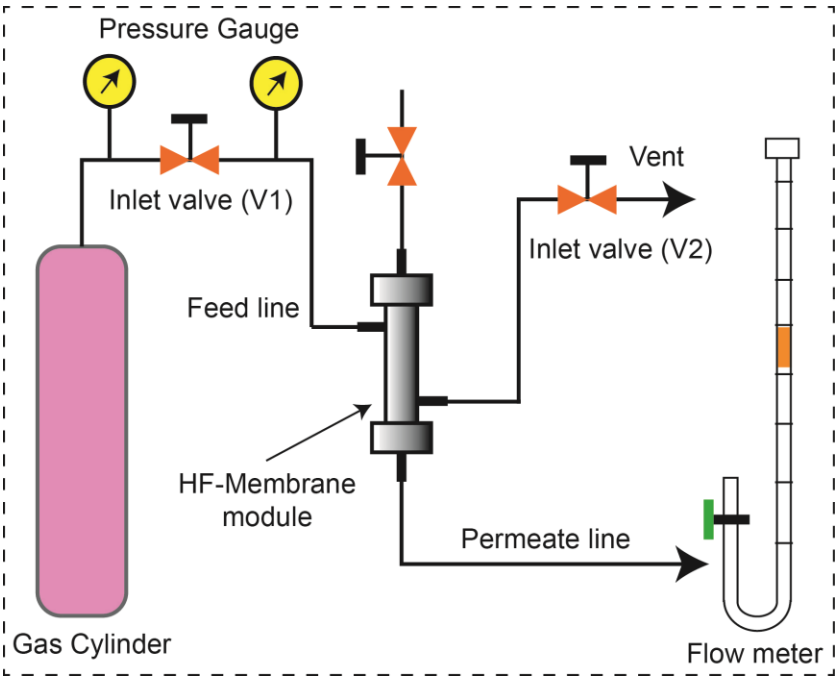

Figure 3.11. *Schematic representation of gas permeation equipment set-up.*

NOTE: The results of this chapter have already been published in *Nanoscale*, **2015**, *7*, 7291-7298, with the title: "*Selective Interfacial Synthesis of Metal-Organic Frameworks on Polybenzimidazole Hollow Fiber Membrane for Gas Separation*". These publications were the results from the group of Dr. Rahul Banerjee and his students Mr. Bishnu Prasad Biswal and Dr. Ulhas K. Kharul and his student Mr. Anand Bhaskar from CSIR-National Chemical Laboratory, Pune, India. Major work was contributed by Mr. Bishnu Prasad Biswal with the help of the instrumental facilities of CSIR-National Chemical Laboratory. Mr. Anand Bhaskar assisted in MOF growth on hollow fiber experiments at the beginning of the project. The manuscript was primarily written by Mr. Bishnu Prasad Biswal under the guidance of Dr. Rahul Banerjee and Dr. Ulhas K. Kharul.

CHAPTER 4

Mechanochemical Approach towards Synthesis of Chemically Stable, Isoreticular Covalent Organic Frameworks

Abstract: *In this chapter, we present a series of thermally and chemically stable covalent organic frameworks (COFs) that were synthesized via room-temperature solvent-free mechanochemical grinding. All these COFs were successfully compared with their solvothermally synthesized counterparts. These solvent-free mechanochemically synthesized COFs have moderate crystallinity with remarkable stability in boiling water, acid (9 N HCl), and base (3 N NaOH). Exfoliation of COF layers (graphene-like layered morphology) was simultaneously observed with COF formation during mechanochemical synthesis. In the later part of this chapter, we disclose that the dynamic covalent bond formation is dramatically accelerated under Liquid-Assisted Grinding (LAG) conditions leading to improved crystalline COFs efficiently at a faster rate and in high yield. We showcase that a variety of symmetric aromatic amine/hydrazide and aldehydes can be utilized for the construction of crystalline Schiff base COFs irrespective of their reactivity and solubility using LAG.*

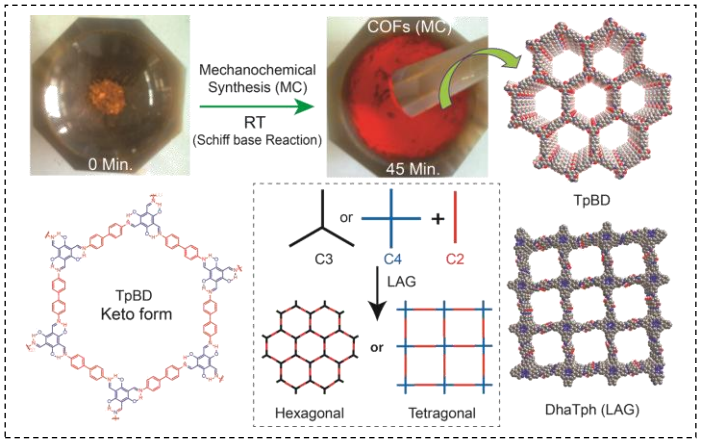

4.1 Introduction

Construction of various bonds through simple, cost-effective and environmentally-friendly mechanochemical route is of considerable interest in contemporary synthetic chemistry [4.1]. In recently years, mechanochemistry has been capably employed to achieve various organic and inorganic transformations [4.2], nanostructures formation [4.3] and to build metal-organic frameworks [4.4]. Thus, this method has become a very good alternative to conventional solution based synthesis. Moreover, modified mechanochemical synthetic approaches such as liquid assisted grinding (LAG) were also employed for the rapid synthesis of metal-organic complexes and frameworks [4.5]. Although, mechano-synthesis approach have been well explored as a most suitable synthetic tool for the formation of covalent bonds, but so far not a single attempt has been made to synthesize 2D/3D covalent organic frameworks (COF) or crystalline porous polymers (CPPs). COFs are lightweight, crystalline porous materials constructed *via* strong covalent bonds between selected lighter elements such as C, Si, B, N and O [4.6]. It is noteworthy that, the COF crystallization is only possible by the employment of reversible organic reactions and the reversibility of covalent bond formation is the foremost criteria. Therefore, achieving the same adopting a mechanochemical approach is remains a dire challenge [4.7]. In general, extremely harsh experimental conditions like reaction in a sealed Pyrex tube, inert atmosphere, choice of suitable solvents, reaction rates, longer reaction time for crystallization etc. are required for highly crystalline and porous COF formation [4.8]. Moreover, once they formed special care is required for their storage due to moisture instability [4.9]. For this reason, an advanced synthetic method like mechanochemical grinding and appropriate optimization of the reaction conditions are highly needed to overcome the aforementioned issues to bring COF materials into real practice. Very recently, Kandambeth et al. have reported two COFs (TpPa-1 and TpPa-2) with outstanding chemical stability, which has been synthesized using a modified Schiff base reaction, wherein the proton tautomerism makes the framework exceptionally robust towards the water, acid and base [4.10]. The outstanding chemical stability of these COFs led us to attempt for alternative simple, solvent free, rapid and scalable room temperature construction of COF using well-known mechanochemistry.

In this work, we for the first time showcase that COF materials can be synthesized in a rapid, solvent-free mechanochemical (MC) way at room-temperature. At first, we have

successfully synthesized two COFs TpPa-1 (MC) and TpPa-2 (MC) by using manual grinding in a mortar and pestle. The products obtained were initially identified by visual colour change, FT-IR spectra and comparing the powder X-ray diffraction (PXRD) profiles with their solvothermally crystallized counterparts and structural modeling. Using a similar protocol of solvent-free mechanochemical route, we further synthesized a new crystalline isoreticular COF namely TpBD (MC) and for the comparison also crystallized the solvothermal counterpart (TpBD). TpBD COF was found to be porous and highly crystalline with remarkable chemical stability in aqueous, acidic (9 N HCl) and in basic (3 N NaOH) conditions. Although, TpPa-1 (MC), TpPa-2 (MC) and TpBD (MC) possess moderate crystallinity as compared to their parent form [TpPa-1, TpPa-2 and TpBD] synthesized solvothermally, but the thermochemical stability remains intact under identical experimental conditions. More interestingly, the mechanochemically synthesized COFs have graphene-like layered morphology (delaminated layers) than the COFs synthesized in a solvothermal way.

In the first part of this chapter, we have discussed the formation of stable COFs *via* simple neat mechanical grinding using a combined reversible and irreversible Schiff base reaction [4.11]. However, it makes an impression that only selected COFs involving a combined reversible and irreversible reaction steps [4.10] can be formed *via* mechanochemical grinding. Also, the important thing we had noticed that the crystallinity of COFs synthesized *via* neat grinding are moderate as compared to the COFs synthesized *via* conventional solvothermal method [4.11a and 4.6]. In this context, liquid-assisted grinding (LAG) or ion- and liquid-assisted grinding (ILAG) methods have recently added momentous advantages to mechanochemical synthesis. A significant improvement in the rate of product formation in the presence of water (formed as a by-product of Schiff base reaction) or a small amount of added solvents was realized due to efficient mass transport and diffusion of reactants [4.5]. To establish the versatility of our mechanochemical synthesis approach, we have slightly altered our strategy by applying LAG approach and further extended to three different Schiff base systems (Imine, Hydrazone-keto-enamine and H-bonded imine) [4.12] to synthesize COFs mechanochemically with improved yield, purity and crystallinity. Although, there are few selected reversible reactions were known to proceed under mechanochemical conditions *i.e.,* boronic acid-alcohol condensation, aldehyde-amine Schiff base reaction etc. [4.3a]. Moreover, due to the dynamic nature [4.13] of imine bonds and its

stability disarmingly made possible its rapid formation under very mild solvothermal or mechanochemical conditions.

As a part of our systematic investigation on mechanochemical synthesis, herein, we showcase the usage of a variety of aromatic amine/hydrazide and aldehydes for the construction of crystalline Schiff base COFs irrespective of their solubility employing LAG. In this part, we have explored the synthesis of 2D-COFs with predetermined topological design (hexagonal and tetragonal) using proper symmetry combinations (C_2+C_3 and C_2+C_4) of the building blocks under mechanochemical condition [4.14]. It is noteworthy that, making COFs of unsubstituted hydrazone linkages with decent crystallinity was extremely challenging even using solvothermal methods due to its low solubility and pH-dependant reversibility [4.12a]. By applying LAG approach, we have successfully synthesized a new crystalline hydrazone-linked COF [TpTh (LAG)] with high chemical stability. Since 2D porphyrin, COFs were known to display high rate charge carrier and photoconductivity owing to the well-aligned long range π-orbital overlapping of porphyrin units. We further decided to extend our LAG strategy to synthesize COFs containing porphyrin building unit [DhaTph (LAG)] [4.12b]. More importantly, we could demonstrate that the COF with chemically labile Schiff base [–C=N] centers such as LZU-1 [4.12c] can also be synthesized with good crystallinity *via* LAG approach. To ensure the formation of these aforementioned COFs, we have synthesized their solvothermal counterparts for comparison. Overall, in this work, we showcase that, by adopting LAG approach imine, hydrazone-keto-enamine and H-bonded imine-based COFs can be synthesized in high purity, yield and faster rate compared to conventional solvothermal and neat mechanochemical methodology.

4.2 Mechanochemical synthesis of chemically stable isoreticular covalent organic frameworks *via* neat grinding

4.3 Result and discussion

4.3.1 *Powder X-ray diffraction and structural analysis*

The solvent-free mechanochemical syntheses of COFs [TpPa-1 (MC), TpPa-2 (MC) and TpBD (MC)] were carried out by using a modified Schiff base aldehyde-amine condensation reaction. In the typical synthesis *1,3,5*-triformylphloroglucinol (Tp) (0.30

mmol), *p*-phenylenediamine (Pa-1) [for TpPa-1 (MC)], *2,5*-dimethyl-p-phenylenediamine [for TpPa-2 (MC)] and benzidine [for TpBD (MC)] (0.45 mmol) was placed in a mortar and grounded using pestle (later we have synthesized them using a ball mill; ***Figure 4.2d-f***) at room temperature, after 5 minutes the mixture turned into light yellow powders (which may be a mixture of oligomers and starting materials) (***Figure 4.1***). As the time progress, the yellow colour changes to orange (15 min.) and then at 40 minutes of grinding results a dark red colour powder [similar to COFs (ST)]. This could be due to the increased conjugated units and complete COF formation.

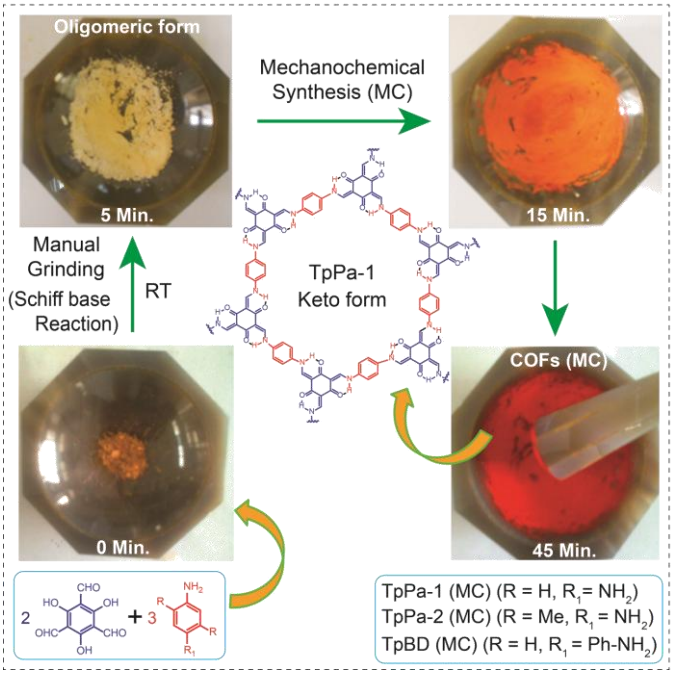

Figure 4.1. *Schematic representation of the synthesis of TpPa-1 (MC), TpPa-2 (MC) and TpBD (MC) through simple Schiff base reaction performed via mechanochemical grinding (MC) using mortar and pestle.*

The PXRD was performed to access the crystallinity of all mechanochemically synthesized COFs. As revealed from PXRD analysis; TpPa-1 (MC), TpPa-2 (MC) and TpBD (MC) showed moderate crystallinity, exhibiting the first peak at low angle 4.7° (2θ), 4.7° (2θ) and 3.3° (2θ) respectively, which corresponds to the (100) reflection plane (***Figure 4.2***). The shift in 2θ (from 4.7° to 3.3°) towards lower value for TpBD (MC) compared to TpPa-1 (MC) and TpPa–2 (MC) could be due to the diamine linker length, which resulted in large pore aperture.

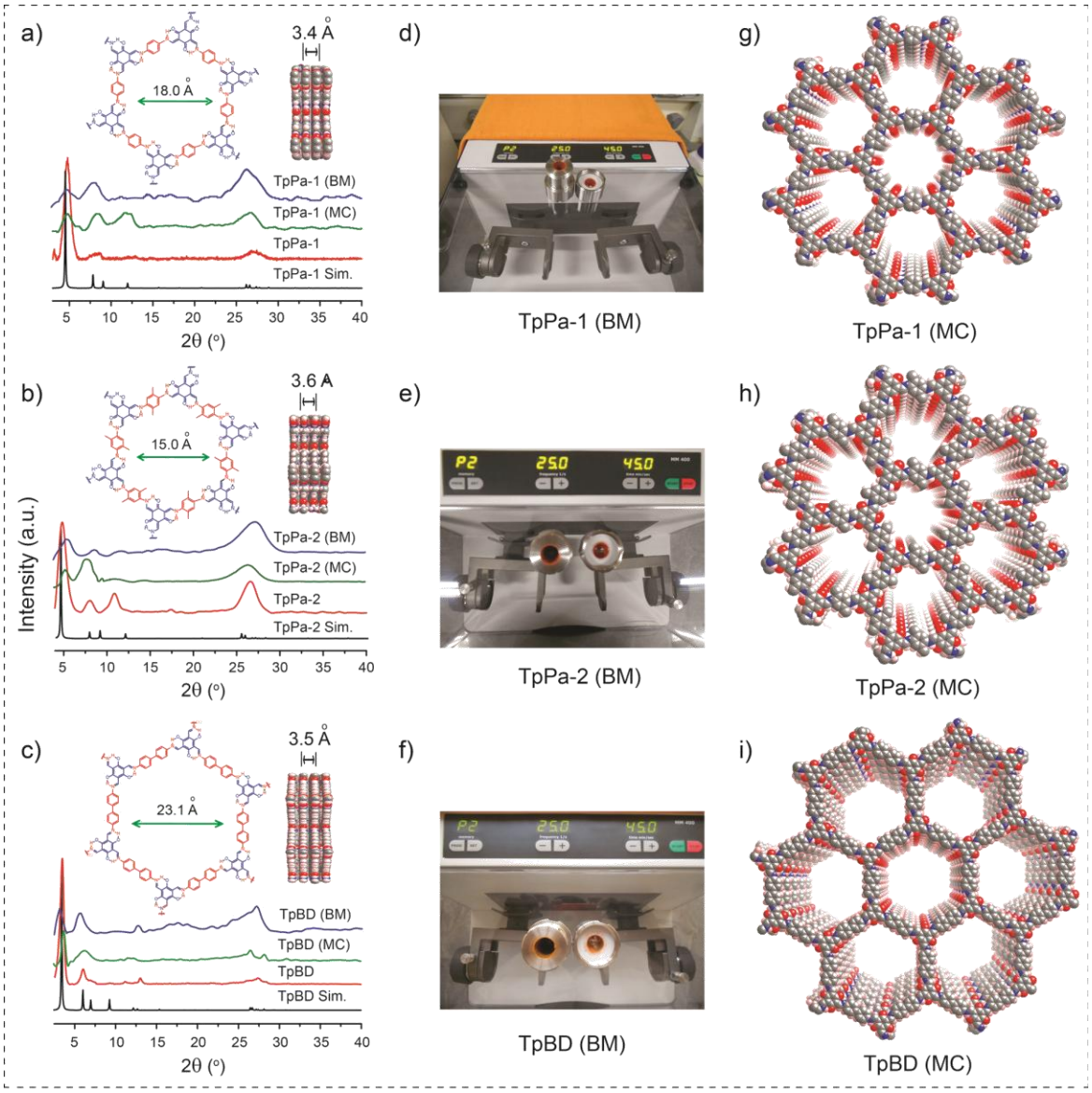

Figure 4.2. *a), b) and c) Comparison of the PXRD patterns; green [synthesized via mechanochemical grinding (MC)], red [synthesized via solvothermal method (ST)], blue [synthesized using ball mill (BM)] and black (simulated) for TpPa-1, TpPa-2, and TpBD respectively. (Inset images showing the pore opening and π-π stacking distance between consecutive 2D layers for all COFs); d), e) and f) Ball Mill used for the synthesis of TpPa-1 (BM), TpPa-2 (BM) and TpBD (BM); g), h) and i) Represents the space filling packing models showing the hexagonal pores for TpPa-1, TpPa-2 and TpBD respectively.*

In comparison to the COFs synthesized solvothermally [TpPa-1, TpPa-2 and TpBD], the first peak is relatively less intense (100 planes) for mechanochemically synthesized COFs. This is due to the random displacement of the 2D layers (delamination occurs) that may hinder the pore accessibility and hence the distributions of eclipsed pores get affected. The broader peak

at higher 2θ (~27°) is mainly due to the π-π stacking between the COF layers and corresponds to the 001 plane. The d-spacing values for these three COFs [TpPa-1 (MC), TpPa-2 (MC) and TpBD (MC)] were found to be *ca.* 3.3, 3.6 and 3.5 Å respectively. The proposed 2D models and the detailed structural description of TpPa-1 and –2 were reported by Kandambeth *et al*. their previous publication [4.10]. However, for newly introduced COF TpBD, two possible 2D models (eclipsed and staggered; ***Figure 4.3a***) were built using self-consistent charge density functional tight-binding (SCC-DFTB) method based on which the unit cell parameters were calculated [4.15a]. All the observed PXRD patterns for mechanochemically synthesized COFs (MC) were matched well with the solvothermally synthesized COFs (ST) along with the simulated patterns obtained from eclipsed staking model (***Figure 4.3***). For **TpBD** the proposed model crystallizes in a hexagonal *P*6/*m* space group with unit cell parameter $a = b = 29.28$, $c = 3.25$ Å; $\alpha = 90^o$, $\beta = 90^o$, $\gamma = 120^o$ derived from the Pawley refinements [4.15b] (***Table 4.1***).

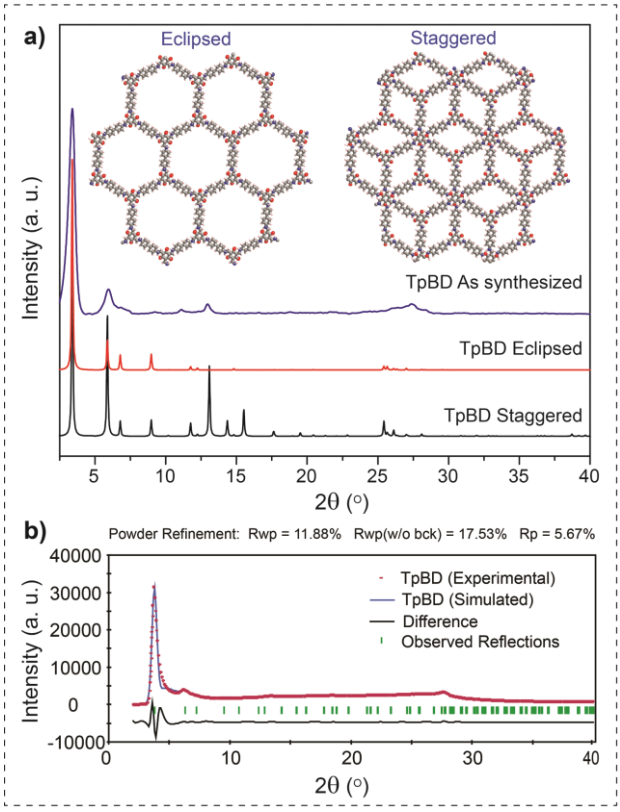

Figure 4.3. *a) PXRD patterns of as-synthesized TpBD (Blue) compared with the Eclipsed (red) and staggered (black) stacking models; b) Experimental (Red) compared with refined (Blue) PXRD profiles of COF-TpBD with an eclipsed arrangement; difference plot is given in (black).*

4.3.2 *Fourier transforms infrared (FT-IR) and ^{13}C CP/MAS NMR*

To achieve a better insight into the bond formation and local mode of binding in mechanochemically synthesized COFs, we have investigated the systematic progress of the reaction employing FT-IR spectra with respect to time.

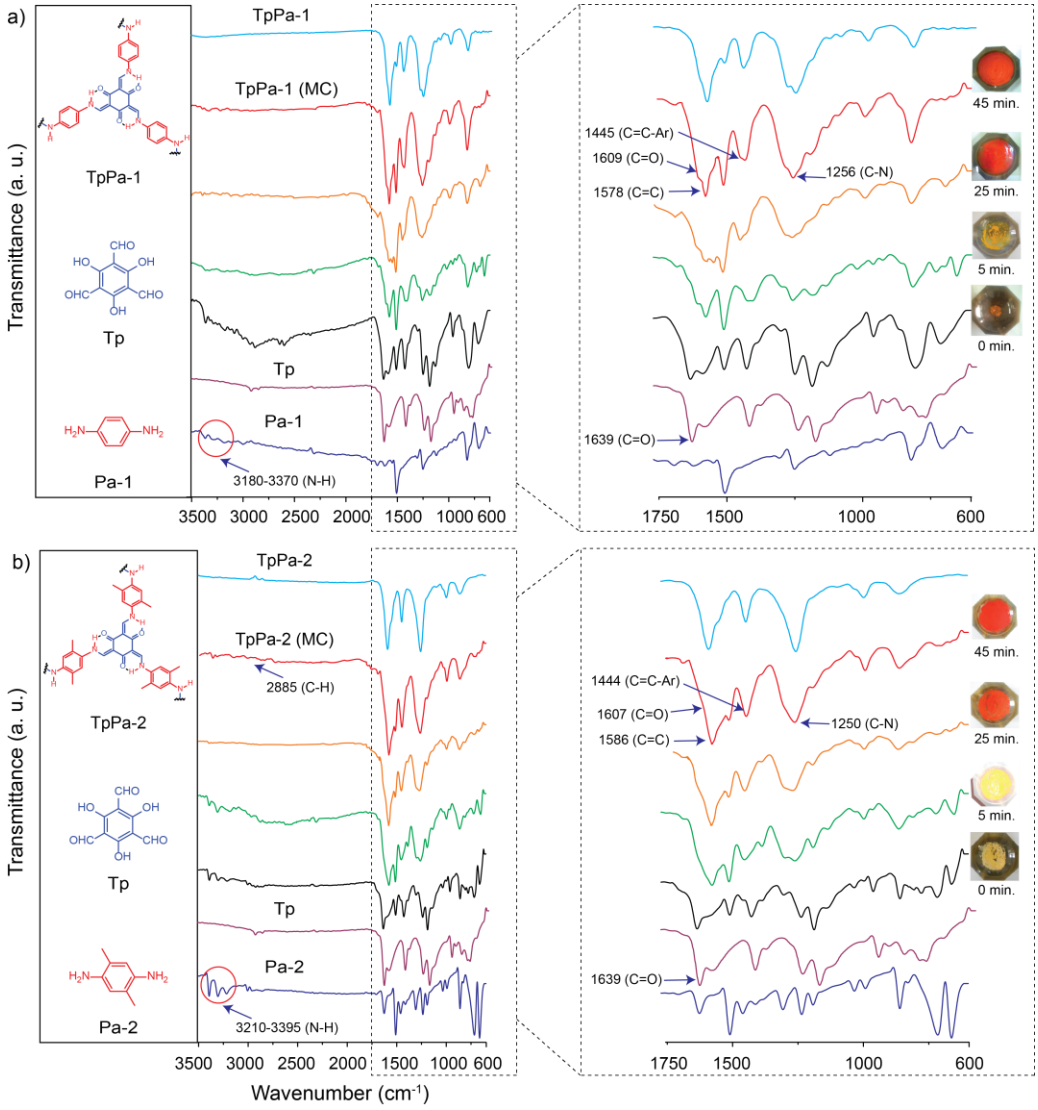

Figure 4.4. *a) and b) Stepwise comparison of the FT-IR spectra showing progress of reaction with time for TpPa-1 (MC) and TpPa-2 (MC); blue, brown, black represents [p-phenylenediamine (Pa-1)], [1,3,5-triformylphloroglucinol (Tp)], [physical mixture of Tp with Pa-1 / Pa-2] and green, golden yellow, red for 5, 25 and 45 minutes grinding of reactants respectively. Cyan represents TpPa-1 and TpPa-2 synthesized by solvothermal method (ST) (right inset images shows the change in colour observed during grinding).*

Finally thus obtained product was successfully compared with the COFs synthesized *via* solvothermal method (***Figure 4.4*** and ***4.5***). All three COFs synthesized mechanochemically showed similar FT-IR spectra like their solvothermally synthesized counterpart. The spectra obtained for all the COFs clearly indicates the complete disappearance of IR band for the characteristic N-H stretching of free diamine (3100-3300 cm^{-1}), which indicates that the starting material (diamines) gets completely consumed. Simultaneously the carbonyl (C=O) peak position (at 1609 cm^{-1} with reference to 1639 cm^{-1} for Tp) gets broadened, shifted and slightly merged with the newly formed C=C bond (1578 cm^{-1}) which occurs due to the existence of strong hydrogen bonding in the keto form of honeycomb 2D framework and confirms the s-cis structure. The unobserved hydroxyl (O-H) and C=N stretching peaks, as well as the appearance of a new peak at 1578 cm^{-1} (C=C), while forming the 2D extended framework gives fairly convincing evidence for the existence of the keto form. Although enol form was the expected one (tautomerism drive the reaction towards keto form instead of enol form), which is further supported by the FT-IR spectra of the reference compound [*2,4,6*-tris-(phenylamino)methylene] made for comparison [4.16].

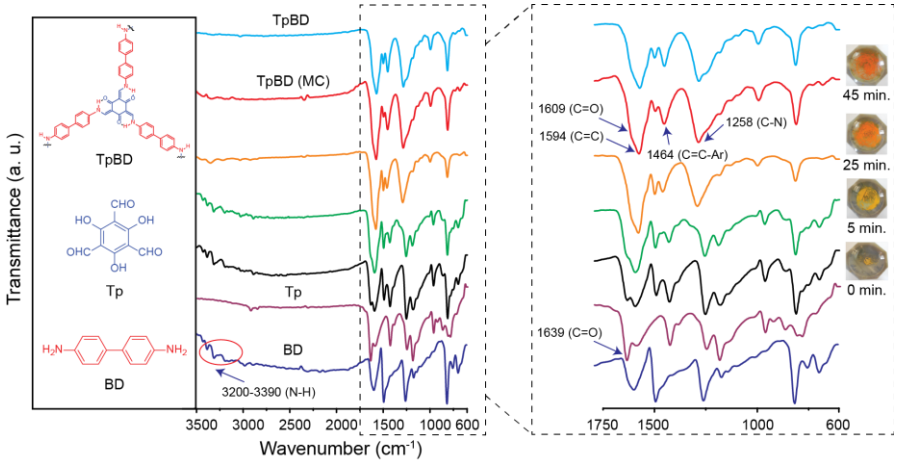

Figure 4.5. *Stepwise comparison of the FT-IR spectra showing progress of reaction with time for TpBD (MC); blue, brown, black represents [Benzidine (BD)], [1,3,5-triformylphloroglucinol (Tp)], [physical mixture of Tp with BD] and green, golden yellow, red for 5, 25 and 45 minutes grinding of reactants respectively. Cyan represents TpBD synthesized by solvothermal method (ST) (right inset images shows the change in colour observed during grinding).*

The appearance of two peaks at 1445 cm^{-1} [C=C(Ar)] and 1256 cm^{-1} (C-N), was assigned due to the aromatic C=C and newly formed C-N bond in the keto form structure. The extra peak observed at 2885 cm^{-1} (C-H) for TpPa-2 (MC) confirms the existence of the

methyl group. In ***Figure 4.4a, b*** and ***4.5***, the FT-IR profile of TpPa-1 (MC), TpPa-2 (MC) and TpBD (MC) has been presented showing how the peak positions change with time while grinding, which indicates new bond formation and subsequently to the construction of COF network happens.

^{13}C cross-polarization magic-angle-spinning (CP-MAS) solid state NMR spectroscopy was performed to verify the structural compositions of the COFs (MC) synthesized *via* mechanochemical grinding approach. All the spectra obtained for COFs (MC) were successfully compared with their respective solvothermally synthesized counterparts and with reference compound [*2,4,6*-tris-(phenylamino)methylene] (***Figure 4.6***). The peak to peak matching of solid state NMR profile indicates that the COF derived from both solvothermal and mechanochemical methods have same local structure. The COFs [TpPa-1 (MC), TpPa-2 (MC) and TpBD (MC)] showed a signal at ~181 ppm, which corresponds to the carbonyl carbon of the keto form structure. The unobserved peak at ~190 ppm gives a clear evidence for the unavailability of starting material (Tp) remain in the mixture (***Figure 4.6***).

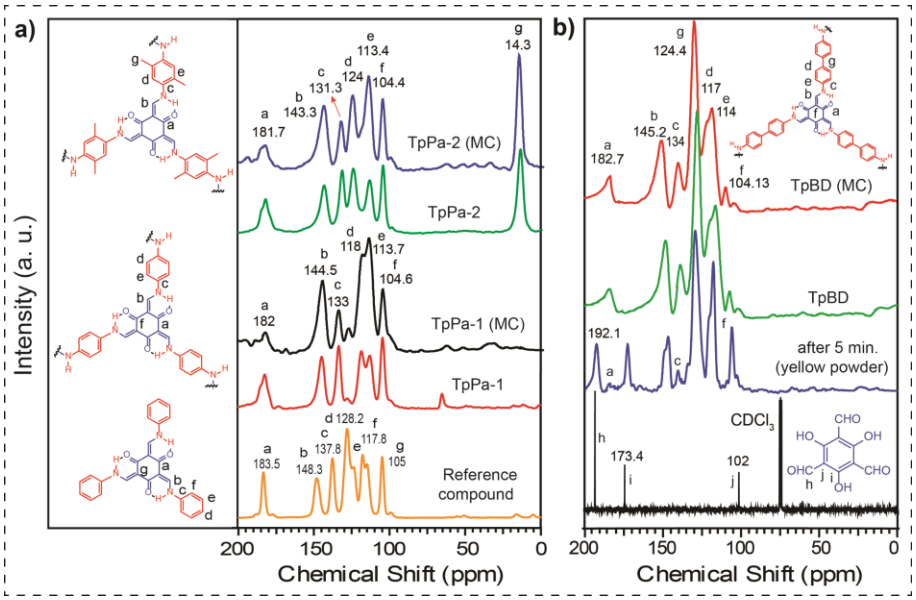

Figure 4.6. *a) Comparison of the ^{13}C CP-MAS solid-state NMR spectra of TpPa-1 (MC) (black), TpPa-2 (MC) (green) with TpPa-1 (red), TpPa-2 (blue) and reference compound 2,4,6-tris[(phenylamino)methylene]cyclohexane-1,3,5-trione (golden yellow). b) ^{13}C CP-MAS spectrum of TpBD (MC) (red), TpBD (green) and oligomers (yellow powder resulted after 5 minutes of grinding) (blue) compared with respect to the solution based ^{13}C NMR of 1,3,5-triformylphloroglucinol (Tp) (black) taken in $CDCl_3$.*

For TpBD and TpBD (MC), at 124 ppm a peak appears for two identical carbons present at the biphenyl junction (***Figure 4.6b***), which is absent in both TpPa-1 (MC) and TpPa-2 (MC) COFs. However, in the case of TpPa-2 and TpPa-2 (MC), there is a peak at 14 ppm, this comes due to the presence of extra methyl group unlike the other two COFs [TpPa-1 (MC) and TpBD (MC)] (***Figure 4.6a***).

4.3.3 *Raman spectra and thermogravimetric analysis (TGA)*

We have also collected the Raman spectra for all the COFs [TpPa-1, TpPa-2, TpBD, TpPa-1 (MC), TpPa-2 (MC) and TpBD (MC)] samples synthesized *via* both mechanochemical (MC) as well as solvothermal methods to prove the structural similarity (***Figure 4.7***). It has been found that the characteristic peaks such as C-N, C=O, C=C, C-C are present in the COF samples synthesized *via* both solvothermal and mechanochemical methods. However, some background peaks were also observed in all cases and no Raman peaks were observed for the reference compound (monomer) (green, at the top of ***Figure 4.7***) (λ = 514.5 nm), that could be suppressed due to fluorescence.

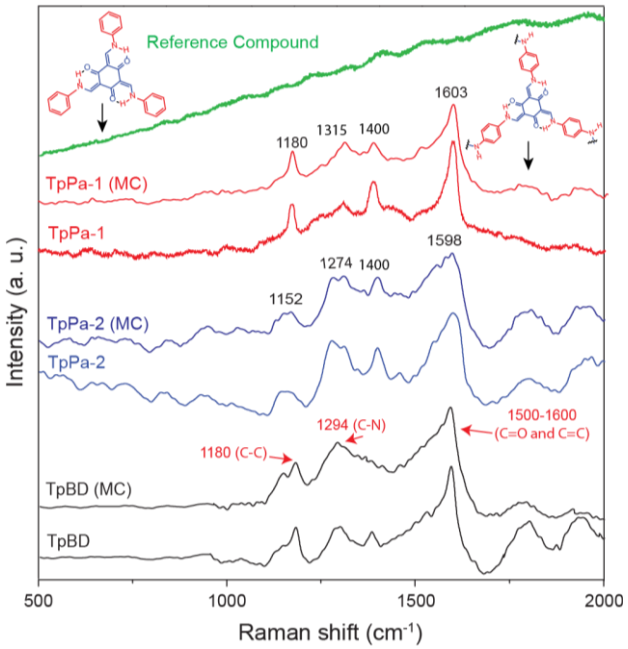

Figure 4.7. *Raman spectra of TpPa-1 (MC), TpPa-2 (MC) and TpBD (MC) [mechanochemically synthesized] in comparison with TpPa-1, TpPa-2, TpBD [solvothermally synthesized] and reference compound measured at 514.5 nm. The Raman spectra presented herein is the average of 5 spectra collected at different spots of the sample stage.*

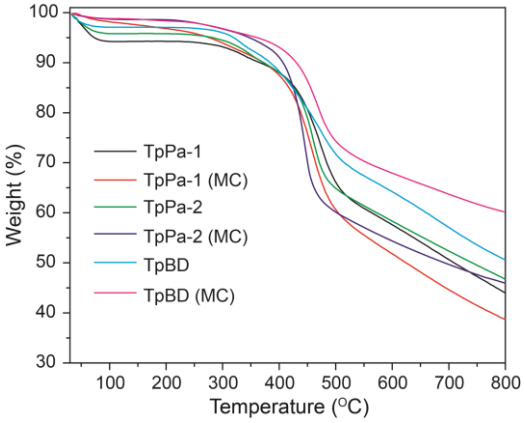

Figure 4.8. *TGA profile of all activated COFs (MC) and COFs (ST) collected under N_2 atmosphere.*

So, from these data we can only say that the matching of Raman peaks of COFs is owing to similar chemical structure and bonding environment synthesized under both solvothermal and mechanochemical methods.

We have performed the thermogravimetric analysis (TGA) experiment to understand the thermal behaviour of these COFs synthesized *via* both solvothermal and mechanochemical methods. The TGA profiles indicate that all the COF (MC and ST) pores are guest free and thus have almost identical thermal stability up to ~350 °C (***Figure 4.8***). However, after 350 °C the framework decomposition occurs with gradual a weight loss of 45-60% for all COFs except TpBD (MC), where only 28% weight loss was observed till 800 °C.

4.3.4 *Electron Microscopy (SEM and TEM)*

Scanning electron microscopy (SEM) images were done to know the external morphology of these mechanochemically synthesized COFs. SEM images indicate that small layers agglomerate to construct spherical shaped particles with relative size ~5-7 μm for TpPa-1 (MC) and TpPa-2 (MC). However, for TpBD (MC) flower-like morphology has been observed similar to TpPa-1 and TpPa-2 reported previously [4.10]. SEM images of TpPa-1 and TpPa-2 are flower-like morphology, which is a new type of morphology seen in COFs (***Figure 4.9a*** and 4.***9b***). Each individual flower is the result of the aggregation of a number of petals. In the case of TpPa-1, petals have spike shaped tips and grown out from a core.

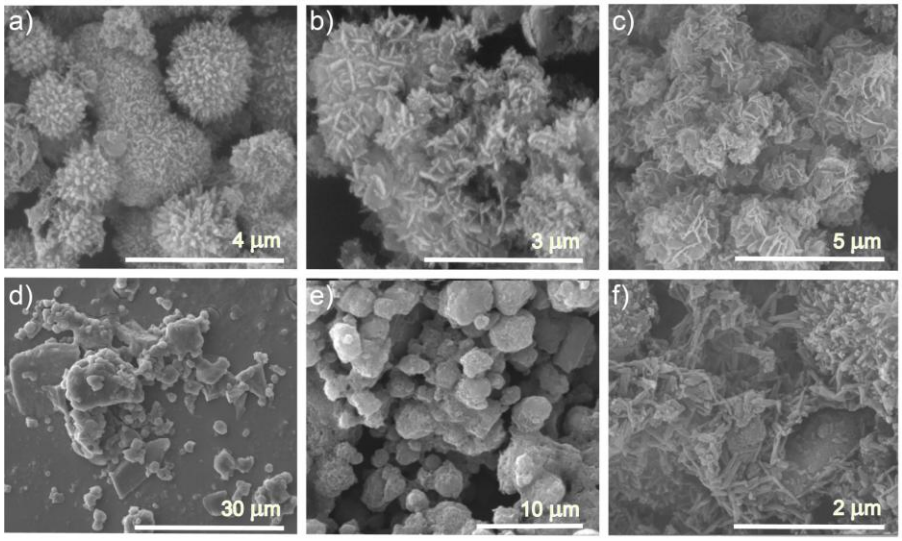

Figure 4.9*. SEM images a), b), and c) represents TpPa-1, TpPa-2, and TpBD synthesized solvothermally; and d), e), and f) for TpPa-1 (MC), TpPa-2 (MC) and TpBD (MC) synthesized mechanochemically respectively.*

But in the case of TpPa-2, petals are grown much broader and longer to form plate-like structures. Moreover, in the case of TpBD (MC) these flower petals are exfoliated, well dispersed and form graphene sheet-like layered morphology.

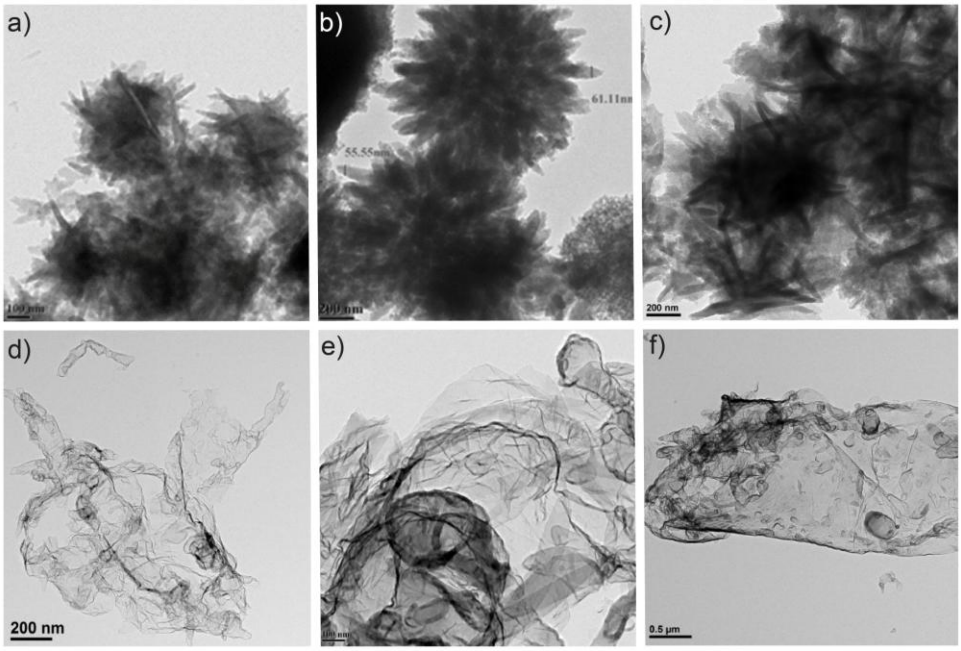

Figure 4.10. *HR-TEM images a), b) and c) represents TpPa-1, TpPa-2 and TpBD synthesized solvothermally; and d), e) and f) for TpPa-1 (MC), TpPa-2 (MC) and TpBD (MC) synthesized mechanochemically respectively.*

From the high-resolution TEM (HR-TEM) images, we have observed such graphene sheet-like layered morphology for TpPa-1 (MC), TpPa-2 (MC) and TpBD (MC) (***Figure 4.10d, e*** and ***f***). The layered like morphology could be a result of the strong mechanochemical force applied to already form COFs (MC). In which the 2D layers get exfoliated/delaminated as a result sheet-like structures were recovered. This kind of mechanochemical exfoliation already been known for graphene and other 2D materials [4.17], but the phenomenon of COF delamination presented in this paper is for the first time observed in COF materials.

4.3.5 *Gas and water vapour adsorption studies*

Nitrogen adsorption-desorption experiments were performed to examine the architectural rigidity, the permanent porosity of all mechanochemically and solvothermally synthesized COFs at 77 K (***Figure 4.11a***).

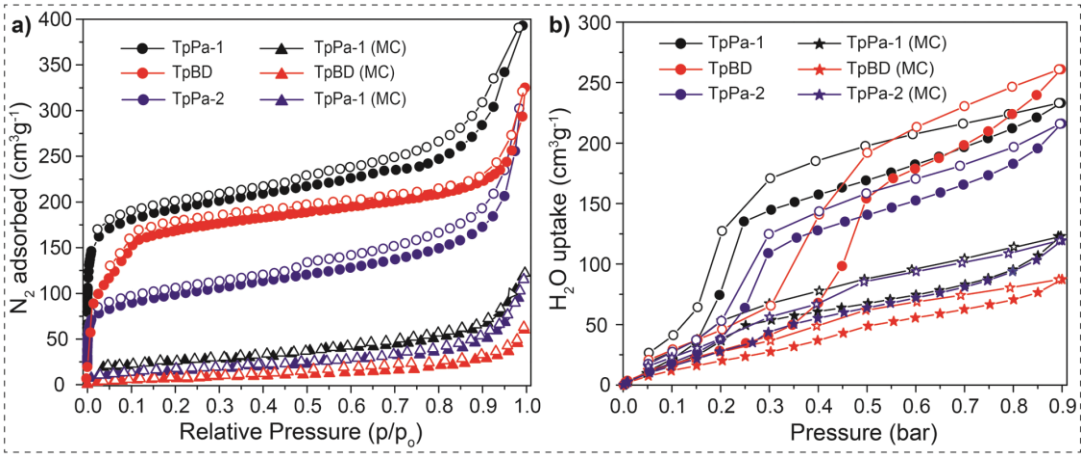

Figure 4.11. *a) Comparison of N_2 adsorption isotherms of TpPa-1 (MC), TpPa-2 (MC), TpBD (MC) with TpPa-1, TpPa-2 and TpBD; [Filled spheres for adsorption and hollow spheres for desorption COFs synthesized via solvothermal method, filled and hollow triangle represents COFs synthesized via Mechanochemical grinding method]. (b) Water adsorption isotherms for COFs (ST) and COFs (MC) at 0.9 P/P_o and 293 K.*

All these COFs were solvent (acetone/dichloromethane) exchanged 4-5 times and activated at 170 °C for 12 h under strong vacuum condition before the analysis to make sure the pores are guest free. All these COFs display reversible type-I isotherms during N_2 adsorption. The Brunauer-Emmet-Teller (BET) surface areas for the activated newly introduced COF TpBD

synthesized solvothermally were found to be 537 m^2g^{-1}. This BET surface area value of TpBD is very close to that of TpPa-1; 535 m^2g^{-1} and higher than TpPa-2; 339 m^2g^{-1} reported previously [4.10]. However, the same COFs synthesized *via* mechanochemically method have low BET surface area and the values are 61 m^2g^{-1} for TpPa-1 (MC), 56 m^2g^{-1} for TpPa-2 (MC) and 35 m^2g^{-1} for TpBD (MC) (***Figure 4.11a).*** Although, the exact reason for the low surface area for COFs (MC) was not fully clear to us but we speculate that due to the mechanochemical delamination thin layered structure results. Therefore, the long range pore formation in COFs (MC) gets hindered followed by only less depth pores accessible for N_2 adsorption. Another possible reason could be the entrapment of oligomeric impurities inside the COF (MC) pores during their formation *via* mechanochemical grinding, although from TGA profile we could not find any such indications. To showcase the usefulness of COFs synthesized via both the methods, we have collected water vapour adsorption isotherms.

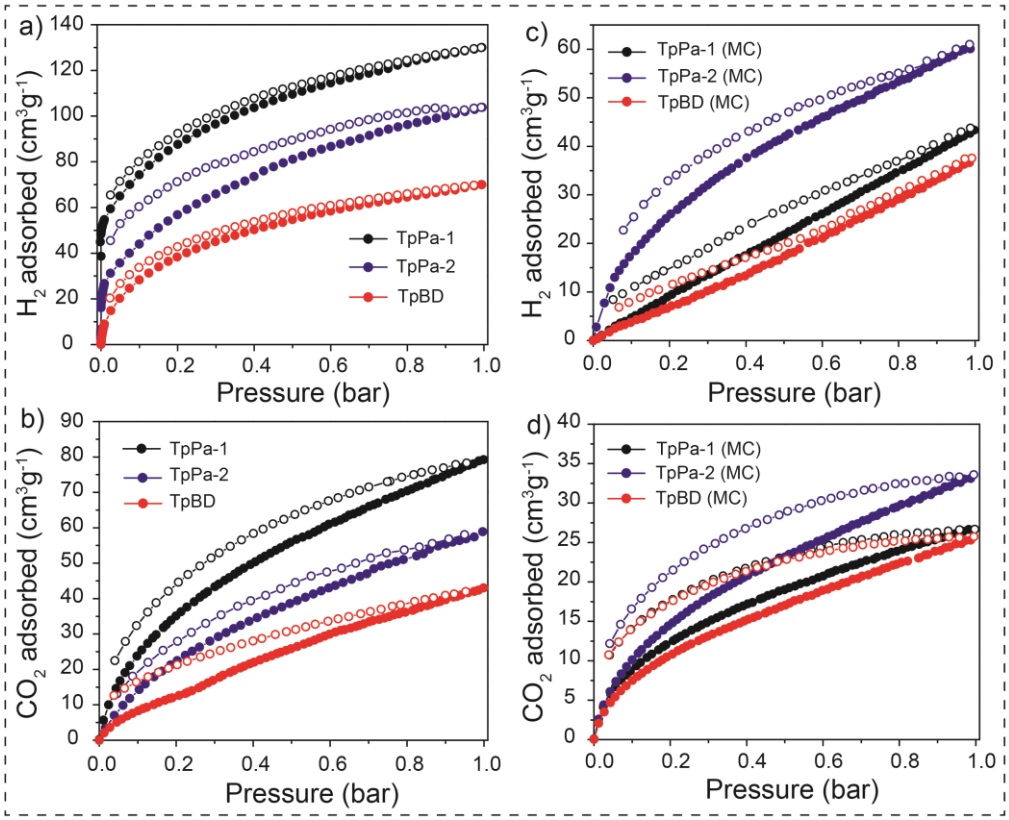

Figure 4.12. *a) and c) Hydrogen adsorption isotherms of TpPa-1, TpPa-1 (MC), TpPa-2, TpPa-2 (MC), TpBD and TpBD (MC) respectively collected at 77 K; b)and d) Carbon dioxide adsorption isotherms of TpPa-1, TpPa-1 (MC), TpPa-2, TpPa-2 (MC), TpBD and TpBD (MC) respectively collected at 273 K.*

From which we found that TpBD have highest water vapour uptake of 268 cm^3g^{-1} at 0.9 (P/P_o) and 293 K, followed by TpPa-1 (249 cm^3g^{-1}) and TpPa-2 (223 cm^3g^{-1}) (***Figure 4.11b***). It is to note that the water uptake value for COFs (ST) is higher than COFs (MC), this could be due to the high surface area and porous nature.

The H_2 uptake capacity of solvothermally and mechanochemically synthesized COFs were checked at 77 K (***Figure 4.12a*** and ***c***). As an example, TpBD found to show a H_2 uptake of 0.7 wt% at 77 K. This uptake is lower than the H_2 uptake of TpPa-1 (1.1 wt%) and TpPa-2 (0.89 wt%) reported previously. Similarly, the CO_2 uptake of TpBD was found to be 43 cm^3g^{-1} at 273 K, whereas for TpPa-1 and TpPa-2 was 78 cm^3g^{-1} and 64 cm^3g^{-1} respectively at 273 K (***Figure 4.12b*** and ***d***). Notably, for COF (MC) both the H_2 and CO_2 uptake values are lower compared to COF (ST), this may be due to the lower porosity and surface area resulted from layered like structures.

4.3.6 *Chemical stability test*

To investigate the stability of COFs (MC and ST) in boiling water, we have submerged 50 mg of each COFs in 10 ml of deionized water and allowed it to stand in boiling condition (100 °C) for 7 days.

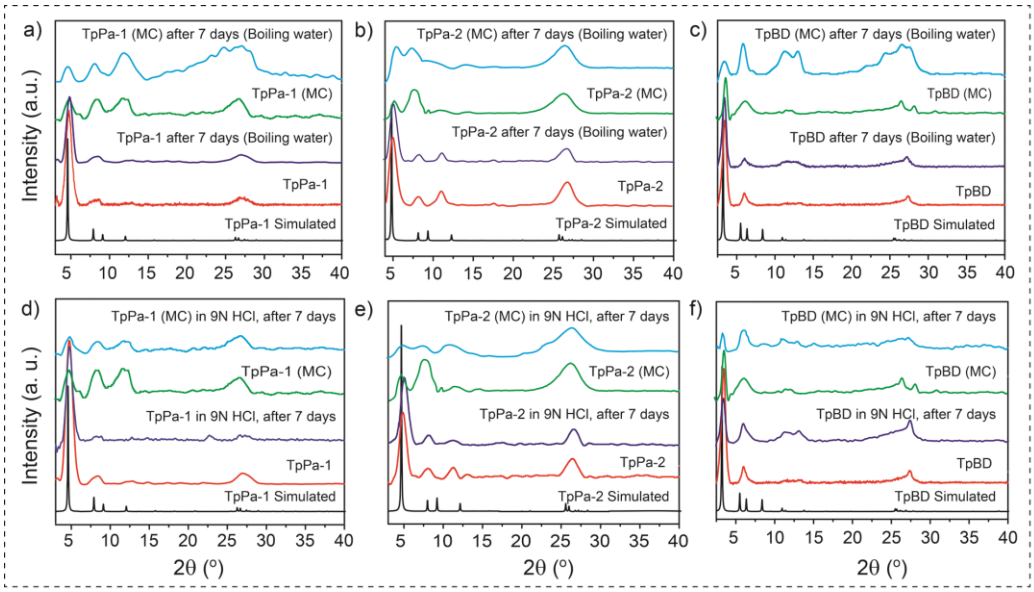

Figure 4.13*. (a), (b) and (c) water stability test for COFs (MC) and COFs (ST) after dipping 7 days in boiling water; (d), (e) and (f) Acid stability test for COFs (MC) and COFs (ST) after dipping 7 days in 9 N HCl.*

After the mentioned period, we took the PXRD to confirm the crystallinity and found that all the PXRD peak positions and the intensity remain intact (***Figure 4.13a-c***). Hence, we conclude that all the COFs synthesized in both (MC) and (ST) methods are highly stable in water. As explained by Kandambeth *et al*., [4.10] the water stability arises due to the irreversible nature of the enol-to-keto tautomerism. Since these COFs (MC) are highly stable in water that motivated us to check the acid and base stabilities as well. We have monitored the acid stability of all three COFs (MC) and the newly made TpBD in 9 N HCl for 7 days (***Figure 13d-f***). Like water, these COFs (MC) are also highly stable in acid, which confirmed by the retention of peak position and intensity in the PXRD profile collected after the acid treatment (9 N HCl) for 7 days. We believe that the same phenomenon of tautomerism (forming only C-N bond) plays a very crucial role for the exceptional acid stabilities of these COFs as well. TpBD and TpBD (MC) were stable in 3 N NaOH as well for about 3 days in comparison to TpPa-1; which is not stable in base even one day, whereas TpPa-2 (MC) was stable for 7 days period due to the presence of hydrophobic $–CH_3$ group near to the Schiff base centers.

4.4 Mechanosynthesis of covalent organic frameworks (COFs) using liquid-assisted grinding (LAG)

4.5 Physical properties of COFs (LAG)

4.5.1 *Powder X-ray diffraction and structural analysis of COF (LAG)*

Synthesis of TpTh (LAG), DhaTph (LAG), and LZU-1 (LAG) were done by the simple Schiff-base reaction using a ball mill. The detailed methods and experimental procedures are given in the experimental section. PXRD patterns of TpTh (LAG) and DhaTph (LAG) showed an intense peaks at 3.8° and 3.4° 2θ, which corresponds to 100 plane reflections along with minor peaks at (6.2° and 24-28°) 2θ and (6.9° and 18-23°) 2θ, which corresponds to 200 and 001 facets respectively. The peak broadening was observed at higher 2θ (001 plane) for the mentioned COFs, this is due to the defects in the π-π stacking between the COF layers. The π-π stacking distances between the COF layers were 3.4 Å and 4 Å for TpTh (LAG) and DhaTph (LAG) respectively, calculated from the d spacing between the 001 planes (***Figure 4.14e*** and ***f***). In the case of LZU-1 (LAG), the PXRD patterns showed a

peak at ~4.6° (2θ) which corresponds to 100 plane reflections along with minor peaks at ~8° and ~26-28° (2θ) which corresponds to 200 and 001 planes. The π-π stacking distances between the COF layers were calculated as 3.4, 3.7 and 4 Å respectively from the d spacing between the 001 planes (***Figure 4.14d-f***). In order to elucidate the structure of these COFs and to calculate the unit cell parameter, possible 2D models were built using SCC-DFTB Method [4.15a]. The experimental PXRD pattern matches well with the simulated pattern of the eclipsed stacking model (***Figure 4.14d-f***). Hence, we believe that the structure close to the *P*6/*m* space group for TpTh (LAG). The structural feature of TpTh (LAG) is closely similar to the COF-42 [4.18]. The unit cell values of TpTh (LAG) were calculated to be $a = b$ = 29.6 Å, c = 3.4 Å; α = 90º, β = 90º and γ = 120º using the Pawley refinement (Table 2).

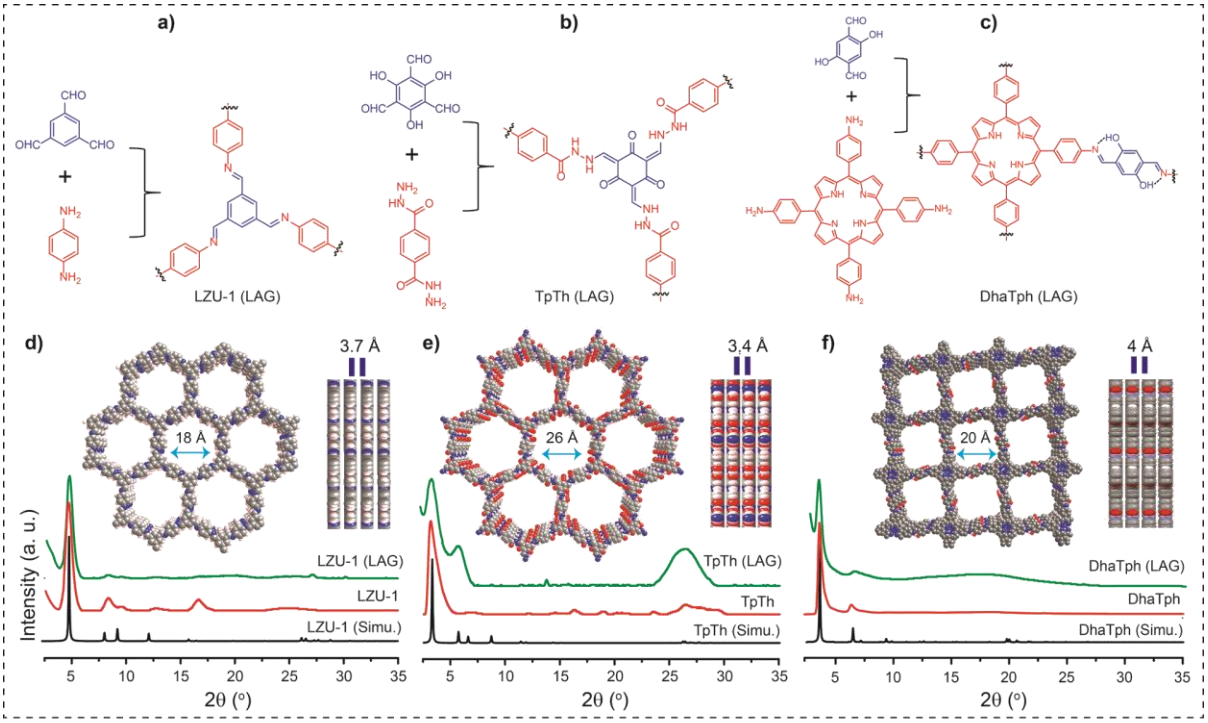

Figure 4.14. *Schematic representation of the synthesis of a) LZU-1 (LAG); b) TpTh (LAG); and c) DhaTph (LAG) through simple Schiff base reaction performed via liquid-assisted grinding (LAG) using a Ball Mill; d), e) and f) Comparison of the PXRD patterns; green [synthesized via LAG approach], red [synthesized via solvothermal method] and black (simulated) for LZU-1 (LAG), TpTh (LAG) and DhaTph (LAG) respectively (Inset images showing the pore opening and π-π stacking distance between consecutive 2D layers for all three COFs).*

For DhaTph (LAG) the proposed structure was close to the *P*4/*m* space group with unit cell values calculated to be $a = b$ = 25.6 Å, c = 4 Å using similar Pawley refinement similar to

DhaTph [4.12b]. LZU-1 (LAG) also crystallizes in the same eclipsed layered structures like the reported LZU-1 [4.12c] (space group of *P*6/*m* with the optimized parameters of $a = b =$ 22.0 Å and $c = 3.7$ Å).

4.5.2 *Fourier transforms infrared (FT-IR) and ^{13}C CP/MAS NMR*

We have collected FT-IR spectra confirm the presence of building blocks in our mechanochemically synthesized COFs (***Figure 4.15a***). The FT-IR spectra of TpTh (LAG) clearly indicate a broadband for the characteristic N-H stretching (3100-3300 cm^{-1}). Simultaneously the carbonyl (C=O) peak position (at 1610 cm^{-1} with reference to 1639 cm^{-1} for Tp) gets broadened, shifted and merged with the newly formed C=C bond (1580 cm^{-1}), this occurs due to the existence of strong hydrogen bonding in the keto form of the 2D framework. The carbonyl stretching of amide unit in the COF framework observed as a merged band at 1660 cm^{-1}, which confirm its presence.

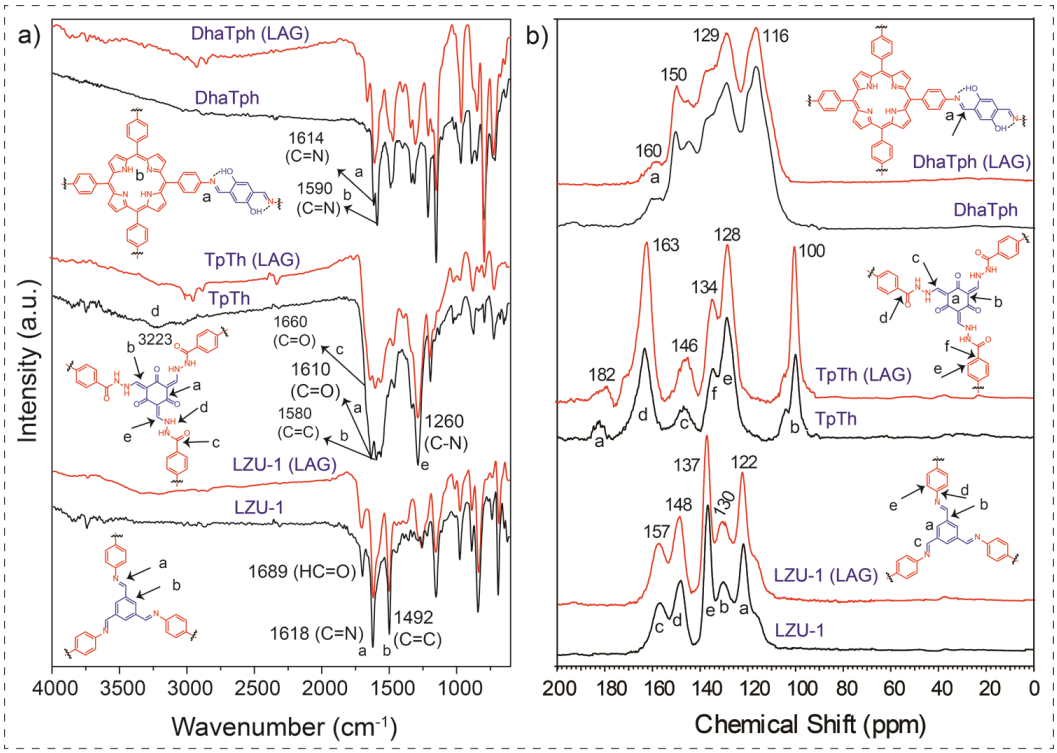

Figure 4.15. *a) Comparison of the FT-IR spectra for LZU-1 and LZU-1 (LAG); TpTh and TpTh (LAG); DhaTph and DhaTph (LAG); (black, synthesized by solvothermal method and red, synthesized by mechanochemical method); b) Comparison of the ^{13}C CP-MAS solid-state NMR spectra for LZU-1 and LZU-1 (LAG); TpTh and TpTh (LAG); DhaTph and DhaTph (LAG); (black, synthesized by solvothermal method and red, synthesized by mechanochemical method).*

The unobserved hydroxyl (O–H) and C=N stretching peaks, as well as the appearance of a new peak at 1580 cm^{-1} (C=C), gives convincing evidence for the existence of the keto form although enol was the expected one. We have also collected the FT-IR spectra of the reference compound {*2,4,6*-tris-[(phenylhydrazino)methylene]cyclohexane-*1,3,5*-trione} made for comparison, which also supported the same fact. The appearance of two peaks at 1465 cm^{-1} [C=C (Ar)] and 1260 cm^{-1} (C-N), were due to the aromatic C=C and newly formed C–N bond in the keto form of the TpTh (LAG) framework. The FT-IR spectrum of DhaTph (LAG) shows characteristic –C=N stretching bands at 1613 cm^{-1} (exists in the enol-imine form) [4.12b] (***Figure 4.15a***). Similarly, the FT-IR spectrum of LZU-1 (LAG) shows a strong C=N stretch at 1618 cm^{-1} indicating the formation of imine bonds. The peak appears at 1689 cm^{-1} and a broadband at (3020-3400 cm^{-1}) is due to the terminal aldehyde and amines present at the edges of LZU-1 (LAG).

We have also carried out ^{13}C CP-MAS solid state NMR spectroscopy to know the structural compositions of these COFs (***Figure 4.15b***). TpTh (LAG) showed a resonance signal at ~182 ppm, which corresponds to the carbonyl carbon of the keto form. This fact is further supported by the ^{13}C NMR spectrum of the reference compound {*2,4,6*-tris-[(phenylhydrazino)methylene]cyclohexane-*1,3,5*-trione}synthesized *via* same LAG approach for comparison. The peak at δ ~163 ppm is due to the amide carbonyl (–CO–NH–), which signifies its presence in the framework. Exact match of solid state ^{13}C NMR profiles indicates the same local structure of COFs obtained *via* both mechanochemical and solvothermal methods (***Figure 4.15b***). ^{13}C CP-MAS NMR of DhaTph (LAG) confirms the formation of the imine bond by showing the characteristic signal at δ 160 ppm, which corresponds to the chemical shift of the –C=N carbon (***Figure 4.15b***). Similarly, the ^{13}C NMR of LZU-1 (LAG) showed a peak at δ ~157 ppm corresponds to the carbon atom of the –C=N bond, which formed by the condensation reaction of aldehyde (TFB) and *p*-phenylenediamine (Pa-1). The signals at ~122, 130, 137, and 148 ppm can be assigned to the carbon atoms of the phenyl groups.

4.5.3 *Thermogravimetric analysis (TGA), Transmission Electron Microscopy (TEM) and N_2 adsorption analysis*

We have confirmed the thermal stability of these activated COFs from TGA (***Figure 4.16b***). Both TpTh and TpTh (LAG) exhibit a thermal stability up to ~300 °C with a gradual weight loss of ~70% (for TpTh) and ~90% [for TpTh (LAG)] respectively at 800 °C. DhaTph and DhaTph (LAG) were observed to be stable up to ~300 °C, and then after the framework slowly decompose with about ~68% weight loss for DhaTph and only ~40% for DhaTph (LAG) respectively at 800 °C. Similarly, LZU-1 (LAG) showed a thermal stability up to 450 °C with a weight loss of ~62% and ~73% respectively at the end of 800 °C (***Figure 4.16b***). The permanent porosity of these mechanochemically synthesized COFs was measured from N_2 adsorption isotherms. These COFs (LAG) showed reversible type II (TpTh and LZU-1) and type IV (DhaTph) adsorption isotherm with low BET surface areas (<100 m^2g^{-1}) for mechanochemically synthesized COFs compared to the solvothermally synthesized COFs, as also previously observed for TpPa-1, -2 and TpBD (MC) [4.11a] (***Figure 4.16c***). The reason for the low surface area could be the strong mechanochemical force applied to the already formed COFs (MC) that sometimes causes delamination of the 2D layers, resulting sheet-like structures. Another possible reason may be the entrapment of insoluble oligomeric impurities inside the pores during the COF formation *via* mechanochemical grinding. The steep increase of N_2 uptake of TpTh and TpTh (LAG) shown at high relative pressure (P/P_0> 0.8) was due to the mesoporous nature (pore aperture = *ca.* 26 Å) and condensation in the inter-particle voids. The TEM images show the layer like morphology and the boundaries of the stacked layers of both TpTh and TpTh (LAG) COFs (***Figure 4.16a***). The formation of the eclipsed structure originates from the strong tendency for the hexagonal units to form coplanar aggregates which could stabilize the π-π stacking interactions between adjacent layers (a distance of ~3.4 Å). TEM images revealed that DhaTph (LAG) is composed of well-defined, squircle-shaped particles that have an almost uniform size of ~40 nm unlike DhaTph, which is perfectly square shaped (~50 nm) (***Figure 4.16a***). Unlike, LZU-1 (LAG) particles were much more elongated in shape and forming thin ribbon-shaped structures (width up to ~40 nm and length more than >500 nm).

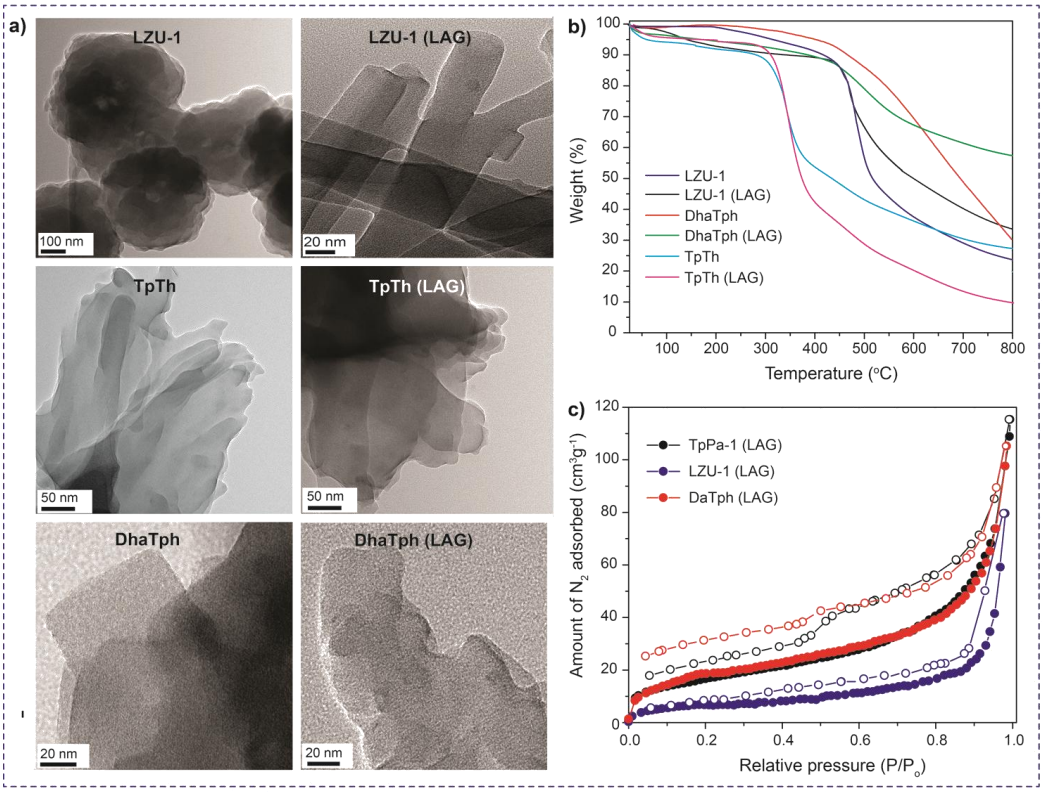

Figure 4.16. *a) HR-TEM images of LZU-1 and LZU-1 (LAG); TpTh and TpTh (LAG); DhaTph and DhaTph (LAG) at different magnifications; b) TGA data of all COFs (ST and LAG) under N_2 atmosphere; c) N_2 adsorption isotherm of TpPa-1 (LAG), LZU-1 (LAG) and DhaTph (LAG).*

The detailed investigations of the stability of these synthesized COFs in the aqueous, acidic and basic medium have been performed. It has been found that all these COFs synthesized *via* LAG approach holds the chemical stability except LZU-1. Since, neither hydrogen bonding nor keto-enol tautomerism exists in LZU-1 (LAG), fast decomposition of the framework results in water or even normal humidified conditions. However, the keto-enol tautomerism (keto-enamine formation) and O–H···N=C intramolecular hydrogen bonding is the key factor for this enhanced hydrolytic stability of TpTh (LAG) and DhaTph (LAG) respectively.

4.6 Conclusions

In the first part of this chapter, we have discussed the first example of a simple, safe and environmentally-friendly mechanochemical synthetic route for the synthesis of three highly water, acid and base stable covalent organic frameworks (COFs). We have

demonstrated that by employing Schiff base mechanochemistry, COFs can be synthesized very rapidly in high yield at room temperature and the progress of the reaction and the product can be observed by the visual colour change. We observed a simultaneous mechanochemical exfoliation of 2D COFs layers during the grinding process, which has not been observed for any COFs materials before. The gas and water adsorption properties of all COFs (MC) were studied and compared with the COFs (ST). In the later part of this chapter, liquid-assisted grinding (LAG) have been employed to synthesize three COFs [TpTh (LAG), DhaTph (LAG) and LZU-1 (LAG)] efficiently at a faster rate and in high yield at room temperature with improved crystallinity compared to only neat grinding. Also, we have focused that the COFs with low chemical stability such as LZU-1 (LAG) can also be readily synthesized with decent crystallinity using the same LAG approach. Although the crystallinity, porosity of these mechanochemically synthesized COFs are moderate, we believe our fundamental findings will provide better insight towards the general synthetic applicability of mechanochemistry and will become a conventional synthetic tool for the large scale COF production in near future. Moreover, the observed 2D layered structures of COFs (MC) will be very much helpful to act as a graphene-like supportive material for various practical applications.

4.7 Experimental procedures

4.7.1 *Materials*

Terephthalic dihydrazide was synthesized from diethyl terephthalate and hydrazine monohydrate by reported procedure [4.19a] and *2,5*-dihydroxyterephthalaldehyde (Dha) was synthesized from *1,4*-dimethoxybenzene [4.19b]. All other reagents and solvents were commercially available and used as received.

4.7.2 *Synthesis*

4.7.2.1 *Synthesis of 1,3,5-triformylphloroglucinol (Tp)*

The 1,3,5-triformylphloroglucinol (Tp) was synthesized using literature procedure [4.16]. To hexamethylenetetraamine (15.098 g, 108 mmol) and dried phloroglucinol (6.014 g, 49 mmol) under N_2 was added 90 mL trifluoroacetic acid. The solution was heated at 100

ºC for ca. 2.5 h. Approximately 150 mL of 3 M HCl was added and the solution was heated at 100 ºC for 1 h. After cooling to room temperature, the solution was filtered through Celite, extracted with ca. 350 mL dichloromethane, dried over magnesium sulfate, and filtered. Rotary evaporation of the solution afforded 1.48 g (7.0 mmol, 14%) of an off-white powder.

a) ***Synthesis of TpPa-1 (MC), TpPa-2 (MC) and TpBD (MC) via neat grinding*****:** *1,3,5*-triformylphloroglucinol (Tp) (0.3 mmol), aromatic diamine [*p*-phenylenediamine (for TpPa-1), *2,5*-dimethyl-p-phenylenediamine (for TpPa-2) and benzidine (for TpBD)] (0.45 mmol) was placed in a mortar (inner diameter = 3 inch or 75 mm) and with either neat or 1-2 drop of mesitylene : dioxane (1: 1) grounded using pestle at room temperature, after 5 minutes a light yellow colour developed. We characterized the yellow powders *via* FT-IR spectra, ^{13}C solid-state NMR, and found that these yellow powders are a mixture of oligomeric form with some unreacted starting materials. As time progress the colour changes to orange (15 minutes) which could be due to the increased number of units and conjugation, finally the dark red colour observed [similar to COFs (ST)] after 30 minutes age of reaction which indicates the complete COFs formation. The dark red powder collected after 45 minutes was then washed with anhydrous acetone, dichloromethane 5-6 times to remove some unreacted starting material and oligomeric impurities, then dried at 180 ^{0}C under vacuum for 24 hours to give a deep red colored powder in ~90% isolated yield. FT-IR was employed to check the reaction progress, after 40 minutes of reaction all the corresponding IR peaks of COFs (MC) were matched well with the COFs (TpPa-1, –2 and TpBD) synthesized solvothermally. **TpPa-1 (MC): IR (powder, cm^{-1});** 1609 (s), 1582 (s), 1579 (w), 1445 (s), 1256 (s), 1093 (m), 990 (s), 825 (s). **Anal. Calcld**. For $C_6H_4N_1O_1$: C, 69.92; H, 3.77; N, 13.20; found: C, 65.2; H, 3.77; N, 11.02. **TpPa-2 (MC): IR (powder, cm^{-1});** 2885 (w), 1587 (s), 1444 (s), 1250 (s), 1090 (w), 995 (s), 859 (m). **Anal. Calcld**. For $C_7H_4N_1O_1$: C, 71.18; H, 3.38; N, 11.86; found: C, 70.51; H, 5.34; N, 10.58. **TpBD (MC): FT-IR (powder, cm^{-1});** 1594 (s), 1579 (w), 1464 (s), 1258 (s), 1093 (m), 990 (s), 825 (s). **Anal. Calcld**. For $C_9H_6N_1O_1$: C, 75.0; H, 4.16; N, 9.72; found: C, 72.51; H, 3.98; N, 8.75.

b) ***Procedure for the synthesis of COF-TpPa-1 (MC), TpPa-2 (MC)*** *and* ***TpBD (MC) using ball mill*****:** *1,3,5*-triformylphloroglucinol (Tp) (0.3 mmol), the aromatic diamine [*p*-phenylenediamine (for TpPa-1) or *2,5*-dimethyl-p-phenylenediamine (for TpPa-2) or benzidine (for TpBD)] (0.45 mmol) was placed in a 5 mL stainless steel jar, with two 7 mm

diameter stainless steel balls and either neat or 1-2 drop of mesitylene : dioxane (1:1). The mixture was ground at room temperature for 45 minutes in a Retsch MM400 mill operated at 25 Hz. The dark red powders [Red for TpPa-1 (MC), TpPa-2 (MC) and yellowish red for TpBD (MC)] collected after 45 minutes was then washed with anhydrous acetone, dichloromethane 5-6 times to remove some unreacted starting material and oligomeric impurities, then dried at 180 ^{0}C under vacuum for 24 hours to give a deep colored powder in ~89% isolated yield. Reactions were repeated to ensure reproducibility.

c) ***COF-TpPa-1 and TpPa-2*****:** A pyrex tube (o.d. × i.d. = 10 × 8 mm^2 and length 18 cm) is charged with *1,3,5*-triformylphloroglucinol (Tp) (63 mg, 0.3 mmol), diamine [*P*-phenylenediamine (Pa-1) (48 mg, 0.45 mmol) for TpPa-1 and *2,5*-dimethy-*p*-phenylenediamine (Pa-2) (61 mg, 0.45 mmol) for TpPa-2], 1.5 mL of mesitylene, 1.5 mL of dioxane, 0.5 mL of 3 M aqueous acetic acid. This mixture was sonicated for 10 minutes in order to get a homogenous dispersion. The tube was then flash frozen at 77 K (liquid N_2 bath) and degassed by three freeze-pump-thaw cycles. The tube was sealed off and then heated at 120 °C for 3 days. A red colored precipitate formed was collected by centrifugation or filtration and washed with anhydrous acetone. The powder collected was then solvent exchanged with anhydrous acetone 5-6 times and then dried at 180 ºC under vacuum for 24 h to give a deep red colored powder in ~80% isolated yield.

d) ***COF-TpBD*****:** A Pyrex tube (o.d. × i.d. = 10 × 8 mm^2 and length 18 cm) is charged with *1,3,5*-triformylphloroglucinol (Tp) (63 mg, 0.3 mmol), Benzidine (BD) (82.9 mg, 0.45 mmol), 1.5 mL of mesitylene, 1.5 mL of dioxane, 0.5 mL of 3 M aqueous acetic acid. This mixture was sonicated for 10 minutes in order to get a homogenous dispersion. The tube was then flash frozen at 77 K (liquid N_2 bath) and degassed by three freeze-pump-thaw cycles. The tube was sealed off and then heated at 120 °C for 3 days. A red colored precipitate formed was collected by centrifugation or filtration and washed with anhydrous acetone. The powder collected was then solvent exchanged with anhydrous acetone 5-6 times and then dried at 180 ºC under vacuum for 24 hours to give a deep red colored powder in 80% isolated yield. **FT-IR (powder, cm^{-1}):** 1594 (s), 1579 (w), 1464 (s), 1258 (s), 1093 (m), 990 (s), 825 (s). **Anal. Calcld**. For $C_9H_6N_1O_1$: C, 75.0; H, 4.16; N, 9.72; found: C, 71.98; H, 3.33; N, 8.82.

e) *2,4,6*-tris((phenylamino)methylene)cyclohexane-*1,3,5*-trione *(Reference compound for TpPa-1)*: The reference compound was synthesized by the reaction between *1,3,5*-triformylphloroglucinol (0.163 g, 0.8 mmol) and aniline (0.5 g, 5.4 mmol) in 70 mL ethanol under refluxing condition for one day. After this time the solution was cooled to room temperature and the precipitate was collected by filtration, washed with ethanol, and dried under vacuum to give 0.210 g (0.5 mmol, 82%) of a yellow solid. **^{1}H NMR (300 MHz, $CDCl_3$):** δ 13.0-13.4 (m, NH), 8.90 (d, HC-N), 8.77 (d, CH), 8.75 (d, CH), 7.44-7.17 (m, Ph) ppm. **FT-IR (powder, cm^{-1}):** 1616 (s), 1581, 1553, 1465, 1444, 1340, 1287, 1236, 1041.

4.7.2.2 *Synthesis of TpTh (LAG)*: *1,3,5*-triformylphloroglucinol (Tp) (63.0 mg, 0.3 mmol), terephthalic dihydrazide (Th) (87.4 mg, 0.45 mmol) was placed in a 5 mL stainless steel jar, with one 7 mm diameter stainless steel ball, 1-2 drop (~100 μL) of mesitylene : dioxane (2:1) and 1 drop (~50 μL) of 3 M acetic acid. The mixture was milled at room temperature for 90 minutes in a Retsch MM400 mill operated at 25 Hz. A yellow colour powder formed was collected and washed with DMA, DMF and finally with acetone repeatedly for 3 days. Further purification was carried out by Soxhlet extraction in DMA for 48 h and then dried at 180 °C under vacuum for 24 hours to give a yellow colour powder in ~78 % (105 mg) isolated yield. **FT-IR (powder, cm^{-1}):** 3223, 1660, 1610, 1580, 1542, 1444, 1337, 1260, 1180, 995, 855. **Anal. Calcld (%)**. For $(C_7O_2N_2H_4)_n$: C, 57.75; H, 3.7; N, 18.9; found : C, 50.33; H, 3.87; N, 18.87.

a) *Synthesis of TpTh*: A pyrex tube (o.d. × i.d. = 10 × 8 mm^2 and length 18 cm) is charged with *1,3,5*-triformylphloroglucinol (Tp) (63.0 mg, 0.3 mmol), terephthalic dihydrazide (87.4 mg, 0.45 mmol), 3.0 mL of mesitylene, 1.5 mL of dioxane, 0.5 mL of 3 M aqueous acetic acid. This mixture was sonicated for 10 minutes in order to get a homogenous dispersion. The tube was then flash frozen at 77 K (liquid N_2 bath) and degassed by three freeze-pump-thaw cycles. The tube was sealed off and then heated at 120 °C for 3 days. A yellow colour precipitate formed was collected by filtration and washed with DMA, DMF and finally with acetone repeatedly for 3 days. Further purification was carried out by Soxhlet extraction in DMA for 48 h and then dried at 180 °C under vacuum for 24 hours to give a yellow powder in ~70 % (94 mg) isolated yield. **FT-IR (powder, cm^{-1}):** 3223, 1660, 1610, 1580, 1542, 1444, 1337, 1260, 1180, 995, 855. **Anal. Calcld (%)**. For $(C_7O_2N_2H_4)_n$: C, 57.75; H, 3.7; N, 18.9; found : C, 49.69; H, 3.89; N, 19.66.

b) ***2,4,6*-tris-[(phenylhydrazino)methylene]cyclohexane-*1,3,5*-trione *(Reference compound for TpTh)*:** 1,3,5-triformylphloroglucinol (Tp) (63.0 mg, 0.3 mmol) and phenyl hydrazide (Ph) (97.2 mg, 0.9 mmol) was placed in a 5 mL stainless steel jar, with one 7 mm diameter stainless steel ball, 1-2 drop (~100 μL) of ethanol and 1 drop (~50 μL) of 3 M acetic acid. The mixture was milled at room temperature for 30 minutes in a Retsch MM400 mill operated at 25 Hz. The powder formed was collected and washed with ethanol, and dried under vacuum to give a dark red solid (yield ~84%); **FT-IR (powder, cm^{-1}):** 1594, 1565, 1436, 1273, 1170, 1109, 986, 812, 710.

c) ***Synthesis of DhaTph (LAG)*:** *2,5*-dihydroxyterephthalaldehyde (Dha) (13.3 mg, 0.08 mmol) and tetra(*p*-amino-phenyl)porphyrin (Tph) (27.0 mg, 0.04 mmol) was placed in a 5 mL stainless steel jar, with one 7 mm diameter stainless steel ball, in that 6 M acetic acid (1 drop) and dichlorobenzene, ethanol (1: 1) as solvent combination (2 drops) was added. The mixture was milled at room temperature for 90 minutes in a Retsch MM400 mill operated at 25 Hz. After the reaction, the COF powders washed with ethanol 5-7 times and dried under vacuum at 150 °C for 12 hours to give purple colored powder in ~75 % (28 mg) isolated yield based on Tph. **FT-IR (powder, cm^{-1})**: 1613, 1590, 1491, 1399, 1338, 1313, 1213, 1149, 968, 888, 849, 797, 718.

d) ***Synthesis of DhaTph*:** The synthesis of DhaTph was carried out by utilizing the standard protocol for COF synthesis with a mixture of *2,5*-dihydroxyterephthalaldehyde (Dha) (13.3 mg, 0.08 mmol) and tetra(*p*-aminophenyl)porphyrin (Tph) (27.0 mg, 0.04 mmol) in presence of 6 M acetic acid (0.2 mL) using dichlorobenzene, ethanol (1: 1) as solvent combination (2 mL). This mixture was sonicated for 10-15 minutes in order to get a homogenous dispersion. The tube was then flash frozen at 77 K (liquid N_2 bath) and degassed by three freeze-pump-thaw cycles. The tube was sealed off and then heated at 120 °C for 3 days. After the reaction the COF powders are filtered out, washed with ethanol and dried under vacuum at 150 °C for 12 h to give purple colored powder in ~79% isolated yield based on Tph.

e) ***Synthesis of LZU-1 (LAG)*:** *1,3,5*-triformylbenzene (TFB) (48.0 mg, 0.3 mmol), *p*-phenylenediamine (Pa-1) (48.0 mg, 0.45 mmol) was placed in a 5 mL stainless steel jar, with one 7 mm diameter stainless steel ball, 1-2 drop of mesitylene : dioxane (1:1) and 1 drop of

3M acetic acid. The mixture was milled at room temperature for 90 minutes in a Retsch MM400 mill operated at 25 Hz. The dark yellow powders collected was then washed with anhydrous DMF and THF, 5-6 times to remove some unreacted starting material and oligomeric impurities. Further purification was carried out by Soxhlet extraction in THF for 48 h and dried at 160 ºC under vacuum for 24 h to yield COF-LZU-1 (LAG) as a dark yellow powder (68.5 mg, ~86% yield). The reaction was repeated to ensure reproducibility. **FT-IR (powder, cm^{-1});** 3382, 2863, 1689, 1618, 1492, 1444, 1250, 1146, 968, 880, 832, 730, 685. **Anal. Calcld (%)**. For $(C_6H_4N)_n$: C, 80.0; H, 4.44; N, 15.55; found : C, 72.31; H, 4.59; N, 13.79.

f) ***Synthesis of COF-LZU-1*:** The detailed synthetic procedure was described by Ding *et al*. [12c].A pyrex tube (o.d. × i.d. = 10 × 8 mm^2 and length 18 cm) is charged with *1,3,5*-triformylbenzene (48 mg, 0.30 mmol), *1,4*-diaminobenzene (48 mg, 0.45 mmol), 3.0 mL of dioxane, 0.6 mL of 3.0 mol/L aqueous acetic acid. This mixture was sonicated for 10 minutes in order to get a homogenous dispersion. The tube was then flash frozen at 77 K (liquid N_2 bath) and degassed by three freeze-pump-thaw cycles. Upon warming to room temperature, the tube was sealed off and then heated at 120 °C for 3 days. A yellow colour precipitate formed was collected by filtration and washed with DMF and finally with dried tetrahydrofuran (THF) repeatedly for 3 days to yield COF-LZU1. (70 mg, ~90% yield). **Anal. Cald (%)** for $(C_6H_4N)_n$: C 80.00; H 4.44; N 15.55. Found: C 76.34; H 4.61; N 14.20. **FT-IR** (powder, cm 1) 3382, 2864, 1694, 1618, 1496, 1444, 1250, 1146, 968, 880, 832, 730, 685. **PXRD** [2θ (relative intensity)] 4.70 (100), 8.05 (110), 9.47 (200), 12.45 (210), 26.22 (001).

4.7.3 *General methods for characterization*

a) ***Powder X-Ray diffraction (PXRD)*:** Powder X-ray diffraction (PXRD) patterns were recorded on a Rigaku Smartlab diffractometer for Cu K_α radiation (λ = 1.5406 Å), with a scan speed of 2° min^{-1}. The tube voltage and amperage were set at 40 kV and 50 mA respectively. Each sample was scanned between 5 and 50° 2θ with a step size of 0.02°. The instrument was previously calibrated using a silicon standard.

b) ***Thermogravimetric analysis (TGA)*:** Thermogravimetric analyses (TGA) were carried out on a TG50 analyzer (Mettler-Toledo) or a SDT Q600 TG-DTA analyzer under N_2 atmosphere at a heating rate of 5 ºC min^{-1} within a temperature range of 30-800 °C.

c) ***FT-IR spectroscopy*:** Fourier transform infrared (FT-IR) spectra were taken on a Bruker Optics ALPHA-E spectrometer with a universal Zn-Se ATR (attenuated total reflection) accessory in the 600-4000 cm^{-1} region or using a Diamond ATR (Golden Gate). 24 scans were collected at 4 cm^{-1} resolution for each sample.

d) ***Electron Microscopy*:** SEM images were obtained with a Zeiss DSM 950 scanning electron microscope and FEI, QUANTA 200 3D Scanning Electron Microscope with tungsten filament as electron source operated at 10 kV. The samples were sputtered with Au (nano-sized film) prior to imaging by a SCD 040 Balzers Union. HR-TEM images were recorded using FEI Tecnai G2 F30 X-TWIN TEM at an accelerating voltage of 300 kV. The TEM Samples were prepared by drop casting the sample from isopropanol on copper grids TEM Window (TED PELLA, INC. 200 mesh).

e) ***^{13}C CP/MAS Solid state NMR and Raman spectroscopy*:** Solid-state NMR (SSNMR) was taken in a Bruker 300 MHz NMR spectrometer and reference compound NMR data were taken in Bruker 200 MHz NMR spectrometer. All Raman measurements were carried out at room temperature on a (Jobin Yvon Horiba, France) using monochromatic radiation emitted by an Ar-laser (514 nm) (NRS 1500 W) operating at 20 mW using 50x long distance objective. The experiment was repeated several times and at different positions to verify the consistency of the measurement. The samples were prepared simply by putting a drop of dispersion of COF materials in isopropanol on a clean piece of Silicon wafer.

f) ***Gas/water adsorption experiments*:** All low-pressure N_2 adsorption experiments (up to 1 bar) were performed on a Quantchrome instrument and water adsorption experiments on Quantachrome Autosorb-iQ-MP automatic volumetric instrument. Approximately 50 mg of the sample was activated after solvent exchange by the use of activation chamber. The activated sample was loaded inside the glass bulb of gas/vapour adsorption instrument and measured the capacity.

4.7.4 *Crystallography*

4.7.4.1 *Structure modeling and atomic coordinates of TpBD and TpTh (LAG)*

As Atomic positions and cell sizes of modeled COF layers were optimized using Self-Consistent-Charge Density-Functional Tight-Binding (SCC-DFTB) Method. Stacking of layers are affected by the Coulomb repulsion between the partial atomic charges in adjacent layers. Hence, we performed Mulliken population analysis for the charges. The adjacent layers were shifted with respect to each other in different directions in order to avoid Coulomb repulsion from charges alike.

Table 4.1. *Fractional atomic coordinates for the unit cell of COF-TpBD.*

COF-TpBD			
Hexagonal: *P*6/*m* *a* = *b* = 29.28 Å, *c* = 3.25 Å α = 90º, β = 90º, γ = 120º			
O	0.2956	0.5612	0
N	0.3872	0.5781	0
C	0.3135	0.6107	0
C	0.4039	0.6298	0
C	0.4195	0.5569	0
C	0.4739	0.5883	0
C	0.5046	0.5656	0
C	0.4829	0.5112	0
C	0.4281	0.4803	0
C	0.3968	0.5027	0
C	0.3684	0.6472	0
H	0.4458	0.6592	0
H	0.4926	0.6314	0
H	0.3442	0.5557	0
H	0.3534	0.4783	0
H	0.5476	0.5916	0
H	0.4091	0.4372	0

Several possibilities were considered, however, the best was taken from a comparison of simulated PXRD pattern with the experimental. Interlayer separation was also determined from the comparison of PXRD patterns. The fractional coordinates of TpBD and TpTh (LAG) are given in ***Table 4.1*** and ***Table 4.2*** respectively. In order to elucidate the structure of these COFs and to calculate the unit cell parameters, possible 2-D models were optimized using Density-Functional Tight-Binding method. Several stacking possibilities were considered for reasons reported in the literature. The experimental PXRD patterns are agreeable with the simulated patterns of some near-eclipsed stacking models. Hence, we propose structures close to hexagonal space group (*P*6/*m*) for **TpBD** by comparing the experimental and simulated PXRD patterns. Refinements of PXRD pattern were done using Reflex module of Material Studio.

Table 4.2. *Fractional atomic coordinates for the unit cell of TpTh (LAG).*

TpTh (LAG)			
Hexagonal: *P*6/*m* $a = b = 29.97$ Å, $c = 3.4$ Å $\alpha = 90^o$, $\beta = 90^o$ and $\gamma = 120^o$			
C1	0.38352	0.67953	0
C2	0.37095	0.71716	0
C3	0.46151	0.44892	0
C4	0.45120	0.48802	0
C5	0.46878	0.57675	0
C6	0.48730	0.53952	0
C7	0.35904	0.58914	0
N1	0.41908	0.56296	0
N2	0.40520	0.59983	0
O1	0.57173	00.30789	1
O2	0.49804	0.62101	0

NOTE: The results presented in this chapter have already been published in *J. Am. Chem. Soc.*, **2013**, *135*, 5328–5331, and *Chem. Commun.*, **2014**, *50*, 12615-12618, with the title: "*Mechanochemical Synthesis of Chemically Stable Isoreticular Covalent Organic Frameworks*" and "*Mechanosynthesis of Imine, β-Ketoenamine, and Hydrogen-Bonded Imine-Linked Covalent Organic Frameworks using Liquid-Assisted Grinding*" respectively. This publication was the results from the group of Dr. Rahul Banerjee and his students Mr. Bishnu Prasad Biswal, Mr. Suman Chandra, Mr. Sharath Kandambeth, Dr. Gobinda Das and Dr. Digambar Balaji Shinde from CSIR-National Chemical Laboratory, Pune, India. Prof. Thomas Heine with his student Mr. Binit Lukose has contributed to the publication by performing computational studies on COFs. Major work was contributed by Mr. Bishnu Prasad Biswal and Dr. Gobinda Das with the help from all co-authors. Both the manuscripts were written by Mr. Bishnu Prasad Biswal in co-ordination with all the co-authors under the guidance of Dr. Rahul Banerjee.

CHAPTER 5

Chemically Stable Covalent Organic Framework-Polymer Hybrid Membranes for Enhanced Gas Separation

Abstract: *In this chapter, we have discussed the fabrication of highly flexible, COF@Polymer hybrid membranes for gas separation. The COF loading into the polymer (PBI-BuI) matrix obtained was substantially high (50%), than generally achieved for MOFs (30%). These hybrid membranes showed exciting enhancement in the permeability (~7 fold) of gases with appreciable separation factors for CO_2/N_2 and CO_2/CH_4. Further, we found that by COF pore modulation, the gas permeability can be systematically enhanced. In the later part of this chapter, we have focused on fabricating Thin Film Composite (TFC) membranes based on COF (TpPa-1) and Styrene Butadiene Rubber (SBR). We found that these TFC membranes are chemically stable and highly flexible even at 70% of COF loading into the polymer matrix. Excitingly, TpPa-1@SBR TFC membranes showed 8-12 fold faster hydrocarbon (propylene and propane) transport compared to pristine SBR-TFC membranes with enhanced reverse separation factor. We believe that the outcome of this work would be useful for significant hydrocarbon vapour recovery from fuel stations/industries.*

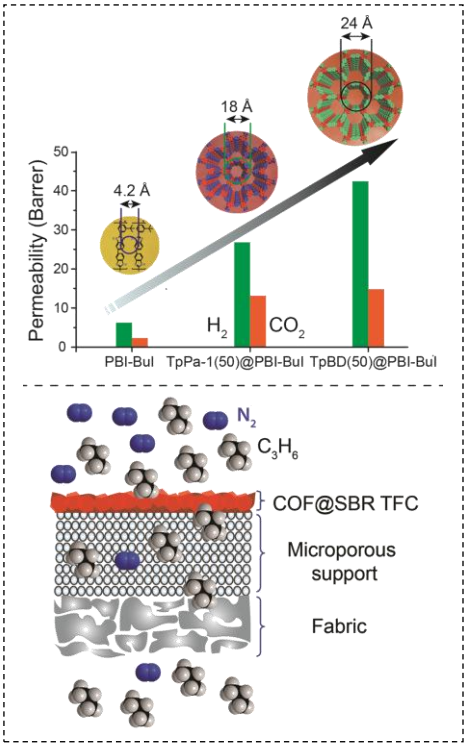

5.1 Introduction

The fabrication of composite membranes based on porous materials for molecular separation has gathered significant interest in recent years [5.1]. Among various membrane materials, polymers are always preferred for separation applications due to easy processability, mechanical stability and scale-up opportunity [5.2]. However, polymeric membranes have certain limitations in terms of permeability-selectivity trade-off, plasticization, and high temperature withstands capacity. These factors are proving to be major concerns and need urgent scientific attention [5.3]. To conquer these shortcomings, constantly researchers are putting efforts for developing various methodologies of incorporating porous material fillers like zeolite [5.4], CNTs [5.5], CMS [5.6], MOFs [5.7], PAFs [5.8] and porous organic cages [5.9] inside the polymer matrix to enhance the composite membrane performance. Although a momentous advancement in MOF-based membranes have been documented, but often face compatibility issues with the polymers, which leads to cracks and defects in the resulting composite membranes [5.10]. This fact motivated us to thought for a fully organic material, which is crystalline, porous and have well-defined nanochannels along with high chemical stability to be used as filler. We anticipate that, due to the fully organic nature, they will offer excellent compatibility with the polymer matrix gives rise to better separation performance.

Covalent organic frameworks (COFs) are a class of crystalline, porous materials linked by covalent bonds between lighter elements (H, B, C, Si, N and O) [5.11]. These materials have attracted numerous interests in the areas like adsorption/storage [5.12], chemical sensors [5.13], catalysis [5.14] and optoelectronics [5.15] due to their highly ordered and low-density framework, with an opportunity to incorporate diverse functional groups at a molecular level. Despite, COF-polymer hybrid membranes are not so far explored for any molecular separations [5.16]. Although researchers have tried to make such membrane but they were not successful because of poor chemical stability in the attempted COFs under operational conditions [5.17]. We have looked at the problem and tried to address this issue by making use of our chemically stable COFs [5.18] for hybrid membrane fabrication with a modified polybenzimidazole (PBI-BuI) and employed them for gas separation.

In the first part of this chapter, we showcase the first usage of chemically stable isoreticular COFs [TpPa-1 and TpBD, pore aperture of 18 Å and 24 Å, respectively] as an active phase incorporated within the polymer (PBI-BuI) matrix for making self-supported TpPa-1@PBI-BuI and TpBD@PBI-BuI hybrid membranes. Considerably high (50%) COF loading to polymer matrix have been achieved unlike MOFs (~30%) [5.19]. These COF@Polymer hybrid membranes display exceptionally high chemical stability and flexibility. Our aim was to create intermolecular interactions between H-bonded benzimidazole groups of PBI with COFs to improve the filler loading and thereby enhance the overall permeability of the composite matrix. Six hybrid membranes, *viz*., TpPa-1(20)@PBI-BuI, TpPa-1(40)@PBI-BuI, TpPa-1(50)@PBI-BuI, TpBD(20)@PBI-BuI, TpBD(40)@PBI-BuI and TpBD(50)@PBI-BuI was prepared with a sequential increase of COF content in the polymer (PBI-BuI) matrix. Notably, both partners contain organic backbone, H-bonding sites and have good thermochemical stability; which are requisites for membrane usability for real life applications such as separations involving H_2 and CO_2 at elevated temperatures. Further, these COF@PBI-BuI hybrid membranes were evaluated for gas permeation performance and found to offer elevated (~7 fold) gas permeability (H_2, N_2, CH_4 and CO_2), while maintaining appreciable selectivities with respect to the pristine PBI-BuI dense membrane.

In the second part of this chapter, we have tried to address the issue associated with mixed matrix composite dense membranes (MMMs) comprising of porous materials (*i.e.* MOF/COF@Polymer) for gas separation [5.20]. These issues are, poor loading of fillers, chemical instability, synthetic difficulty, membrane brittleness, higher thickness or compatibility issues, which restricted their use in potential applications such as hydrocarbon recovery [5.20b and e]. Moreover, hydrocarbon recovery is a long-standing problem in many fuel industries and filling stations, which demand a very high flux membrane material with an outstanding selectivity of hydrocarbons with respect to other gases such as air components [5.10]. We anticipate, these shortcomings can be met by utilising the core property (flexibility and good affinity towards gases) of a well-chosen polymer matrix in combination with a suitable porous material (that would provide a free path for the gas transport) in adequate membrane form, such as thin film composite (TFC) membranes. Notably, TFC membranes serve best as it demands very less active materials and offers higher fluxes as

compared to other membrane types owing to their ultrathin selective skin layers [5.21]. It is noteworthy that, most of the composite gas separation membranes reported are made-up of glassy polymers because of their good mechanical strength and low plasticization effect. However, due to glassy nature, these polymers possess very low hydrocarbon permeance [5.22]. This motivated us to select a rubbery polymer [styrene butadiene rubber (SBR)], which have a very high affinity towards hydrocarbons and a crystalline, porous, chemically stable COF (TpPa-1) possessing well-defined nanochannels as a filler to make the TFC membranes for hydrocarbon separation.

We devote our effort to make use of chemically stable COF [TpPa-1] as a transport-active phase incorporated within the polymer (SBR) matrix to make TpPa-1@SBR thin film composite (TFC) membranes. Three TFC membranes, *viz.*, TpPa-1(30)@SBR, TpPa-1(50)@SBR and TpPa-1(70)@SBR, were prepared with a sequential increase of COF content. These TpPa-1@SBR TFCs membranes are stable, flexible and can be easily processable. Our motivation behind the use of rubbery polymer (SBR) was to improve upon the filler (COF) loading, to achieve membrane flexibility and thereby hydrocarbon affinity. This would lead to enhancing the overall hydrocarbon permeance of the composite matrix that is highly required in applications such as hydrocarbon vapour recovery in fuel filling stations. A maximum of 70% of TpPa-1 could be loaded into the SBR matrix as both associates contain pure organic backbone. This loading (%) is higher than ever made any MMMs based on porous materials [5.20], even compared to COF@PBI-BuI discussed in the first part of this chapter. So obtained COF@SBR TFC membranes were tested for gas permeation performance and found to offer 8-12 times faster hydrocarbon permeance (propylene and propane) with respect to pristine SBR-TFC membranes. The increase in reverse selectivity compared to the pristine SBR TFC membrane was a highly promising outcome of this work.

5.2 Chemically stable covalent organic framework (COF)-polybenzimidazole based hybrid membranes

5.3 Result and discussion

5.3.1 *Wide-angle X-ray diffraction (WAXD) analysis*

A solution casting method using *N*,*N*-dimethylformamide (DMAc), was employed for the fabrication of COF(n)@PBI-BuI hybrid membranes by varying incremental COF content (where, n = 20, 40 or 50 wt% of TpPa-1 and TpBD) (***Figure 5.1***). In these hybrid membranes, the COF loading could be successfully achieved till 50%. Beyond this composition, defects in the membrane was observed. Importantly, all prepared COF-polymer hybrids are quite flexible even at higher (50%) COF loading (***Figure 5.2***) unlike their MOF membrane counterparts; where only 30% ZIF-8 loading was possible [5.19].

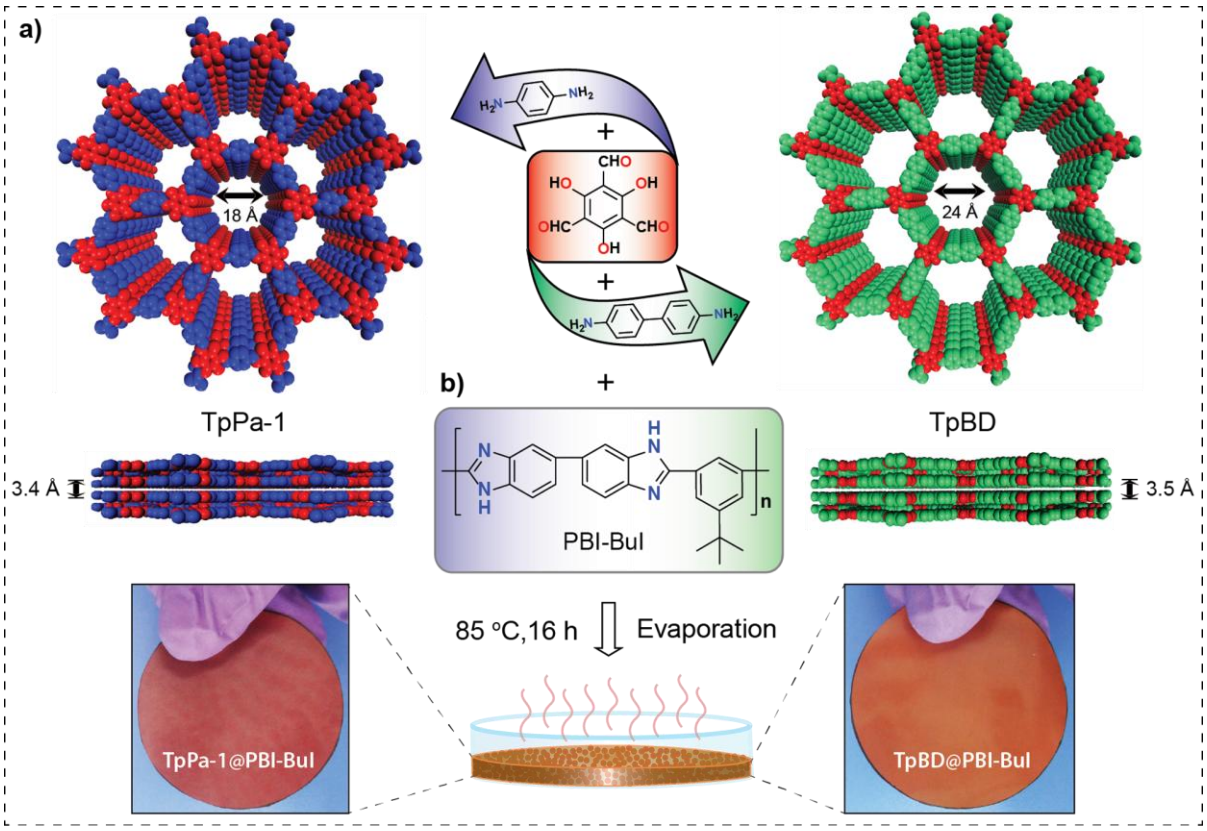

Figure 5.1. *a) Schematic representations of the synthesis of COFs and their packing models indicating the pore aperture and stacking distances; b) Overview of the solution casting method for the COF@PBI-BuI hybrid membrane fabrication with Digital photographs of TpPa-1(50)@PBI-BuI and TpBD(50)@PBI-BuI hybrid membranes.*

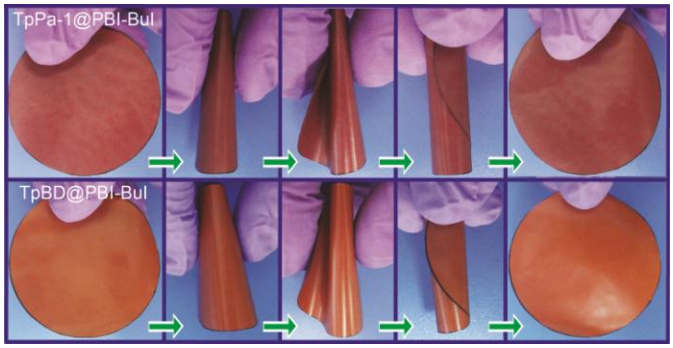

Figure 5.2. *The flexibility of TpPa-1(50)@PBI-BuI and TpBD(50)@PBI-BuI hybrid membranes.*

We have performed the wide-angle X-ray diffraction (WAXD) studies on the as-synthesized TpPa-1, TpBD, PBI-BuI and all hybrid membranes. WAXD patterns of TpPa-1 and TpBD matched well with their simulated patterns. The pristine PBI-BuI membrane showed one major broad hump at 2θ, 15°-30°, which indicates its complete amorphous nature. The TpPa-1(n)@PBI-BuI and TpBD(n)@PBI-BuI membranes were analyzed by WAXD to ensure the phase purity of TpPa-1 and TpBD embedded inside the matrix (***Figure 5.3***).

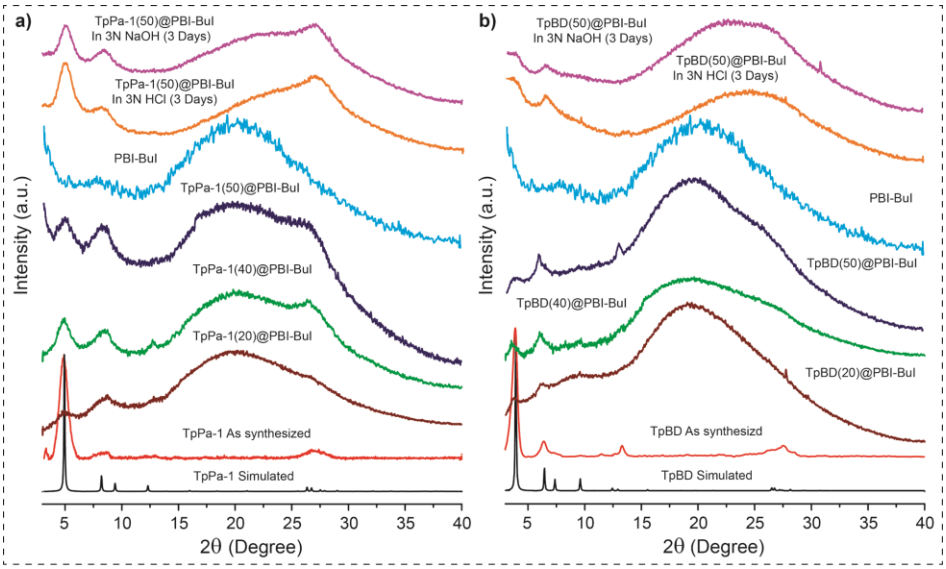

Figure 5.3. *X-ray diffraction of a) TpPa-1@PBI-BuI and b) TpBD@PBI-BuI hybrid membranes in comparison with pristine PBI-BuI, TpPa-1 and TpBD.*

In the WAXD pattern of hybrid membranes, a crystalline peaks at 4.7° and 3.4° (2θ), corresponds to 100 planes of TpPa-1 and TpBD confirm their stability in the formed hybrid membranes. In addition to that, the characteristic amorphous hump of host PBI-BuI was also

observed in the hybrid membranes. We have also studied the chemical stability of these hybrid membranes by putting them in 3 N NaOH and 3 N HCl. From WAXD patterns, it is observed that there is no change in the characteristic patterns and thus these hybrid membranes have good acid and base resistance capacity (***Figure 5.3***).

5.3.2 *Fourier transforms infrared (FT-IR) analysis*

The FT-IR spectrum of pristine PBI-BuI-HF was characterized by absorption in the range of 1430-1650 cm^{-1} for benzimidazole repeat units (***Figure 5.4***). The broadband at ~3145 cm^{-1} was ascribed to the N–H···N hydrogen bonding and the peak at 2862 cm^{-1} is due to the presence of *tert*-butyl group of PBI-BuI [5.23a].

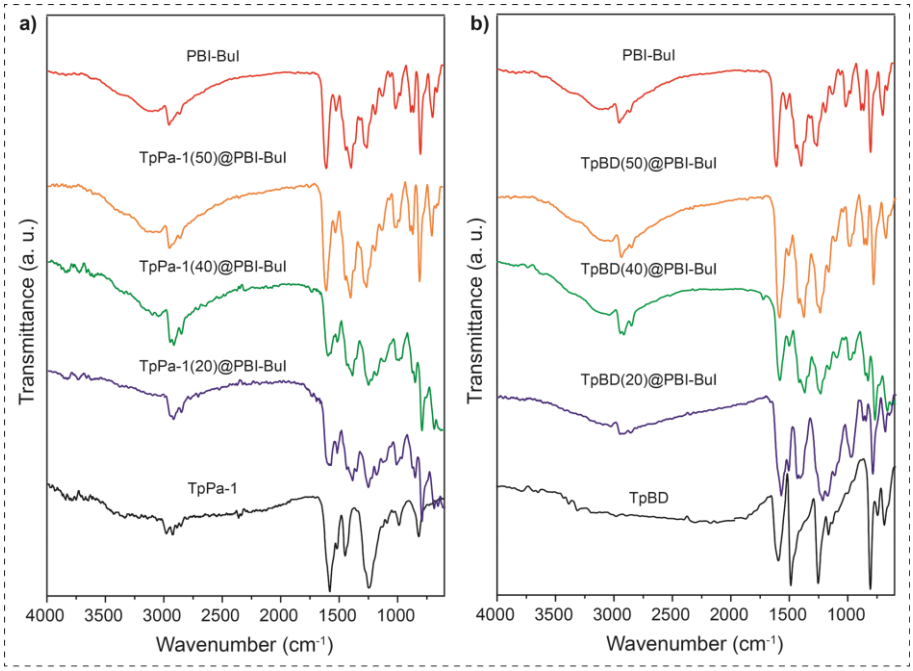

Figure 5.4. *FT-IR of a) TpPa-1(n)@PBI-BuI and b) TpBD(n)@PBI-BuI hybrid membranes in comparison with pristine PBI-BuI, TpPa-1 and TpBD. [where, n = 20, 40 and 50].*

However, for TpPa-1@PBI-BuI and TpBD@PBI-BuI hybrid membranes, major bands of TpPa-1 and TpBD are found to be merged with the pristine PBI-BuI bands. The appearance of a peak at ~1578 cm^{-1} is due to the exocyclic C=C bond of *1,3,5*-triformylphloroglucinol (Tp). The peaks at 1445 cm^{-1} [C=C(Ar)] and 1256 cm^{-1} (C-N), corresponded to the aromatic C=C and C-N bond in the keto-enamine form of TpPa-1 and TpBD (***Figure 5.4***).

5.3.3 *Scanning Electron Microscopy (SEM)*

The scanning electron microscopy (SEM) images indicated that TpPa-1 and TpBD have a spherical flower-like morphology with an average size of 5−7 μm, similar to that observed previously [5.19]. The SEM cross-section of the TpPa-1(n)@PBI-BuI (***Figure 5.5***) and TpPa-1(n)@PBI-BuI hybrid membranes (***Figure 5.6***) confirms the distribution of spherical COF particles throughout the membrane matrix.

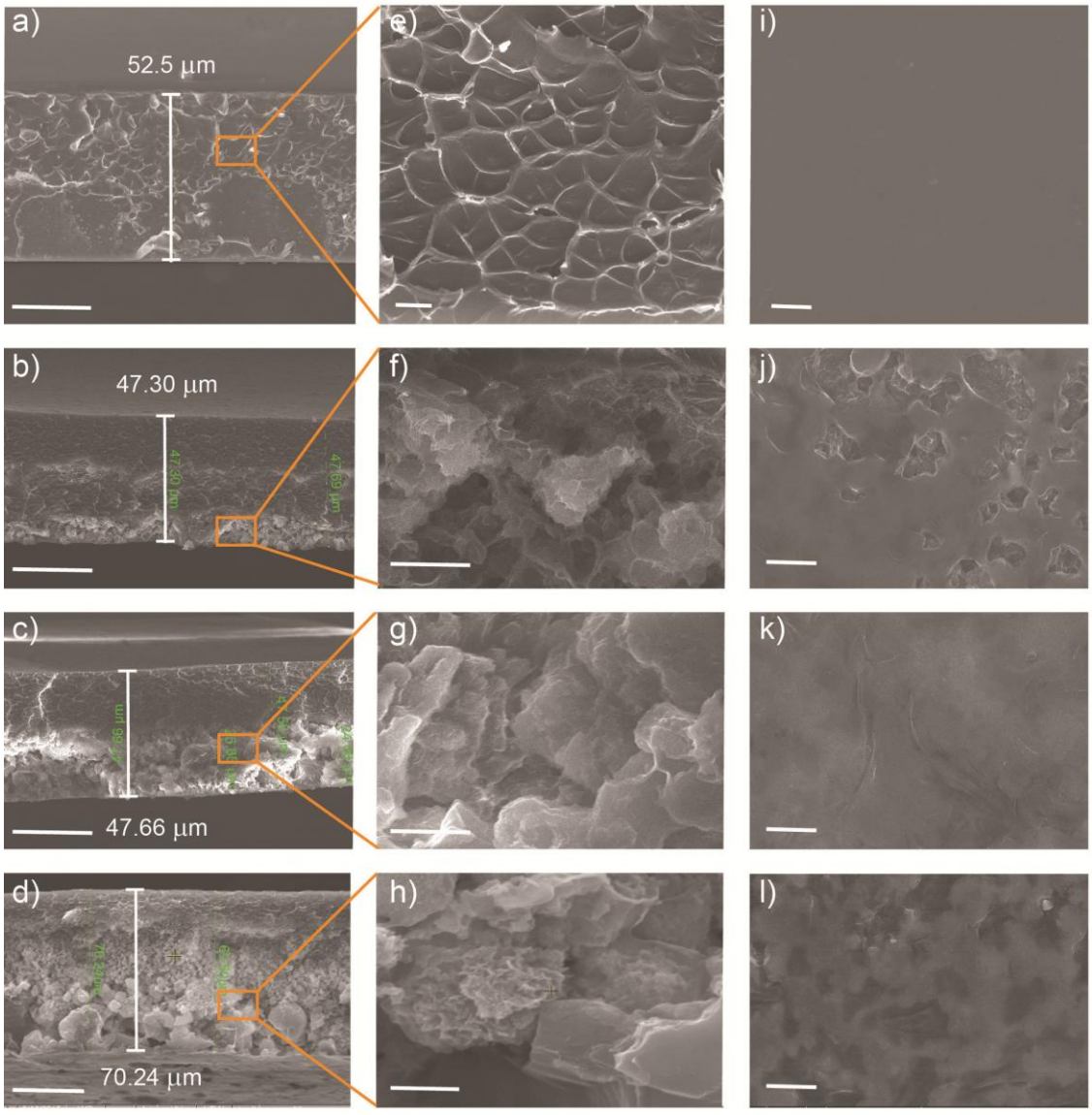

Figure 5.5. *SEM images showing cross-section of a) pristine PBI-BuI; b) TpPa-1(20)@PBI-BuI; c) TpPa-1(40)@PBI-BuI; and d) TpPa-1(50)@PBI-BuI membranes respectively; e), f), g) and h) are their respective zoomed view; and i), j), k) and l) represents the top membrane surfaces respectively. Scale bar represents (a-d) 50 μm, (e-h) 3 μm and i) 0.5 μm, j-l) 5 μm.*

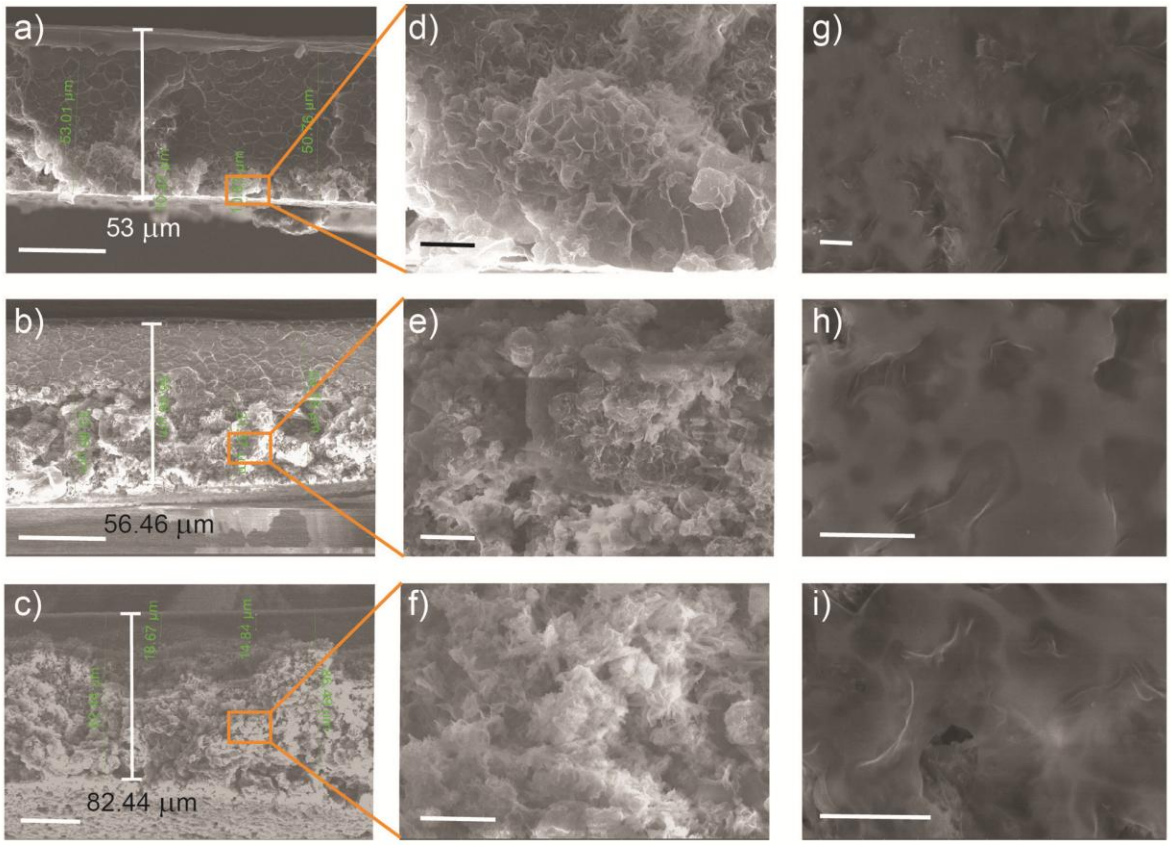

Figure 5.6. *SEM images showing cross-section of a) TpBD(20)@PBI-BuI; b) TpBD(40)@PBI-BuI; and c) TpBD(50)@PBI-BuI membranes respectively; d), e), and f) are their respective zoomed view; g), h), and i) represents the top membrane surfaces respectively. Scale bar represents a-c) 30 µm, d-e) 5 µm and f) 3 µm, g-i) 5 µm.*

It has been seen from the SEM cross-section images that the average thicknesses of the representative hybrid membranes are between ~47 to 80 µm. In both TpPa-1 and TpBD based hybrid membranes, the cross-section and the surface did not show any visible cracks or tears at the COF-polymer interface. Further, the COF particles are firmly bound with the PBI-BuI backbone, which does not allow the COFs to leach out from the polymer matrix. Notably, we have tried to re-dissolve the hybrid membranes in DMAc but found that COF and PBI-BuI are not completely separable from each other. This observation indicates a very good compatibility and adhesion between the polymer and COFs, as both contain pure organic backbone with H-bonding sites [5.24].

5.3.4 *Thermogravimetric analysis (TGA) and Mechanical property*

Thermogravimetric analysis (TGA) was performed to understand the thermal behavior of these fabricated hybrid membranes. TGA profile indicates that the COFs (TpPa-1 and TpBD) have guest-free pores, and no visible weight loss was observed till 350 °C. However, a gradual weight loss of ~ 65% (TpPa-1) and 90% (TpBD) was observed up to 800 °C. PBI-BuI showed a thermal stability of 525 °C, which is consistent with the literature reports [5.21]. All these hybrid membranes showed a thermal stability up to ~ 400 °C, which lies between the thermal stability of PBI-BuI and COFs (***Figure 5.7***). The higher stability of these hybrid membranes than that of COFs is a sign of attractive interactions between COF and PBI-BuI.

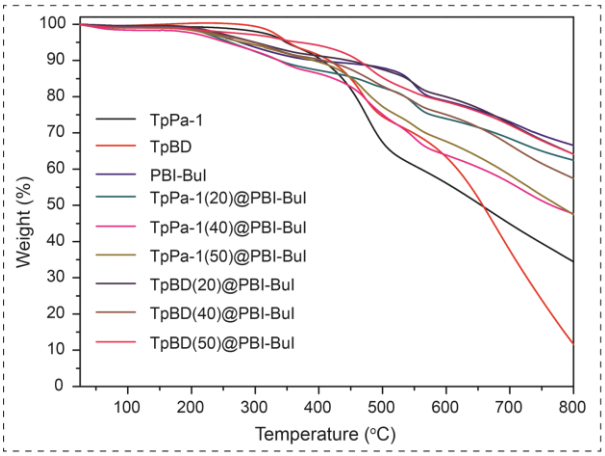

Figure 5.7. *TGA profiles of PBI-BuI, TpPa-1, TpBD and their hybrid membranes measured under N_2 atmosphere.*

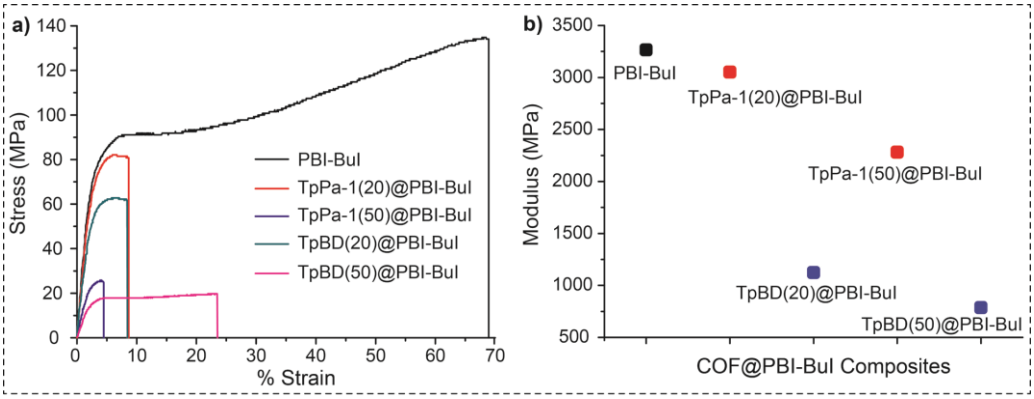

Figure 5.8. *a) Tensile strength and b) Modulus of TpPa-1@PBI-BuI and TpBD@PBI-BuI based hybrid membranes respectively.*

Moreover, mechanical properties analysis of COF(n)@PBI-BuI hybrid membranes showed a decrease of tensile strength and modulus with an increase in COF loading (from 20 to 50%) compared to the pristine PBI-BuI membrane (***Figure 5.8***). This result indicates that at higher COF loading (50%) into the polymer matrix the continuity of the polymer phase is decreased.

5.3.5 *N_2 adsorption isotherms and pore size distribution*

We have performed the N_2 adsorption isotherm study on TpPa-1(50)@PBI-BuI and TpBD(50)@PBI-BuI hybrid membranes, compared with their respective parent materials to understand the pore structure and change in BET surface area of the COFs inside the membrane matrix (***Figure 5.9***).

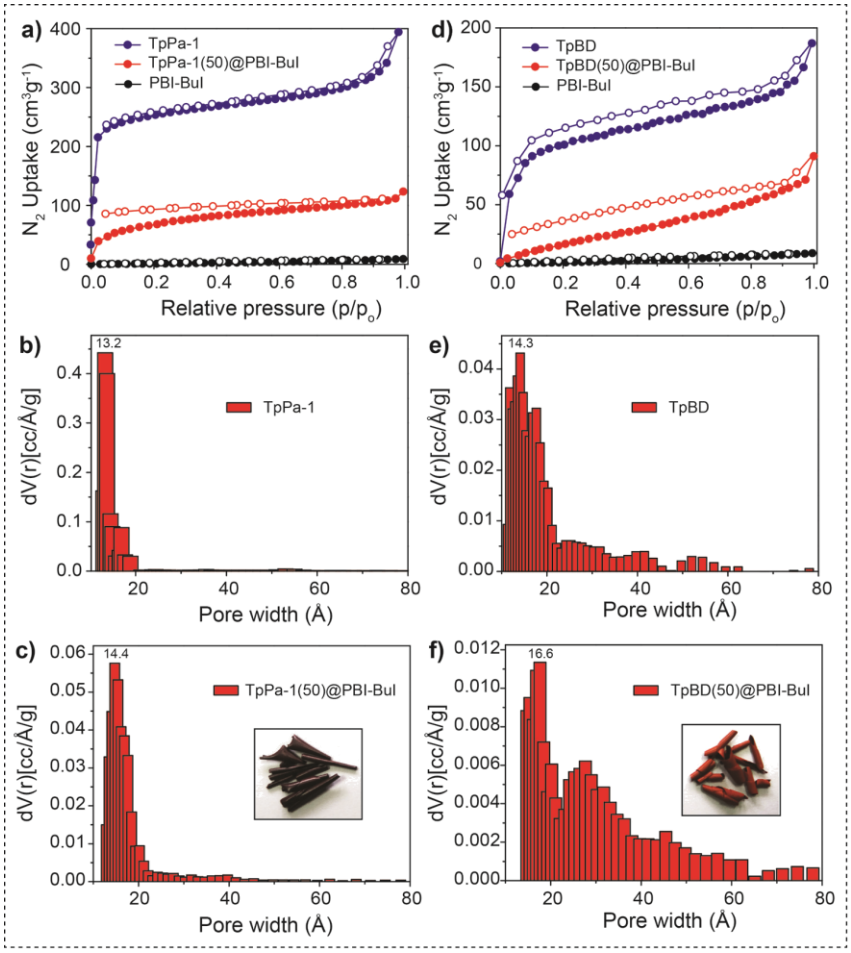

Figure 5.9. *a, d) N_2 adsorption isotherms; b, e) and c, f) Pore size distribution of TpPa-1, TpBD, TpPa-1(50)@PBI-BuI and TpBD(50)@PBI-BuI hybrid membranes.*

From the results, we have found that the BET surface area of these composite membranes are slightly decreased [from expected BET for 50% Polymer: 50% COF], that could be due to the fact that the COF pores are partially covered by polymer chains in the composite membrane matrix and hence, they are not fully exposed to the N_2 gas. The BET surface area values of all these materials are, PBI-BuI: 13 m^2g^{-1}, TpPa-1: 801 m^2g^{-1}, TpBD: 341 m^2g^{-1}, TpPa-1(50)@PBI-BuI: 237 m^2g^{-1} and TpBD(50)@PBI-BuI: 85 m^2g^{-1}. However, the pore size distributions (maxima) of COFs (TpPa-1 and TpBD) in polymer matrix has remained almost constant (slightly increased by 1Å for TpPa-1(50)@PBI-BuI, and 2Å TpBD(50)@PBI-BuI) as compared to the pristine COF powders. This result indicates that majority of the COF pores are not blocked by polymer chains.

5.3.6 *Gas permeation study of dense membranes*

Polybenzimidazoles (PBIs) are famous owing to their excellent thermochemical stability and outstanding mechanical properties at high temperature and useful in many exciting applications [5.23]. In this work, our motivation is to demonstrate an increase of gas permeance of a polymer (PBI-BuI) by introducing a 2D organic porous, crystalline framework (COF) material within it. The beauty of these COF materials lies in their chemical stability, tunable porosity and opportunity of pore engineering. Further, it is anticipated that by selection of COFs with a wide range of pore aperture, the molecular sieving properties can be achieved, which is an essential criterion for various gas/liquid separation. In this study, we have performed gas permeance through COF based hybrid dense membranes using H_2, N_2, CH_4 and CO_2 at 35 ºC and 20 atm upstream pressure. Such high-pressure withstand capacity for composite membranes composed of COF with high filler loading (~ 50%) is not known so far. The permeation data presented here is the average numbers of three samples (3.8 cm active membrane diameter). All these gas permeance and selectivity values are listed in ***Table 5.1*** and ***5.2***. ***Figure 5.10a*** and ***5.10b***, attributed to H_2 and CO_2 permeability of PBI-BuI based hybrid and found to be increased almost linearly with the amount of COF loading (20, 40 and 50%) in them. A three times elevation in H_2 permeability from 6.2 Barrer (for pristine PBI-BuI) to 18.8 Barrer was observed for TpPa-1(40)@PBI-BuI hybrid membrane. This is associated with an increase in H_2/CH_4 selectivity from 155 to 165.5 and H_2/N_2 selectivity from 69 to 79. Although CO_2/N_2 selectivities (***Figure 5.10b***) are slightly decreased, CO_2/CH_4

selectivity remained appreciable even with 40% of TpPa-1 loading as 46.3. This is found to be higher than the selectivity obtain for commonly used gas separation membrane materials such as matrimid, polysulfone (PSF) and polycarbonate (PC) [$\alpha(CO_2/CH_4)$ = 36, 22 and 19, respectively] [5.25]. Further, we have compared our results along with some common membrane materials (PSF, matrimid, PC, PPO) with reference to Robeson's upper bound (1991 and 2008) [5.3] (***Figure 5.11a*** and ***5.11b***).

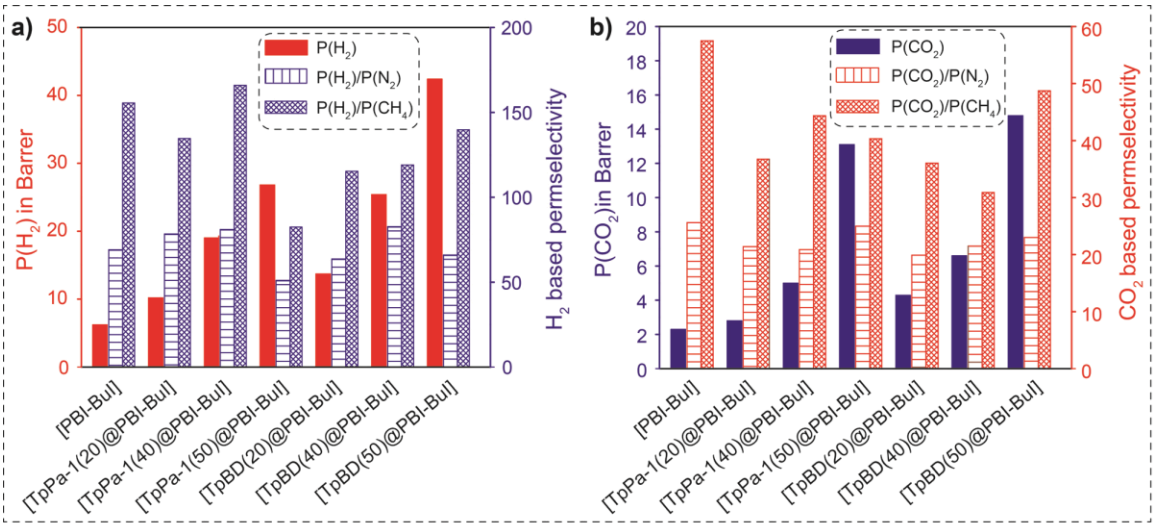

Figure 5.10. *Variation in (a) H_2 permeability and its selectivity over N_2 and CH_4; b) CO_2 permeability and its selectivity over N_2 and CH_4 with respect to COF loading in TpPa-1(n)@PBI-BuI and TpBD(n)@PBI-BuI hybrid membranes.[where, n = 20, 40 and 50].*

These results depict that the TpBD(50)@PBI-BuI hybrid outperforms the aforementioned materials (PSF, matrimid and PC) regarding CO_2 permeability and comparable with CO_2/CH_4 selectivity, except for polyphenylene oxide (PPO), where the selectivity is lower, but the permeability is higher. We have also compared our gas permeation results with the previously reported ZIF-8@PBI-BuI based hybrid membranes [5.19]. It has been found that TpBD(50)@PBI-BuI based membranes are showing better CO_2 (14.8) and CH_4 (0.3) permeability with slightly higher CO_2/CH_4 selectivity (48.7) as compared to the Z_{30}@PBI-BuI [P_{CO2}: 5.23, P_{CH4}: 0.12 and CO_2/CH_4 selectivity was 43.6]. The effect of pore modulation, aperture 18 Å (TpPa-1) to 24 Å (TpBD) of COF in gas permeation was prominently seen. Almost ~7 fold elevation in H_2 permeability than the pristine case was achieved with 50% TpBD loading into PBI-BuI (***Figure 5.10a***). This was coupled with comparable H_2/N_2 (from 69 to 66) and a slight decrease in H_2/CH_4 (155.5 to 139.7)

selectivity than that of unloaded PBI-BuI. Thus, these selectivity values are still very well comparable with that of commonly used commercial gas separation membrane materials like PSF [5.25c]. The H_2 permeability for PSF is reported to be 14 Barrer, which is 3 times lower than the H_2 permeability (42.5 Barrer) of TpBD(50)@PBI-BuI. An increase in CO_2 permeability from 3.2 Barrer (for pristine PBI-BuI) to 13.1 and 14.8 Barrer for TpPa-1(50)@PBI-BuI and TpBD(50)@PBI-BuI hybrid membrane was generous (***Figure 5.10b***).

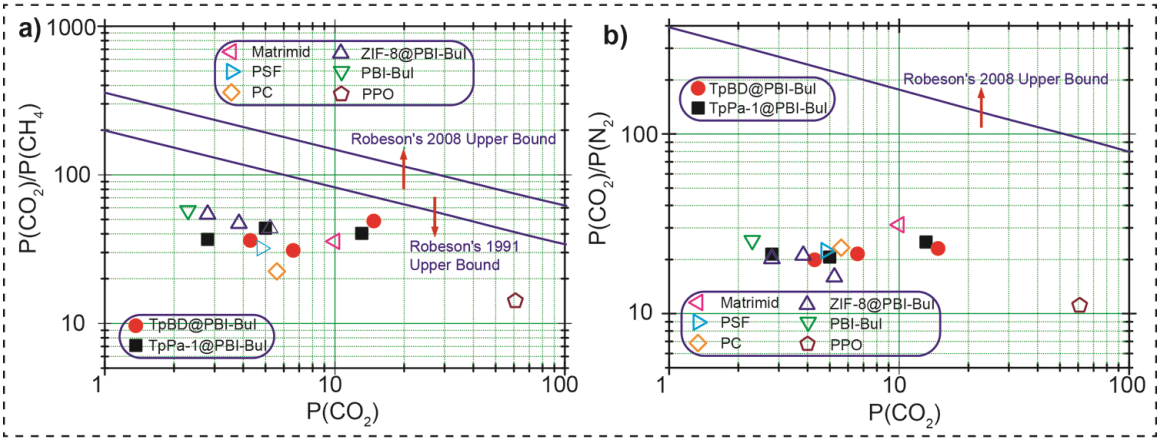

Figure 5.11. *a) and b) The single gas CO_2 permeability and ideal CO_2/CH_4 and CO_2/N_2 selectivity of TpPa-1@PBI-BuI (black, filled squares) and TpBD@PBI-BuI (red, filled circles) hybrid membranes respectively are plotted on Robeson's Upper Bound.*

Table 5.1. *The gas permeability of pristine PBI-BuI and COFs@PBI-BuI dense hybrid membranes.*

	P(H_2)	**P(N_2)**	**P(CH_4)**	**P(CO_2)**
PBI-BuI	6.22	0.09	0.04	2.3
TpPa-1(20)@PBI-BuI	10.2	0.13	0.08	2.8
TpPa-1(40)@PBI-BuI	18.8	0.24	0.11	5.0
TpPa-1(50)@PBI-BuI	26.8	0.52	0.33	13.1
TpBD(20)@PBI-BuI	13.7	0.22	0.12	4.3
TpBD(40)@PBI-BuI	25.4	0.31	0.21	6.6
TpBD(50)@PBI-BuI	42.4	0.64	0.30	14.8

Table 5.2. *Gas perm-selectivity of pristine PBI-BuI and COFs@PBI-BuI dense hybrid membranes.*

	α(H_2/N_2)	**α(H_2/CH_4)**	**α(H_2/CO_2)**	**α(CO_2/N_2)**	**α(CO_2/CH_4)**
PBI-BuI	69.1	155.5	2.7	25.6	57.5
TpPa-1(20)@PBI-BuI	78.4	134.6	3.7	21.4	36.7
TpPa-1(40)@PBI-BuI	78.9	165.5	3.8	20.9	46.3
TpPa-1(50)@PBI-BuI	51.1	82.4	2.0	25.0	40.3
TpBD(20)@PBI-BuI	63.7	115.3	3.2	19.9	36.1
TpBD(40)@PBI-BuI	82.7	119.0	3.9	21.5	30.9
TpBD(50)@PBI-BuI	66.0	139.7	2.9	23.0	48.7

One of the peculiarities seen in the case of COF@PBI-BuI based hybrid membranes was the linear increase in permeability from 20 to 50% of COF loading. When we have compared the elevation in permeability in the case of TpPa-1 loaded PBI-BuI with TpBD loaded PBI-BuI, the effect of pore modulation, was prominently evident. Improved gas permeation while maintaining the base polymer (PBI-BuI) selectivity in the case of COF@PBI-BuI hybrid membranes concludes that benefits of COF pores can be better drawn by lowering the diffusion resistance. However, the base selectivity probably is still governed by the polymer matrix (PBI-BuI). This could be made possible by avoiding agglomeration or defect inhibition. As the COF pores (~13 Å for TpPa-1 and ~15 Å for TpBD; from pore size distribution ***Figure 5.9***) are much larger than the kinetic diameters of gases [(2.89 Å (H_2), 3.64 Å (N_2), 3.3 Å (CO_2) and 3.8 Å (CH_4)], hence molecular sieving of gases (enhancement of selectivity) is not really expected from COFs. Notably, in some of the MOF-based MMMs, high enhancement in selectivity was evidenced due to narrow pore aperture (3-4 Å) of MOFs. In the present case, the COFs (TpBD) contributes to a significant increase in permeability of PBI-BuI, with small deviations in selectivity. It can be further expected that if the COFs with even higher pore aperture are chosen, elevation in permeability could be more pronounced.

5.4 Covalent organic framework-styrene butadiene rubber based thin-film composite (TFC) membranes

5.5 Physical properties of COF based thin-film composite membranes

5.5.1 *Wide-angle X-ray diffraction (WAXD) and Fourier transforms infrared (FT-IR) analysis*

The fabrication of TpPa-1@SBR TFC was done using a systematic dip coating strategy as shown in ***Figure 5.12***. To verify the crystallinity and phase purity of all these membrane materials, we have performed the WAXD analysis. WAXD pattern of as-synthesized TpPa-1 matched well with the simulated one, having a sharp peak at 4.7° (2θ) assigned to 100 reflection planes (***Figure 5.12a***).

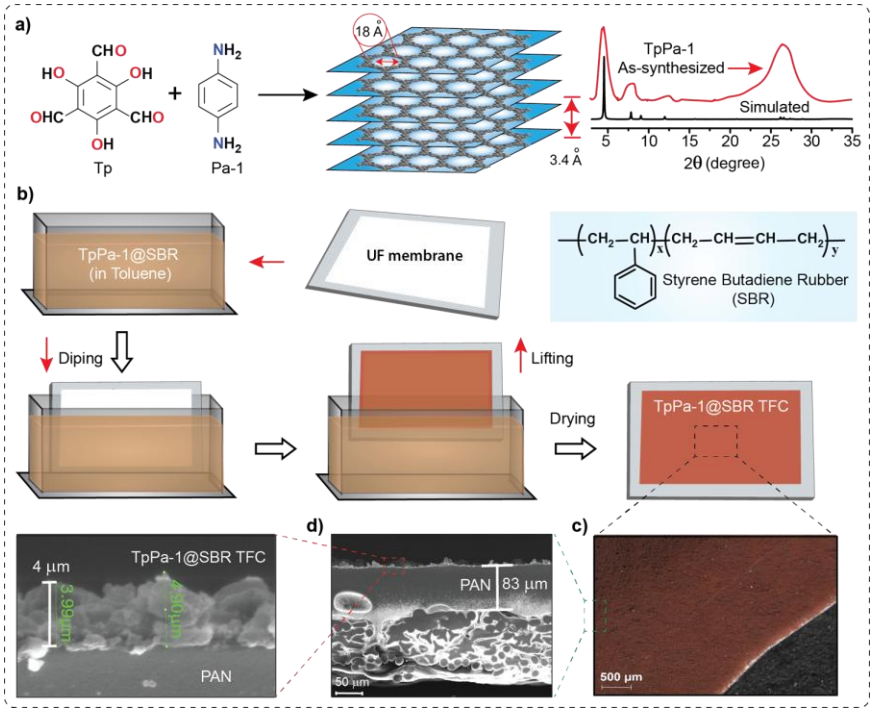

Figure 5.12. *Schematic representations of a) synthesis of TpPa-1; b) step-wise detail of the fabrication of TpPa-1@SBR based TFC membrane; c) digital photographs; d) SEM image of TpPa-1@SBR membranes fabricated on PAN ultrafiltration support.*

The polyacrylonitrile (PAN) ultrafiltration (UF) support shows three broad peaks in the WAXD pattern; the first peak appears at $2\theta = 17^{o}$ and other two broad peaks at $2\theta = 22.5^{o}$ and $2\theta = 26.3^{o}$, which signifies the moderate crystalline nature of PAN. However, the polymer (SBR) shows one broad hump at around $2\theta = 20^{o}$, indicating its complete

amorphous nature. The three different composites, *i.e.*, TpPa-1(30)-SBR@PAN, TpPa-1(50)-SBR@PAN and TpPa-1(70)-SBR@PAN showed three broad peaks at the same 2θ value as that of PAN support and no peak of SBR and TpPa-1 was prominently seen in the WAXD pattern (***Figure 5.13a***). This is mainly attributed due to the fact that the PAN support is crystalline in nature. Another reason could be the amount of SBR and the added filler (TpPa-1) is very less as compared to the PAN; therefore, the peaks of SBR and TpPa-1 have been merged with the WAXD patterns of PAN support.

The FT-IR spectrum of fabricated COF-SBR TFC membranes were collected and compared with the parent materials. The FT-IR spectra of the pristine SBR showed a strong absorption band near 2918 cm^{-1}, which ascribed due to the stretching vibrations of the C–H bonds in the SBR repeat unit. In addition, other distinct bands are observed at 1451 cm^{-1} and 960 cm^{-1}, these are due to the alkane C–C stretch and out-of-plane vibrations of $–CH_2–$ groups from SBR. The same three bands can also be observed in the FT-IR spectrum of TpPa-1@SBR TFC membranes but with slightly decreased intensity (***Figure 5.13b***).

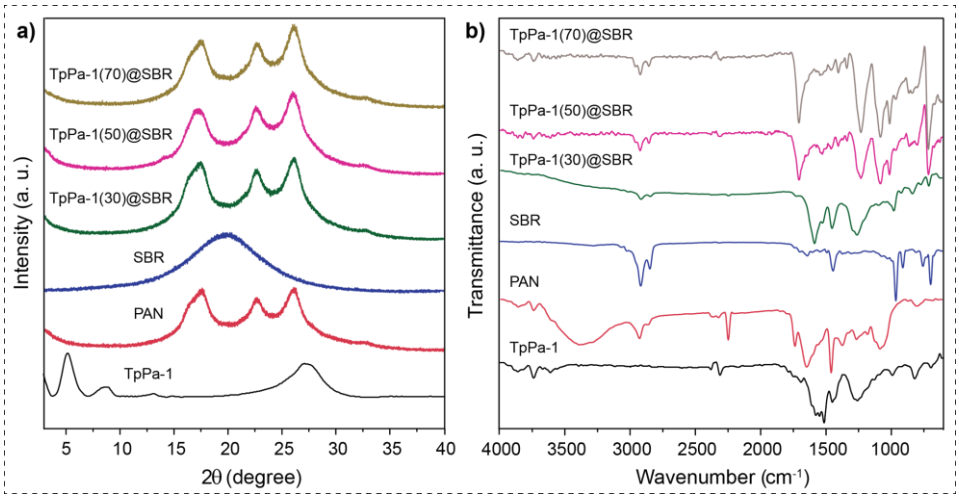

Figure 5.13. *Comparative a) WAXD patterns and b) FT-IR spectra of TpPa-1(X)@SBR on PAN support TFC membranes (X = 30, 50 and 70), PAN, TpPa-1 and SBR.*

In the FT-IR spectrum of the keto-enamine form of TpPa-1, two distinct bands are observed, one at 1265 cm^{-1} due to the C–N stretching vibrations and another at 1524 cm^{-1} that is due to the –C=C stretch. All these major bands found to be present in all TpPa-1@SBR TFC membranes. This confirms the presence of both SBR and TpPa-1 in the same matrix (***Figure 5.13b***).

5.5.2 *Scanning Electron Microscopy (SEM)*

The SEM cross-section of the TpPa-1@SBR TFC membranes confirms the distribution of spherical COF particles all over the skin layer membrane matrix (***Figure 5.14***).

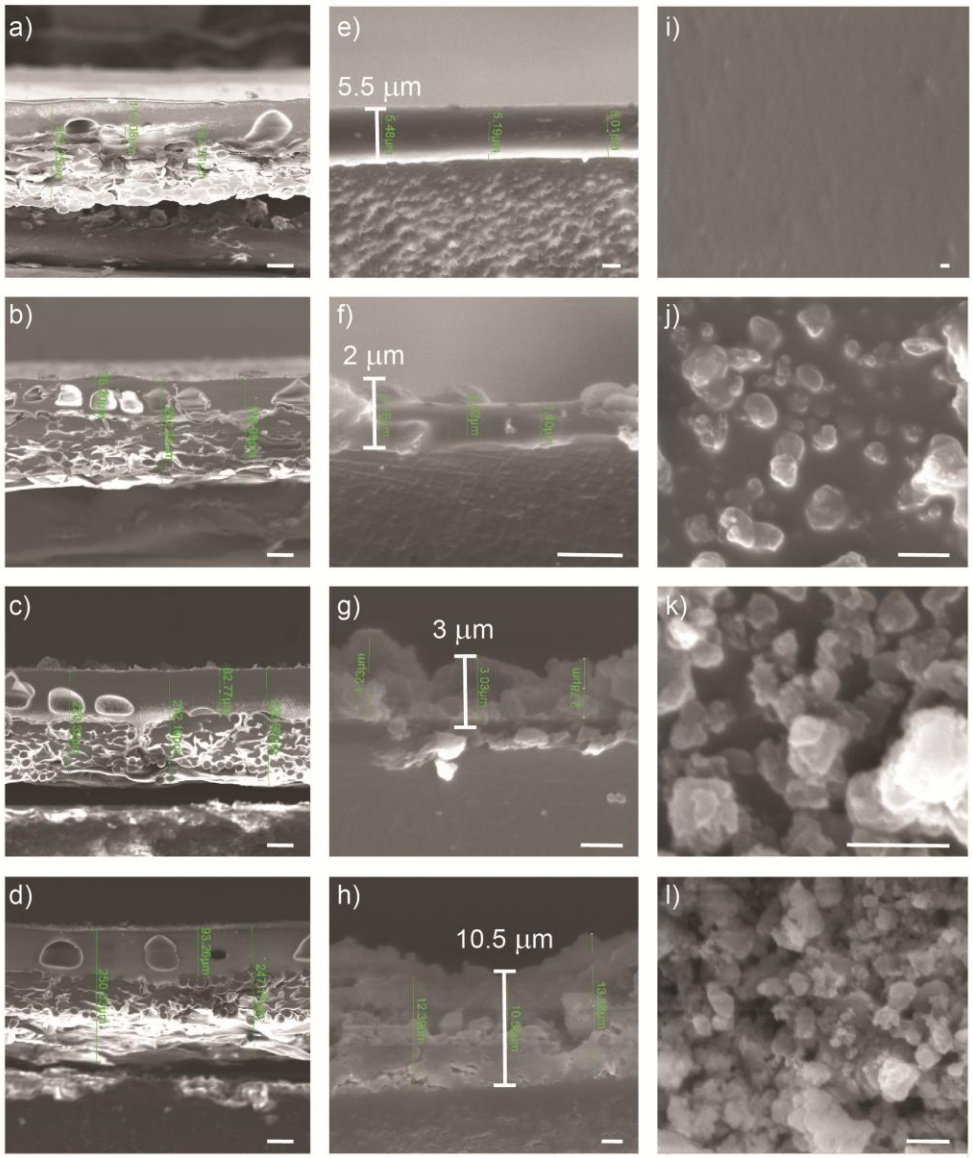

Figure 5.14. *SEM images showing the cross-section of a) SBR; b) TpPa-1(30)@SBR; c) TpPa-1(50)@SBR; d) TpPa-1(70)@SBR; e), f), g) and h) are their respective zoomed view; i), j), k) and l) are the membrane surfaces respectively. [Scale bar: a-d) 50 µm, e-h) 2 µm and i-l) 2 µm).*

From SEM cross-sectional images, successful formation of TpPa-1@SBR thin layer on the surface of PAN UF membrane support was clearly observed. SEM images of pristine SBR-

TFC membrane showed a distinct phase boundary between the UF support and SBR layer with an average thickness of around ~5.5 μm. The selective upper layer of TpPa-1@SBR TFC consists of blends of SBR and flower like TpPa-1 COF particles. The average thickness of the top layer was found to be ~2 μm for TpPa-1(30)@SBR TFC membrane. As the COF content increases from 50 and 70%, the thickness of the TFC layer also increases (~3 μm and ~10.5 μm, respectively). The successive increase in the thickness of the thin layers is due to the dense population of COF particles within the SBR matrix. Most importantly, in the present case, the membrane cross-section, as well as the surface, did not show any visible cracks or defects (***Figure 5.15i-l***). This conveys the success of choosing rubbery polymer for making TFC membrane. Further, the TpPa-1 crystallites are tightly bound with the SBR matrix and not easily leach out from the membrane. This observation signifies that a good compatibility and adhesion is obtainable between the SBR (polymer) and COFs, as both contain organic backbone.

5.5.3 *Gas permeation study of TFC membranes*

The motivation behind the fabrication of TFC membranes is to demonstrate faster transport of hydrocarbons (C_3H_6 and C_3H_8) using a rubbery polymer (SBR) and by introducing 2D organic porous crystalline framework material within, which will provide a free pathway for gas transport. As proven earlier, the beautiful features of our COF materials are the chemical stability, tunable porosity and an opportunity of pore engineering [5.18]. Hence, it is expected that by judicious selection of COFs with a definite pore aperture, the effective molecular transport properties can be tuned. To validate our logic, we have performed the gas permeance study using H_2, N_2, C_3H_6 and C_3H_8 gases at ambient temperature and 3 atm upstream pressure. The gas permeation data, we have presented here is the average of three membrane samples (3.8 cm active membrane diameter). The ***Figure 5.15a*** and ***5.15b*** attribute to the single gas permeance of four gases under study and their selectivities with each other. The permeance value for pristine SBR-TFC membrane is considered as the base value for the further analysis of the results. It is observed from the gas permeance data that as percentage of the TpPa-1 increases in the SBR matrix, the gas permeance of the TFC membranes also increases. This proves the hypothesis of faster gas diffusion through COFs, rather than the surrounding polymer matrix.

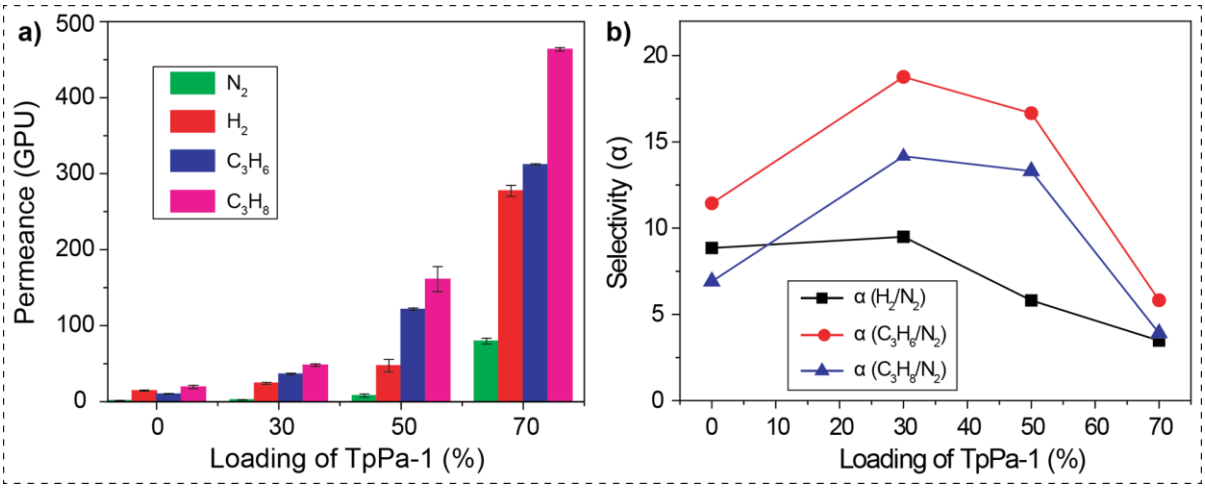

Figure 5.15. *a) Comparison of the single gas permeance of H_2, N_2, propylene (C_3H_6) and propane (C_3H_8); b) the ideal H_2/N_2, C_3H_6/N_2 and C_3H_8/N_2 selectivity of TpPa-1@SBR TFC membranes respectively. [1GPU = 1×10^{-6} cm^3 (STP)/ (cm^2 s cmHg)].*

The purpose of using TpPa-1 for TFC membrane fabrication was to increase the gas permeance due to the high porosity of the filler material. The same is reflected in the results. As we increased the filler concentration from 30 to 70 %, the permeance value for different gases was increased linearly (***Table 5.3***). A ~8 fold elevation in C_3H_6 permeance from 19 GPU (for pristine SBR) to 161 GPU was observed for TpPa-1(50)@SBR TFC membrane associated with slight increase in C_3H_6/N_2 reverse selectivity from 13 to 20.

Table 5.3. *The gas permeance of TpPa-1@SBR TFC membranes.*

	P(H_2)	**P(N_2)**	**P(C_3H_6)**	**P(C_3H_8)**
SBR-TFC	14.4±(0.7)	1.5±(0.24)	19.3±(2.1)	10.4±(0.25)
TpPa-1(30)@SBR	24.3±(1.2)	2.6±(0.2)	48±(1.8)	36.3±(1.4)
TpPa-1(50)@SBR	47.3±(8)	8.1±(2)	161.3±(16.5)	121.6±(1.8)
TpPa-1(70)@SBR	277.5±(7.16)	79.7±(3.9)	463.6±(2)	311.9±(1.1)

Similarly, almost ~12 fold increase in C_3H_8 permeance than the pristine SBR was achieved with 50% TpPa-1 loading into SBR. This was coupled with C_3H_8/N_2 reverse selectivity (from 7 to 15) compared to only SBR based TFC membrane (***Table 5.4***). The trade-off relationship is a well-known term in the membrane research, which states that as the flux of the membrane increases, it's selectively decreases and vice versa [5.3]. However, in the present

case, as the concentration of the TpPa-1 increases, the selectivity is slightly increased up to 50% of TpPa-1 loading to SBR. Notably, the highest reverse separation factor is observed in the case of TpPa-1(50)@SBR as well. Moreover, in the case of TpPa-1(70)@SBR the permeance of all gases is very high associated with lower selectivity than the pristine SBR TFC. ***Figure 5.15b*** shows the selectivity relationship of different gases for different TFC membranes.

Table 5.4*. Gas perm-selectivity of TpPa-1@SBR TFC membranes.*

	α(H_2/N_2)	**α (C_3H_6/C_3H_8)**	**α(C_3H_6/N_2)**	**α(C_3H_8/N_2)**
SBR-TFC	9.56	1.85	12.81	6.91
TpPa-1(30)@SBR	9.50	1.32	18.77	14.17
TpPa-1(50)@SBR	5.81	1.33	19.81	14.94
TpPa-1(70)@SBR	3.48	1.49	5.82	3.91

We believe, the very high flux could be attributed due to two major factors, i) the rubbery and hydrophobic nature of SBR that interacts with hydrocarbons and thereby enhance flux, and ii) fast diffusion of gases (kinetic diameter: ~4 Å) through the pore aperture of TpPa-1 (~ 18 Å). The first aspect derives the reverse selectivity phenomena and the second one governs the high permeance observed in all TFC membranes. Higher concentration of COF in TFC membranes although showed a decrease in selectivity of gases, a large enhancement in the permeance values was achieved. It can also be further expected that, if COFs with large pore aperture are chosen, more increase in permeance could be pronounced, provided polymer matrix offers good affinity towards hydrocarbons.

5.6 Conclusions

In the first part of this chapter, we showcase a methodology to fabricate a new class of self-supported COF@polymer hybrid membranes. These self-supported membranes are highly flexible, reproducible and display high degree of thermal and chemical stabilities; showing its potentiality for a wider range of applications in the gas/liquid separation. As a proof of concept, we have performed the gas permeation analysis, which revealed that almost 7 fold elevations in permeability of gases (H_2, N_2, CH_4 and CO_2) than the pristine membrane

with 50% TpBD loading with appreciable CO_2/N_2 (23) and CO_2/CH_4 (48.7) selectivity was achievable. Interestingly, the effect of isoreticulation in COF towards elevating the gas permeability was prominently seen in these COF@PBI-BuI based hybrid membranes. In the later part, we have introduced a methodology to fabricate COF@polymer (TpPa-1@SBR) thin film composite (TFC) membranes. We also performed the gas permeation analysis, which revealed almost 8 to 12 fold elevation in permeance of hydrocarbon gases (C_3H_6 and C_3H_8) than the pristine SBR based TFC membrane. With 50% TpPa-1 loading, appreciable C_3H_8/N_2 and C_3H_6/N_2 reverse selectivity (15 and 20) was achievable. The outcome of this work of obtaining TFC membranes of chemically stable functional COF with high flux and reverse selectivity is of significant use in vapour recovery from fuel stations/industries. Overall, the findings presented in this chapter demonstrate a versatile approach of preparing chemically stable functional COF/polymer hybrid membranes that could significantly contribute to the advancement of such materials in near future.

5.7 Experimental procedures

5.7.1 *Materials*

1,3,5-triformylphloroglucinol was prepared using reported literature procedure [5.26]. All starting materials were purchased from a commercial source and used without further purification.

5.7.2 *Synthesis and membrane fabrication*

5.7.2.1 Preparation of PBI-BuI and its membrane

A three-neck round-bottomed flask equipped with a mechanical stirrer, N_2 inlet and outlet was charged with 300 gm of polyphosphoric acid and heated with stirring at 140 ºC under a constant flow of N_2. A 10 gm (0.0467 mol) of *3,3'*-diaminobenzidine (DAB) was added to the reaction mixture. The temperature was maintained at 140 ºC. After complete dissolution of DAB, 10.4 gm (0.0467 mol) of *5-t*-butylisophthalic acid (BuI) was added. After that, the temperature of the mixture was slowly raised to 170 °C and maintained for 3.5 hrs under a constant flow of N_2. The temperature was further raised to 200 °C and then maintained for 5 hrs. After completion of the reaction, the temperature was lowered, and the

highly viscous reaction mixture was poured onto the stirred water. The precipitated polymer was crushed and thoroughly washed with water until a neutral to pH. The polymer was then kept overnight in 10% aqueous $NaHCO_3$, washed with water until a neutral to pH and kept in methanol for 8 hrs. Dried polymer (100 °C, 3 days) was further purified by dissolving in DMAc to get a 3 wt% solution, removing undissolved material, if any, by centrifugation at 3000 rpm for 3 hrs and reprecipitation onto the stirred water. The polymer was kept in methanol for 8 hrs, filtered, dried at 60 °C for 24 hrs and then dried in a vacuum oven at 100 °C for a week. The inherent viscosity (η_{inh}) was determined using 0.2 g dL^{-1} of PBI-BuI solution in concentrated H_2SO_4 at 35 °C.

The solution of PBI-BuI in *N,N'*-dimethylacetamide (DMAc) (3% w/v) was prepared and filtered through a 5 μm filter paper. Then the resulting solution was poured on a flat glass surface maintained at 85 °C, and the solvent was evaporated under dry condition for 16 hrs. The membrane was peeled off from the glass surface and was kept in a vacuum oven at 100 °C for a week in order to remove traces of the solvent.

a) ***Synthesis of COFs (TpPa-1 and TpBD)*:** A pyrex tube (o.d. × i.d. = 24 × 22 mm^2 and length 30 cm) is charged with *1,3,5*-triformylphloroglucinol (Tp) (3 mmol), and aromatic diamines (4.5 mmol) [*p*-phenylenediamine (Pa-1) for TpPa-1 and Benzidine (BD) for TpBD], 15 mL of mesitylene, 15 mL of dioxane, 5 mL of 3 M aqueous acetic acid. This mixture was sonicated for 10 minutes in order to get a homogenous dispersion. The tube was then flash frozen at -196 ºC (liquid N_2 bath) and degassed by three freeze-pump-thaw cycles. The tube was sealed off and then heated at 120 °C for 3 days. A red colored precipitate (TpBD is yellow) formed was collected by centrifugation or filtration and washed with anhydrous acetone. The powder collected was then solvent exchanged with anhydrous acetone 5-6 times and then dried at 180 ^{0}C under vacuum for 24 hrs to give a deep red colored powder in ~80% isolated yield.

b) ***Preparation of COFs@PBI-BuI hybrid membrane*:** PBI-BuI based hybrid membranes with varying weight fraction [(COF)(n)@PBI-BuI(m); n: m = 20: 80, 40: 60 and 50: 50 on w/w basis] of synthesized COFs (TpPa-1 or TpBD) were prepared by the solution casting method. PBI-BuI solution in DMAc was mixed with the stock suspension of COFs stirred for 15 minutes followed by bath sonication for 30 minutes in order to obtain a homogeneous suspension. It was poured on a flat glass surface maintained at 85 °C, and the

solvent was evaporated under the dry condition for 16 hrs. The membrane was peeled off from the glass surface and was kept in a vacuum oven at 100 °C for a week in order to remove traces of the solvent.

5.7.2.2 *Preparation PAN based ultrafiltration membrane*

Flat-sheet polyacrylonitrile (PAN) membranes were prepared using Hollytex-3324 as the porous support. A dope solution containing 11 wt. % of PAN powder and 4 wt. % of citric acid (CA) as pore controller additive in DMF was prepared while stirring for 48 hrs under dry conditions. The prepared dope solution was degassed and then centrifuged at ~2700 rpm for 3 hrs. The membrane was casted on a moving nonwoven support fabric using pilot scale continuous membrane casting facility at 20 °C gelation temperature and 40 °C curing temperature. The formed membrane had an average thickness of ~ 250 μm and was stored with aq. formalin solution (0.5 %) at 4 ºC until further use. The water flux analysis of thus formed PAN membrane was performed in a stirred cell of membrane active area 11 cm^2. The water permeance value was 413 $Lm^{-2}h^{-1}bar^{-1}$.

a) ***Preparation of SBR-TFC membrane*:** Styrene butadiene rubber (SBR) with 25 % of styrene content was mixed with toluene to give a 2 % (wt/v) solution. The solution was stirred until the SBR was totally dissolved. The PAN porous support of 15 × 10 cm^2 size was used for the thin-film composite (TFC) membrane preparation by dip coating method. In this method, PAN support of was initially mounted on a glass plate with all four sides taped to avoid back penetration of the polymer solution during dipping. The glass plate with support was then dipped into the prepared SBR solution in toluene for 15 Sec. It was then allowed to dry by keeping the membrane in the oven at 40 ºC for 30 minutes. Further, coupons were the obtained thin film composite (TFC) membrane for gas permeation analysis and further characterization.

b) ***Processing of TpPa–1 COF for TFC membrane preparation*:** The TpPa-1 powder was ground gently using a mortar and pestle for 5 min. to reduce the particle size and to break down the agglomeration prior to use for the TFC membrane fabrication.

c) ***Preparation of TpPa-1@SBR TFC membrane*:** A solution of SBR 2% (w/v) was prepared in toluene by taking the required amount of the polymer and the solvent. After

having a solution of SBR in toluene, it was filtered in another clean conical flask so as to have a clear solution of SBR free from impurities. Then to this clear solution the stock suspension of TpPa-1was added in different compositions [TpPa-1(X)SBR(Y)@PAN (X: Y = 30: 70, 50: 50 and 70: 30 on w/w basis]. It was stirred on a magnetic stirrer for 30 minutes followed by a bath sonication for 30 minutes in order to get a homogeneous suspension of TpPa-1@SBR solution. Then the PAN support was taped on a glass plate from all four sides, and it was allowed to dry at 40 ^{o}C for 15 minutes. Once dried, the PAN support was dipped in the SBR@TpPa-1 suspension for 15 sec. and after that, the plate was placed in an oven for drying at 40 ^{o}C up to 45 minutes. Further, coupons were taken out of the coated support (TFC membrane) for gas permeation analysis and further characterization.

5.7.3 *General methods for characterization*

a) ***Wide angle X-Ray diffraction (WAXD)*:** The WAXD analysis of the hybrid membranes were carried on a Rigaku SmartLab X-ray diffractometer in reflection mode using CuKα radiation (λ = 1.54 Å). The 2θ range from 2° to 40° was scanned with a scan rate of 3° min^{-1}. The instrument was previously calibrated using a silicon standard.

b) ***Thermogravimetric analysis (TGA)*:** Thermogravimetric analyses (TGA) were carried out on a TG50 analyzer (Mettler-Toledo) or an SDT Q600 TG-DTA analyzer under N_2 atmosphere at a heating rate of 10 ºC min^{-1} within a temperature range of 30-800 °C.

c) ***FT-IR spectroscopy*:** The Fourier transform infrared (FT-IR) spectra were taken on a Bruker Optics ALPHA-E spectrometer with a universal Zn-Se ATR (attenuated total reflection) accessory in the 600-4000 cm^{-1} region or using a Diamond ATR (Golden Gate). The spectra were measured over the range of 4000-400 cm^{-1}.

d) ***Scanning Electron Microscopy (SEM)*:** SEM was performed on an FEI Nova NanoSEM 650 Scanning Electron Microscope instrument with a field emitter as an electron source. SEM images of membrane cross section were taken after freeze fracture of membranes in LN_2. Samples for SEM were gold sputtered before analyses.

e) ***Mechanical property*:** Mechanical properties of these hybrid membranes were studied using a Linkam TST-350 micro-tensile testing instrument, where the membrane

samples were analyzed at a strain rate of 20 μm s^{-1}. The mechanical property analysis for each hybrid membrane was repeated with eight samples prepared under identical conditions.

f) ***N_2 adsorption experiment*:** All low-pressure N_2 adsorption experiments (up to 1 bar) were performed on a Quantchrome instrument. Approximately 50 mg of the sample was activated after solvent exchange by the use of activation chamber. The activated sample was loaded inside the glass bulb of N_2 adsorption instrument and measured the capacity.

5.7.4 *Gas permeation measurements*

The variable volume set-up was used for the determination of gas permeability. The pure gases used (H_2, N_2, CH_4, CO_2, C_3H_6 and C_3H_8) had a minimum purity of 99.8%. These gases were selected because of their industrial significance. Membrane sample of 3.8 cm active diameter was used for gas permeation analysis at ambient temperature and at 20 atm (3 atm for TFC membranes) upstream pressure.

A schematic diagram of permeation equipment is shown in ***Figure 5.16***. One end of the feed side of the cell was connected through valve V_1 to the feed gas cylinder outlet and an electronic pressure gauge (0-999 psi range). The valve V_2 was a vent and used to control the feed pressure. On the permeate side of the permeation cell, a mercury flowmeter was connected. The displacement of mercury slug was monitored against time.

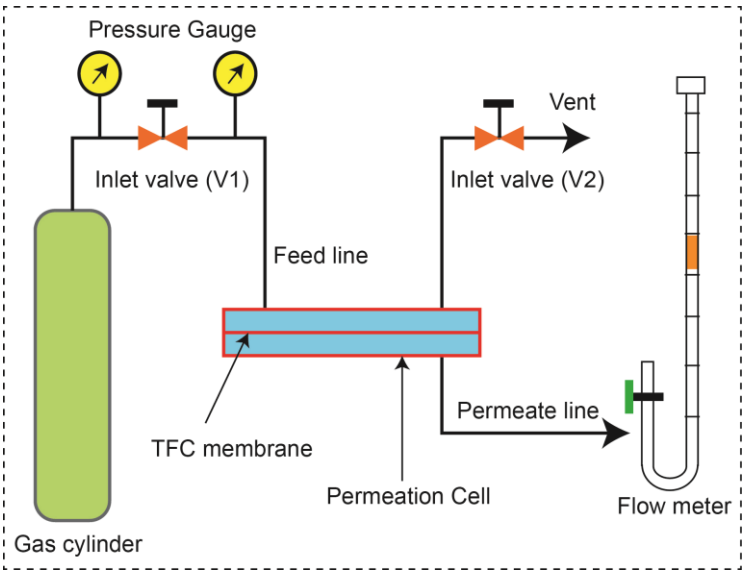

Figure 5.16. *Schematic representation of gas permeation equipment set-up.*

The permeability (*P*) was calculated using the Equation 5.1.

$$P = \frac{J \times l}{\Delta P} \qquad (5.1)$$

where, *J* = Flux of gas ($cm^3.cm^{-2}.s^{-1}$), *l* = thickness of the membrane (cm), Δ*p* = pressure difference across the membrane (cm Hg), and *P* is the permeability expressed in Barrer (1 Barrer = 10^{-10} cm^3(STP)cm.$cm^{-2}.s^{-1}$.cm Hg^{-1}).

The permeance (*P*) of TFC membranes was calculated using the Equation 5.2.

$$P = \frac{14.7 \times d \times F.C}{76 \times A \times t \times \Delta P} \qquad (5.2)$$

where, d = Distance travelled by mercury (cm), F.C. = Flow meter constant [volume of the flow meter capillary per unit length (cm^3/cm)], A= Effective membrane area (cm^2), t = Time (sec), P = Pressure (psi), and *P* is the permeance expressed in GPU [1 GPU = 1×10^{-6} cm^3 (STP)/ (cm^2 s cmHg)].

The ideal selectivity (α) was calculated as the ratio of permeability/permeance of two gases. The permeation measurements were repeated with at least 3 different membrane samples prepared under identical conditions and the data was averaged. The ideal selectivity of various gases was calculated using the Equation 5.3.

$$\alpha = \frac{P_x}{P_y} \qquad (5.3)$$

where, P_x and P_y are the permeance of respective pure gases.

NOTE: The work presented in this chapter is a collaborative work between the group of Dr. Rahul Banerjee with his student Mr. Bishnu Prasad Biswal from the Physical/Materials Chemistry Division and the group of Dr. Ulhas K. Kharul with his student Mr. Harshal D. Chaudhari, Ms. Taranpreet Kaur and Mr. Shebeeb Kunjattu H., from the Polymer Science and Engineering Division at CSIR-National Chemical Laboratory, Pune. The experimental results depicted in the first part of this chapter have already been published in *Chem. Eur. J.*, **2016**, *22*, 4695-4699, with the title: "*Chemically Stable Covalent Organic Framework (COF)-Polybenzimidazole Hybrid Membranes: Enhanced Gas Separation through Pore Modulation*". The results presented in the later part of this chapter have submitted for possible publication with the title: "*Transforming Covalent Organic Framework into Thin-film Composite Membranes for Faster Hydrocarbon Recovery*." The major work has been contributed by Mr. Bishnu Prasad Biswal. He was involved in the synthesis of COF and COF@PBI-BuI composite membrane fabrication, characterizations of the materials etc. In this work, Mr. Harshal D. Chaudhari helped in PBI-BuI synthesis and to carry out the mechanical property measurement. Ms. Taranpreet Kaur and Mr. Shebeeb Kunjattu H. assisted in carrying out TFC membrane fabrication at the beginning of this project. Both the manuscripts were primarily written by Mr. Bishnu Prasad Biswal under the supervision of Dr. Rahul Banerjee and Dr. Ulhas K. Kharul.

CHAPTER 6

Conclusions of all Chapters and Future Directive

6.1 Conclusions

The first chapter of the thesis includes the introduction of advanced porous crystalline frameworks such as metal-organic frameworks (MOFs) and covalent organic framework (COFs), their synthetic development and important applications with a special emphasis on membrane-based gas separation. The synthetic difficulties and the chemical stability of these crystalline, porous materials have been thoroughly discussed. In the later part, we have outlined the advantages of using these crystalline, porous, stable nanoporous framework materials for composite membrane fabrication and gas separation application evidenced with appropriate literature reports.

In the second chapter, we have entrapped a highly porous, water stable Co(II) based ZIF [CoNIm (RHO)] and thoroughly observed the crystal growth and time-dependent phase transformation from CoNIm (RHO) to a less porous CoNIm (SOD) ZIF. The CoNIm (RHO) displayed a highest BET surface area as 1858 m^2g^{-1} among all ZIFs reported. CoNIm (RHO) shows unusually high water stability and thus water vapour uptake compared to CoNIm (SOD) and other ZIFs known. In addition, CoNIm (RHO) shows promising H_2 uptake capacity of 1.5 wt% at (77 K and 1 bar) along with CO_2 uptake capacity of 2.99 mmol g^{-1} (273 K and 1 bar) and 1.92 mmol g^{-1} (298 K and 1 bar) respectively.

In the third chapter, we revealed a methodology to grow MOF crystals selectively on preferred surfaces (inner or outer) of a porous polymeric (PBI-BuI-HF) substrate employing interfacial synthesis method. The methodology, we have demonstrated has its own merits owing to the ease of MOF growth without any pre-seeding. Moreover, we introduced the use of volatile solvents ($CHCl_3$, IBA and H_2O) to synthesize MOF membranes. The separation performance of gases such as He, N_2 and C_3H_8 through MOF-HF composite membranes demonstrated that MOFs extensively take part in the molecular discrimination. Among all

composite membranes synthesized in this work, CuBTC@PBI-BuI-Out displayed an appreciable permeance and selectivity of 12 (He/N_2) and 17 (He/C_3H_8).

In the fourth chapter, we showcased the first example of a simple, safe and environmentally-friendly mechanochemical synthetic route for the synthesis of highly water, acid and base stable COFs. We have demonstrated that by employing Schiff base mechanochemistry, COFs can be synthesized very rapidly in high yield at room temperature and the progress of the reaction can be monitored by the visual colour change. We observed a simultaneous mechanochemical exfoliation of 2D COFs layers during the grinding process, which has not been observed for any COFs materials before. The gas and water adsorption properties of all COFs (MC) were studied and compared with the COFs (ST). In the later part of this chapter, liquid-assisted grinding (LAG) have been employed to synthesize a diverse class of COFs [TpTh (LAG), DhaTph (LAG) and LZU-1 (LAG)] efficiently at a faster rate and in high yield at room temperature with improved crystallinity compared to only neat grinding.

In the fifth chapter, we discussed a methodology to fabricate a new class of self-supported COF@polymer hybrid membranes. These self-supported membranes are highly flexible, reproducible and display a high degree of thermal and chemical stabilities; showing its potentiality for a wider range of applications in the gas/liquid separation. We have performed the gas permeation analysis, which revealed that almost 7 fold elevations in permeability of gases (H_2, N_2, CH_4 and CO_2) than the pristine membrane with 50% TpBD loading with appreciable CO_2/N_2 (23) and CO_2/CH_4 (48.7) selectivity was achievable. Interestingly, the effect of isoreticulation in COF towards elevating the gas permeability was prominently seen. In the later part, we demonstrated a methodology to fabricate COF@polymer (TpPa-1@SBR) thin film composite (TFC) membranes. The gas permeation analysis shows almost 8 to 12 fold elevation in permeance of hydrocarbon gases (C_3H_6 and C_3H_8) than the pristine SBR based TFC membrane. With 50% TpPa-1 loading, appreciable C_3H_8/N_2 and C_3H_6/N_2 reverse selectivity (15 and 20) was achievable. The outcome of this work of obtaining TFC membranes of chemically stable functional COF with high flux and reverse selectivity is of significant use in vapour recovery from fuel stations/industries.

6.2 Future directive

Design and synthesis of crystalline, porous 2D polymers for photocatalytic CO_2 reduction to renewable fuels.

The aim of this future plan is to address the most challenging concern of today's society to replace the current use of fossil fuels by sustainable energy conversion processes [6.1]. As the overall work presented in this thesis is based on the facile synthesis of chemically stable, crystalline porous materials and membranes for gas separation. Next, we are planning to fabricate thin films based on porous materials for energy application. The idea behind this plan is to design and synthesise porous, chemically stable, crystalline 2D polymeric thin films as heterogeneous CO_2 reduction catalysts.

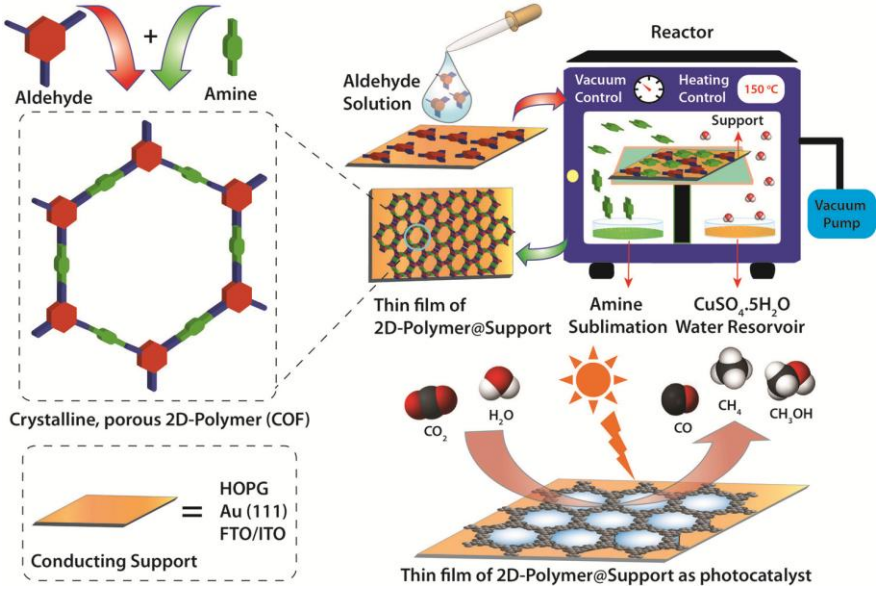

Figure 6.1. *Schematic of the proposed strategy toward the direct growth of the 2D-polymeric thin film on conducting surfaces for CO_2 reduction to fuels.*

We expect, highly conjugated metal-porphyrin based COF systems will enhance the photoresponse towards the visible region [6.2]. Next, the ideology of designing hetero-metallic COFs will have uniqueness over monometallic systems as the primary metal-porphyrin/salen framework will be responsible for CO_2 activation/adsorption in the COF framework and the secondary metal-ligand system linked to the Schiff base centres will act as electro-photocatalyst, which may facilitates the CO_2 reduction to produce products such as CO, CH_4 and CH_3OH [6.3].

Page left intentionally blank

REFERANCES

CHAPTER 1

[1.1] (a) M. E. Davis, *Nature* **2002**, *417*, 813; (b) A. Oterhals, M. Solvang, R. Nortvedt, M. H. G. Berntssen, *Eur. J. Lipid Sci. Tech.,* **2007**, *109*, 691; (c) T. Sawaki, T. Dewa, Y. Aoyama, *J. Am. Chem. Soc.*, **1998**, *120*, 8539; (d) D. Wang, *Sep. Purif. Technol.*, **2004**, *35*, 125; (e) R. Dawson, E. Stöckel, J. R. Holst, D. J. Adams, A. I. Cooper, *Energy Environ. Sci.*, **2011**, *4*, 4239.

[1.2] (a) A. Corma, *Chem. Rev*. **1997**, *97*, 2373. (b) F. Schüth and W. Schmidt, *Adv. Mater.* **2002**, *9*, 629.

[1.3] J. Lee, J. Kim, and T. Hyeon, *Adv. Mater.*, **2006**, *18*, 2073.

[1.4] (a) Y. Ma, W. Tong, H. Zhou, S. L Suib, *Microporous Mesoporous Mater.*, **2000**, *37*, 243; (b) S. Cavenati, C. A. Grande and A. E. Rodrigues, *J. Chem. Eng. Data*, **2004**, *49*, 1095.

[1.5] (a) O. M. Yaghi, H. Li, *J. Am. Chem. Soc.*, **1995**, *117*, 10401; (b) O. M. Yaghi, G. Li, H. Li, *Nature*, **1995**, *378*, 703.

[1.6] A. P. Côté, A. I. Benin, N. W. Ockwig, A. J. Matzger, M. O'Keeffe, O. M. Yaghi, *Science* **2005**, *310*, 1166.

[1.7] J. Rouquerol, D. Avnir, C. W. Fairbridge, D. H. Everett, J. H. Haynes, N. Pernicone, J. D. F. Ramsay, K. S. W. Sing, K. K. Unger, *Pure and Applied Chemistry*, **1994**, *66*, 1739.

[1.8] (a) M. Eddaoudi, D. B. Moler, H. Li, B. Chen, T. M. Reinekee, M. O'Keeffe, O. M. Yaghi, *Acc. Chem. Res.* **2001**, *34*, 319; (b) C. Janiak, *Angew. Chem., Int. Ed. Engl.*, **1997**, *36*, 1431; (c) A. J. Blake, N. R. Champness, P. Hubberstey, W.-S. Li, M. A. Withersby, M. Schroder, *Coord. Chem. Rev.*, **1999**, *183*, 117; (d) B. Kesanli, Y. Cui, M.Smith, E. Bittner, B. Bockrath, W. Lin, *Angew. Chem., Int. Ed.*, **2005**, *44*, 72; (e) S. Kitagawa, R. Kitaura, S. -I. Noro, *Angew. Chem., Int. Ed.*, **2004**, *43*, 2334; (f) G. Ferey, *Chem. Soc. Rev.* **2008**, *37*, 191; (g) B. Chen, S. Xiang, G. Qian, *Acc. Chem. Res.*, **2010**, *43*, 1115; (h) L. Ma, C. Abney, W. Lin, *Chem. Soc. Rev.*, **2009**, *38***,** 124; (i) Z. G. Gu, Y. P. Cai, H. C. Fang, Z. Y. Zhou, P. K. Thallapally, J. A. Tian, J. Liu,

G. J. Exarhos, *Chem. Commun.*, **2010**, *46*, 5373; (j) B. Chen, M. Eddaoudi, S. T. Hyde, M. O'Keeffe, O. M. Yaghi, *Science*, **2001**, *291*, 1021; (k) P. Pachfule, Y. Chen, J. Jiang, R. Banerjee *J. Mater. Chem.*, **2011**, *21*, 17737; (l) J. W. Yoon, S. H. Jhung, Y. K. Hwang, S. M. Humphrey, P. T. Wood, J. -S. Chang, *Adv. Mater.* **2007**, *19*, 1830; (m) K. L. Mulfort, O. K. Farha, C. D. Malliakas, M. G. Kanatzidis and. J. T. Hupp, *Chem. Eur. J.*, **2010**, *16*, 276; (n) H. -S. Choi, M. P. Suh, *Angew. Chem*. **2009**, *121*, 6997; (o) X. Gu, Z.-H. Lu, Q. Xu, *Chem. Commun* **2010**, *46*, 7400; (p) S**.** -T. Zheng, J. T. Bu, Y. Li, T. Wu, F. Zuo, P. Feng, X. Bu. *J. Am. Chem. Soc.* **2010**, *132*, 17062; (q) J. An, N. L. Rosi, *J. Am. Chem. Soc.* **2010**, *132*, 5578; (r) A. G. Wong-Foy, O. Lebel, A. J. Matzger, *J. Am. Chem. Soc.* **2007**, *129*, 15740; (s) H. Chun, D. N. Dybtsev, H. Kim, K. Kim, *Chem. Eur. J.* **2005**, *11*, 3521; (t) J. Rowsell, A. Millward, K. Park, O. Yaghi *J. Am. Chem. Soc.* **2004**, *126*, 5666.

[1.9] (a) H. Furukawa, K. E. Cordova, M. O'Keeffe, O. M. Yaghi, *Science*, **2013**, *341*, 6149; (b) R. J. Kupplera, D. J. Timmonsb, Q. –R. Fanga, J. –R. Lia, T. A. Makala, M. D. Younga, D. Yuana, D. Zhaoa, W. Zhuanga, H .-C. Zhou. *Coord. Chem. Rev.*, **2009**, **253**, 3042; (c) A. Morozan, F. Jaouen, *Energy Environ. Sci.*, **2012**, *5*, 9269; (d) A. U. Czaja, N. Trukhan, U. Müller, *Chem. Soc. Rev.*, **2009**, *38*, 1284; (e) U. Mueller, M. Schubert, F. Teich, H. Puetter, K. Schierle-Arndt and J. Pastré *J. Mater. Chem.*, **2006**, *16*, 626.

[1.10] (a) N. Stock, S. Biswas *Chem. Rev*. **2012**, *112*, 933; (b) C. Dey, T. Kundu, B. P. Biswal, A. Mallick and R. Banerjee, *Acta Crystallogr., Sect. B. **2014**, B70, 3*.

[1.11] (a) C. Wang, & J. Y. Ying, *Chem. Mater.*, **1999**, *11*, 3113; (b) A. Lagashetty, V. Havanoor, S. Basavaraja, S. D. Balaji, & A. Venkataraman, *Sci. Technol. Adv. Mater.*, **2007**, *8*, 484; (c) A. Pichon, A. Lazaun-Garay, S. L. James, *CrystEngComm*. **2006**, *8*, 21; (d) T. Friščić, L. R. MacGillivray, *Chem. Commun*., **2003**, 1306; (e) T. Friščić, I. Halasz, P. J. Beldon, A. M. Belenguer, F. Adams, S. A. J. Kimber, V. Honkimäki, R. E. Dinnebier, *Nat. Chem.* **2013**, *5*, 66; (f) A. Martinez Joaristi, J. Juan-Alcaniz, P. Serra-Crespo, F. Kapteijn, & J. Gascon, *Cryst. Growth Des.* **2012**, *12*, 3489; (g) N. Arul Dhas, C. P. Raj & A. Gedanken, *Chem. Mater*. **1998**, *10*, 3278; (h) J. Kim, S. Yang, S. B. Choi, J. Sim, J. Kim, & W. Ahn, *J. Mater. Chem.*, **2011**, *21*, 3070.

[1.12] (a) L. J. Murray, M. Dincă, J. R. Long, *Chem. Soc. Rev.*, **2009**, *38*, 1294; (b) Y. Tao, H. Kanoh, L. Abrams, K. Kaneko, *Chem. Rev.* **2006**, *106*, 896.

[1.13] (a) M. P. Suh, H. J. Park, T. K. Prasad, D. -W. Lim, *Chem. Rev.*, **2012**, *1128*, 782; (b) D. J. Collinsa, H. –C. Zhou, *J. Mater. Chem.*, **2007**, *17*, 3154.

[1.14] M. P. Suh, H. J. Park, T. K. Prasad, D.-W. Lim, *Chem. Rev.*, **2012**, *112*, 782.

[1.15] (a) N. L. Rosi, J. Eckert, M. Eddaoudi, D. T. Vodak, J. Kim, M. O'Keeffe, O.M. Yaghi, *Science* **2003**, *300*, 1127; (b) Y. Yan, X. Lin, S. Yang, A. J. Blake, A. Dailly, N. R. Champness, P. Hubberstey and M. Schröder *Chem. Commun.*, **2009**, 1025; (c) O. K. Farha, A. O. Yazaydin, I. Eryazici, C. D. Malliakas, B. G. Hauser, M. G. Kanatzidis, S. T. Nguyen, R. Q. Snurr, J. T. Hupp, *Nat. Chem*. **2010**, *2*, 944.

[1.16] H. Furukawa, N. Ko, Y. B. Go, N. Aratani, S. B. Choi, E. Choi, A. O. Yazaydin, R. Q. Snurr, M. O'Keeffe, J. Kim, O. M. Yaghi, *Science* **2010**, *329*, 424.

[1.17] (a) O. K. Farha, A. O. Yazaydın, I. Eryazici, C. D. Malliakas, B. G. Hauser, M. G. Kanatzidis, S. T. Nguyen, R. Q. Snurr, J. T. Hupp, *Nat. Chem.* **2010**, *2*, 944; (b) Y. Yan, X. Lin, S. Yang, A. J. Blake, A. Dailly, N. R. Champness, P. Hubbersteya, M. Schroder, *Chem. Commun*., **2009**, 1025; (c) D. Yuan, D. Zhao, D. Sun, Hong-Cai Zhou, *Angew. Chem. Int. Ed.* **2010**, *49*, 5357; (d) M. Dinca, A. Dailly, Y. Liu, C. M. Brown, D. A. Neumann, J. R. Long, *J. Am. Chem. Soc.* **2006**, *128*, 16876; (e) X. Lin, J. Jia, X. Zhao, K. M. Thomas, A. J. Blake, G. S. Walker, N. R. Champness, P. Hubberstey, M. Schroder, *Angew. Chem.* **2006**, *118*, 7518; (f) O. K. Farha, K. L. Mulfort, J. T. Hupp, *Inorg. Chem.*, **2008**, *47*, 10223; (g) O. K. Farha, A. M. Spokoyny, K. L. Mulfort, M. F. Hawthorne, C. A. Mirkin, J. T. Hupp, *J. Am. Chem. Soc.*, **2007**, *129*, 12680; (h) D. F. Sava, V.C. Kravtsov, J. Eckert, J. F. Eubank, F. Nouar, M. Eddaoudi, *J. Am. Chem. Soc.*, **2009**, *131*, 10394; (i) A. G. Wong-Foy, O. Lebel, A. J. Matzger *J. Am. Chem. Soc.* **2007**, *129*, 15740; (j) S. R. Caskey, A. G. Wong-Foy, A. J. Matzger, *J. Am. Chem. Soc.* **2008**, *130*, 10870; (k) H. Chun, D. N. Dybtsev, H. Kim, K. Kim, *Chem. Eur. J.* **2005**, *11*, 3521.

[1.18] (a) X. B. Zhao, B. Xiao, A. J. Fletcher, K. M. Thomas, D. Bradshaw, M. J. Rosseinsky, *Science* **2004**, *306*, 1012; (b) D. Sun, S. Ma, Y. Ke, D. J. Collins, H. C. Zhou, *J. Am. Chem. Soc.* **2006**, *128*, 3896; (c) Y. Yan, I. Telepeni, S. Yang, X. Lin,

W. Kockelmann, A. Dailly, A. J. Blake, W. Lewis, G. S. Walker, D. R. Allan, S. A. Barnett, N. R. Champness, M. Schroder, *J. Am. Chem. Soc.* **2010**, *132*, 4092; (d) S.-T. Zheng, J. T. Bu, Y. Li, T. Wu, F. Zuo, P. Feng, X. Bu, *J. Am. Chem. Soc.* **2010**, *132*, 17062; (e) F. Debatin, A. Thomas, A. Kelling, N. Hedin, Z. Bacsik, I. Senkovska, S. Kaskel, M. Junginger, H. Muller, U. Schilde, C. Jager, A. Friedrich, H. J. Holdt, *Angew. Chem. Int. Ed.* **2010**, *49*, 1258; (f) O. K. Farha, A. M. Spokoyny, K. L. Mulfort, S. Galli, J. T. Hupp, C. A. Mirkin, *small*, **2009**, *5*, 1727; (g) T. Panda, P. Pachfule, Y. Chen, J. Jiang, R. Banerjee *Chem. Commun.*, **2011**, 2011; (i/h) J. An, S. J. Geib, N. L. Rosi *J. Am. Chem. Soc.* **2010**, *132*, 38.

[1.19] (a) X. –S. Wang, S. Ma, P. M. Forster, D. Yuan, J. Eckert, J. J. Lopez, B. J. Murphy, J. B. Parise, H. –C. Zhou *Angew. Chem. Int. Ed.* **2008**, *47*, 7263; (b) Z. Guo, H. Wu, G. Srinivas, Y. Zhou, S. Xiang, Z. Chen, Y. Yang, W. Zhou, M. O'Keeffe, B. Chen, *Angew. Chem. Int. Ed.* **2011**, *50*, 3178; (c) S. Ma, D. Sun, J. M. Simmons, C. D. Collier, D. Yuan, H.-C. Zhou, *J. Am. Chem. Soc.*, **2008**, *130*, 1012; (d) X. Lin, I. Telepen, A. J. Blake, A. Dailly, C. M. Brown, J. M. Simmons, M. Zoppi, G. S. Walker, K. M. Thomas, T. J. Mays, P. Hubberstey, N. R. Champness, M. Schroder, *J. Am. Chem. Soc.*, **2009**, *131*, 2159; (e) X. S. Wang, S. Ma, K. Rauch, J. M. Simmons, D. Yuan, X. Wang, T. Yildirim, W. C. Cole, J. J. Lspez, A. de Meijere, H. C. Zhou, *Chem. Mater.*, **2008**, *20*, 3145; (f) X. Lin, J. H. Jia, X. B. Zhao, K. M. Thomas, A. J. Blake, G. S. Walker, N. R. Champness, P. Hubberstey, M. Schroder, *Angew. Chem., Int. Ed.*, **2006**, *45*, 7358; (g) C. Tan, S. Yang, N. R. Champness, X. Lin, A. J. Blake, W. Lewis, M. Schroder, *Chem. Commun.*, 2**011**, 4487; (h) B. Chen, N. W. Ockwig, A. R. Millward, D. S. Contreras, O. M. Yaghi, *Angew. Chem. Int. Ed.* **2005**, *44*, 4745; (i) M. Dinca, W. S. Han, Y. Liu, A. Dailly, C. M. Brown, J. R. Long, *Angew. Chem., Int. Ed.*, **2007**, *46*, 1419; (j) F. Nouar, J. F. Eubank, T. Bousquet, L. Wojtas, M. J. Zaworotko, M. Eddaoudi, *J. Am. Chem. Soc.*, **2008**, *130*, 1833; (k) X. Gu, Z. –H. Lu, Q. Xu, *Chem. Commun.*, **2010**, *46*, 7400.

[1.20] (a) J. Grigg, *Arch Dis Child*, **2002**, *86*, 79; (b) D. Lüthi, M. Le Floch, B. Bereiter, T. Blunier, J. M. Barnola, U. Siegenthaler, D. Raynaud, J. Jouzel, H. Fischer, K. Kawamura, T. F. Stocker, *Nature*, **2008**, *453*, 379; (c) *Health Effects of Climate Change in the UK*, **2008**, UK Department of Health.

[1.21] (a) F. Barzagli, F. Mani, M. Peruzzini, *Energy Environ. Sci.* **2010**, *3*, 772; (b) C.-H. Yu, C.-H. Huang, C.-S. Tan, *Aerosol Air Qual. Res.* **2012**, *12*, 745; (c) W. M. Budzianowski, *Energy*, **2012**, 37.

[1.22] (a) A.-H. Lu, G.-P. Hao, *Annu. Rep. Prog. Chem., Sect. A: Inorg. Chem.*, **2013**, *109*, 484; (b) A.-H. Lu, S. Dai, *Springer-Verlag Berlin Heidelberg*, **2014**.

[1.23] (a) K. Sumida, D. L. Rogow, J. A. Mason, T. M. McDonald, E. D. Bloch, Z. R. Herm, T.-H. Bae, J. R. Long, *Chem. Rev.*, **2012**, *112*, 724; (b) Y. Liu, U. Z. Wang, H.-C. Zhou, *Greenhouse Gases: Sci. Technol.* **2012**, *2*, 239; (c) J. Liu, P. K. Thallapally, B. P. McGrail, D. R. Brown, J. Liu, *Chem. Soc. Rev.*, **2012**, *41*, 2308; (d) Z. Zhang, Y. Zhao, Q. Gong, Z. Li, J. Li, *Chem. Commun.*, **2013**, *49*, 653.

[1.24] (a) A. R. Millward, O.M. Yaghi, *J. Am. Chem. Soc.*, **2005**, *127*, 17998; (b) P. D. C. Dietzel, R. E. Johnsen, H. Fjellvag, S. Bordiga, E. Groppo, S. Chavan, R. Blom, *Chem. Commun.* **2008**, 5125; (c) T. M. McDonald, D. M. D'Alessandro, R. Krishna, J. R. Long, *Chem. Sci.* **2011**, *2*, 2022; (d) S. S.-Y. Chui, S. M.-F. Lo, J. Charmant, A. G. Orpen, I. D. Williams, *Science*, **1999**, *283*, 1148; (e) D. Britt, H. Furukawa, B. Wang, T. G. Glover, O. M. Yaghi, *Proc. Natl. Acad. Sci. U. S. A.*, **2009**, *106*, 20637; (f) P. Nugent, Y. Belmabkhout, S. D. Burd, A.J. Cairns, R. Luebke, K. Forrest, T. Pham, S. Ma, B. Space, L. Wojtas, M. Eddaoudi, M. J. Zaworotko, *Nature*, **2013**, *495*, 80; (g) K. Sumida, D. L. Rogow, J. A. Mason, T. M. McDonald, E. D. Bloch, Z. R. Herm, T. -H. Bae, J. R. Long, *Chem. Rev.*, **2012**, *112*, 724.

[1.25] D. Aaron, C. Tsouris, *Sep. Sci. Technol.*, **2005**, *40*, 321.

[1.26] (a) K. S. Park, N. Zheng, A. -P. Cöté, J. Y. Choi, R. Huang, F. J. Uribe-Romo, H. K. Chae, M. O'Keeffe, O. M. Yaghi, *Proc. Natl. Acad. Sci. U.S.A.*, **2006**, *103*, 10186; (b) X. -C. Huang, Y. -Y. Lin, J. -P. Zhang, X. -M. Chen, *Angew. Chem., Int. Ed.*, **2006**, *45*, 1557; (c) R. Banerjee, A. Phan, B. Wang, C. Knobler, H. Furukawa, M. O'Keeffe, O. M. Yaghi, *Science*, **2008**, *319*, 939; (d) R. Banerjee, H. Furukawa, D. Britt, C. Knobler, M. O'Keeffe, O. M. Yaghi, *J. Am. Chem. Soc.*, **2009**, *131*, 3875; (e) B. Wang, A. P. Cöté, H. Furukawa, M. O'Keeffe, O. M. Yaghi, *Nature*, **2008**, *453*, 207; (f) A. J. Cairns, J. A. Perman, L. Wojtas, V. Ch. Kravtsov, M. H. Alkordi, M. Eddaoudi, M. J. Zaworotko, *J. Am. Chem. Soc.*, **2008**, *130*, 1560; (g) F. Debatin, A.

Thomas, A. Kelling, N. Hedin, Z. Bacsik, I. Senkovska, S. Kaskel, M. Junginger, H. Muller, U. Schilde, C. Jager, A. Friedrich, H. -J. Holdt, *Angew. Chem., Int. Ed*. **2010**, *49*, 1258; (h) B. Chen, N. W. Ockwig, A. R. Millward, D. S. Contreras, O. M. Yaghi, *Angew. Chem., Int. Ed.*, **2005**, *44*, 4745; (i) W. Morris, B. Leung, H. Furukawa, O. K. Yaghi, N. He, H. Hayashi, Y. Houndonougbo, M. Asta, B. B. Laird, O. M. Yaghi, *J. Am. Chem. Soc.*, **2010**, *132*, 11006.

[1.27] (a) Z. Bao, L. Yu, Q. Ren, X. Lu, S. J. Deng, *Colloid Interface Sci*. **2011**, *353*, 549; (b) A. O. Yazaydin, R. Q. Snurr, T.-H. Park, K. Koh, J. Liu, M. D. LeVan, A. I. Benin, P. Jakubczak, M. Lanuza, D. B. Galloway, J. L. Low, R. R. *J. Am. Chem. Soc*. **2009**, *131*, 18198; (c) J. A. Mason, K. Sumida, Z. R. Herm, R. Krishna, J. R. Long, *Energy Environ. Sci*. **2011**, *4*, 3030; (d) D. Britt, H. Furukawa, B. Wang, T. G. Glover and O. M. Yaghi, *Proc Natl Acad Sci USA* **2009**, *106*, 20637; (e) S. R. Caskey, A. G. Wong-Foy, A. J. Matzger, *J. Am. Chem. Soc.*, **2008**, *130*, 10870; (f) A. O. Yazaydin, A. I. Benin, S. A. Faheem, P. Jakubczak, J. L. Low, R. Willis, R. R. Q. Snurr, *Chem. Mater*. **2009**, *21*, 1425; (g) J. Liu, Y. Wang, A. I. Benin, P. Jakubczak, R. R. Willis, M. D. LeVan, *Langmuir*, **2010**, *26*, 14301; (h) P. D. C. Dietzel, R. E. Johnsen, H. Fjellvag, S. Bordiga, E. Groppo, S. Chavan, R. Blom, *Chem. Commun*., **2008**, 5125; (i) P. Aprea, D. Caputo, N. Gargiulo, F. Iucolano, F. Pepe, *J. Chem. Eng. Data*, **2010**, *55*, 3655; (j) P. Chowdhury, C. Bikkina, D. Meister, F. Dreisbach, S. Gumma, *Microporous Mesoporous Mater.* **2009**, *117*, 406; (k) J. Liu, Y. Wang, A. I. Benin, P. Jakubczak, R. R. Willis, M. D. LeVan, *Langmuir*, **2010**, *26*, 14301; (l) D. Farrusseng, C. Daniel, C. Gaudillère, U. Ravon, Y. Schuurman, C. Mirodatos, D. Dubbeldam, H. Frost, R. Q. Snurr, *Langmuir,* **2009**, *25*, 7383; (m) J. Kim, S. -T. Yang, S. B. Choi, J. Sim, J. Kim, W. -S. Ahn, *J. Mater. Chem*. **2011**, *21*, 3070; (n) T. M. McDonald, D. M. D'Alessandro, R. Krishna, J. R. Long. *Chem. Sci*. **2011**, *2*, 2022; (o) J. An, S. J. Geib, N. Rosi, *J. Am. Chem. Soc.,* **2009**, *132*, 38; (p) A. Demessence, D. M. D'Alessandro, M. L. Foo, J. R. Long, *J. Am. Chem. Soc*. **2009**, *131*, 8784; (q) R. Vaidhyanathan, S. S. Iremonger, K. W. Dawson, G. K. H. Shimizu, *Chem. Commun*. **2009**, 5230; (r) B. Arstad, H. Fjellvåg, K. O. Kongshaug, O. Swang, R. Blom, *Adsorption* **2008**, *14*, 755; (s) T. K. Prasad, D. H. Hong, M. P. Suh, *Chem.. Eur. J.* **2010**, *16*, 14043; (t) K. Sumida, S. Horike, S. S. Kaye, Z. R. Herm, W. L. Queen, C. M. Brown, F. Grandjean,

G. J. Long, A. Dailly, J. R. Long, *Chem. Sci.* **2010**, *1*, 184; (u) J. Kim, S. -T. Yang, S. B. Choi, J. Sim, J. Kim, W. -S. Ahn. *J. Mater. Chem*. **2011**, *21*, 3070; (v) H. Kanoh, A. Kondo, H. Noguchi, H. Kajiro, A. Tohdoh, Y. Hattori, W. -C. Xu, M. Inoue, T. Sugiura, K. Morita, H. Tanaka, T. Ohba, K. J. Kaneko, *Colloid Interface Sci*. **2009**, *334*, 1; (w) O. K. Farha, C. D. Malliakas , M.G. Kanatzidis, J. T. Hupp *J. Am. Chem. Soc.* **2010**, *132*, 950; (x) Y. -S. Bae, O. K. Farha,J. T. Hupp, R. Q. Snur, *J. Mater. Chem.*, **2009**, *19*, 2131; (y) Y. -S. Bae, O. K. Farha, A. M. Spokoyny, C. A. Mirkin, J. T. Hupp, R. Q. Snurr. *Chem. Commun*., **2008**, 4135.

[1.28] a) S. K. Henninger, H. A. Habib, C. Janiak, *J. Am. Chem. Soc*., **2009**, *131*, 2776; b) E. Kang, G. S. Jeong, Y. Y. Choi, K. H. Lee, A. Khademhosseini, S. H. Lee, *Nat. Mater*. **2011**, *10*, 877; c) H. Yang, H. Zhu, M. M. R. M. Hendrix, N. J. H. G. M. Lousberg, G. de With, A. C. C. Esteves, J. H. Xin, *Adv. Mater*. **2013**, *25*, 1150; d) M. N. Golubovic, H. D. M. Hettiarachchi, W. M. Worek, Int. *J. Heat Mass Transfer* **2006**, *49*, 2802; e) D. Fröhlich, S. K. Henninger, C. Janiak, *Dalton Trans.*, **2014**, *43*, 15300.

[1.29] (a) W. H. Tao, T. C. K. Yang, Y. N. Chang, L. K. Chang, T. W. J. Chung, *Environ. Eng.* **2004**, *130*, 1210; (b) J. Rodriguez-Mirasol, J. Bedia, T. Cordero, J. J. Rodriguez, *Sep. Sci. Technol.* **2005**, *40*, 3113; (c) D. Ferreira, R. Magalhaes, P. Taveira, A. Mendes, *Ind. Eng. Chem. Res.* **2011**, *50*, 10201.

[1.30] P. Kanchanalai, R. P. Lively, M. J. Realff, Y. Kawajiri, *Ind. Eng. Chem. Res*. **2013**, *52*, 11132.

[1.31] (a) P. Kusgens, M. Rose, I. Senkovska, H. Froede, A. Henschel, S. Siegle, S. Kaskel, *Microporous Mesoporous Mater.* **2009**, *120*, 325; (b) F. Jeremias, A. Khutia, S. K. Henninger, C. Janiak, *J. Mater. Chem.* **2012**, *22*, 10148; (c) G. Akiyama, R. Matsuda, S. Kitagawa, *Chem. Lett.* **2010**, *39*, 360; (d) G. D. Pirngruber, L. Hamon, S. Bourrelly, P. L. Llewellyn, E. Lenoir, V. Guillerm, C. Serre, T. Devic, *ChemSusChem.*, **2012**, *5*, 762; (e) M. Wickenheisser, F. Jeremias, S. K. Henninger, C. Janiak, *Inorg. Chim. Acta* **2013**, *407*, 145; (f) Q. M. Wang, D. M. Shen, M. Bulow, M. L. Lau, S. G. Deng, F. R. Fitch, N. O. Lemcoff, J. Semanscin, *Microporous Mesoporous Mater.* **2002**, *55*, 217; (g) Y. Wang, M. D. J. LeVan, *Chem. Eng. Data*, **2009**, *54*, 2839.

[1.32] J. J. Low, A. I. Benin, P. Jakubczak, J. F. Abrahamian, S. A. Faheem and R. R. Willis, *J. Am. Chem. Soc*., **2009**, *131*, 15834.

[1.33] (a) H. Furukawa, F. Gandara, Y.-B. Zhang, J. Jiang, W. L. Queen, M. R. Hudson and O. M. Yaghi, *J. Am. Chem. Soc.*, **2014**, *136*, 4369; (b) S. S. Kaye, A. Dailly, O. M. Yaghi and J. R. Long, *J. Am. Chem. Soc.*, **2007**, *129*, 14176; (c) M. Gaab, N. Trukhan, S. Maurer, R. Gummaraju and U. Muller, *Microporous Mesoporous Mater.*, **2012**, *157*, 131; (d) P. Kuesgens, M. Rose, I. Senkovska, H. Froede, A. Henschel, S. Siegle and S. Kaskel, *Microporous Mesoporous Mater.*, **2009**, *120*,325; (e) A. Khutia, H. U. Rammelberg, T. Schmidt, S. Henninger and C. Janiak, *Chem. Mater.*, **2013**, *25*, 790; (f) G. Akiyama, R. Matsuda, H. Sato, A. Hori, M. Takata and S. Kitagawa, *Microporous Mesoporous Mater.*, **2012**, *157*, 89; (g) F. Jeremias, V. Lozan, S. K. Henninger and C. Janiak, *Dalton Trans.*, **2013**, *42*, 15967; (h) H. Furukawa, F. Gandara, Y.-B. Zhang, J. Jiang, W. L. Queen, M. R. Hudson and O. M. Yaghi, *J. Am. Chem. Soc.*, **2014**, *136*, 4369; (i) G. E. Cmarik, M. Kim, S. M. Cohen and K. S. Walton, *Langmuir*, **2012**, *28*, 15606; (j) J. Canivet, J. Bonnefoy, C. Daniel, A. Legrand, B. Coasneand, D. Farrusseng, *New J. Chem.*, **2014**, *38*, 3102; (k) H. Reinsch, B. Marszalek, J. Wack, J. Senker, B. Gil and N. Stock, *Chem. Commun.*, **2012**, *48*, 9486; (l) H. Reinsch, M. A. van der Veen, B. Gil, B. Marszalek, T. Verbiest, D. de Vos and N. Stock, *Chem. Mater.*, **2013**, *25*, 17; (m) K. Zhang, R. P. Lively, M. E. Dose, A. J. Brown, C. Zhang, J. Chung, S. Nair, W. J. Koros and R. R. Chance, *Chem. Commun.*, **2013**, *49*, 3245; (n) C. R. Wade, T. Corrales-Sanchez, T. C. Narayan and M. Dinca, *Energy Environ. Sci.*, **2013**, *6*, 2172.

[1.34] Y. Li, R. T. Yang, *AIChE J.* **2008**, *54*, 269.

[1.35] (a) L. M. Robeson, *J. Membr. Sci.* **2008**, *320*, 390; (b) D. L. Gin, R. D. Noble, *Science*, **2011**, *332*, 674.

[1.36] P. Gorgojo, S. Uriel, C. Téllez, J. Coronas, *Micropor. Mesopor. Mater.*, **2008**, *115*, 85.

[1.37] (a) S. Keskin, T. M. van Heest and D. S. Sholl, *ChemSusChem.* **2010**, *3*, 879; (b) S. Basu, A. Cano-Odena and I. F. J. Vankelecom, *J. Membr. Sci.* **2010**, *362*, 478; (c) X. Liu, Y. S. Li, G. Q. Zhu, Y. J. Ban, L. Y. Xu, and W. S. Yang, *Angew. Chem. Int. Ed.*

2011, *50*, 10636; (d) J. A. Thompson, K. W. Chapman, W. J. Koros, C. W. Jones and S. Nair, *Micropor. Mesopor. Mater.* **2012**, *158*, 292.

[1.38] (a) S. Hermes, F. Schröder, R. Chelmowski, C. Wöll, R. A. Fischer, *J. Am. Chem. Soc.* **2005**, *127*, 13744; (b) Y. Yoo, H. K. Jeong, *Chem. Commun*., **2008**, 2441; (c) M. Arnold, P. Kortunov, D. J. Jones, Y. Nedellec, J. Kärger, J. Caro, *Eur. J. Inorg. Chem.*, **2007**, 60; (d) J. Gascon, S. Aguado, F. Kapteijn, *Microporous Mesoporous Mater.*, **2008**, *113*, 132; (e) H. Guo, G. Zhu, I. J. Hewitt, S. Qiu, *J. Am. Chem. Soc.* **2009**, *131*, 1646; (f) Y. Liu, Z. Ng, E. A.Khan, H. K. Jeong, C. B. Ching, Z. P. Lai, *Microporous Mesoporous Mater.*, **2009**, *118*, 296; (g) Y. S. Li, H. Bux, A. Feldhoff, G. L. Li, W. S. Yang, J. Caro, *Adv. Mater.* **2010**, *22*, 3322; (h) Z. Zhong, J. Yao, R. Chen, Z. Low, M. He, J. Z. Liuc and H. Wang, *J. Mater. Chem. A*, **2015**, *3*, 15715; (i) J. P. Nan, X. L. Dong, W. J. Wang, W. Q. Jin, N. P. Xu, *Langmuir*, **2011**, *27*, 4309; (j) L. Fan, M. Xue, Z. Kang, H. Li and S. Qiu, *J. Mater. Chem.*, **2012**, *22*, 25272; (k) D. Nagaraju, D. G. Bhagat, R. Banerjee, and U. K. Kharul, *J. Mater. Chem. A* **2013**, *1*, 8828; (l) M. N. Shah, M. A. Gonzalez, M. C. McCarthy, and H.-K. Jeong, *Langmuir*, **2013**, *29*, 7896; (m) O. Shekhah, R. Swaidan, Y. Belmabkhout, M. Plessis, T. Jacobs, L. J. Barbour, I. Pinnau and M. Eddaoudi, *Chem. Commun.*, **2014**, *50*, 2089.

[1.39] (a) I. Erucar, G.Yilmaz, and S. Keskin, *Chem. Asian J.* **2013**, *8*, 1692; (b) J. Hu, H. Cai, H. Q. Ren, Y. M. Wei, Z. L. Xu, H. L. Liu, Y. Hu, *Ind. Eng. Chem. Res.*, **2010**, *49*, 12605; (c) S. Basu, A. Cano-Odena, I. F. J Vankelecom, *J. Membr. Sci.*, **2010**, *362*, 478; (d) S. Basu, A. Cano-Odena, I. F. J. Vankelecom, *Sep. Sci. Technol.*, **2011**, 8131; (e) A. Bhaskar, R. Banerjee and U. K. Kharul, *J. Mater. Chem. A* **2014**, *2*, 12962; (f) L. Ge, W. Zhou, V. Rudolph and Z. Zhu, *J. Mater. Chem. A*, **2013**, *1*, 6350.

[1.40] (a) J. Yao, D. Dong, D. Li, L.He, G. Xu and H. Wang, *Chem. Commun.*, **2011**, *47*, 2559; (b) C. Carbonell, I. Imaz, D. Maspoch, *J. Am. Chem. Soc.*, **2011**, *133*, 2144.

[1.41] (a) R. Ameloot, F. Vermoortele, W. Vanhove, M. B. J. Roeffaers, B. F. Sels and D. E. De Vos, *Nat. Chem.* **2011**, *3*, 382; (b) H. Lu and S. Zhu, *Eur. J. Inorg. Chem.*, **2013**, 1294.

[1.42] (a) R. Ranjan, M. Tsapatsis, *Chem. Mater.* **2009**, *21*, 4920; (b) H. Bux, F. Y. Liang, Y. S. Li, J. Cravillon, M. Wiebcke, J. Caro, *J. Am. Chem. Soc.* **2009**, *131*, 16000; (c) Y.

S. Li, F. Y. Liang, H. Bux, A. Feldhoff, W.S. Yang, J. Caro, *Angew. Chem., Int. Ed.* **2010**, *49*, 548; (d) A. Huang, H. Bux, F. Steinbach, J. Caro, *Angew. Chem., Int. Ed.* **2010**, *49*, 4958; (e) S. R. Venna, M. A. Carreon, *J. Am. Chem. Soc.*, **2010**, *132*, 76; (f) Y. Yoo, V. Varela-Guerrero, H.-K. Jeong, *Langmuir*, **2011**, *27*, 2652.

[1.43] (a) S. Takamizawa, Y. Takasaki and R. Miyake, *J. Am. Chem. Soc.*, **2010**, *132*, 2862; (b) Y. Li, F. Liang, H. Bux, W. Yang and J. Caro, *J. Membr. Sci.*, **2010**, *354*, 48; (c) M. C. McCarthy, V. V. Guerrero, G. V. Barnett and H.-K. Jeong, *Langmuir*, **2010**, *26*, 14636; (d) H. Bux, A. Feldhoff, J. Cravillon, M. Wiebcke, Y.-S. Li and J. Caro, *Chem. Mater.*, **2011**, *23*, 2262; (e) K. Huang, S. Liu, Q. Li and W. Jin, *Sep. Purif. Technol.*, **2013**, *119*, 94; (f) A. Huang, W. Dou and J. Caro, *J. Am. Chem. Soc.*, **2010**, *132*, 15562; (g) A. Huang and J. Caro, *Angew. Chem., Int. Ed.*, **2011**, *50*, 4979; (h) A. Huang, Y. Chen, N. Wang, Z. Hu, J. Jiang and J. Caro, *Chem. Commun.*, **2012**, *48*, 10981; (i) X. Dong, K. Huang, S. Liu, R. Ren, W. Jin and Y. S. Lin, *J. Mater. Chem.*, **2012**, *22*, 19222; (j) S. Zhou, X. Zou, F. Sun, H. Ren, J. Liu, F. Zhang, N. Zhao and G. Zhu, *Int. J. Hydrogen Energy*, **2013**, *38*, 5338; (k) A. Huang, Y. Chen, Q. Liu, N. Wang, J. Jiang and J. Caro, *J. Membr. Sci.*, **2014**, *454*, 126; (l) F. Zhang, X. Zou, X. Gao, S. Fan, F. Sun, H. Ren and G. Zhu, *Adv. Funct. Mater.*, **2012**, *22*, 3583; (m) Y. Hu, X. Dong, J. Nan, W. Jin, X. Ren, N. Xu and Y. M. Lee, *Chem. Commun.*, **2011**, *47*, 737; (n) Y. Yoo, Z. Lai and H.-K. Jeong, *Microporous Mesoporous Mater.*, **2009**, *123*, 100; (o) T. Ben, C. Lu, C. Pei, S. Xu and S. Qiu, *Chem. – Eur. J.*, **2012**, *18*, 10250; (p) S. Zhou, X. Zou, F. Sun, F. Zhang, S. Fan, H. Zhao, T. Schiestel and G. Zhu, *J. Mater. Chem.*, **2012**, *22*, 10322; (q) S. Aguado, J. Canivet, D. Farrusseng, *J. Mater. Chem.* **2011**, *21*, 7582.

[1.44] (a) X. Feng, X. Dinga, D. Jiang, *Chem. Soc. Rev*. **2012**, *41*, 6010; (b) P. Kuhn, M. Antonietti, A. Thomas, *Angew. Chem., Int. Ed.* **2008**, *47*, 3450; (c) B. P. Biswal, S. Chandra, S. Kandambeth, B. Lukose, T. Heine, R. Banerjee, *J. Am. Chem. Soc.* **2013**, *135*, 5328; (d) E. L. Spitler, W. R. Dichtel, *Nature Chem*. **2010**, *2*, 672; (e) S. Kandambeth, V. Venkatesh, D. B. Shinde, S. Kumari, A. Halder, S. Verma, R. Banerjee, *Nat. Commun*. **2015,** *6*, 6786.

[1.45] J. W. Colson and W. R. Dichtel, *Nature Chemistry*, **2013**, *5*, 453.

[1.46] (a) J. F. Dienstmaier, D. D. Medina, M. Dogru, P. Knochel, T. Bein, W. M. Heckl, M. Lackinger, *ACS Nano* **2012**, *6*, 7234; (b) S. Y. Ding, J. Gao, Q. Wang, Y. Zhang, W. G. Song, C. Y. Su, W. Wang, *J. Am. Chem. Soc.* **2011**, *133*, 19816; (c) D. B. Shinde, S. Kandambeth, P. Pachfule, R. R. Kumar and R. Banerjee. *Chem Commun.*, **2015**, *51*, 310; (d) G. Das, B. P. Biswal, S. Kandambeth, V. Venkatesh, G. Kaur, M. Addicoat, T. Heine, S. Verma, R. Banerjee, *Chem. Sci.* **2015**, *6*, 3931.

[1.47] (a) S. Kandambeth, A. Mallick, B. Lukose, V. M. Mane, T. Heine, R. Banerjee, *J. Am. Chem. Soc.* **2012**, *134*, 19524; (b) X. S. Ding, J. Guo, X. Feng, Y. Honsho, J. D. Guo, S. Seki, P. Maitarad, A. Saeki, S. Nagase and D. Jiang, *Angew. Chem., Int. Ed.*, **2011**, *50*, 1289; (c) X. Feng, L. Chen, Y. P. Dong and D. Jiang, *Chem. Commun.*, **2011**, *47*, 1979.

[1.48] S.-Y. Ding and W. Wang, *Chem. Soc. Rev.*, **2013**, *42*, 548.

[1.49] (a) N. L. Campbell, R. Clowes, L. K. Ritchie and A. I. Cooper, *Chem. Mater.*, **2009**, *21*, 204; (b) M. Dogru, A. Sonnauer, A. Gavryushin, P. Knochel and T. Bein, *Chem. Commun.*, **2011**, *47*, 1707; (c) D. D. Medina, J. M. Rotter, Y. Hu, M. Dogru, V. Werner, F. Auras, J. T. Markiewicz, P. Knochel and T. Bein, *J. Am. Chem. Soc.*, **2015**, *137*, 1016; (d) J. W. Colson, A. R. Woll, A. Mukherjee, M. P. Levendorf, E. L. Spitler, V. B. Shields, M. G. Spencer, J. Park and W. R. Dichtel, *Science*, **2011**, *332*, 228.

[1.50] (a) H. Furukawa and O. M. Yaghi, *J. Am. Chem. Soc.*, **2009**, *131*, 8875; (b) J. R. Hunt, C. J. Doonan, J. D. LeVangie, A. P. Cote and O. M. Yaghi, *J. Am. Chem. Soc.*, **2008**, *130*, 11872; (c) C. J. Doonan, D. J. Tranchemontagne, T. G. Glover, J. R. Hunt and O. M. Yaghi, *Nat. Chem.*, **2010**, *2*, 235; (d) S. Dalapati, S. Jin, J. Gao, Y. Xu, A. Nagai and D. Jiang, *J. Am. Chem. Soc.*, **2013**, *135*, 17310; (e) S. Wan, J. Guo, J. Kim, H. Ihee and D. Jiang, *Angew. Chem., Int. Ed.*, **2008**, 47, 8826; (f) S. Wan, J. Guo, J. Kim, H. Ihee and D. Jiang, *Angew. Chem., Int. Ed.*, **2009**, *48*, 5439.

[1.51] (a) L. M. Lanni, R. W. Tilford, M. Bharathy, J. J. Lavigne, *J. Am. Chem. Soc.* **2011**, *130*, 11872; (b) E. Spitler, M. Giovino, S. White, W. Dichtel, *Chem. Sci.* **2011**, *2*, 1588; (c) Y. Du, K. Mao, P. Kamakoti, P. Ravikovitch, C. Paur, S. Cundy, Q. Li, D. Calabro, *Chem. Commun.*, **2012**, *48*, 4606.

[1.52] J. H. Chong, M. Sauer, B. O. Patrick, M. MacLachlan, *Org. Lett.* **2003**, *5*, 3823.

CHAPTER 2

[2.1] (a) K. S. Park, Z. Ni, A. P. Côté, J. Y. Choi, R. D. Huang, F. J. Uribe- Romo, H. K. Chae, M. O'Keeffe and O. M. Yaghi, *Proc. Natl. Acad. Sci*. U. S. A, **2006**, *103*, 10186; (b) R. Banerjee, A. Phan, B. Wang, C. Knobler, H. Furukawa, M. O'Keeffe and O. M. Yaghi, *Science*, **2008**, *319*, 939; (c) K. Li, D. H. Olson, J. Seidel, T. J. Emge, H. Gong, H. Zeng, and J. Li, *J. Am. Chem. Soc*., **2009**, *131*, 10368; (d) F. Wang, Z. S. Liu, H. Yang, Y. X. Tan and J. Zhang, *Angew. Chem. Int. Ed*., 2011, **50**, 450; (e) W. Morris, C. J. Doonan, H. Furukawa, R. Banerjee and O. M. Yaghi, *J. Am. Chem. Soc.*, **2008**, *130*, 12626; (f) Y. Liu, V. Ch. Kravtsov, R. Larsen and M. Eddaoudi, *Chem. Commun.*, **2006**, 1488; (g) Y. Q. Tian, S. Y. Yao, D. Gu, K. H. Cui, D. W. Guo, G. Zhang, Z. X. Chen and D. Y. Zhao, *Chem. Eur. J.*, **2010**, *16*, 1137.

[2.2] (a) C. Y. Lee, O. K. Farha, B. J. Hong, A. A. Sarjeant, S. T. Nguyen, J. T. Hupp, *J. Am. Chem. Soc.* **2011**, *133*, 15858; (b) S. Xiang, Z. Zhang, C.-G. Zhao, K. Hong, X. Zhao, D.-R. Ding, M.-H. Xie, C.-D. Wu, M. C. Das, R. Gill, K. M. Thomas, B. Chen *Nat. Commun.* **2011**, *2*, 204; (c) S. A. Kumalah Robinson, M.-V. L. Mempin, A. J. Cairns, K. T. Holman, *J. Am. Chem. Soc.* **2011**, *133*, 1634; (d) B. Zheng, J. Bai, J. Duan, L. Wojtas, M. J. Zaworotko, *J. Am. Chem. Soc.* **2011**, *133*, 748; (e) C. Scherb, A. Schoedel, T. Bein, *Angew. Chem., Int. Ed.***, 2008**, *47*, 5777; (f) K. Otsubo, T. Haraguchi, O. Sakata, A. Fujiwara, H. Kitagawa *J. Am. Chem. Soc.* **2012**, *134*, 9605; (g) J. L. Atwood, L. J. Barbour, S. J. Dalgarno, M. J. Hardie, C. L. Raston and H. R. Webb, *J. Am. Chem. Soc.* **2004**, *126*, 13170.

[2.3] (a) S. A. Moggach, T. D. Bennett and A. K. Cheetham, *Angew. Chem. Int. Ed*., **2009**, *121*, 7221; (b) D. Fairen-Jimenez, S. A. Moggach, M. T. Wharmby, P. A. Wright, S. Parsons and T. Duren, *J. Am. Chem. Soc.*, **2011**, *133*, 8900.

[2.4] (a) R. Banerjee, H. Furukawa, D. Britt, C. Knobler, M. O'Keeffe, and O. M. Yaghi, *J. Am. Chem. Soc.* **2009**, *131*, 3875; (b) S. S. Han, S.-H. Choi, W. A. Goddard, *J. Phys. Chem. C*, **2011**, *115*, 3507.

[2.5] (a) Y.-S. Li, F.-Y. Liang, H. Bux, A. Feldhoff, W.-S. Yang and J. Caro, Angew. Chem., Int. Ed., 2010, 49, 548–551; (b) C. Gücüyener, J. van den Bergh, J. Gascon and F. Kapteijn, *J. Am. Chem. Soc.* **2010**, *132*, 17704; (c) Y. Pan and Z. Lai, *Chem. Commun.* **2011**, *47*, 10275.

[2.6] C.-Y. Sun, C. Qin, X.-L. Wang and Z.-M. Su, *Expert Opin. Drug Delivery*, **2013**, *10*, 89.

[2.7] (a) Lien T. L. Nguyen, Ky K. A. Le, Hien X. Truong and Nam T. S. Phan, *Catal. Sci. Technol.*, **2012**, *2*, 521-528; (b) O. Karagiaridi, M. B. Lalonde, W. Bury, A. A. Sarjeant, O. K. Farha, and J. T. Hupp, *J. Am. Chem. Soc.* **2012**, *134*, 18790.

[2.8] G. Lu and J. T. Hupp**,** *J. Am. Chem. Soc.*, **2010**, *132*, 7832.

[2.9] A. Phan, C. J. Doonan, F. J. Uribe-Romo, C. B. Knobler, M. O'Keeffe and O. M. Yaghi, *Acc. Chem. Res.*, **2010**, *43*, 58.

[2.10] (a) Q.-L. Zhu and Q. Xu, *Chem. Soc. Rev.*, **2014**, *43*, 5468; (b) Han, J.-Y.; Fang, J.; Chang, H.-Y.; Dong, Y.; Liang, S., *Acta Crystallogr*. **2005**, *E61*, m2667.

[2.11] H. Greer, P. S. Wheatley, S. E. Ashbrook, R. E. Morris and W. Zhou, *J. Am. Chem. Soc.*, **2009**, *131*, 17986.

[2.12] E. Bayram, J. Lu, C. Aydin, N. D. Browning, S. Özkar, E. Finney, B. C. Gates, and R. G. Finke, *ACS Catal.*, **2015**, *5*, 3514.

[2.13] B. Li, H. Wang, B. Chen, *Chem. Asian J.*, **2014**, *9*, 1474.

[2.14] W. Morris, B. Leung, H. Furukawa, O. K. Yaghi, N. He, H. Hayashi, Y. Houndonougbo, M. Asta, B. B. Laird, and O. M. Yaghi, *J. Am. Chem. Soc.*, **2010**, *132*, 11006.

[2.15] F. Wang, Z. S. Liu, H. Yang, Y. X. Tan and J. Zhang, *Angew. Chem. Int. Ed*., **2011**, *50*, 450.

[2.16] (a) B. Wang, A. P. Côté, H. Furukawa, M. O'Keeffe & O. M. Yaghi, *Nature*, **2008**, *453*, 207; (b) R. Ananthoji, J. F. Eubank, F. Nouar, H. Mouttaki, M. Eddaoudi and J. P. Harmon, *J. Mater. Chem.*, **2011**, *21*, 9587.

[2.17] (a) R. P. Lively, M. E. Dose, J. A. Thompson, B. A. McCool, R. R. Chanceab and W. J. Korosb, *Chem. Commun.,* **2011**, *47*, 8667; (b) P. Küsgens, M. Rose, I. Senkovska,

H. Fröde, A. Henschel, S. Siegle, S. Kaskel, *Micropor. Mesopor. Mater.*, **2009**, *120*, 325.

[2.18] J. Kahr, J. P. S. Mowat, A. M. Z. Slawin, R. E. Morris, D. Fairen-Jimenez and P. A. Wright, *Chem. Commun*., 2012, **48**, 6690.

[2.19] (a) J. An, S. J. Geib and N. L. Rosi, *J. Am. Chem. Soc*., **2010**, *132*, 38; (b) J. L. C. Roswell, A. R. Milward, K. S. Park, O. M. Yaghi, *J. Am. Chem. Soc.*, **2004**, *126*, 5666; (c) S.-T. Zheng, J. T. Bu, Y. Li, T. Wu, F. Zuo, P. Feng, X. Bu, *J. Am. Chem. Soc*. **2010**, *132*, 17062; (d) T. Wu, J. Zhang, C. Zhou, L. Wang, X. Bu, and P. Feng, *J. Am. Chem. Soc*., **2009**, *131*, 6111; (e) H. Hayashi, A. P. Côté, H. furukaya, M. O'keeffe and O. M. Yaghi, *Nat. Mater*., **2007**, *6*, 501; (f) H. J. Park and M. P. Suh, *Chem. Eur. J*., **2008**, *14*, 8812; (g) J. L. C. Roswell and O. M. Yaghi, *J. Am. Chem. Soc.*, **2006**, *128*, 1304; (h) H. Kim, S. Das, M. G. Kim, D. N. Dybtsev, Y. Kim, and K. Kim, *Inorg. Chem.*, **2011**, *50*, 3691; (i) M. P. Suh, H. J. Park, T. K. Prasad, and D.W. Lim, *Chemical Reviews*, **2012**, *112*, 782.

[2.20] T. Panda, P. Pachfule, Y. F. Chen, J. W. Jiang and R. Banerjee, *Chem. Commun.*, **2011**, *47*, 2011.

[2.21] K. S. Walton, R. Q. Snurr, *J. Am. Chem. Soc.*, **2007,** *129*, 8552.

[2.22] (a) CrysAlisPro, Version 1.171.33.66; *Oxford Diffraction Ltd*.: Abingdon, U.K., **2010**; (b) Sheldrick, G. M. (**1997**). SHELXS '97 and SHELXL '97. *University of Göttingen*, Germany; (c) A. L. Spek (**2005**) PLATON, *A Multipurpose Crystallographic Tool*, Utrecht University, Utrecht, The Netherlands; (d) L. A. Dakin, P. C. Ong, J. S. Panek, R. J. Staples, and P. Stavropoulos, *Organometallics*, **2000**, *19*, 2896; (e) S. Noro, R. Kitaura, M. Kondo, S. Kitagawa, T. Ishii, H. Matsuzaka, and M. Yamashita, *J. Am. Chem. Soc.*, **2002**, *124*, 2568; (f) M. Eddaoudi, J. Kim, D. Vodak, A. Sudik, J. Wachter, M. O'Keeffe, and O. M. Yaghi, *Proc. Natl. Acad. Sci.*, USA, **2002**, *99*, 4900; (g) R. A. Heintz, H. Zhao, X. Ouyang, G. Grandinetti, J. Cowen, and K. R. Dunbar, *Inorg. Chem.*, **1999**, *38*, 144; (h) K. Biradha, Y. Hongo, and M. Fujita, *Angew. Chem. Int. Ed.*, **2000**, *39*, 3843; (i) P. Grosshans, A. Jouaiti, M. W. Hosseini, and N. Kyritsakas, *New J. Chem*, (*Nouv. J. Chim.*), **2003**, *27*, 793; (j) N. Takeda, K. Umemoto, K. Yamaguchi, and M. Fujita, *Nature* (London), **1999**, *398*, 794; (k) M.

Eddaoudi, J. Kim, N. Rosi, D. Vodak, J. Wachter, M. O'Keeffe, and O. M. Yaghi, *Science*, **2002**, *295*, 469; (l) B. Kesanli, Y. Cui, M. R. Smith, E. W. Bittner, B. C. Bockrath, and W. Lin, *Angew. Chem. Int. Ed.*, **2005**, *44*, 72; (m) F. A. Cotton, C. Lin, and C. A. Murillo, *Inorg. Chem*., **2001**, *40*, 478.

CHAPTER 3

[3.1] (a) C. Y. Lee, O. K. Farha, B. J. Hong, A. A. Sarjeant, S. T. Nguyen and J. T. Hupp, *J. Am. Chem. Soc.* **2011**, *133*, 15858; (b) S. A. K. Robinson, M.-V. L. Mempin, A. J. Cairns and K. T. Holman, *J. Am. Chem. Soc.* **2011**, *133*, 1634; (c) O. M. Yaghi, M. O'Keeffe, N. W. Ockwig, H. K. Chae, M. Eddaoudi and J. Kim, *Nature* **2003**, *423*, 705; (d) D. J. Tranchemontagne, J. R. Hunt and O. M. Yaghi, *Tetrahedron* **2008**, *64*, 8553; (e) J. Cravillon, S. Munzer, S.-J. Lohmeier, A. Feldhoff, K. Huber, and M. Wiebcke, *Chem. Mater.* **2009**, *21*, 1410; (f) J.-L. Zhuang, D. Ceglarek, S. Pethuraj, and A. Terfort, *Adv. Funct. Mater.* **2011**, *21*, 1442; (g) S. Tominaka, H. Hamoudi, T. Suga, T. D. Bennett, A. B. Cairns and A. K. Cheetham, *Chem. Sci.*, **2015**, DOI: 10.1039/C4SC03295K; (h) C. Dey, T. Kundu, B. P. Biswal, A. Mallick and R. Banerjee, *Acta Crystallogr., Sect. B.* **2014**, *B70*, 3.

[3.2] B. Zheng, J. Bai, J. Duan, L. Wojtas and M. J. Zaworotko, *J. Am. Chem. Soc.* **2011**, *133*, 748;

[3.3] P. Horcajada, S. Surble,.C. Serre, D.-Y. Hong, Y.-K. Seo, J.-S. Chang, J.-M. Greneche, I. Margiolaki and G. Ferey, *Chem. Commun.* **2007**, 2820.

[3.4] H.-J. Son, S. Jin, S. Patwardhan, S. J. Wezenberg, N. C. Jeong, M. So, C. E. Wilmer, A. A. Sarjeant, G. C. Schatz, R. Q. Snurr, O. K. Farha, G. P. Wiederrecht, and J. T. Hupp, *J. Am. Chem. Soc.* **2013**, *135*, 862.

[3.5] L. Sun, M. G. Campbell, M. Dincă, *Angew. Chem. Int. Ed.* **2016**, *55*, 3566.

[3.6] M. L. K. Taylor-Pashow, J. D. Rocca, Z. Xie, S. Tran, and W. Lin, *J. Am. Chem. Soc.* **2009**, *131*, 14261.

[3.7] (a) S. Keskin, T. M. van Heest and D. S. Sholl, *ChemSusChem.* **2010**, *3*, 879; (b) S. Basu, A. Cano-Odena and I. F. J. Vankelecom, *J. Membr. Sci.* **2010**, *362*, 478; (c) X. Liu, Y. S. Li, G. Q. Zhu, Y. J. Ban, L. Y. Xu, and W. S. Yang, *Angew. Chem. Int. Ed.*

2011, *50*, 10636; (d) J. A. Thompson, K. W. Chapman, W. J. Koros, C. W. Jones and S. Nair, *Micropor. Mesopor. Mater.* **2012**, *158*, 292.

[3.8] (a) O. Shekhah, L. Fu, R. Sougrat, Y. Belmabkhout, A. J. Cairns, E. P. Giannelis and M. Eddaoudi, *Chem. Commun.* **2012**, *48*, 11434; b) D. Zacher, A. Baunemann, S. Hermes and R. A. Fischer, *J. Mater. Chem.* **2007**, *17*, 2785;

[3.9] H. Bux, A. Feldhoff, J. Cravillon, M. Wiebcke, Y. S. Li and J. Caro, *Chem. Mater.* **2011**, *23*, 2262;

[3.10] (a) V. V. Guerrero, Y. Yoo, M. C. McCarthya and H. K. Jeong, *J. Mater. Chem.* **2010**, *20*, 3938; b) L. Dumee, L. He, M. Hill, B. Zhu, M. Duke, J. Schutz, F. She, H. Wang, S. Gray, P. Hodgson and L. Kong, *J. Mater. Chem. A* **2013**, *1*, 9208.

[3.11] M. Shah, M. C. McCarthy, S. Sachdeva, A. K. Lee, and H.-K. Jeong, *Ind. Eng. Chem. Res*. **2012**, *51*, 2179.

[3.12] (a) D. Nagaraju, D. G. Bhagat, R. Banerjee, and U. K. Kharul, *J. Mater. Chem. A* **2013**, *1*, 8828; (b) D. Bradshaw, A. Garai and J. Huo, *Chem. Soc. Rev*. **2012**, *41*, 2344.

[3.13] (a) I. Erucar, G.Yilmaz, and S. Keskin, *Chem. Asian J*. **2013**, *8*, 1692; (b) Y. Hu, X. Dong, J. Nan, W. Jin, X. Ren, N. Xu and Y. M. Lee, *Chem. Commun.* **2011**, *47*, 737; (c) Y. Liu, S. Li, X. Zhang, H. Liu, J. Qiu, Y. Li, K. L. Yeung, *Inorg. Chem. Commun*. **2014**, *48*, 77; (d) H. B. T. Jeazet, C. Staudt and C. Janiak, *Dalton Trans.* **2012**, *41*, 14003.

[3.14] (a) Y. Dai, J. R. Johnson, O. Karvan, D. S. Sholl, W. J. Koros, *J. Membr. Sci.* **2012**, *401*, 76; b) J. Hu, H. Cai, H. Ren, Y. Wei, Z. Xu, H. Liu, and Y. Hu, *Ind. Eng. Chem. Res.* **2010,** *49*, 12605; c) K. Huang, Z. Dong, Q. Li and W. Jin, *Chem. Commun.* **2013**, *49*, 10326; (d) A. J. Brown, J. R. Johnson, M. E. Lydon, W. J. Koros, C.W. Jones, and S. Nair, *Angew. Chem. Int. Ed.* **2012**, *51*, 10615.

[3.15] (a) A. J. Brown, N. A. Brunelli, K. Eum, F. Rashidi, J. R. Johnson, W. J. Koros, C. W. Jones, S. Nair, *Science* **2014**, *345*, 72; (b) F. Cacho-Bailoa, S. Catalána, M. Etxeberría-Benavidesb, O. Karvanb, V. Sebastiána, C. Télleza, J. Coronas, *J. Membr. Sci.* **2015**, *476*, 277.

[3.16] (a) A. T. Yang, Y. Xiao and T. -S. Chung, *Energy Environ. Sci.* **2011**, *4*, 4171; (b) S. C. Kumbharkar, K. Li, *J. Membr. Sci.* **2012**, *415*, 793; (c) S. C. Kumbharkar, P. B. Karadkar, U. K. Kharul, *J. Membr. Sci.* **2006**, *286*, 161.

[3.17] A. Bhaskar, R. Banerjee and U. K. Kharul, *J. Mater. Chem. A* **2014**, *2*, 12962.

[3.18] (a) H. Guo, G. Zhu, I. J. Hewitt and S. Qiu, *J. Am. Chem. Soc.*, **2009**, *131*, 1646; (b) J. Nan, X. Dong, W. Wang, W. Jin and N. Xu, *Langmuir*, **2011**, *27*, 4309; (c) T. Ben, C. Lu, C. Pei, S. Xu and S. Qiu, *Chem. – Eur. J.*, **2012**, *18*, 10250; (d) S. Zhou, X. Zou, F. Sun, F. Zhang, S. Fan, H. Zhao, T. Schiestel and G., *J. Mater. Chem*., **2012**, *22*, 10322.

[3.19] H. Lohokare, Y. Bhole, S. Taralkar, U. Kharul, *Desalination,* **2011**, *282*, 46.

[3.20] (a) G. R. Desiraju, *Acc. Chem. Res*. **2002,** *35*, 565; (b) G. R. Desiraju, T. Steiner, The Weak Hydrogen Bond in Structural Chemistry and Biology, *Oxford University Press*, Oxford, **1999**.

CHAPTER 4

[4.1] (a) L. R. MacGillivray, J. L. Reid, and J. A. Ripmeester, *J. Am. Chem. Soc.* **2000**, *122*, 7817; (b) R. E. Morris, and S. L. James, *Angew. Chem. Int. Ed.* **2013**, *52*, 2163; (c) C. B. Aakeröy, A. S. Sinha, K. N. Epa, C. L. Spartz, and J. Desper, *Chem. Commun.*, **2012**, *48*, 11289; (d) S. L. James, C. J. Adams, C. Bolm, D. Braga, P. Collier, T. Friščić, F. Grepioni, K. D. M. Harris, G. Hyett, W. Jones, A. Krebs, J. Mack, L. Maini, A. G. Orpen, I. P. Parkin, W. Ch. Shearouse, J. W. Steed, and D. C. Waddell, *Chem. Soc. Rev.*, **2012**, *41*, 413; (e) K. Tanaka, F. Toda, *Chem. Rev.* **2000**, *100*, 1025; (f) O. Dolotko, J. W. Wiench, K. W. Dennis, V. K. Pecharskya, V. P. Balema, *New J. Chem.*, **2010**, *34*, 25; (g) G. Rothenberg, A. P. Downie, C. L. Raston, J. L. Scott, *J. Am. Chem. Soc.* **2001**, *123*, 8701.

[4.2] (a) T. Friščić, *Chem. Soc. Rev.*, **2012**, *41*, 3493; (b) J. Stojakovic, B. S. Farris, and L. R. MacGillivray, *Chem. Commun*. **2012**, *48*, 7958.

[4.3] (a) B. Icli, N. Christinat, J. Tonnemann, C. Schuttler, R. Scopelliti, and K. Severin, *J. Am. Chem. Soc.*, **2009**, *131*, 3154; (b) A. Orita, L. Jiang, T. Nakano, N. Ma, J. Otera,

Chem. Commun. **2002**, 1362; (c) D. Braga and F. Grepioni, *Angew. Chem., Int. Ed.*, **2004**, *43*, 4002.

[4.4] (a) A. Pichon, A. Lazaun-Garay, S. L. James, *CrystEngComm*. **2006**, *8*, 21; (b) T. Friščić, L. R. MacGillivray, *Chem. Commun*., **2003**, 1306; (c) T. Friščić, I. Halasz, P. J. Beldon, A. M. Belenguer, F. Adams, S. A. J. Kimber, V. Honkimäki, R. E. Dinnebier, *Nat. Chem.* **2013**, *5*, 66.

[4.5] (a) T. Friščić, , D. G. Reid, I. Halasz, R. S. Stein, R. E. Dinnebier, and M. J. Duer, *Angew. Chem., Int. Ed.*, **2010**, *49*, 712; (b) W. Yuan, T. Friščić, D. Apperley, and S. L. James, *Angew. Chem. Int. Ed.,* **2010**, *49*, 3916.

[4.6] (a) A. P. Côté, A. I. Benin, N. W. Ockwig, A. J. Matzger, M. O'Keeffe, O. M. Yaghi, *Science* **2005**, *310*, 1166; (b) J. F. Dienstmaier, D. D. Medina, M. Dogru, P. Knochel, T. Bein, W. M. Heckl, M. Lackinger, *ACS Nano.* **2012**, *6*, 7234; (c) P. Kuhn, M. Antonietti, A. Thomas, *Angew. Chem. Int. Ed*. **2008**, *47*, 3450; (d) J. W. Colson, A. R. Woll, A. Mukherjee, M. P. Levendorf, E. L. Spitler, V. B. Shields, M. G. Spencer, J. Park, W. R. Dichtel, *Science* **2011**, *332*, 228.

[4.7] (a) H. Furukawa, O. M. Yaghi, *J. Am. Chem. Soc.* **2009,** *131***,** 8875; (b) Wan, S.; Guo, J.; Kim, J.; Ihee, H.; Jiang, D. *Angew. Chem. Int. Ed.* **2008**, *120*, 8958.

[4.8] (a) J. W. Colson and W. R. Dichtel, *Nature Chemistry*, **2013**, *5*, 453; (b) P. J. Waller, F. Gandara and O. M. Yaghi, *Acc. Chem. Res*. **2015**, *48*, 3053.

[4.9] L. M. Lanni, R. W. Tilford, M. Bharathy, J. Lavigne, J. *J. Am. Chem. Soc.* **2011**, *130***,** 11872.

[4.10] S. Kandambeth, A. Mallick, B. Lukose, V. M. Mane, T. Heine, R. Banerjee, *J. Am. Chem. Soc*., **2012**, *134*, 19524.

[4.11] (a) B. P. Biswal, S. Chandra, S. Kandambeth, B. Lukose, T. Heine and R. Banerjee, *J. Am. Chem. Soc.* **2013**, *135*, 5328; (b) S. Chandra, S. Kandambeth, B. P. Biswal, B. Lukose, S. M. Kunjir, M. Chaudhary, R. Babarao, T. Heine and R. Banerjee, *J. Am. Chem. Soc.* **2013**, *135*, 17853.

[4.12] (a) S. Wan, F. Gandara, A. Asano, H. Furukawa, A. Saeki, S. K. Dey, L. Liao, M. W. Ambrogio, Y. Y. Botros, X. Duan, S. Seki, J. F. Stoddart and O. M. Yaghi, *Chem. Mater*. **2011**, *23*, 4094; (b) S. Kandambeth, D. B. Shinde, M. K. Panda, B. Lukose, T.

Heine and R. Banerjee, *Angew. Chem., Int. Ed.* **2013**, *52*, 13052; (c) S .Y. Ding, J. Gao, Q. Wang, Y. Zhang, W. G. Song, C. Y. Su and W. Wang, *J. Am. Chem. Soc.* **2011**, *133*, 19816.

[4.13] M. E. Belowich and J. F. Stoddart, *Chem. Soc. Rev*., **2012**, ***41***, 2003.

[4.14] X. Feng, X. Dinga and D. Jiang, *Chem. Soc. Rev.*, **2012**, *41*, 6010.

[4.15] (a) B. Lukose, A. Kuc, T. Heine, *Chem. Eur. J*., **2011**, *17*, 2388; (b) Accelrys, Material Studio Release Notes, Release 4.2, *Accelrys Software*, San Diego **2006**.

[4.16] J. H. Chong, M. Sauer, B. O. Patrick, M. MacLachlan, *Org. Lett.* **2003**, *5*, 3823.

[4.17] (a) C. Borriello, A. De Maria, N. Jovic, A. Montone, M. Schwarz, and M. V. Antisari, *Materials and Manufacturing Processes*, **2009**, *24*, 1053. (b) I-Y. Jeon, H-J. Choi, S-M. Jung, J-M. Seo, M-J. Kim, L. Dai, and J-B. Baek, *J. Am. Chem. Soc*. **2013**, *135*, 1386.

[4.18] F. J. Uribe-Romo, J. R. Hunt, H. Furukawa, C. Klock, M. O'Keeffe, O. M. Yaghi, *J. Am. Chem. Soc*. **2009**, *131*, 4570.

[4.19] (a) X.-b. Zhang, B.-C. Tang, P. Zhang, M. Li, W.-J. Tian, *Journal of Molecular Structure*, **2007,** *846*, 55; (b) T. Kretz, J. W. Bats, H.-W. Lerner and M. Wagner, *Z. Naturforsch.* **2007**, *62b*, 66.

CHAPTER 5

[5.1] (a) S. Keskin, T. M. van Heest and D. S. Sholl, *ChemSusChem.* **2010**, *3*, 879; (b) S. Basu, A. Cano-Odena and I. F. J. Vankelecom, *J. Membr. Sci.* **2010**, *362*, 478; (c) H. B. T. Jeazet, C. Staudt and C. Janiak, Chem. Commun., 2012, **48**, 2140; (d) D. Nagaraju, D. G. Bhagat, R. Banerjee, and U. K. Kharul, *J. Mater. Chem. A*, **2013**, *1*, 8828; (e) A. J. Brown, N. A. Brunelli, K. Eum, F. Rashidi, J. R. Johnson, W. J. Koros, C. W. Jones, S. Nair, *Science*, **2014**, *345*, 72.

[5.2] (a) D. L. Gin, R. D. Noble, *Science* **2011**, *332*, 674; (b) N. Du, H. B. Park, G. P. Robertson, M. M. Dal-Cin, T. Visser, L. Scoles and M. D. Guiver, *Nature mater.*, **2011**, *10*, 372.

[5.3] L. M. Robeson, *J. Membr. Sci.* **2008**, *320*, 390.

[5.4] P. Gorgojo, S. Uriel, C. Téllez, J. Coronas, *Micropor. Mesopor. Mater.*, **2008**, *115*, 85.

[5.5] S. Kim, L. Chen, J. K. Johnson and E. Marand, *J. Membr. Sci.*, **2007**, *294*, 147.

[5.6] D. Q. Vu, W. J. Koros and S. J. Miller, *J. Membr. Sci.*, **2003**, *211***,** 311.

[5.7] B. A. Al-Maythalony; O. Shekhah; R. Swaidan; Y. Belmabkhout; I. Pinnau; M. Eddaoudi, *J. Am. Chem. Soc.* **2015**, *137*, 1754.

[5.8] C. H. Lau, P. T. Nguyen, M. R. Hill, A. W. Thornton, K.Konstas, C. M. Doherty, R. J. Mulder, L. Bourgeois, A. C. Y. Liu, D. J. Sprouster, J. P. Sullivan, T. J. Bastow, A. J. Hill, D. L. Gin, and R. D. Noble; *Angew. Chem. Int. Ed.* **2014**, *126*, 5426.

[5.9] A. F. Bushell, P. M. Budd, M. P. Attfield, J. T. A. Jones, T. Hasell, A. I. Cooper, P. Bernardo, F. Bazzarelli, G. Clarizia, and J. C. Jansen, *Angew. Chem. Int. Ed.* **2012**, *52*, 1253.

[5.10] B. Zornoza, C. Tellez, J. Coronas, J. Gascon and F. Kapteijn, *Micropor. Mesopor. Mater.*, **2013**, *166*, 67.

[5.11] (a) A. P. Côté, A. I. Benin, N. W. Ockwig, A. J. Matzger, M. O'Keeffe, O. M. Yaghi, *Science* **2005**, *310*, 1166; (b) X. Feng, X. Dinga, D. Jiang, *Chem. Soc. Rev*. **2012**, *41*, 6010; (c) P. Kuhn, M. Antonietti, A. Thomas, *Angew. Chem., Int. Ed.* **2008**, *47*, 3450; (d) B. P. Biswal, S. Chandra, S. Kandambeth, B. Lukose, T. Heine, R. Banerjee, *J. Am. Chem. Soc.* **2013**, *135*, 5328; (e) E. L. Spitler, W. R. Dichtel, *Nature Chem*. **2010**, *2*, 672; (f) S. Kandambeth, V. Venkatesh, D. B. Shinde, S. Kumari, A. Halder, S. Verma, R. Banerjee, *Nat. Commun*. **2015,** *6*, 6786.

[5.12] J. F. Dienstmaier, D. D. Medina, M. Dogru, P. Knochel, T. Bein, W. M. Heckl, M. Lackinger, *ACS Nano* **2012**, *6*, 7234.

[5.13] G. Das, B. P. Biswal, S. Kandambeth,V. Venkatesh,G. Kaur, M. Addicoat, T. Heine, S. Verma, R. Banerjee, *Chem. Sci.*, **2015**, *6*, 3931.

[5.14] S .Y. Ding, J. Gao, Q. Wang, Y. Zhang, W. G. Song, C. Y. Su, W. Wang, *J. Am. Chem. Soc.* **2011**, *133*, 19816.

[5.15] S. Wan, J. Guo, J. Kim, H. Ihee, D. Jiang, *Angew. Chem., Int. Ed*. **2009**, *48*, 5439.

[5.16] (a) D. D. Hao, J. N. Zhang, H. Lu, W. G. Leng; R. L. Ge, X. N. Dai, Y. Gao, *Chem. Commun.* **2014**, *50*, 1462; (b) H. Lu, C. Wang, J. Chen, R. Ge, W. Leng, B. Dong, J. Huang and Y. Gao, *Chem. Commun.* **2015**, *51*, 15562.

[5.17] (a) L. M. Lanni, R. W. Tilford, M. Bharathy, J. J. Lavigne, *J. Am. Chem. Soc*. **2011**, *130*, 11872; (b) E. Spitler, M. Giovino, S. White, W. Dichtel, *Chem. Sci*. **2011**, *2*, 1588.

[5.18] (a) S. Kandambeth, A. Mallick, B. Lukose, V. M. Mane, T. Heine, R. Banerjee, *J. Am. Chem. Soc*. **2012**, *134*, 19524; (b) S. Chandra, S. Kandambeth, B. P. Biswal, B. Lukose, S. M. Kunjir, M. Chaudhary, R. Babarao, T. Heine, R. Banerjee, *J. Am. Chem. Soc*. **2013**, *135*, 17853.

[5.19] A. Bhaskar, R. Banerjee and U. K. Kharul, *J. Mater. Chem. A* **2014**, *2*, 12962.

[5.20] (a) B. P. Biswal, H. D. Chaudhari, R. Banerjee, U. K. Kharul, *Chem. Eur. J.*, **2016**, *22*, 4695; (b) B. Seoane, J. Coronas, I. Gascon, M. E. Benavides, O. Karvan, J. Caro, F. Kapteijn and J. Gascon, *Chem. Soc. Rev.*, **2015**, *44*, 2421; (c) I. Erucar, G. Yilmaz, and S. Keskin, *Chem. Asian J*. **2013**, *8*, 1692; (d) G. Dong, H. Li and V. Chen, *J. Mater. Chem. A,* **2013**, *1*, 4610; (e) Z. X. Kang, Y. W. Peng, Y. H. Qian, D. Q. Yuan, M. A. Addicoat, T. Heine, Z. G. Hu, L. Tee, Z. G. Guo, D. Zhao, *Chem. Mater.* **2016**, *28*, 1277.

[5.21] (a) W. J. Lau, A. F. Ismail, N. Misdan, M. A. Kassim, *Desalination*, **2012**, *287***,** 190; b) B. Khorshidi, T. Thundat, B. A. Fleck, M. Sadrzadeh, *Sci. Rep.*, **2016**, *6*, 22069, 1.

[5.22] A. Mushtaq, H. B. Mukhtar, A. M. Shariff, H. A. Mannan, *IJET-IJENS*, **2013**, *13*, 53.

[5.23] (a) S. C. Kumbharkar, P. B. Karadkar, U. K. Kharul, *J. Membr. Sci.* **2006**, *286*,161; (b) T. Yang, Y. Xiao and T. -S. Chung, *Energy Environ. Sci.* **2011**, *4*, 4171; (c) S. C. Kumbharkar, K. Li, *J. Membr. Sci.* **2012**, *415*, 793.

[5.24] (a) G. R. Desiraju, *Acc. Chem. Res*. **2002,** *35*, 565; (b) G. R. Desiraju, T. Steiner, The Weak Hydrogen Bond in Structural Chemistry and Biology, Oxford University Press, Oxford, **1999**; (b) G. R. Desiraju, *Acc. Chem. Res*. **2002,** *35*, 565.

[5.25] (a) W. F. Yong, F. Y. Li, Y. C. Xiao, P. Li, K. P. Pramod, Y. W. Tong and T. S. Chung, *J. Membr. Sci.*, **2012**, *47*, 407; (b) J. S. McHattie, W. J. Koros and D. R. Paul,

Polymer, **1992**, *33*, 1701; (c) M. W. Hellums, W. J. Koros, G. R. Husk and D. R. Paul, *J. Membr. Sci.*, **1989**, *46***,** 93.

[5.26] J. H. Chong, M. Sauer, B. O. Patrick, M. MacLachlan, *Org. Lett.* **2003**, *5*, 3823.

CHAPTER 6

[6.1] (a) C. D. Windle, R. N. Perutz, *Coord. Chem. Rev*. **2012**, *256*, 2562; (b) V. S. Vyas, F. Haase, L. Stegbauer, G. Savasci, F. Podjaski, C. Ochsenfeld, B. V. Lotsch, *Nat. Commun.*, **2015**, *6*, 8508; (c) Ș. Neațu , J. A. Maciá-Agulló and H. Garcia, *Int. J. Mol. Sci.* **2014**, *15*, 5246; (d) C. Costentin, M. Robert, J. Saveant, *Chem. Soc. Rev.* **2013**, *42*, 2423; (e) A. T. Najafabadi, *Int. J. Energy Res.* **2013**, *37*, 485; H. Jhong, S. Ma, P. Kenis, *Curr. Opin. Chem. Eng*. **2013**, *2*, 191.

[6.2] (a) S. Kandambeth, D. B. Shinde, M. K. Panda, B. Lukose, T. Heine**,** R. Banerjee. *Angew. Chem. Int. Ed.*, **2013**, *52*, 13052; (b) P. Maitarad, S. Namuangruk, D. Zhang, L. Shi, H. Li, L. Huang, B. Boekfa, and M. Ehara, *Environ. Sci. Technol*. **2014**, *48*, 7101; (c) Z. Wang, S. Yuan, A. Mason, B. Reprogle, D.-J. Liu and L. Yu, *Macromolecules* **2012**, *45*, 7413.

[6.3] (a) S. Lin, C. S. Diercks, Y.-B. Zhang, N. Kornienko, E. M. Nichols, Y. Zhao, A. R. Paris, D. Kim, P. Yang, O. M. Yaghi, C. J. Chang, *Science*, **2015**, *349*, 6253; (b) N. Kornienko, S. Lin, Y. Zhao, C. J. Chang, C. S. Kley, O. M. Yaghi, C. Zhu, D. Kim, and P. Yang, *J. Am. Chem. Soc.* **2015**, *137*, 14129; (c) E. V. Kondratenko, G. Mul, J. Baltrusaitis, G. O. Larrazabal and J. Perez-Ramirez, *Energy Environ. Sci.*, **2013**, *6*, 3112.

ABOUT THE AUTHOR

Mr. Bishnu Prasad Biswal, son of Sj. Giridhari Biswal and Smt. Durgabati Biswal, was born in Bartanda village of Jajpur district, Odisha, India, in 1988. He did his schooling from Chandra Sekhar Behera Zilla School, Sambalpur (2003) and higher secondary education from Sukinda College, Sukinda, Jajpur, Odisha (2005). He has completed his B.Sc. (Chemistry) from Dhenkanal Autonomous College, Dhenkanal affiliated to Utkal University, Odisha in the year 2008. Then he moved to Department of Chemistry, Utkal University, Bhubaneswar, Odisha to pursue his M.Sc. (Chemistry). After qualifying all India CSIR-UGC National Eligibility Test (NET-JRF) examination, he joined Physical and Materials Chemistry Division, CSIR-National Chemical Laboratory, Pune, India to pursue his Ph.D. degree in July 2011 under the guidance of Prof. Dr. Rahul Banerjee. He has received the research fellowship (JRF and SRF) from University Grant Commission (UGC), New Delhi, India for the period of July 2011 - June 2016 to carry out the Ph.D. thesis work.

Page left intentionally blank

LIST OF PUBLICATIONS

1. **Bishnu P. Biswal**, Shebeeb Kunjattu H., Taranpreet Kaur, Rahul Banerjee* and Ulhas K. Kharul* *"Transforming Covalent Organic Framework into Thin-film Composite Membranes for Faster Hydrocarbon Recovery"* **2017**, Submitted.
2. Suvendu Karak, Sharath Kandambeth, **Bishnu P. Biswal**, Himadri Sekhar Sasmal, Sushil Kumar, Pradip Pachfule and Rahul Banerjee* *"Constructing Ultraporous Covalent Organic Frameworks in Seconds via an Organic Terracotta Process"*

   ***J. Am. Chem. Soc.*, 2017,** 139, 1856–1862.
3. Sharath Kandambeth,[†] **Bishnu P. Biswal**,[†] Harshal D. Chaudhari, Kanhu Charan Rout, Shebeeb Kunjattu H., Shouvik Mitra, Anuja Das, Rabibrata Mukherjee, Ulhas K. Kharul* and Rahul Banerjee* *"Selective Molecular Separation in Self-standing Porous Covalent Organic Membranes (COMs) made by Molecular Baking"* ***Adv. Mater.*, 2017,** 29, 1603945. ([†]**SK** and **BPB** contributed equally to this work).
4. Jayshri Thote, Harshitha Barike Aiyappa, Rahul Raya Kumar, Sharath Kandambeth, **Bishnu P Biswal**, Digambar Balaji Shinde, Neha Chaki Roy and Rahul Banerjee* *"Constructing Covalent Organic Frameworks in Water via Dynamic Covalent Bonding"* ***IUCrJ*, 2016**, Accepted Article.
5. Arjun Halder,[†] Sharath Kandambeth,[†] **Bishnu P. Biswal**,[†] Gagandeep Kaur, Neha Chaki Roy, Matthew Addicoat, Jagadish K. Salunke, Subhrashis Banerjee, Kumar Vanka, Thomas Heine, Sandeep Verma and Rahul Banerjee* "*Decoding the Morphological Diversity in Two Dimensional Crystalline Porous Polymers by Core Planarity Modulation*" ***Angew. Chem. Int. Ed.*, 2016**, *55*, 7806–7810.

   ([†]**AH, SK** and **BPB** contributed equally to this work).
6. Shouvik Mitra,[†] Sharath Kandambeth,[†] **Bishnu P. Biswal**,[†] Abdul Khayum M., Chandan K. Choudhury, Mihir Mehta, Gagandeep Kaur, Subhrashis Banerjee, Asmita Prabhune, Sandeep Verma, Sudip Roy, Ulhas K. Kharul and Rahul Banerjee* "*Self-Exfoliated Guanidinium-Based Ionic Covalent Organic Nanosheets (iCONs)*"

   ***J. Am. Chem. Soc.*, 2016**, *138*, 2823–2828. ([†]**SM, SK** and **BPB** contributed equally to this work).

7. **Bishnu P. Biswal**, Harshal D. Chaudhari, Rahul Banerjee* and Ulhas K. Kharul* "*Chemically Stable Covalent Organic Frameworks (COF)-Polybenzimidazole Hybrid Membranes: Enhanced Gas Separation through pore modulation*"

   ***Chem. Eur. J.,* 2016**, *22*, 4695–4699.

8. Digambar Balaji Shinde, Harshitha Barike Aiyappa, Mohitosh Bhadra, **Bishnu P. Biswal**, Pritish Wadge, Sharath Kandambeth, Bikash Garai, Shrikant M. Kunjir, Tanay Kundu, Sreekumar Kurungot* and Rahul Banerjee* "*A Mechanochemically Synthesized Covalent Organic Framework as Proton-conducting Solid Electrolyte*"

   ***J. Mater Chem. A*, 2016**, *4*, 2682–2690.

9. **Bishnu P. Biswal**, Sharath Kandambeth, Suman Chandra, Digambar Balaji Shinde, Saibal Bera, Suvendu Karak, Bikash Garai, Ulhas K. Kharul and Rahul Banerjee* "*Pore Surface Engineering in Porous, Chemically Stable Covalent Organic Frameworks for Water Adsorption*" ***J. Mater Chem. A*, 2015**, *3*, 23664–23669.

10. Gobinda Das,[†] **Bishnu P. Biswal**,[†] Sharath Kandambeth,[†] V. Venkatesh, Gagandeep Kaur, Matthew Addicoat, Thomas Heine, Sandeep Verma, Rahul Banerjee* "*Chemical Sensing in Two Dimensional Porous Covalent Organic Nanosheets*" ***Chem. Sci.*, 2015**, *6*, 3931–3939. ([†]**GD, BPB** and **SK** contributed equally to this work).

11. **Bishnu P. Biswal**, Anand Bhaskar, Rahul Banerjee* and Ulhas K. Kharul* "*Selective Interfacial Synthesis of Metal-Organic Frameworks on polybenzimidazole Hollow Fiber Membrane for Gas Separation" **Nanoscale,* 2015**, *7*, 7291–7298.

12. Gobinda Das, Digambar Balaji Shinde, Sharath Kandambeth, **Bishnu P. Biswal** and Rahul Banerjee* "*Mechanosynthesis of Imine, β-Ketoenamine, and Hydrogen-Bonded Imine-Linked Covalent Organic Frameworks using Liquid-Assisted Grinding*". ***Chem. Commun.*, 2014**, *50*, 12615–12618. *(Selected as the "inside front cover page" of the journal **Chem. Commun.**).*

13. Chandan Dey, Tanay Kundu, **Bishnu P. Biswal**, Arijit Mallick* and Rahul Banerjee* *"Crystalline Metal Organic Frameworks (MOFs): Synthesis, Structure and Function"* ***Acta Cryst.*** *B70,* 2014, 3–10. *(Published in the Special issue on Crystal Engineering).*

14. Suman Chandra, Sharath Kandambeth, **Bishnu P. Biswal**, Binit Lukose, Shrikant M. Kunjir, Minakshi Chaudhary, Ravichandar Babarao, Thomas Heine and Rahul Banerjee* *"Chemically Stable Multi-layered Covalent Organic Nanosheets from Covalent Organic Frameworks via Mechanical Delamination"*

***J. Am. Chem. Soc.,* 2013**, *135*, 17853–17861.

15. **Bishnu P. Biswal**, Dhanraj B. Shinde, Vijayamohanan Pillai* and Rahul Banerjee* *"Stabilization of Graphene Quantum Dots (GQDs) by Encapsulation inside Zeolitic Imidazolate Framework Nanocrystals for Photoluminescence Tuning"*

***Nanoscale*, 2013**, *5*, 10556–10561.

16. **Bishnu P. Biswal**,† Suman Chandra,† Sharath Kandambeth,† Binit Lukose, Thomas Heine and Rahul Banerjee* "*Mechanochemical Synthesis of Chemically Stable Isoreticular Covalent Organic Frameworks*"

***J. Am. Chem. Soc.,* 2013**, *135*, 5328–5331. (†**BPB, SC** and **SK** contributed equally to this work).

17. Thangavelu Palaniselvam,† **Bishnu P. Biswal**,† Rahul Banerjee* and Sreekumar Kurungot* "*Zeolitic Imidazolate Frameworks (ZIFs) Derived Hollow Core-Nitrogen doped Carbon Nanostructures for Oxygen Reduction Reactions in PEFCs*"

***Chem. Eur. J.,* 2013**, *19*, 9335–9342. (†**TP** and **BPB** contributed equally to this work).

18. **Bishnu P. Biswal**, Tamas Panda and Rahul Banerjee* "*Solution Mediated Phase Transformation (RHO to SOD) in Porous Co-Imidazolate based Zeolitic Framework with High Water Stability*" ***Chem. Commun.,* 2012**, *48*, 11868–11870. *(Published as part of* ***ChemComm*** *Emerging Investigators issue 2013).*

19. Pradip Pachfule, **Bishnu P. Biswal** and Rahul Banerjee* "*Control over Porosity using Isoreticular Zeolitic Imidazolate Frameworks (IRZIFs) as Template for Porous Carbon Synthesis*" ***Chem. Eur. J.,* 2012**, *18*, 11399–11408.

LIST OF PATENTS

1. Rahul Banerjee, Ulhas K. Kharul, Sharath Kandambeth, **Bishnu P. Biswal**, Harshal D. Chaudhari, Suvendu Karak *"Self Standing Crystalline, Porous Covalent Organic Membranes for Molecular Separation*" Provisional Filing No. 201611009671; Filing Date: 21th Mar. **2016**.
2. Ulhas K. Kharul, **Bishnu P. Biswal**, Rahul Banerjee, Harshal D. Chaudhari *"Polymer Composite Membranes based on Covalent Organic Frameworks (COFs) and Covalent Organic Nanosheets (CONs)"* Complete Filing No. 201611018307; Filing Date: 1st June **2015**.
3. Ulhas K. Kharul, Rahul Banerjee, **Bishnu P. Biswal**, Anand Bhaskar *"Growth of MOFs on Polymeric Hollow Fiber Membranes via Interfacial Synthesis Approach Can Be Made More General*" Provisional Filing No. 3324/DEL/2014; Filing Date: 18th Nov. **2014**.
4. Rahul Banerjee, **Bishnu P. Biswal**, Suman Chandra, Sharath Kandambeth *"Two Dimensional Porous Crystalline Organic Frameworks with High Chemical Stability" Provisional* Filing No. 1112/DEL/2013; Filing Date: 15th Apr. **2013**.

CONFERENCES AND PRESENTATIONS

1. Presented a poster in "*International Conference on Metal Organic Frameworks and Porous Polymers (EuroMOF)* **2015**, Potsdam, Germany.
2. Oral presentation in "*International Conference on Membranes*" **2015**, Kochi, Kerala.
3. Presented poster in *International Conference on Membrane based Separation "MEMSEP"* **2015**, Vadodara, Gujarat.
4. Presented poster in "*9th CRSI-RSC and CRSI-NSC-17 symposia*" **2015**, Pune.
5. Presented poster in *International Conference on* "*Structural Chemistry of Molecules and Materials (SCOMM)*" **2014**, Kolkata.
6. Presented poster in *National Conference on* "*Chemical Frontiers*" **2014**, Goa.